

FERARI: A multi-protein tethering platform involved in endocytic recycling

Inauguraldissertation zur Erlangung der Würde eines Doktors der
Philosophie vorgelegt der Philosophisch-Naturwissenschaftlichen

Fakultät der Universität Basel

Von

Harun-Or Rashid

Basel, 2021

Originaldokument gespeichert auf dem Dokumentenserver der Universität Basel
<https://edoc.unibas.ch>

Genehmigt von der Philosophisch-Naturwissenschaftlichen Fakultät
auf Antrag von

Pr. Dr. Anne Spang

Pr. Dr. Martin Spiess

Pr. Dr. Jean Gruenberg

Basel, 27 April 2021

Prof. Dr. Marcel Mayor

Dekan der Philosophisch-
Naturwissenschaftlichen
Fakultät

Dedictory

This thesis is dedicated to my parents and my other family members:

My mom, who passed away when I was an infant.

My father, who taught me how to read and write.

My siblings, with whom I share a tight bonding. They cared me and raised me.

Finally to my loving wife, Sheuli Begum. Thanks for being there when I needed you the most.

Statement of my thesis

This work has been performed in the group of Prof. Dr. Anne Spang at the Biozentrum of University of Basel in Switzerland.

My Ph.D committee members are:

Prof. Dr. Anne Spang

Prof. Dr. Martin Spiess

Prof. Dr. Jean Gruenberg

My Ph.D. thesis consists of a synopsis and an introduction covering a variety of aspects related to my work. Furthermore, this thesis contains a scientific publication, a manuscript ready to submit, and additional unpublished data. Finally, I discuss various aspects of my major findings. The figure numbering has been adapted to each subchapter.

Table of contents

Summary	7-8
1. Introduction	
1.1 The basics of membrane trafficking	9-10
1.2 Different methods of membrane trafficking.....	10-12
1.3 Major steps in vesicular trafficking	12
1.4 Cellular mechanisms of vesicle delivery.....	13
1.5 Membrane tethering in vesicular transport.....	13-15
1.6 SNARE-mediated vesicle fusion at the target organelle.....	15-17
1.7 Organelle identity in endocytic trafficking process	
1.7.1 Rab GTPases in maintenance of organelle identity.....	17-20
1.7.2 Phosphatidylinositol phospholipids (PIPs) in organelle identity.....	20-21
1.8 Cargo trafficking to the plasma membrane from SE through recycling process.....	21-22
1.8.1 Fast recycling process.....	22
1.8.2 Slow recycling process.....	23
1.9 Regulators of slow Recycling process	
1.9.1 Rab11-FIPs	23-24
1.9.2 EHD proteins	24-25
1.9.3 Rabenosyn-5 and VPS45 in endocytic recycling.....	26-27
1.10 Cargo sorting for endocytic recycling from SEs.....	27-28
1.11 Formation of transport carrier for recycling	
1.11.1 Role of Sorting Nexins (SNXs) and associated complexes in recycling carrier formation.....	28-29
1.11.2 WASH complex-mediated membrane stabilization and endocytic recycling.....	30
1.11.3 Retromer –mediated cargo recycling towards TGN.....	31
1.11.4 Retromer –mediated cargo recycling towards PM.....	31
1.11.5 ESCPE-1-mediated cargo sorting for recycling.....	32
1.11.6 Retriever complex-mediated cargo sorting for recycling.....	32
1.11.7 CCC complex-mediated cargo sorting for recycling.....	32-33
1.12 Tethering complexes in endocytic recycling	
1.12.1 Coiled-coil tethers.....	33-34
1.12.2 Multi-subunit tethering complexes.....	34-36
2. Open questions and aim of the thesis	
2.1 Open questions.....	37-39
2.2 The aim of the thesis.....	39

3. FERARI is required for Rab11-dependent recycling	
3.1 Summary.....	41
3.2 Introduction.....	41
3.3 Results.....	41-49
3.4 Discussion and outlook.....	49-51
3.5 References.....	51-52
3.6 Methods.....	53-55
3.7 Supplementary information.....	56-65
4. FERARI coordinates cargo flow through sorting endosomes	
4.1 Summary.....	68
4.2 Introduction.....	68-69
4.3 Results.....	69-83
4.4 Discussion and outlook.....	83-85
4.5 Materials and methods.....	86-91
4.6 References.....	91-92
4.7 Supplementary material.....	93-96
5. Purification of FERARI	
5.1 Summary.....	98
5.2 Introduction.....	99-100
5.3 Results.....	100-103
5.4 Materials and methods	104-105
6. FERARI regulates primary ciliogenesis	
6.1 Summary.....	107
6.2 Introduction	
6.2.1 Types of cilia and their development.....	108-109
6.2.2 Signaling through primary cilia.....	109-110
6.2.3 Vesicular transport and Rab-GTPases in cilia development.....	110-111
6.3 Aim of the study.....	112
6.4 Results.....	112-117
6.5 Discussion and outlook.....	118-119
6.6 Materials and methods.....	119-121
7. Further discussion and outlook.....	122-127
8. Abbreviation Index.....	128-129
9. References.....	130-145
10. Acknowledgements.....	146
11. Curriculum Vitae.....	147

Summary

Eukaryotic cells have developed intracellular membrane-bound organelles through evolution. These organelles maintain an extended communication system using shuttling vesicles or contact sites. Vesicles bud from the donor organelles or the plasma membrane and transport proteins, lipids, and nutrients across the cytosol to the acceptor membrane. This endomembrane trafficking is a thoroughly regulated process to guarantee correct cargo transport to the right destination organelle or the plasma membrane.

The sorting endosome is a hub for diverse trafficking pathways, including recycling towards plasma membrane, secretion, or protein degradation into the lysosome. Multiple fusion and fission events regulate protein and lipid transport along the eukaryotic endomembrane system. Multi-subunit tethering complexes contribute to the fusion of two opposing membranes with the help of Rab GTPases and SNARE proteins. Co-ordinated function of Rab GTPases, tethers, and SNAREs are required for membrane tethering and fusion. Studies in yeast have identified multiple tethering factors in regulation of membrane tethering and fusion. However, due to the diversification of the cargo and duplication of genes involved in cargo trafficking, membrane tethering is much more complex in higher eukaryotes, especially in the mammalian system. Furthermore, how cargo recycling is regulated from the sorting endosomes is largely obscure, and the involvement of any tethering complex in this process needs to be thoroughly investigated. The presented work is aimed to provide a better understanding of cargo recycling from sorting endosomes in connection with a multi-subunit tethering platform.

In parallel a work conducted in the with *C. elegans*, I have characterized a conserved six member-tethering platform, Factors for Endosome Recycling and Rab Interactions (FERARI) in the mammalian system. We found that, in human cell lines, the FERARI member VIPAS39 interacts with five other subunits: VPS45, Rabenosyn-5, EHD1, Rab11-FIP5 and ANK3. FERARI, as a platform, regulates cargo recycling from sorting endosomes via Rab11-positive recycling vesicles. Transferrin recycling is partially impaired when FERARI is depleted. Rab11-FIP5 and Rabenosyn-5 are two Rab interacting subunits of FERARI that bind Rab11 and Rab5, respectively. FERARI tethers Rab11 containing recycling vesicles to Rab5 positive endosomes, which is then followed by membrane fusion through SNARE proteins regulated by the FERARI subunit Sec1/Munc18 protein VPS45.

Surprisingly, unlike conventional tethering complexes, FERARI contains the membrane fission protein EHD1. Thus, FERARI probably couples fusion and fission activity of recycling vesicles on sorting endosomes through the SM protein VPS45 and membrane pinchase activity of EHD1 respectively. Interestingly, we also found that FERARI is associated with the BAR domain protein SNX1, which is involved in membrane tubulation. ANK3, an actin regulator associated with FERARI, might stabilize SNX1 positive compartments.

In the second part of this thesis, we focused on cargo uptake process by the recycling vesicles from sorting endosomes. Most notably, in HeLa cells, endogenously tagged GFP-Rab11 vesicles transiently associates with SNX1 positive structure and dissociates, suggesting a combination of kiss-and-run process. Furthermore, we have found that the cargo adaptor protein SNX6, but not SNX5, interacts with Rabenosyn-5 and VIPAS39. Combined knockout of *snx5* and *snx6* resulted in a FERARI like phenotype, enlarged Rab11 structure. While the association of SNX1 with Rab11 is reduced Rab5 colocalization was increased in *snx5+6* KO cells.

In the third part of this thesis, I discuss the current study of purification of FERARI. To purify entire FERARI complex, we over-expressed GFP-Rabenosyn-5 in HEK-293 cells and pulled down other subunits heterologously expressed in yeast.

Finally, to gain insight into the biological significance of FERARI, we analyzed cilia development in retinal epithelial cells by knocking out FERARI subunits. We demonstrated that cilia size is shorter in FERARI depleted condition. Normally, Rab11 mediated polarized cargo trafficking is crucial for cilia development. However, in FERARI KO cell Rab11 is not efficiently recruited to the ciliary base. Overall, this work represents the first characterization of FERARI in mammalian cells.

1. Introduction

1.1 The basics of membrane trafficking

Eukaryotes are distinguished from their common ancestors, bacteria, and archaea, by the presence of a sophisticated network of intracellular membrane-bound organelles. Noble prize winning work of Christian De Duve and George Palade demonstrated the presence of membrane-bound compartments/organelles in higher eukaryotes with distinct functions (Duve, 1975; Palade, 1975). Presence of distinct membrane-bound organelles in eukaryotic cells is crucial to compartmentalize particular functions like protein synthesis and degradation, metabolism, signaling, lipid breakdown and ATP production at definite cellular sites. However, to take benefit of such well-developed system of membrane-enclosed compartments, they need to communicate and share information and materials in a specific and controlled manner. Now the question is how these organelles exchange material between them. This can occur through either the formation of contact sites or the generation of shuttling vesicles (Stefan et al., 2017). In eukaryotes, cellular materials follow two distinct trafficking routes- a) the endocytic pathway, and b) the secretory pathway. The former pathway maintains the inward flow of molecules from the cell surface and includes various organelles, such as endosome, Golgi, lysosomes, as well as the plasma membrane itself, whereas the latter transports biosynthetic molecules to the cell exterior, endosomes and lysosomes from the ER via the Golgi apparatus (Alberts et al., 2002b; Schwartz, 1990).

In the endocytic pathway extracellular and the plasma membrane materials enter the cell, in vesicular form, through various processes like clathrin-dependent and independent endocytosis. Irrespective of their mode of internalization, the primary destination of the internalized materials are Early/Sorting Endosomes (EE/SE) (Cavalli et al., 2001). To avoid confusion, I will use the term sorting endosome throughout this thesis. SEs are distinct membrane-bound endocytic organelle. Furthermore, SEs receive cargo transported from trans-Golgi network (TGN), such as newly synthesized lysosomal hydrolases transport from ER to TGN and then to SEs via TGN derived vesicles (Braulke & Bonifacino, 2009). The SEs are the short-term reservoir of cargo from different sources. As shown in Fig. 1.1, SEs have tubule vesicular shape and the fate of the cargo is determined here. From SEs cargoes again separate along different paths. The majority of the cargoes recycle back to the plasma membrane through tubular recycling endosomes (RE). Some of the remaining components follow another transport route that connects SE to the TGN. Any remaining cargo stays in the globular part of the SEs forms intra-luminal vesicles (ILV) through inward invagination of rate-limiting membrane, which leads to the formation of multi-vesicular bodies (MVB)/matured endosomes and follows degradative pathway (Babst, 2011). The endocytic trafficking process culminates with the fusion of mature endosomes with lysosomes. Lower lysosomal pH and the presence of proteases provide suitable condition for cargo degradation delivered by mature endosomes upon fusion (Vellodi, 2005).

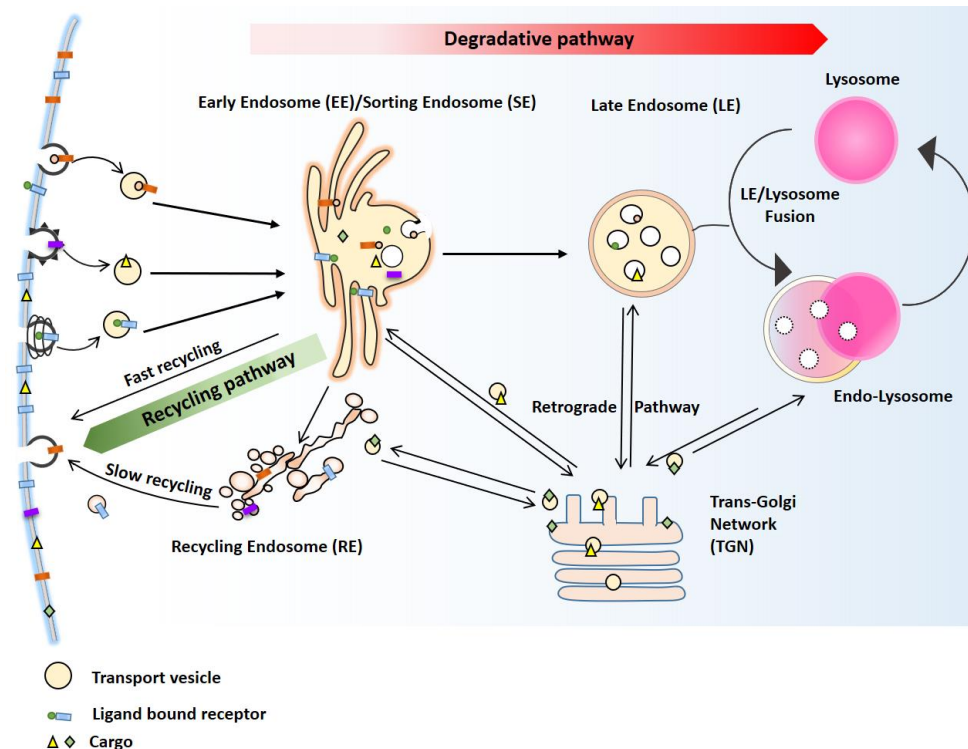


Figure 1.1: The endocytic trafficking: Lipids, and proteins enter the cell through vesicles, and their primary destination are early endosomes. With time, early endosomes transform into tubulo-vesicular structures called SE. Based on the target destination, cargoes are sorted into different subdomains at the SE. A substantial amount of internalized cargoes recycles back to the plasma membrane through the fast and slow recycling pathways. Some cargoes are targeted to TGN through the retrograde pathway. Over time, the tubule-vesicular shape of the SE is changed to more globular shape and it becomes late endosomes. The remaining cargoes in the globular structure are sorted into the intraluminal vesicles that begins from the early endosomal stage. Finally, the endocytic process culminates through the fusion of late endosomes with lysosomes. Adapted from (Huotari & Helenius, 2011).

1.2 Different methods of membrane trafficking

In most cases, cargo transport between organelles is a complex bidirectional process, which is how organelle individuality is preserved while cargoes move through the organelles. Furthermore, organelles need to take the decision, which cargo to keep and which one to extradite from a massive flow of cargo and resident proteins. For maintaining the proper size of the compartments, a regulated flow of cargo is also required (Bonifacino & Glick, 2004). Eukaryotic cells use different modes of cargo transport.

A vital method of communication between the organelles is vesicular transport (Fig. 1.2), which links the cell with its environment. In this process, cargo-laden vesicles are generated at a donor organelle, which are then directed to the correct target compartment, to which they tether and dock, and finally fuse to deliver the cargo. Vesicular trafficking facilitates cargoes in membrane-bound vesicles to transport between the intracellular compartments, including the plasma membrane (Bonifacino & Glick, 2004). However, cargoes can be

transported to their final destination in alternative approaches, such as maturation of the cargo containing compartments by acquiring required lipids and proteins. Maturation of endosomes into MVB is an example of such transport process where endosomal cargoes are packaged into ILVs and eventually degraded in lysosome. Recently, Naava Naslavsky and Steve Caplan have suggested a possible model where EEs can move along microtubules and converts into recycling endosomes through recruitment of particular recycling proteins and lipids on the way to the perinuclear region (Naslavsky & Caplan, 2018). Another model could be a kiss-and-run process (Fig. 1.2), where transport carrier may transiently fuse with the donor/acceptor organelle and deliver/receive respective cargoes. Neuro-transmitter release at the synaptic junction has been suggested to follow kiss-and-run process (Fesce et al., 1994; Ryan, 2003). Furthermore, EEs have also been implicated in kiss-and-run dependent partial fusion at the early stage of lysosome biogenesis (Duclos et al., 2003). Maturing endosomes have been reported to move towards perinuclear region where they form larger bodies by fusing with each other. These larger bodies then transiently contact or 'kiss' with lysosomes, followed by a dissociation or 'run' (kiss-and-run) (Huotari & Helenius, 2011). This process resembles vesicular trafficking, as it still requires vesicle tethering and docking on the target membrane. In case of vesicular transport, identity of the vesicle is lost once it fuses with target membrane. However, in the kiss-and-run process both the vesicle and the acceptor organelle maintain their molecular identity while exchange cargoes (Henkel & Almers, 1996; Solinger et al., 2020). However, the core molecular machineries regulating the kiss-and-run process are mostly obscure.

The formation of the hybrid organelles is another method of cargo transport that mainly takes place between mature endosomes and lysosomes (Fig. 1.2). In this process, instead of formation of cargo containing vesicles or transient contact between two membrane bound organelles, mature endosome and lysosome fuse permanently that leads to the intermixing of luminal content from both of the organelles (Bright et al., 2005; Luzio et al., 2007).

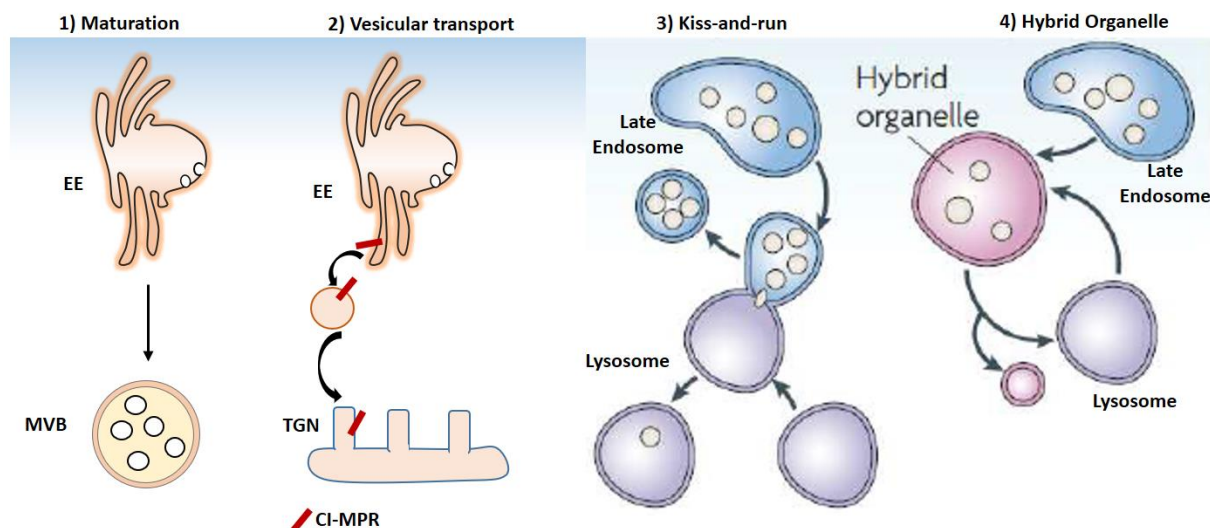


Figure 1.2: This model is depicting the multiple methods of cargo delivery. 1. In the maturation process, cargo-containing organelle undergoes changes in shapes and physical properties through recruitment of various proteins and lipids, and thus matures into a new compartment. 2. Vesicular transport, on the other hand, depends on the generation of cargo containing vesicles from a donor organelle and delivering it to another pre-existing compartment. Cation-independent mannose-6-phosphate receptor trafficking to and from TGN is an example for vesicular trafficking. 3. A kiss-and-run process differs from vesicular transport in the cargo delivery part, where vesicle generated at the donor organelle fuses transiently to acceptor organelle instead of complete fusion. Transient fusion between the late endosomes and the lysosomes is an example of a kiss-and-run process. 4. Late endosomes and lysosomes may fuse permanently that give rise to formation of a hybrid organelle. Adapted from (Luzio et al., 2007).

1.3 Major steps in vesicular trafficking

Membrane trafficking is mostly carried out by transport carriers which are tubular and vesicular in shape. Vesicular transport is a four step process: (i) Cargo (lipid/protein) sorting and generation of transport carrier (i.e. vesicles, tubules); (ii) microtubule and molecular motors based trafficking of vesicles towards their target destination; (iii) vesicle tethering on the target membrane; (iv) and finally the fusion of cargo containing vesicles with their target membrane (Bonifacino & Glick, 2004; Miaczynska & Munson, 2020).

Each of these steps needs to be achieved in an orderly way so that the cargoes are sorted in the right vesicles and follow the correct trafficking route towards their destination. Maintaining the organelle identity is a challenging task for cells while processing cargoes into vesicles for transport.

1.4 Cellular mechanisms of vesicle delivery

The cytoplasm of eukaryotic cells is similar to that of a busy highway full of different membrane-bound organelles and vesicles. Due to the diversity of the membrane system, the transport vesicles are much likely to come across multiple potential membranes before they reach the destination (Alberts et al., 2002a). Therefore, vesicle must be highly selective in choosing the target membrane with which to fuse. Molecular markers exhibited on the cytosolic surface of membrane-bound compartments function as signaling cues to avoid non-specific vesicle targeting. However, multiple compartments can display identical membrane marker, and thus additional control is required for ensuring target specificity. Nevertheless, the exact directionality of vesicles is established because the molecular markers displayed by the vesicles define their type and the origin, and the target organelles display markers that is complementary to the vesicular marker. This critical identification phase is thought to be organized primarily by two different classes of proteins: Rab-GTPases and N-ethylmaleimide-sensitive factor attachment protein receptor (SNARE) proteins (Alberts et al., 2002a; Cai et al., 2007). Rab-GTPases specify the organelle identity whereas the SNARE proteins play central role in both providing membrane specificity and catalyzing the vesicle fusion with target membrane. There is another crucial factor known as “tethering factor” (TF) that regulates initial tethering and docking of vesicles to their target compartment. Rab-GTPases work in concert with tethering factors to regulate the vesicle tethering and docking to the corresponding membrane. Rabs and tethers provide the initial level of membrane recognition, which is then augmented by SNARE pairings (Cai et al., 2007).

In the following paragraph, I will briefly discuss about the regulation of membrane fusion by SNARE and tethering factors. However, we should keep it in mind that coats and adaptor proteins, and molecular motors are also potential determinant of vesicular membrane trafficking. While the coat proteins form a scaffold around the budding vesicle from the donor organelle, the adaptors simultaneously bind to coats and to transmembrane proteins and facilitate the vesicle formation at the right time and place in the cell (Owen et al., 2004). Molecular motors propel the vesicles to the specific direction. Once the vesicle is near to the target destination tethering factors acts as a bridge between two opposing membranes bringing them in close proximity and make the initial contact. When two lipid bilayers are in close contact, SNAREs present on vesicles and the target membrane begins to make a 4-helix bundle and lead to the lipid bilayer mixing and eventually fusion of membranes and inter mixing of cargoes.

1.5 Membrane tethering in vesicular transport

Vesicles enriched with cargo generated at the donor organelles must overcome the distance to reach the acceptor organelles. Upon arriving at their correct destination, vesicles require machinery for docking, tethering, and fusion with the target membrane. Vesicle tethering

defines the development of a protein bridge that stimulates the connection of a vesicle with its target organelle before the two membranes come in contact. Any protein or complex of proteins involved in the membrane tethering process are called “tethering factors.” Tethering is a loose reversible physical connection of a vesicle with its target membrane upstream of SNAREs involvement. Vesicle tethering is followed by docking, which is a robust non-reversible binding between two membranes involving SNAREs. While docking involves bringing two membranes close enough to let the proteins protruding from lipid bilayers interact and adhere, fusion requires bringing the lipid bilayers much closer within the 1.5 nm range (S. R. Pfeffer, 1999)(Bonifacino & Glick, 2004). When the membranes are in such close apposition, lipids can flow from one bilayer to the other. Finally, fusion is the SNARE-mediated process of lipid bilayer mixing of two membranes followed by intermixing luminal contents. Thus, the initial recognition of membranes through tethering proteins has seemed to provide fidelity to the SNARE-mediated membrane fusion. Although tethering is a purely protein-mediated process, the lipid composition of the vesicle, and its radius, can be active agents that influence the tethering factors' binding strength to the membrane. Most tethering factors, if not all, have a lipid-binding property and interact with two different classes of proteins having a related function in membrane trafficking: Rab GTPases and SNAREs (Cai et al., 2007; Hutagalung & Novick, 2011).

Two broad classes of tethering molecules are conserved through evolution from yeast to human. Namely, long putative coiled-coil tethers and multi-subunit tethering complexes (MTCs) (Bröcker et al., 2010; Dubuke & Munson, 2016; Hutagalung & Novick, 2011; Whyte & Munro, 2002). Tethers are extensively distributed throughout the eukaryotic cells, and both classes of tethers are involved in endocytic and secretory membrane trafficking events. Through biochemical and structural studies, significant progress has been made in the elucidation of molecular mechanisms of tethering factors. Scientists are discovering new tethers, and their potential roles in membrane trafficking are being studied extensively. For example, FERARI (Factors for Endosome Recycling and Rab Interaction) is a potential multi-subunit tethering platform (Solinger et al., 2020) that I tried to characterize in the mammalian system and discussed in this thesis. Tethering complexes have certain features, such as most of the tethers are recruited on the membrane through interaction with small GTPases (Mima, 2017; Takemoto et al., 2018). Furthermore, an increasing number of studies have suggested that tethering complexes organize correct SNAREs at the vesicle-docking site (WanJin Hong & Lev, 2014). Therefore, membrane tethering requires a coordinated functions of Rab-GTPases, tethers, and SNARE proteins. As shown in Fig. 1.3, membrane tethering begins with the initial recognition of the transport vesicle through Rab binding subunits of the tethering complexes, followed by docking and fusion. Membrane fusion and pore formation require SM protein-mediated SNARE activation (Südhof & Rothman, 2009). A detailed description of tethering factors is written in section 1.12 of this thesis.

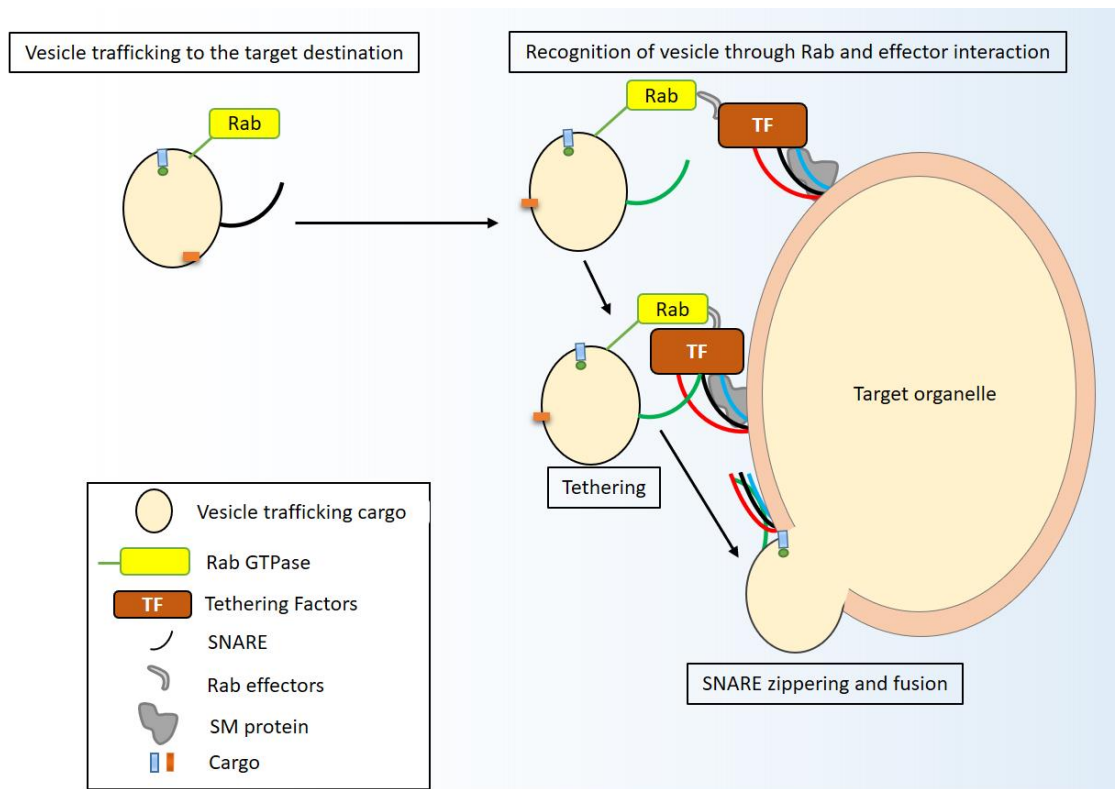


Figure 1.3: The Current model of membrane tethering through MTCs. Rab-binding sub-units of MTC recognize vesicles carrying specific Rabs. Initial interaction between Rab and effectors brings the vesicle in close proximity to the target organelle. SM proteins of tethering complexes regulate SNARE bundle formation and membrane fusion. Adapted from (Bröcker et al., 2010)

1.6 SNARE-mediated vesicle fusion at the target organelle

Delivery of the cargo to the target organelle requires vesicular and organelle membrane fusion. This event is mediated by SNARE proteins (Y. A. Chen & Scheller, 2001). SNAREs are a group of membrane-associated small proteins with 38 members in humans and 25 in yeast. Based on their localization, SNAREs are divided into two groups: vesicular SNARE (v- SNARE) and target membrane SNAREs (t-SNARE) (Wanjin Hong, 2005). Both v and t-SNAREs contain a stretch of approximately 60 amino acids that can form coiled-coils, called the SNARE motif. Generally, the SNARE motif is unstructured, but through interaction with another SNARE motif, it naturally assembles as an alpha-helical structure that develops a parallel form of a four-helix bundle. The bundle zippered between cognate v-SNARE and t-SNARE is called *trans*-SNARE complex or SNAREpin, which pulls two different membranes in close apposition and catalyzes the membrane fusion. As shown in Fig. 1.4, in general a SNAREpin contains VAMP, syntaxin, and SNAP-25 homologs — and a minimum of two SNARE proteins must be attached in the target membranes and vesicles through their carboxy-terminal transmembrane domains (Yoon & Munson, 2018). Given that SNAREpin formation is an exothermic event, the energy produced is utilized to accelerate membrane fusion. The remaining SNARE bundles on the fused membrane after lipid bilayer mixing are termed as *cis*-SNARE complex. Most

interestingly, a single SNARE participates in several rounds of membrane fusion, and thus it needs to be recycled from the fused membrane. This requires disassembly of the cis-SNARE complex, which is catalyzed by ATPase N-ethylmaleimide-sensitive fusion protein (NSF) and its associated cofactor soluble NSF attachment protein (SNAP) (Wanjin Hong, 2005).

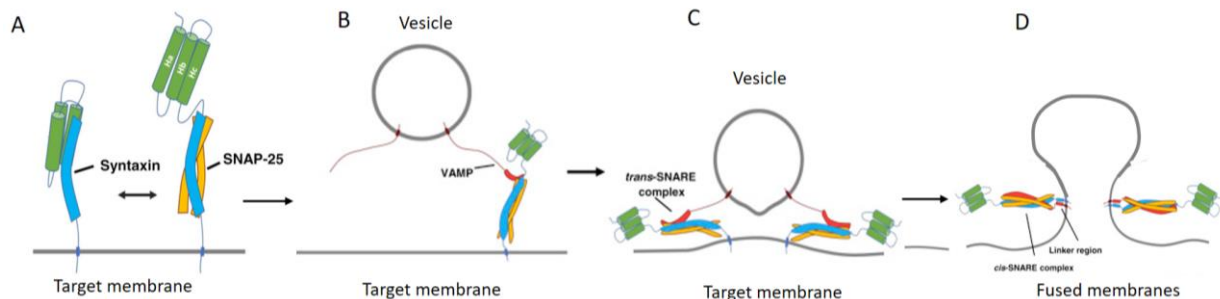


Figure 1.4: Example of trans-SNARE complex formation and vesicle fusion. (A) Upon stimulation, SNARE proteins undergo a conformational change. Generally, SNAREs remain in the closed conformation, and at the beginning of SNARE assembly, SNAREs are in their open conformation (such as Syntaxin in the picture), which is then followed by (B) partial zippering with the other SNAREs. (C, D) SNARE zippering initiates from the amino-terminal end and carries on towards the transmembrane domains and forms the trans-SNARE complex. Completion of trans-SNARE complex assembly causes membrane fusion and pore formation. Taken from (Yoon & Munson, 2018)

SNARE nomenclature based on the subcellular localization is often ambiguous as many SNAREs are localized on both target membranes and vesicles. Therefore, a different classification has been developed depending on their structural features (Fasshauer et al., 1998). Crystal structures revealed that the central position of a quaternary SNARE bundle contains one arginine (R) and three glutamine (Q) residues. This finding classified SNAREs into two types, namely, R-SNARE and Q-SNARE. A functional quaternary SNARE complex is comprised of 3 Q-SNAREs and 1 R-SNARE (Bock et al., 2001; Fasshauer et al., 1998; Katz & Brennwald, 2000). Most of the R-SNAREs are localized on vesicles and the Q-SNARE are on the target membranes with some exceptions where Q-SNAREs, such as GS15, Bet1, and Slt1, function as v-SNARE (Wanjin Hong, 2005). It was believed that the presence of particular SNARE proteins on the vesicle and potential target membrane is adequate to make them compatible for fusion. However, multiple facets of this model do not entirely fit with experiments associated with membrane fusion. For example, in-vitro trans-SNARE assembly is much slower than membrane fusion rate (Brennwald et al., 1994, p. 9; Fasshauer et al., 2002). Furthermore, in some particular cases, membrane fusions are regulated downstream to SNARE complex assembly (Müller et al., 2002). Since the SNAREs are recycled after each fusion event, a single SNARE can be associated with multiple trans-SNARE complexes and thus regulate several fusion events on both anterograde and retrograde pathway (Y. A. Chen & Scheller, 2001; Götte & von Mollard, 1998). Recent studies have shown that the SM (Sec1/Munc18-like) proteins and associated tethering factors play a vital role in trans-SNARE complex formation between particular membranes and thus regulate the specificity of the

membrane fusion (Bacaj et al., 2010; Südhof & Rothman, 2009; Yu et al., 2018). Tethering factors seem to regulate trans-SNARE complex formation in different ways, such as stabilization of individual SNARE proteins or stabilization of SNARE complex in quaternary form. Tethers can further condensate t-SNAREs on the target membrane along with initiation of the complex assembly through interaction with SM proteins (S. R. Pfeffer, 1999).

1.7 Organelle identity in endocytic trafficking process

Membrane-bound organelles along the endocytic trafficking pathway are identified by their differential recruitment and activation of Rab-GTPases and their phosphatidylinositol phospholipid (PIP) compositions. PIPs are phosphorylated intermediates of phosphatidylinositol that play a crucial role in regulating vesicular transport and organelle identification. The unique localization of certain PIPs at specific membranes makes these components exclusively suited to drive organelle-specific trafficking reactions. In this function, PIPs cooperate specifically with Rab and Arf-GTPases (Mayinger, 2012). In the following paragraph, I will briefly describe Rab-GTPases and that will be followed by contribution of PIPs in organelle identification.

1.7.1 Rab GTPases in maintenance of organelle identity

Rab GTPases are the largest branch of small GTPases with a molecular weight of around 20-25 KD of the Ras superfamily. The human genome encodes about 70 Rab proteins, including isoforms with overlapping, yet distinct roles. However, only some of the mammalian Rabs have been studied comprehensively. On the membrane, Rab proteins cycle between active and inactive states through binding with GTP and GDP, respectively (Fig. 1.5). GTPase-activating proteins (GAPs) and Guanine-nucleotide exchange factors (GEFs) proteins regulate the GDP–GTP cycle, respectively. GTP-bound Rab can recruit and interact with downstream effector proteins, including tethering factors, sorting adaptors, motor proteins, lipid kinases, and phosphatases (S. Pfeffer, 2005).

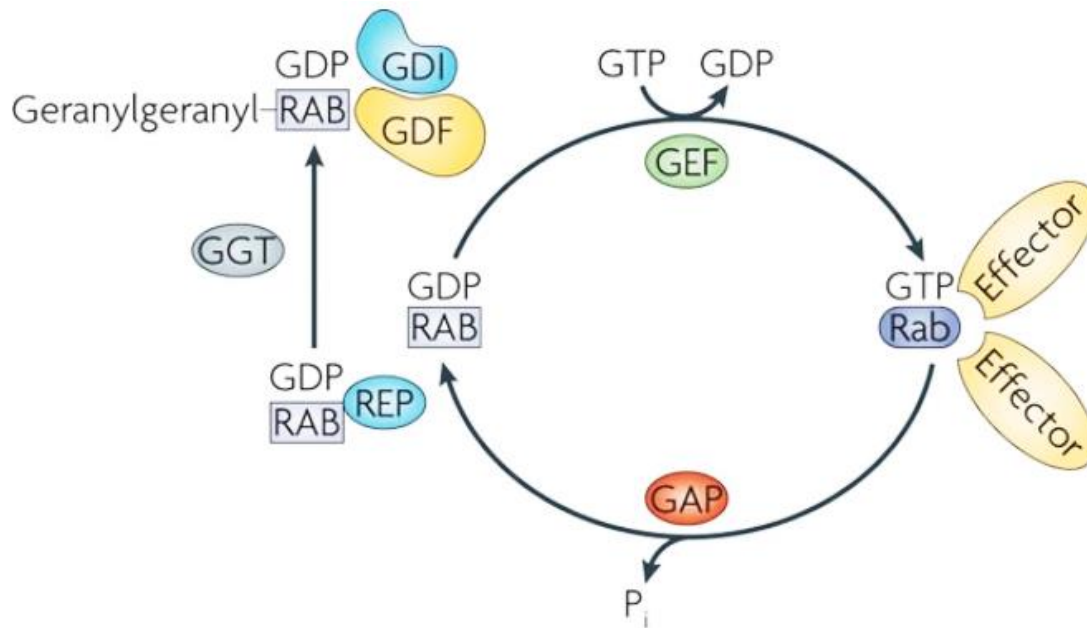


Figure 1.5 : This model shows life cycle of Rab GTPases. The newly synthesized Rab GTPases, in GDI bound form, undergo prenylation by geranylgeranyl-transferase (GGT). Prenylated Rabs are inserted into the membrane and cycles between GDP and GTP through GEF and GAP proteins, respectively. GDP bound Rabs are segregated into the cytosol through interaction with Rab GDI-dissociation inhibitors (Rab-GDI), which regulates the membrane cycle of the Rab. Rab-GDI complex is targeted to specific membranes through interaction with a membrane-bound GDI displacement factor (GDF). Taken from Harald Stenmark (2009).

Rab GTPases are mostly ubiquitous, but many display tissue specificities in expression. The discovery of the localization of different Rab proteins on different intracellular membranes (displayed in Fig. 1.6) preceded our understanding of Rab functions. Rab GTPases organize the lipid and protein composition on the residing membrane, which is crucial for membrane identity (Zerial & McBride, 2001). Most notably, each of the Rabs has distinct intracellular localization, and thus Rab-GTPases provides identity to the organelle and the domains of organelles. The Rab proteins are targeted to their designated membrane through a poorly understood mechanism. It has been suggested that GDI displacement factors (GDFs) plays central role in this process. GDFs recognizes particular Rab-GDI complex and sequesters them apart, consequently enabling the relevant membrane association of the geranylgeranylated Rab GTPase (R. N. Collins, 2003).

Receptors containing vesicles generated at the plasma membrane enter into a complex network of endocytic trafficking process. These vesicles acquire Rab5 at first and reach their first endocytic compartment of a dynamic structure called Sorting Endosomes (SE). Despite the presence of various Rabs on SE, Rab5 is the central organizer of the SE. GTP bound Rab5 interacts with various effector proteins including VPS34, EEA1, and Rabenosyn-5 (Langemeyer et al., 2018).

Different Rab proteins mark different sub-domains of SE where they regulate distinct endocytic events. Cargoes move through distinct sub-domains of endosomes. Suggesting that there is compartmentalization within the membrane (Murk et al., 2003; Wandinger-Ness & Zerial, 2014). For example, Rab4 and Rab11 dependent cargo recycling happens on the tubular part of Rab5 positive SE towards the plasma membrane. These dynamic compartments do not show notable intermix over time (Sönnichsen et al., 2000).

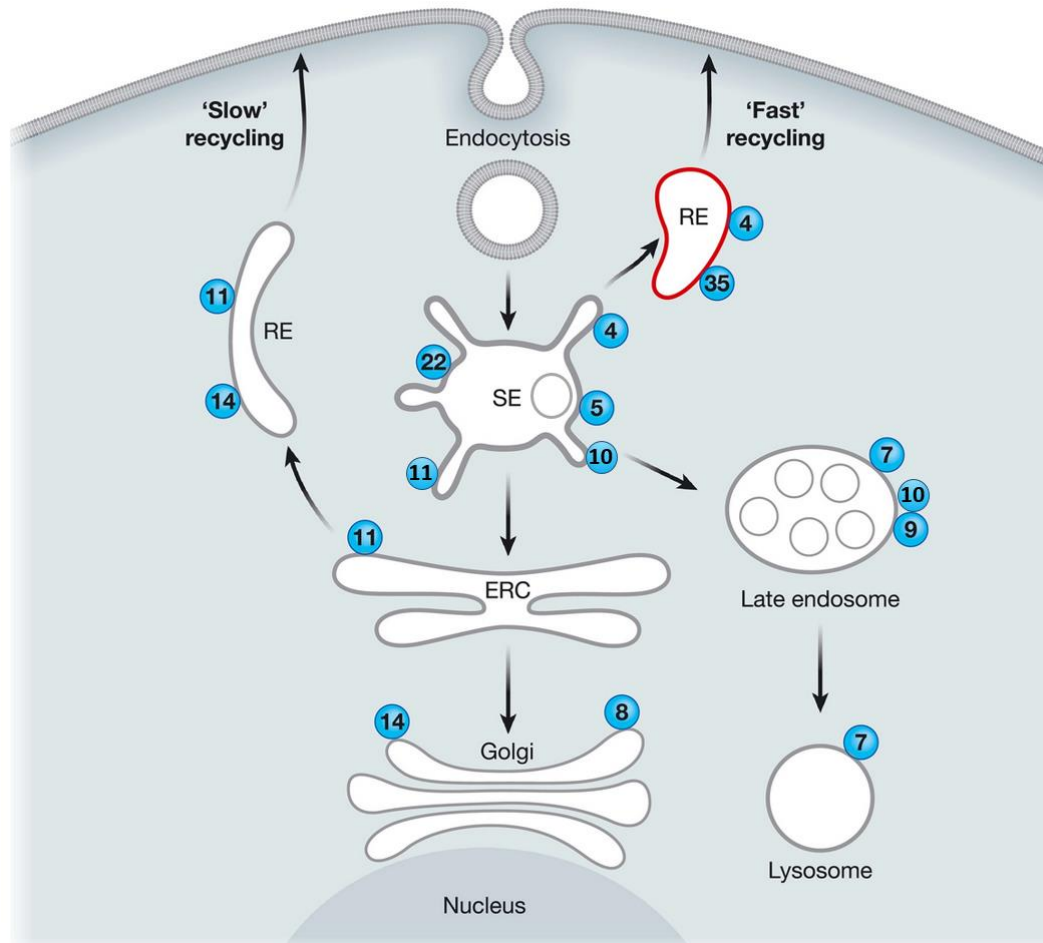


Figure 1.6 : Representation most commonly studied Rabs involved in membrane trafficking system. Adapted from (Allgood & Neunuebel, 2018); (B. Chen et al., 2010).

With time, SE undergoes further morphological changes from a tubulo-vesicular structure to globular structure and Rab7 replaces Rab5. The Rab7 positive globular structure matures into MVB through formation of ILVs (Rink et al., 2005) and it fuses with the lysosomes. Hydrolytic enzymes of lysosomes cause degradation of cargoes (Mindell, 2012). Cargo retrieval from the degradative pathway also can take place from Rab7 positive maturing endosomes. Rab9 regulates retrograde trafficking of cargoes towards TGN from maturing endosomes. Rab7 and Rab9 are on the same endosome but on different sub-domains. This is probably due to the

fact that they are recruited on membranes through different machineries (Barbero et al., 2002).

Sorting of membrane proteins and lipids from luminal content and the generation of membrane tubules emanating from endosomes can lead to the entry of the membrane proteins and lipids into fast recycling pathways (see also in endocytic recycling chapter). Alternatively, they can transfer to a later, juxtanuclear endocytic recycling compartment (ERC) from which recycling endosomes emerge (Grant & Donaldson, 2009). The former pathway is mostly regulated by Rab4 dependent manner. Besides Rab4, Rab35 has been suggested to involve in the fast recycling process as well (Dutta & Donaldson, 2015). However, the latter one is a more complicated and a multistep process, and is defined by the presence of Rab11 on the tubular structure en-route to the plasma membrane. Many studies have shown that Rab11 is one of the main regulators of the endocytic recycling process (Bouchet et al., 2016; Grant & Donaldson, 2009; Kelly et al., 2010; Vale-Costa & Amorim, 2016). The presence of Rab11 on Rab4 and Rab5 positive sorting endosomes, ERC, TGN, and tubule-vesicular recycling endosomes and vesicles makes it more complex to define Rab11 positive structures (Campa et al., 2018).

Rab10 is another recycling endosome-associated Rab that belongs to a Rab subfamily composed of two additional members, Rab8 and Rab13. The function of Rab10 has been well established in polarized epithelial cells, where it regulates early endosome to recycling endosome and TGN trafficking. The involvement of Rab8 in the recycling process is not well understood. However, Rab13 is the third member of this protein family that regulates the recycling of particular cargoes to the cell surface, especially in polarized epithelial cells (Sun et al., 2010). Due to the overlapping function multiple Rabs, it is extremely difficult to distinguish the cargo trafficking pathways they regulate. Therefore, it is crucial to understand molecular machinery for each trafficking path that is defined by specific Rabs.

1.7.2 Phosphatidylinositol phospholipids (PIPs) in organelle identity

PIPs are a group of lipids found in the cytosolic leaflets of all intracellular membranes. PIPs are synthesized in the ER and delivered to intracellular membranes. They cycle between phosphorylated and dephosphorylated forms at their 3, 4, and 5 positions of the inositol ring through lipid kinases and phosphatases, respectively on the intracellular membranes. Based on the number of phosphorylation at the 3, 4, and 5 positions of inositol ring, seven PIPs have been detected in cells (Dickson & Hille, 2019). PIs are differentially enriched on diverse intracellular membrane compartments (Fig. 1.7), where they are involved in spatio-temporal regulation of membrane trafficking events. While the PI(4,5)P₂ is mostly localized on the inner leaflet of the plasma membrane, PI(3)P has been shown to present in SEs (David J. Gillooly et al., 2003; D.J. Gillooly et al., 2000; Marat & Haucke, 2016; Tan et al., 2015). On the other hand, the cellular level of PI(3,5)P₂ is extremely low compared to some other PIPs, and it has a

particular localization on MVB and lysosomes (Behnia & Munro, 2005; Lees et al., 2020). Apart from plasma membrane localization, PI(4,5)P₂ is also present on REs (Shi & Grant, 2013; Tan et al., 2015). PI(4)P is localized on two membrane-bound organelles REs and the Golgi apparatus (Dickson et al., 2014; Jović et al., 2009, p. 15).

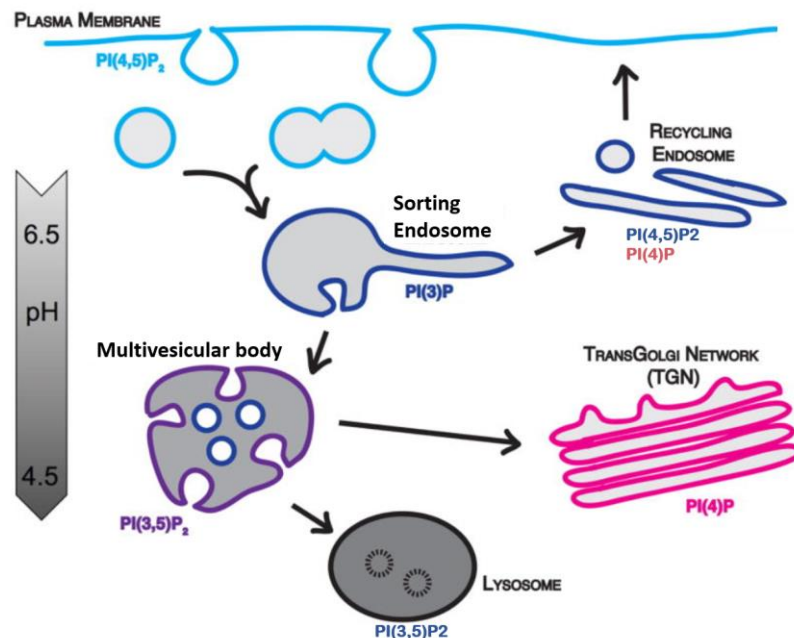


Figure 1.7 : Localization of different PIs on different intracellular membranes. Adapted from Sarah R. Elkin (2016)

PIPs can recruit Rab-GEFs and GAPs on the membrane and thus regulate the Rab activation on endosomal membrane (Novick, 2016). Furthermore, PIP kinases and phosphatases are Rab effectors. For instance, class III PI3-kinase VPS34 is a Rab5 effector that regulates PI(3)P synthesis on SEs. Furthermore, the Rab5 effector proteins EEA1 and Rabenosyn-5 have lipid-binding FYVE domain through which they interact with PI(3)P and are recruited to the early endosomal membrane (Law et al., 2017, p. 34; Law & Rocheleau, 2017, p. 34; Mayinger, 2012). Therefore, Rab-GTPases and PIPs co-ordinate actions to provide a mechanism for membrane identity.

1.8 Cargo trafficking to the plasma membrane from SE through recycling process

The cell surface contains different types receptors through which cells respond to extracellular stimuli by binding with corresponding ligands. For maintaining a constant signaling response, the recycling process ensures the correct density and distribution of the pool of available receptors on the cell surface. It is estimated that, cells internalize the equivalent of one to five times their cell surfaces per hour. Cargo follows two different recycling kinetics to get back to the PM from SE.

- Fast recycling process
- Slow recycling process

These processes contribute to recycling 70-80% of the internalized materials to maintain proper plasma membrane composition (Grant & Donaldson, 2009). The balance between endocytic uptake and recycling regulates various cellular processes, including cell adhesion, migration, polarity, cytokinesis, signal transduction, nutrient uptake, and other cellular activities. Impairment in endocytic recycling leads to the development of various diseases, such as ciliopathies, cancer, different neurological disorders, and Down syndromes (Grant & Donaldson, 2009; Maxfield & McGraw, 2004). In the following part, I will describe underlying mechanisms of fast and slow endocytic recycling processes.

1.8.1 Fast recycling route

Some molecules return to the cell surface through the fast recycling route ($t_{1/2}=1-5$ min). This rapid recycling process can happen directly from SEs, or earlier stages of SEs (Caspar T. H. Jonker et al., 2020; Lakadamyali et al., 2006; Mahmutefendić et al., 2018; Stoorvogel et al., 1987, p. 2). A substantial percentage of cargoes like TfnR or lipid analogues are readily available on the cell surface within 2 minutes or less after internalization (Mahmutefendić et al., 2018; Hao & Maxfield, 2000; Dunn et al., 1989). A fast recycling process regulates the direct return of these cargoes to the cell surface, and the rest follow the slow recycling pathway. The availability of tools to measure the rate, kinetics, and efficiency of TfnR recycling make this membrane protein an ideal candidate for endocytic recycling assay.

The dual nature of TfnR to follow fast recycling directly from EEs and a slow process via downstream endosomes provide crucial information about the mechanistic insight of the recycling process. A distinct set of Rab GTPases are associated with divergent recycling routes. Studies show that Rab4 is one of the main regulator of the rapid recycling of cargoes, such as, TfnR and glycosphingolipids (Choudhury et al., 2004). However, the exact role of Rab4 is not well understood. Expression of GDP-locked (dominant-negative) Rab4 depletes the fast recycling pool of TfnR and lipid molecules. Still, a certain pool of these receptors can recycle faster under the SiRNA-mediated knock-down of Rab4. This ambiguity could be due to the blockage of transitioning from rapid to slow recycling pathway (Yudowski et al., 2009). Besides Rab4, Rab35 plays a crucial role in the fast endocytic recycling pathway. In COS-7 cells, depletion of Rab35 blocks rapid recycling of a LDLR family member megalin from sorting endosomes (Chaineau et al., 2013). Similar to that of Rab4, Rab35 also regulates TfnR recycling kinetics (Grant & Donaldson, 2009).

1.8.2 Slow recycling process

In the slow recycling process, tubular recycling carriers generated from the SEs, travel towards the microtubule-organizing center (MTOC) and accumulates with preexisting recycling carriers to form an endocytic recycling compartment (ERC). Cargoes are then transported to the PM from the ERC. This two-step recycling process takes a longer time than that of direct recycling from SE. In most of the cell-types, other than polarized epithelial cell lines, ERCs tend to accumulate at MTOC, and they are mainly associated with microtubules (Grant & Donaldson, 2009). Morphologically, ERC are a collection of narrow tubular-shaped organelles with a diameter of ~60 nm (Figueiredo et al., 2001; Grant & Donaldson, 2009). The development of ERC is a complex and enigmatic process. At the molecular level, ERC is defined by the presence of Rab11, and Eps15 homology domain (EHD) proteins, tubular morphology, and the geometrical location at the pericentriolar region (Maxfield & McGraw, 2004).

Not all recycling tubules have the same lifespan. Some recycling tubules are long-lasting, and some are short-lived (Puthenveedu et al., 2010). Studies showed that TfnR efficiently enters into recycling tubules, which are short-lived (<30 seconds) (Puthenveedu et al., 2010; Sneeggen et al., 2019, p. 2). In contrast, the beta-adrenoreceptor recycles mostly via longer-lived longer-lived recycling tubules (>30 seconds), and their accessibility towards shorter-lived tubules is very poor. Beta-adrenoreceptor-containing tubules are stabilized by actin (Puthenveedu et al., 2010). However, what drives the cargoes to be segregated into different tubules with distinct life spans is not well understood. Recent studies show that many signaling receptors are sorted into tubule in a more guided process instead of passive diffusion into the recycling tubule. Receptors having a particular sorting sequence at their cytosolic surface can follow the regulated pathway of sequence-dependent recycling (Hanyaloglu & von Zastrow, 2008; Puthenveedu et al., 2010).

1.9 Regulators of slow Recycling process

Recycling endosomes are dynamic, and several regulatory proteins are associated with the slow recycling process. Different Rab-GTPases and their effector proteins, Eps15 homology domain proteins (EHD1–4), membrane remodeling proteins, such as sorting nexins, are major players in the regulation of cargo trafficking through slow recycling pathway (Grant & Donaldson, 2009; Pelham, 2002).

1.9.1 Rab11-FIPs

Rab11 forms mutually exclusive complexes with Rab11-FIPs, which appears to be involved in regulating different sorting/transport pathways via recycling endosomes. Structurally, Rab11-FIPs contain Rab11 binding domain (RaBD) at their C-terminus. Homodimerization of RaBD causes formation of two identical interfaces to bind with two Rab11 molecules simultaneously

(Jing & Prekeris, 2009). FIP binding leads to the conformational change of the GTP-bound Rab11, and that might enhance the binding affinity of Rab11 and Rab11-FIPs (Eathiraj et al., 2006). Based on this finding, it has been proposed that Rab11 recruits Rab11-FIPs on the endosomal membrane, and that causes cytoplasmic exposure of large portions of Rab11-FIPs, providing a surface to recruit other interactors involved in the endocytic recycling process. There are five Rab11-FIP proteins in the mammalian system divided into two classes- class I, class II, based on their sequence homology.

A distribution of Rab11-FIPs in endocytic recycling pathway is depicted in the Fig. 1.8. Different Rab11FIPs interact with distinct proteins involved in the endomembrane trafficking and thus regulate distinct membrane trafficking events. Rab11-FIP1, 2, and 5 belong to class I Rab11-FIP as they contain calcium-dependent phospholipid-binding C2 domain near to the N-terminus (Machesky, 2019). Class I Rab11-FIPs regulate membrane tubulation and cargo trafficking to the plasma membrane via ERC. Depletion of class I FIPs impedes Rab11-mediated recycling of numerous cell membrane receptors, such as TfnR, epidermal growth factor receptor (EGFR), chemokine receptors, $\alpha 5\beta 1$ integrins, GLUT4, FAT/36 and the low density lipoprotein receptor (LDLR) (Caswell et al., 2008; Lindsay & McCaffrey, 2002). Furthermore, Rab11-FIP2 regulates tethering and actin-based transport of recycling vesicles through interaction with Rab11 and actin-based motor myo5 (Lindsay & McCaffrey, 2004). Rab11-FIP5, on the other hand, is localized on peripheral endosomes regulating cargo sorting into the ERC-mediated slow recycling process through interaction with kinesin II. In metastatic prostate cancer cells, Rab11-FIP5 regulates the surface expression of the laminin-associated integrins $\alpha 6\beta 1$. In laminin-rich tissues, $\alpha 6\beta 1$ is accumulated in the Rab11 recycling compartment upon Rab11-FIP5 depletion (Das et al., 2018). Moreover, in polarized epithelial Rab11-FIP5 regulates the apical to basolateral trafficking of polymeric immunoglobulin A (pIgA) by changing the distribution of Rab11 positive compartments (Su et al., 2010). In neurons, Rab11-FIP5 regulates the sorting of presynaptic adhesion molecule neurexin from sorting endosome to RE (Ribeiro et al., 2019, p. 1).

Rab11-FIP3 and Rab11-FIP4 belong to class II Rab11-FIP. Functionally Rab11-FIP3 and Rab11-FIP4 are different from class I FIPs as their depletion does not change TfnR recycling kinetics. Instead, Rab11-FIP3 and Rab11-FIP4 play a crucial role in other cellular processes, such as cell division (L. L. Collins et al., 2012, p. 3).

1.9.2 EHD proteins

C. elegans receptor-mediated endocytosis (RME-1) proteins have four human orthologs EHD1-4. These proteins are evolutionary conserved ATPases. Molecular functions of EHDs share some properties with dynamin family proteins, such as low nucleotide binding affinity, in vitro liposome tubulation ability, and formation of ring-like structures around lipid membrane tubules when oligomerized (Melo et al., 2017).

Mammalian EHDs are highly homologous and all of them carry a single Eps15 homology (EH) domain at the C-terminus (Grant & Caplan, 2008). Recent studies suggest that EHDs are recruited to the endosomal membrane through interaction with PIPs. Their recruitment is crucial for the generation of tubular transport carriers. Although EHDs are highly homologous, they regulate distinct phases of endocytic trafficking. While EHD1, EHD3, and EHD4 decorate vesicular/tubular recycling membranes, the localization of EHD2 is at the plasma membrane. EHD2 function is associated with both endo- and exocytosis (Morén et al., 2012; Yang et al., 2018). The distribution of EHDs in subcellular organelles is shown in Fig. 1.8.

EHD1 is the best-characterized protein of the EHD family and has been implicated in vesicle budding and fission. The combination of EHD1's membrane recruitment and ATP hydrolysis functions are crucial for endocytic recycling (Deo et al., 2018). Once EHD1 is recruited to the endosomal membrane it can form membrane scaffolds that bulge membrane tubules in an ATP-dependent manner. Self-assembly of the membrane scaffold forms a ring around the neck of the endosomal membrane upon ATP hydrolysis. The formation of such EHD1 rings on membrane tubes below 25 nm in radius can lead to the membrane scission and formation of recycling tubules. EHD1 interacts with several other proteins to regulate cargo sorting into forming recycling tubules (Deo et al., 2018). A physical connection between EHDs and Rab11 has not been reported yet. It is speculated that EHDs are connected to Rab11 via other proteins. Naava Naslavsky and colleagues demonstrated that class I Rab11 effector Rab11-FIP2 is the direct interacting partner of both EHD1 and EHD3, and that the membrane recruitment of Rab11FIP2 is EHD1 dependent. Functionally, association between Rab11FIP and EHD1 regulate the release of TfnR and MHC1 cargo from the ERC (Cullis et al., 2002; Naslavsky et al., 2006). Over-expression of EHD3 localizes extensively on EHD1 positive tubule-vesicular structures. They regulate, however, two different steps in the endocytic trafficking process. While EHD1 depletion accumulates cargo in the perinuclear ERC, EHD3 deletion aggregates cargo in the early endosome (Grant & Caplan, 2008). On the other hand, EHD4 recruits and interact with EHD1 at the early endosomal membrane (Jones et al., 2020; Sharma et al., 2008, p. 4).

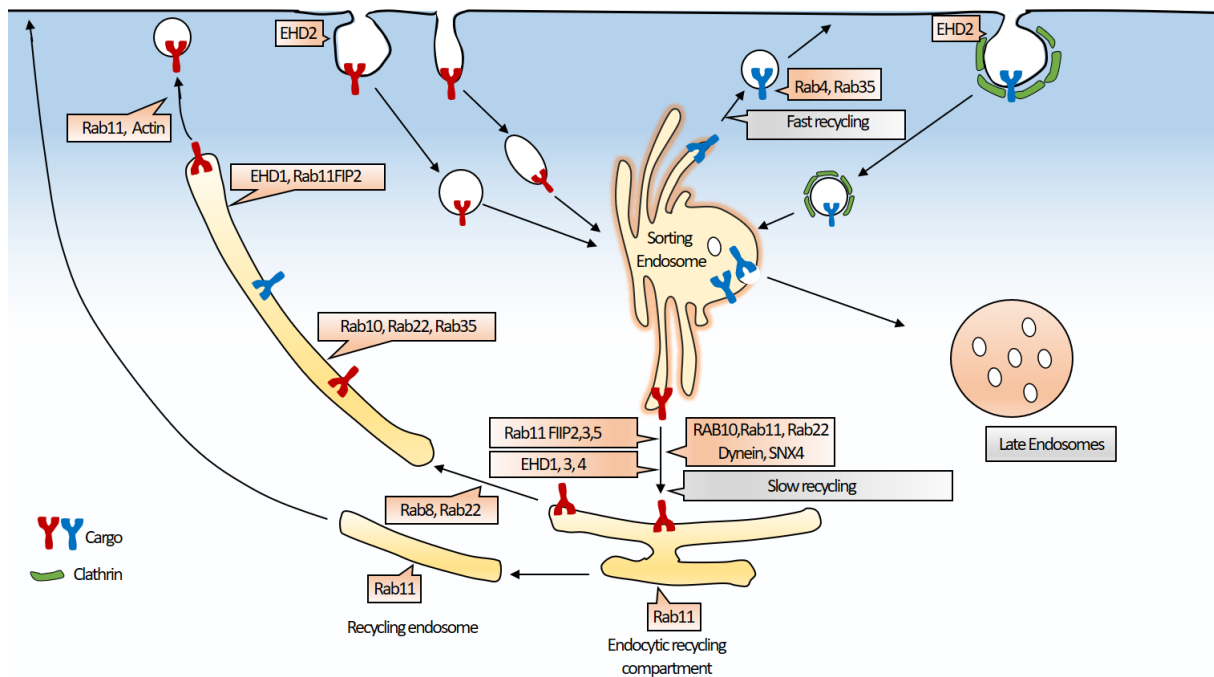


Figure 1.8: Current model of cargo recycling. Early/Sorting endosomes receive cargo from plasma membrane through distinct endocytic processes. Immediately after internalization, some cargoes recycle back to the plasma membrane through Rab4 and Rab35 positive structures. Some cargoes move from sorting endosomes to the endocytic recycling compartment (ERC). This process requires different Rabs, Rab11-FIPs, Dyneins, SNXs and EHDs. From the ERC, recycling of cargoes depends on Rab11. Rab11-FIP2, EHD1, and Rab10, 11, 22 and Rab35 are involved in tubular recycling endosome formation. Adapted from (Grant & Donaldson, 2009)

1.9.3 Rabenosyn-5 and VPS45 in endocytic recycling

Rabenosyn-5 is one of the central regulators of endosomal sorting and recycling, as it is predominantly expressed on specific endosomal subdomains decorated with Rab5 and Rab4 (De Renzis et al., 2002). Rabenosyn-5 is recruited to the membrane in a PI3K-dependent manner, where it acts as a scaffold for multiple protein interactors. Rabenosyn-5 plays a crucial role in endocytosis and recycling of TfnR. After clathrin-mediated endocytosis, TfnR is delivered into Rabenosyn-5 enriched particular endosomal subpopulations. Reduced TfnR uptake couples with rerouting from recycling pathway to lysosomal degradative pathway under Rabenosyn-5 depleted condition (Navaroli et al., 2012). For SE to recycling endosomal trafficking, EHDs potentially interact with many early endosomal proteins. The multivalent Rab GTPase effector and phosphoinositide-binding protein Rabenosyn-5 interacts with EHD1 and sequentially regulates cargo recycling from SEs to the plasma membrane via recycling endosomes (Naslavsky et al., 2004). A recent study showed that Rabenosyn-5 in association with EHD4 recruit EHD1 to sorting endosome and regulate receptor recycling (Jones et al., 2020, p. 15).

Rabenosyn-5 recruits an SM protein VPS45 on Rab5 positive domain of SE through direct interaction. Human VPS45 is primarily associated with receptor recycling and acts downstream of the Rab5 function on the EE (Rahajeng et al., 2010). Similar to the EHD1, association of VPS45 with Rabenosyn-5 is crucial for receptor recycling. Additionally, retrograde transport to TGN is impaired in VPS45 and Rabenosyn-5 depleted condition (Naslavsky et al., 2004; Navaroli et al., 2012). VPS45 is also involved in EE formation and cargo trafficking to the lysosome degradation in *Drosophila melanogaster* and *C. elegans* (Mottola et al., 2010). Furthermore, VPS45 regulates GLUT4 sorting to specialized storage vesicles from recycling compartment (Foley & Klip, 2014; Roccisana et al., 2013).

1.10 Cargo sorting for endocytic recycling from SEs

How cargoes are sorted in the endocytic trafficking process is a deep-rooted question in cell biology. SEs receive internalized cargo for around 10-15 minutes (Maxfield & McGraw, 2004). Afterwards new endocytosed vesicles cannot fuse with SEs. SEs then move along microtubules and become more acidic by acquiring acid hydrolases (Gagescu et al., 2000; Hu et al., 2015; Perret et al., 2005). Lower pH in the endosomal lumen causes conformational change of proteins and allows the dissociation of ligand from the receptors mix with internalized solute molecules (Jovic et al., 2010; Leloup et al., 2017). Dissociation of the receptors from their corresponding ligands is the first step of cargo sorting in SE (Mukherjee et al., 1997). Many cargoes, without having any specific targeting information, are sorted away from the soluble materials of SE directly back to the PM, mostly by bulk membrane flow. This process requires generation and fission of narrow tubules. Tubular part of the SE comprises up to 80% of the endosomal surface area, which helps in effective recycling by accumulating different membrane proteins (Maxfield & McGraw, 2004). The globular domain of the SEs sort cargoes into ILVs, through inward budding of endosomal membrane. ILV formation is regulated by the endosomal sorting complexes required for transport (ESCRT) complexes in association with endosomal maturation. Four ESCRT complexes, ESCRT-0, ESCRT-I, ESCRT-II, and ESCRT-III, take part in cargo sorting into ILVs (Schmidt & Teis, 2012). In this process, soluble molecules, lipids and a subset of membrane proteins reach the matured endosomes without actually departing the endosomal lumen. TGN bound cargoes release their ligands in the late endosomes when the pH is around ~5.5 (e.g., mannose-6-phosphate receptor) (Huotari & Helenius, 2011; Robinson & Neuhaus, 2016). In contrast, some signaling receptors are long-lasting (e.g. the epidermal growth factor receptor), and they can be actively bind their ligands in pH as low as ~4.5 and provide continuous signaling for a longer period of time (Diering & Numata, 2014).

A subset of membrane receptors do not follow the bulk recycling and degradation pathways, and are instead recycled in a regulated manner (Puthenveedu et al., 2010). The discovery of sorting signals on cargoes and the recognition of cargo adaptors and associated coat complexes are now providing mechanistic insight for this highly orchestrated endosomal cargo

recycling process. A detail description of the sequence-based cargo sorting is depicted in the following chapter.

From the SE, sorting of TGN and lysosomal bound cargo has been studied extensively and the underlying mechanisms are mostly known. However, cargo sorting for recycling is an enigmatic process and it requires extensive study. In the next section, I will discuss how the formation of tubulo-vesicular transport carriers are coupled with cargo selection for recycling.

1.11 Formation of transport carrier for recycling

1.11.1 Role of Sorting Nexins (SNXs) and associated complexes in recycling carrier formation and cargo sorting for recycling

Sorting nexin (SNX) proteins are key players of tubule-based sorting from SEs. There are 12 SNX–BAR proteins (SNX1, SNX2, SNX4–SNX9, SNX18, SNX32, and SNX33) in mammalian cells (Fig. 1.9). SNX–BAR family proteins contain two membrane-binding domains: a phox homology (PX) and a BAR (Bin-Amphiphysin-Rvs) domain. The PX domain can interact with PI3P-containing endosomal membrane. Besides PX and BAR domains, there are sub-classes of SNXs that contain PDZ and FERM domains. These types of SNXs leverage their PDZ and FERM domain to interact with cargoes and act as cargo adaptors for recycling, such as SNX17 and SNX27 (Chi et al., 2015; van Weering et al., 2010, p.). Upon dimerization, BAR domains form a crescent-shaped positively charged surface that binds to positively curved membranes through electrostatic interactions. Recruitment of SNX–BAR proteins on high curvature tubular microdomains of endosomes is called coincidence detection as it requires the combined properties of PX and BAR domain (van Weering et al., 2010). SNX–BARs oligomerize on the endosomal membrane, which in turn propels the topological transition of the spherical endosome to a coated, narrow tubule—suggesting that SNX–BARs aid in forming tubular transport carriers from SEs (van Weering, Sessions, et al., 2012).

The SNX-dimer not only regulates the cargo loading and tubule formation for retrograde trafficking but also involved in cargo recycling towards the plasma membrane. SNX–BAR localization studies suggest that around 25% of SNX1 positive tubules overlap with the fast recycling compartment Rab4, and for SNX4, this rises above 35%. Furthermore, 15% of SNX4 tubules overlap with Rab11 positive recycling structures (van Weering, Verkade, et al., 2012; Vazquez-Sanchez et al., 2020). Besides that, there is little co-localization between Rab11 and SNX1 or SNX8 (van Weering, Verkade, et al., 2012). Altogether, SNX–BARs regulate the cargo loading and tubular carrier generation for cargo recycling towards TGN and the plasma membrane.

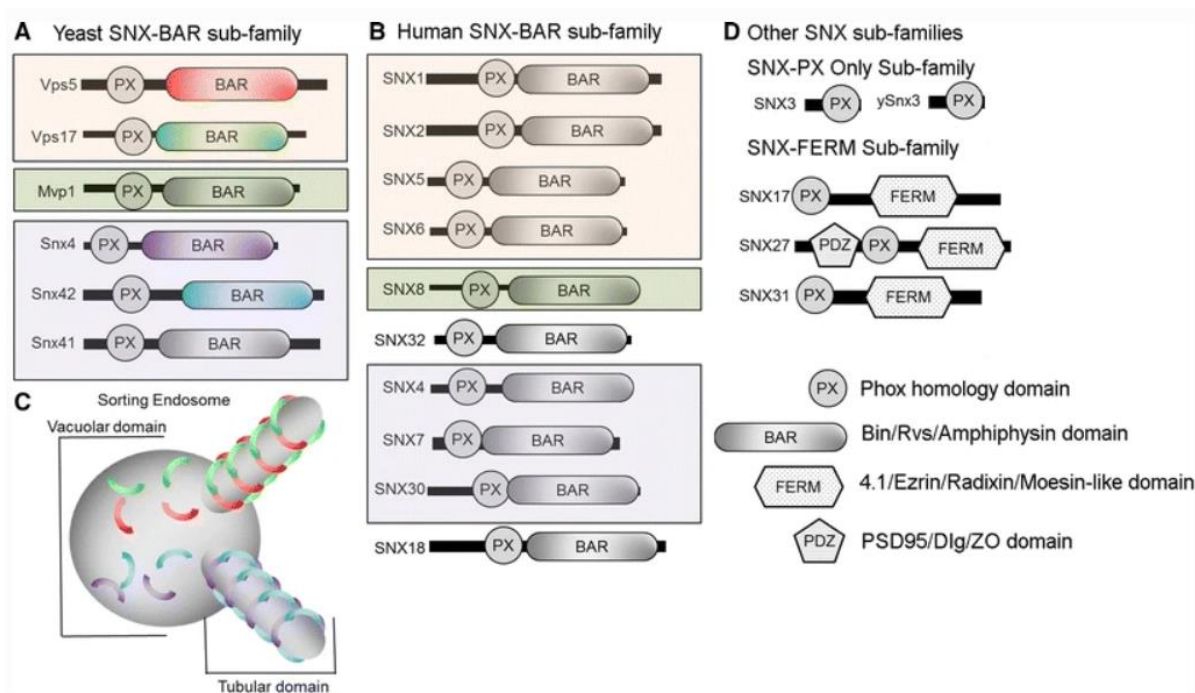


Figure 1.9: Essential characteristics of sorting nexins that regulate export from the SE. The evolutionarily conserved PX domain is common for all sorting nexins. (A, B) Members of the SNX-BAR sub-family of sorting nexins, (A) in yeast and (B) humans contain BAR dimerization domain and oligomerizes on curved surface generating from SE to form transport carriers. (C) Model of endosome-derived tubular transport carrier formation by SNX-BARs. SNX-BAR protomers are recruited to both the globular/vacuolar and tubular parts of the endosome through their PX domain. SNX-BAR protomers oligomerize to coat the endosome-derived tubular transport carrier. (D) Other evolutionarily conserved SNX proteins involved in export from the endosome. Taken from (Chi et al., 2015)

Membrane receptors with a particular sequence for recycling are guided into biochemically distinct specialized endosomal tubules. SNXs are in the center for cargo sorting and recycling transport carrier formation. However, the molecular machinery of cargo delivery to recycling vesicles from SNXs positive compartments has not been studied yet.

Over the last decade, many membrane proteins have been discovered that follow sequence-dependent sorting. The identification of sorting motifs in the cytosolic tails of transmembrane proteins that provide the signature for export and the membrane remodeling complexes that recognize these signatures and drive packaging into recycling transport carriers is central to the understanding of endosomal recycling. Recycling tubule formation, sorting of cargo into the tubules, and stabilization and scission of the newly formed tubules have been reported to be regulated by various protein complexes. For example, different multi-protein complexes such as WASH, Retromer, Retriever, ESCPE, and COMMD/CCDC22/CCDC93 (CCC) are involved in cargo sorting and recycling (Bartuzi et al., 2016; McNally et al., 2017b; Seaman, 2012; Singla et al., 2019).

1.11.2 WASH complex-mediated membrane stabilization and endocytic recycling

Cargo sorting and tubule formation require polymerization and organization of actin filaments on SEs. The Actin-Related Proteins-2/3 (ARP2/3) complex is an actin nucleator. Arp2/3 complex and its activator, Wiskott Aldrich Syndrome protein and SCAR homolog complex (WASH complex), regulate the actin polymerization and the formation of branched actin networks. In mammalian cells, WASH is mostly associated with actin filaments enriched at Rab5 and Rab11-positive endosomal structures. WASH is a pentameric protein complex composed of WASH1 (WASHC1), FAM21A/B/C (WASHC2A/B/C), CCDC53 (WASHC3); strumpellin and WASH interacting protein (SWIP/WASHC4); and strumpellin (WASHC5). This complex, along with associated proteins, generate forces required for membrane budding, tubulation, and scission (Fig. 1.10). WASH complex-mediated localized generation of actin patches on SEs regulates the distribution of recycling and degradative cargoes in discrete sub-domains (Derivery et al., 2009, p. 3; Ryder et al., 2013; F. Wang et al., 2014). This may geometrically separate cargo into either degradative or retrieval sub-domains depending on the identification of ubiquitinated cargo by ESCRT or sequence-based recognition of integral membrane proteins by retrieval machineries. By doing so, the WASH complex regulate endosome-to-Golgi retrieval of CI-MPR and the endosome-to-cell surface recycling of certain cargo proteins, such as the TfnR, the β 2-adrenergic receptor, α 5 β 1 integrin, T cell receptor, glucose transporter GLUT1, and MHC II molecules (Deng et al., 2015). Deletion/depletion of WASH members affects cargo movement from SE as it blocks recycling, retrograde and endolysosomal trafficking pathways. Furthermore, depletion of WASH interactors in HeLa cells destroys the barrier between degradative and retrieval sub-domain, thus leads to the intermixing of the cargoes destined for either lysosomal degradation or recycling (Helfer et al., 2013; Lee et al., 2016). These results suggest that the development and maintenance of endosomal sub-domains depend on localized actin polymerization on the endosome.

1.11.3 Retromer –mediated cargo recycling towards TGN

Our knowledge of SNX-BARs in cargo sorting and tubule generation mainly comes from studies associated with endosome to TGN transport (retrograde trafficking shown in Fig. 1.10). Retromer, an evolutionary conserved multi-protein complex, regulates retrograde trafficking. The mammalian retromer comprises two main sub-complexes: a cargo selective trimeric sub-complex composed of vacuolar protein sorting-associated protein 26 (VPS26)-VPS29-VPS35 and a membrane associated SNX-BAR dimer (SNX1/5 or SNX2/6). Retromer regulates the retrieval and trafficking of cation-independent mannose 6-phosphate receptor (CI-MPR) from the endosome and thus prevents the degradation of CI-MPR in the lysosome. CI-MPR shuttles between TGN and endosome and on its way to the endosome, it carries lysosomal hydrolases. With the help of retromer, CI-MPR returns back to TGN for another round of cargo (hydrolases) trafficking (Seaman, 2012; Simonetti et al., 2019; Wassmer et al., 2009). Retromer is recruited to the endosome via interaction with GTP-bound Rab7. The cargo selective

trimeric sub-complex, Vps26/29/35, specially binds to GTP-bound Rab7 (Liu et al., 2012; Rojas et al., 2008).

1.11.4 Retromer –mediated cargo recycling towards PM

As shown in Fig. 1.10, the distinctive association of retromer with different SNXs at the endosomal membrane develops heterogeneity in cargo recycling. Interaction of Retromer with SNX3 regulates retrograde trafficking of Wntless/Evi (McGough et al., 2018). When associates with SNX27 and WASH complex, retromer regulates the recycling of metal and glucose ion transporters towards the plasma membrane. β 2AR follows Rab4 decorated fast recycling pathway, and this process depends on the interaction of retromer with SNX27 (Temkin et al., 2011, p. 27). There are still some facets in this model as it cannot describe the tubules generated by the coordinated function of retromer and SNXs directly transport the cargo to the PM or Rab4/Rab11 containing vesicles uptake cargo from these tubular transport carriers.

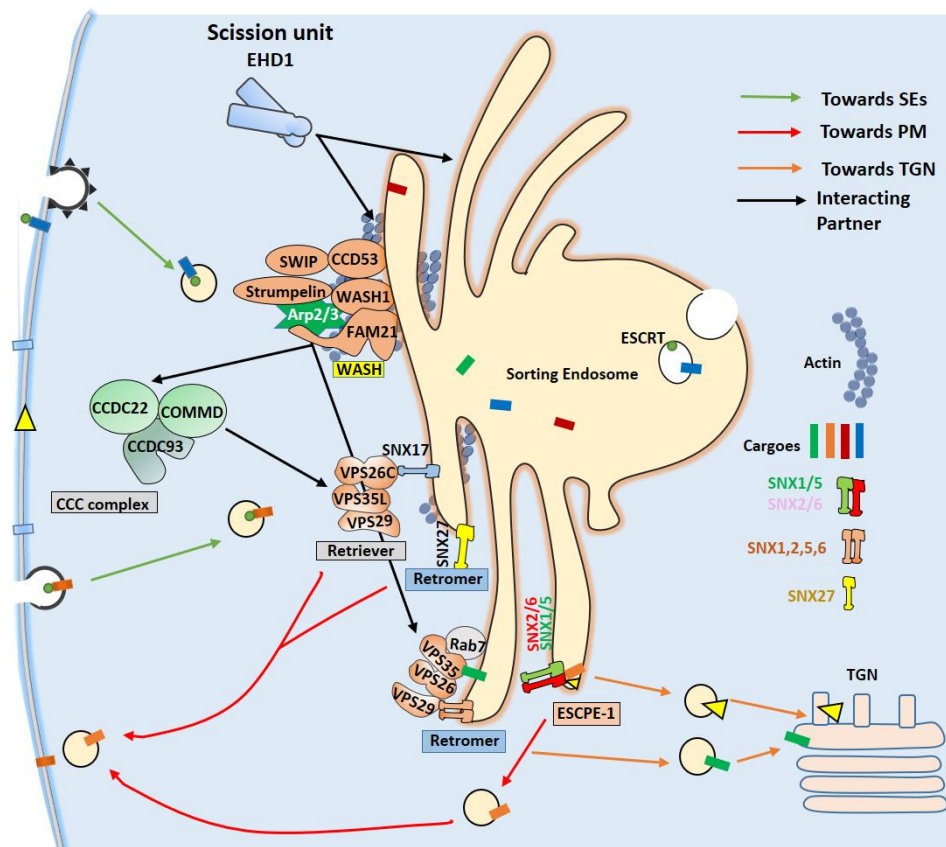


Figure 1.10: Newly formed tubules are stabilized by polymerized actin through WASH complex. Different protein complexes (Retriever, Retromer with SNX27, ESCPE-1 and CCC complex) regulate cargo sorting on specific domain for recycling towards plasma membrane. EHD1 acts as scission unit and regulates pinching off of newly formed tubules from SEs. While the colored arrows showing direction of vesicular transport, black arrow is showing interaction between proteins of different complexes. Adapted from (Naslavsky & Caplan, 2018).

1.11.5 ESCPE-1-mediated cargo sorting for recycling

Recently, a multi-protein complex, endosomal SNX–BAR sorting complex for promoting exit-1' (ESCPE-1), has been described by the group of Peter J. Cullen, which is in the cross-road of cargo sorting for TGN and plasma membrane recycling (Fig. 1.10). Their study suggests that SNX1/SNX2–SNX5/SNX6 form an endosome-associated coat complex that couples sequence-dependent cargo recognition with SNX-BAR mediated membrane remodeling to develop recycling and retrograde cargo-enriched tubulo-vesicular transport carriers. This study shows that SNX-BARs itself- independent of retromer- are sufficient to promote tubular recycling carrier formation and cargo sorting into these tubules through recognizing $\Phi\chi\Omega\chi\Phi$ consensus motif (Evans et al., 2020; Simonetti et al., 2019). Again, cargo sorting and tubule formation machinery can be described with this model but the downstream mechanism for recycling towards plasma membrane requires further study.

1.13.6 Retriever complex-mediated cargo sorting for recycling

Retriever, a multi-protein complex similar to that of Retromer, together with FERM domain-containing adaptor protein SNX17, regulates the recycling of ~120 plasma membrane proteins, including solute transporters, signaling receptors, and integrins. Retriever is a heterotrimeric complex comprised of VPS29, DSCR3, and C16orf62/VPS35L (Fig. 1.10). Endosomal recruitment of the retriever requires interaction with the CCC and the WASH complexes. Retriever localizes to endosomes to drive the retrieval and recycling of NPxY/NxxY-motif-containing cargo proteins, such as β 1 integrin, EGFR, LDLR, and LRP1, by coupling to SNX17 (and SNX31), a cargo adaptor essential for the homeostatic maintenance of numerous cell surface proteins associated with processes that include cell migration, cell adhesion, nutrient supply, and cell signaling. Low-density lipoprotein (LDL) receptor is sorted into the recycling compartment through interaction with FERM domain of SNX17 present on endosomal surface (McNally et al., 2017b, 2017a).

1.11.7 CCC complex-mediated cargo sorting for recycling

COMMD/CCDC22/CCDC93 (CCC) complex is closely associated with retriever as they share a common sub-unit VPS35L/C16orf62 (Fig. 1.10). On SEs, the CCC complex co-localizes with retromer, retriever, and the WASH complex, and participate in the recycling of various cargoes, such as ATP7A, LDLR, and Notch2 to the plasma membrane (Bartuzi et al., 2016). The CCC complex regulates PI(3)P turnover on endosomal membrane through recruitment of phosphatase MTMR2. In the absence of the CCC complex, PI(3)P level is elevated on endosomal membranes, which in turn causes aberrant recruitment of the WASH complex. Mechanistically, higher level of WASH complex on SE causes excessive production of F-actin, and leads to the entrapment of internalized receptors inside the endosomal compartment (Bartuzi et al., 2016; Phillips-Krawczak et al., 2015, p. 1; Singla et al., 2019).

All these proteins and protein complexes are involved in tubular recycling compartment formation and organization of the cargoes for recycling. However, these complexes cannot explain how Rab11 positive vesicle uptake cargo from tubular recycling compartment. Furthermore, there must be connection between fast/slow endocytic recycling regulators and the protein complexes involved in recycling compartment formation.

1.12 Tethering complex-mediated endocytic recycling

Two broad classes of tethering molecules are evolutionarily conserved in higher eukaryotes. Long putative coiled-coil tethers and multi-subunit tethering complexes (MTCs). They are involved in both endocytic and secretory membrane trafficking events. However, only a few of them have been reported to involve in endocytic recycling (Schindler et al., 2015).

1.12.1 Coiled-coil tethers

Coiled-coil tethers are mostly peripheral membrane proteins with a significant association with the Golgi. Large coiled-coil tethers are attached to a membrane at one end that allows them to look for passing vesicles at their surroundings and finally bind to them. A coiled-coil tether has two globular heads connected by long homodimeric coiled-coil domains lengths up to several times the diameter of a vesicle. Given their hydrophilic nature and immense length, coiled-coil tethers are capable of capturing vesicles over long distance of more than 200 nm (Bröcker et al., 2010). Coiled-coil tether can bind to membranes in three ways: through an adaptor protein like Arf GTPases, directly through the carboxy-terminal transmembrane domain or through direct interaction with specific lipids (Gillingham, 2017; Gillingham & Munro, 2003). The intracellular distribution of the coiled-coil tethers is depicted in Fig. 1.11.

A family of around 20 Golgi-associated coiled-coil tethers, called golgins, have been involved in the transport and tethering of coat protein complex I (COPI) vesicles to different Golgi cisterna (Chia & Gleeson, 2014; Witkos & Lowe, 2015). Early embryonic antigen 1 (EEA1) is a well-characterized early endosomal coiled-coil tether involved in the tethering of Rab5-positive and PI3P-containing membranes tethering. EEA1 interacts with GTP-bound Rab5 through zinc-finger motif present on N-terminus and recognizes PI(3)P containing endosomal membrane through FYVE domain present on C-terminus (Mills et al., 2001). Rabenosyn-5 is another early endosomal coiled-coil tether, which has been reported to be a master regulator of cargo recycling (Mottola et al., 2010; Naslavsky et al., 2004; Navaroli et al., 2012). However, whether the tethering function of Rabenosyn-5 is independent of its role in recycling remains unknown.

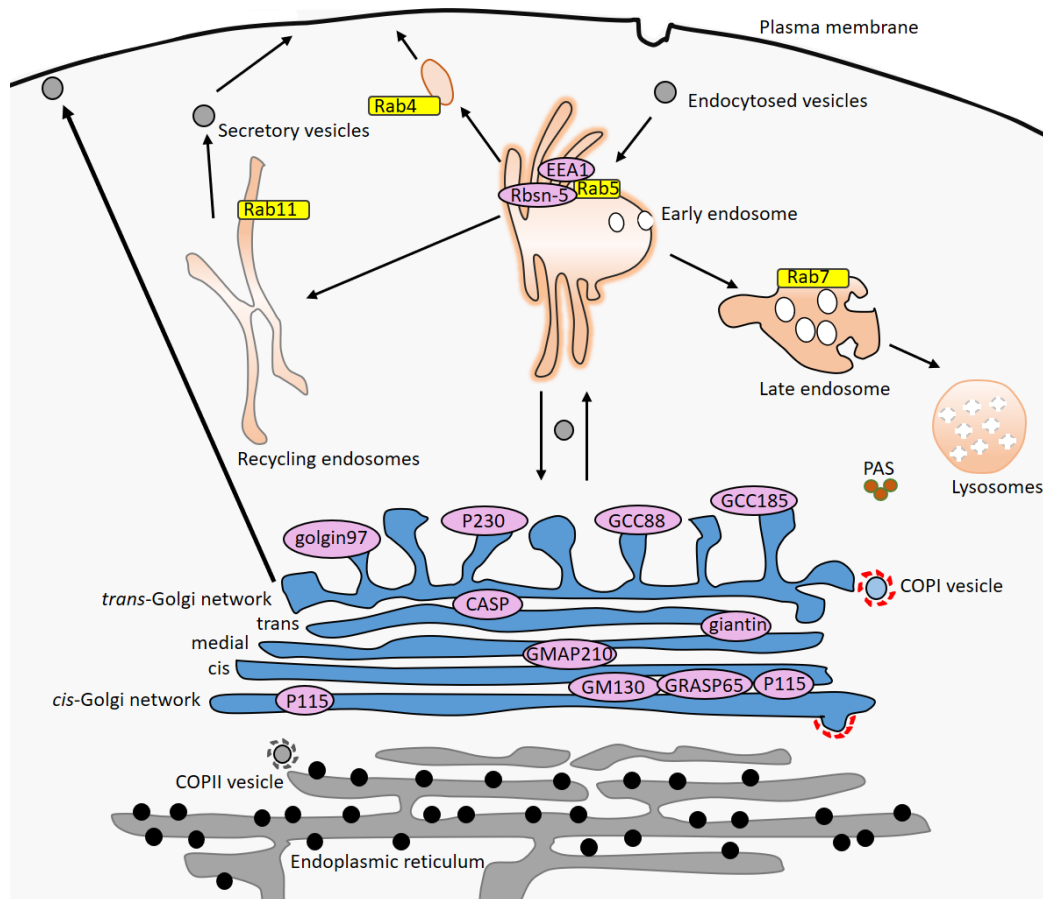


Figure 1.11: Intracellular localization of coiled-coil tethers. Taken from (Chia & Gleeson, 2014)

1.12.2 Multi-subunit tethering complexes

MTCs are the second group of tethers with two to ten sub-units, and the size of the individual subunit can vary from 50 to 140 kDa. MTCs are composed of divergent family of proteins with diverse functions in comparison to the coiled-coil tether (Bröcker et al., 2010). Although MTCs contain up to 10 sub-units, they probably span distances only within the 30 nm range, while coiled-coil tethers can reach beyond 200 nm. However, a 30 nm range should be enough to capture a passing vesicle. The primary function of MTCs is twofold: Firstly, membrane recognition via Rab GTPases and secondly, regulation of SNARE-mediated membrane fusion (Solinger & Spang, 2013). Thus, MTCs are multipurpose protein complexes. GTP-bound Rab preferentially binds with effector subunit present on MTCs and presents a specific membrane compartment to the MTCs (Bröcker et al., 2010).

In the mammalian cells, 10 MTCs have been discovered until now. Which are COG, Exocyst, Dsl1, GARP, EARP, TRAPPI, TRAPP II, TRAP III, CORVET, HOPS and CHEVI (Bröcker et al., 2010; Schindler et al., 2015). MTCs are localized various intracellular organelles and the PM are shown Fig. 1.12. COG, exocyst, Dsl1, and GARP are involved in membrane fusion with organelles of the secretory pathway (Bröcker et al., 2010). CORVET and HOPS are two MTCs

that regulate membrane fusion with organelles of the endosomal pathway (Solinger & Spang, 2013). TRAPPs are multi-protein tether having GEF property towards Rabs and combines coat recognition with tethering. Most recently, TRAPP has been found in the regulation of endocytic recycling by facilitating the actions of Rab11 at the RE (X. Wang et al., 2020). EARP is another MTC, which has a known role in endocytic recycling. While GARP is regulating endosome-derived vesicle tethering on TGN, EARP is localized on RE. GARP and EARP both contain three common subunits- VPS51, VPS52, VPS53, and 4th subunit for GARP is VPS54, which is replaced by syndetin in EARP (Schindler et al., 2015). The presence of syndetin in place of EARP leads to the differential localization of the complex from Golgi to REs, respectively (Schindler et al., 2015). However, from this study it is not clear how vesicle tethering is regulated by EARP at the recycling compartments.

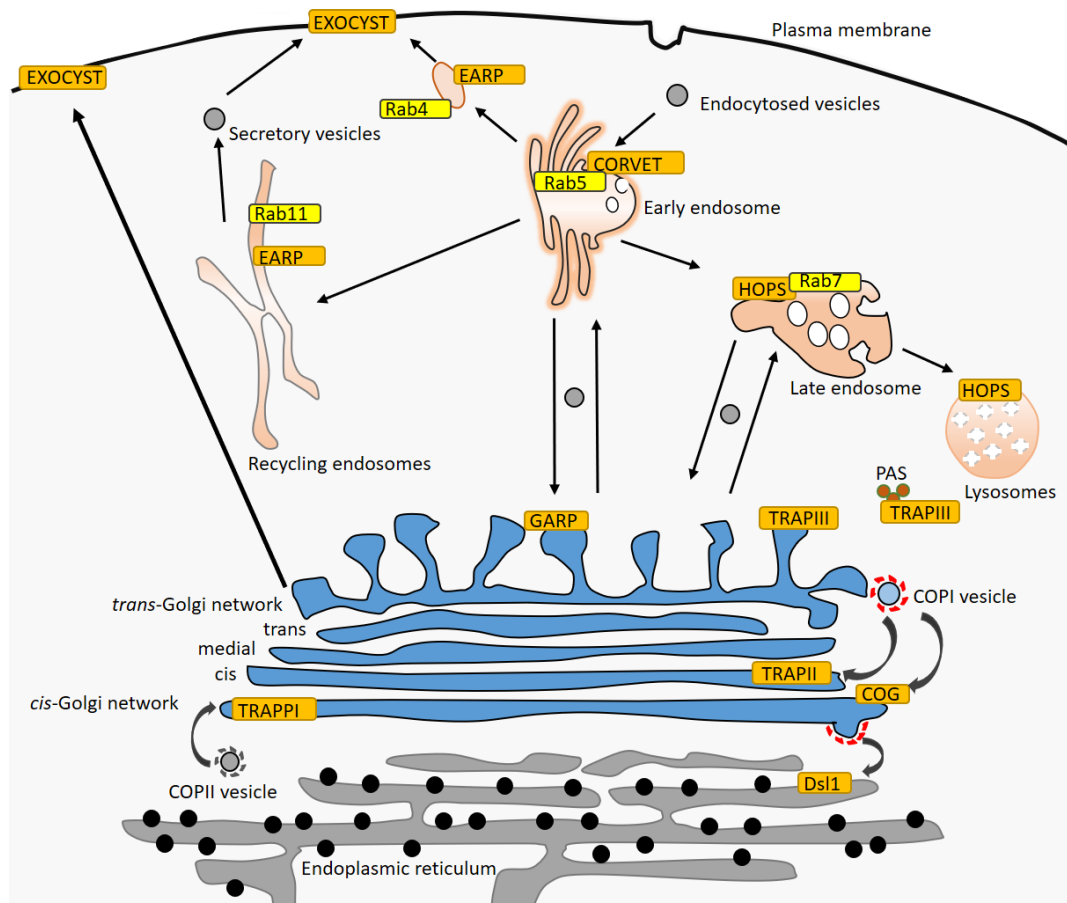


Figure 1.12: This figure is showing the Multi-subunit tethering complexes and their localization. While CORVET regulates early endosomal fusion, HOPS is involved in fusing the late endosomes with lysosomes. EARP regulates Rab4 and Rab11 mediated recycling from sorting endosomes. GARP is localized on TGN and regulates fusion vesicles derived from sorting endosomes. TRAPPI, II, and III are localized on cis, median, and trans-Golgi networks, respectively. TRAPIII is also present on pre-autophagosomal structure (PAS) and regulates autophagosome formation. Dsl1 is the only ER-resident MTC that regulates the tethering of vesicles from the cis-Golgi network. Adapted from (Chia & Gleeson, 2014).

CORVET and HOPS are two heterohexameric tethering complexes involved in early and late endosomal fusion through interaction with Rab5 and Rab7, respectively. These two MTCs share four subunits (VPS11, VPS16, VPS18, and VPS33), called class C vacuolar protein sorting (VPS) proteins, and differ from each other by their Rab interacting proteins present on opposite ends of each complex. A speculated diagram of membrane-bound HOPS and CORVET tethering complexes is depicted in the Fig 1.13. VPS3 and VPS8 are two subunits of CORVET, which can interact with Rab5 (Solinger & Spang, 2013). This particular interaction of CORVET with Rab5 specifies its connection to early endosomal membrane tethering. On the other hand, HOPS possesses VPS39 and VPS41 instead of VPS3 and VPS8, respectively. VPS39 and VPS41 are the binding partners of Rab7 and thus regulate late endosomal membrane fusion (Bröcker et al., 2010; Solinger & Spang, 2013).

In HeLa cells, Rab5 binding subunits of CORVET, Vps3 and Vps8 (also known as Vps3/TGFBRAP1 and Vps8/TRAP1), have been shown to localize on Rab4 positive recycling vesicles and regulates endocytic recycling of β integrin. Furthermore, Vps3 and Vps8 co-localize with on Rab11 positive recycling compartments. However, endocytic recycling function of Vps3 and Vps8 is independent of CORVET as other members do not localize on recycling compartments (C. T. H. Jonker et al., 2018, p. 8). The mechanisms of cargo recycling from recycling compartment is still far from being elucidated at the molecular level. To develop a mechanistic model for this process, we need to understand the molecular aspect of cargo recycling.

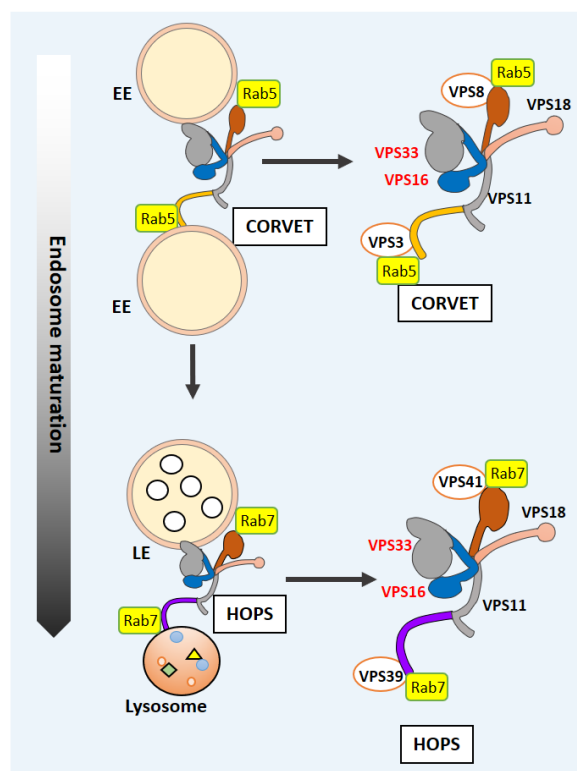


Figure 1.13: Speculated diagram of CORVET and HOPS complex regulating membrane fusion. CORVET is recruited on the membrane through interaction with GTP bound Rab5 present on EEs. VPS3 and VPS8 interacts with Rab5 on opposite membranes, which in turn, leads to the fusion of Rab5 positive compartments. Late endosomes acquire Rab7 and recruit HOPS tethering complex. VPS39 and VPS41

present on two opposite sides of HOPS and connect two Rab7 containing organelles. Adapted from (Balderhaar & Ungermann, 2013; Beek et al., 2019).

2. Open questions and aim of this thesis

In spite of all the knowledge gained in recent years there is still a profound lack of mechanistic insight in endosomal trafficking. Below, I will outline some major questions that need to be addressed.

2.1 Open questions

HOPS and CORVET complexes can interconvert by dynamic changes of a Rab binding subunit, leading to the formation of two intermediate complexes in yeast (Peplowska et al., 2007). Furthermore, deletion of Rab interacting proteins of HOPS complex demonstrated a weaker phenotype than class C components ("Organelle Assembly in Yeast," 1988). Therefore, SM proteins and the core complex might regulate additional cellular functions. In Metazoan, two genes encoding orthologs of yeast Vps33, VPS33A and VPS33B. In *C. elegans*, HOPS and CORVET, each contains individual SM proteins VPS-33.1 (VPS33A) and VPS-33.2 (VPS33B), respectively. Under certain conditions, VPS-33.1 can be exchanged with VPS-33.2 in *C. elegans* (Solinger & Spang, 2014).

Blood platelet studies suggest that alpha granule biogenesis is impaired due to a missense mutation in mouse VPS33A (Gissen et al., 2005; Xie et al., 2009). A mutation in human VPS33B causes a platelet-associated disease called arthrogryposis-renal dysfunction-cholestasis syndrome (Bull et al., 2006), suggesting that, both of the VPS33A and VPS33B are required for platelet formation. VPS33A regulates in dense granule biogenesis process while VPS33B is involved in α -granule biogenesis of platelet development (Urban et al., 2012), indicating that, VPS33A and VPS33B guide two different vesicular events. Thus, it can be speculated that VPS33 homologs are part of two different tethering complexes.

Surprisingly, current data suggest that VPS33A is the sole SM protein for both HOPS and CORVET (Perini et al., 2014; Solinger & Spang, 2014; Wartosch et al., 2015). Interaction between VPS33A and VPS16 is essential for endosome and lysosomal fusion whereas siRNA depletion of VPS33B does not have any impact on endo-lysosomal fusion. Furthermore, in mammalian cells, neither HOPS nor CORVET is physically associated with VPS33B (Urban et al., 2012). This further highlights the intricacy of tethering complexes in higher eukaryotes and raises a question about the potential role of VPS33B in mammalian system. Similar to that of VPS33, VPS16 has two homologs, Vps16 and VIPAR/VIPAS39/SPE-39/fob/Vps16B, in metazoans (Spang, 2016). While VPS16 is part of both HOPS and CORVET, recent studies, however, suggest that VIPAS39 is neither a part of HOPS nor CORVET; instead, it is associated with SM protein VPS33B (Wartosch et al., 2015, p. 33). It is speculated that VIPAS39-VPS33B

interaction might serve as a core component for another HOPS and CORVET like tethering complex called CHEVI (class C Homologs in Endosome-Vesicle Interaction) (Spang, 2016) (Fig. 2.1). Functional role for CHEVI in mammalian cells has already been established. The CHEVI complex has been shown to interact with Rab11A and regulates apical-basolateral polarity in the liver and kidney (Cullinane et al., 2010). Furthermore, CHEVI plays vital role in platelet formation (Urban et al., 2012).

In a complex endocytic membrane trafficking system, SEs receive cargoes from different sources, such as PM and TGN, and the presence of HOPS and CORVET are not sufficient to explain the complex trafficking at the SE. Inevitably that raises a question-

Whether there are other tethering complexes in the endocytic trafficking system?

The third endosomal SM protein VPS45 interacts with multiple SNAREs and thus regulates membrane fusion (Cowles et al., 1994; Dulubova et al., 2002, p. 2; Shanks et al., 2012, p. 1). Unlike HOPS and CORVET, SM proteins are not intrinsic part of most MTCs (Spang, 2016). Therefore, there is a possibility that VPS45 might be a part of tethering complex. Moreover, SM proteins have non-SNARE interacting partners (Spang, 2016). For example, VPS45 has been suggested to interact with Rabenosyn-5 at the SE. This interaction plays vital role in cargo recycling towards plasma membrane (Rahajeng et al., 2010). Rabenosyn-5 connects VPS45 to Rab5 containing endosomal membrane and thus suggests a CORVET and HOPS-like multi subunit-tethering platform with minimal components to connect membranes and proofread SNAREs for membrane fusion (Spang, 2016). The function of VPS45 and Rabenosyn-5 on EEs implicates this speculated multi-subunit tether in the regulation of cargo trafficking from sorting endosome to recycling pathway.

Based on the target sequence, cargoes are sorted in an appropriate sub-compartment, which would require discrete types of machinery for the development of transport vesicles and traffic to the corresponding destinations. Especially cargo recycling from sorting endosomes is quite a robust process with multiple recycling routes to the plasma membrane and the TGN. While Rab4 and Rab11 mediate recycling to the plasma membrane, Rab9 and Rab10 regulate recycling to the TGN (Chua & Tang, 2018; Wandinger-Ness & Zerial, 2014). Furthermore, Rab8a is distributed into tubular and vesicular REs and regulates transferrin recycling towards plasma membrane (Hattula et al., 2006). Since within an hour, cells internalize one to five times of their cell surfaces, PM-bound recycling pathways must be robust and coordinately regulated. The robustness of the endocytic recycling system suggests a possible existence of machineries that regulate cargo recycling through different vesicles in a coordinated way. Different tethering platform might regulate the tethering of various Rab-containing vesicles on the busy crossroad of sorting endosomes.

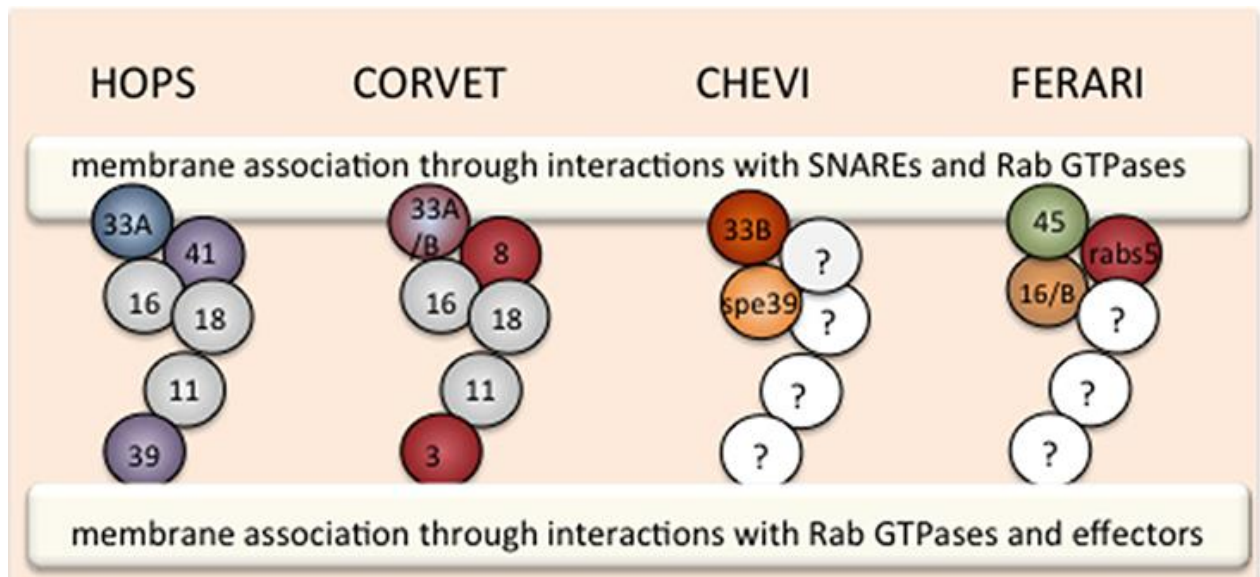


Figure 2.1: This model showing speculated model of two tethering platforms, CHEVI and FERARI, which are similar to HOPS and CORVET. Taken from (Spang, 2016)

2.2 The aim of the thesis

The aim is to identify and characterize a novel tethering complex in mammalian cells.

Work from our lab in *C. elegans* indicated the presence of a novel tethering platform, FERARI, at the SE. Main focus of this thesis is establish whether this tethering platform is conserved in mammalian system, elucidate the function and provide mechanistic insight into this tethering platform, and finally investigate the biological significance of FERARI.

3. FERARI is required for Rab11-dependent recycling

The following manuscript is published on *Nature Cell Biology*; Volume 22; February 2020; 213-224.

Statement of contributions: I conducted all the mammalian experiments. Jachen A. Solinger conducted all the experiments in *C. elegans*. Cristina Prescianotto-Baschong conducted the electron microscopy.

Professor Anne Spang wrote and supervised the manuscript. I wrote the figure legends and materials and methods for mammalian part.

FERARI is required for Rab11-dependent endocytic recycling

Jachen A. Solinger^{1,2}, Harun-Or Rashid^{1,2}, Cristina Prescianotto-Baschong¹ and Anne Spang^{1*}

Endosomal transport is essential for cellular organization and compartmentalization and cell-cell communication. Sorting endosomes provide a crossroads for various trafficking pathways and determine recycling, secretion or degradation of proteins. The organization of these processes requires membrane-tethering factors to coordinate Rab GTPase function with membrane fusion. Here, we report a conserved tethering platform that acts in the Rab11 recycling pathways at sorting endosomes, which we name factors for endosome recycling and Rab interactions (FERARI). The Rab-binding module of FERARI consists of Rab11FIP5 and rabenosyn-5/RABS-5, while the SNARE-interacting module comprises VPS45 and VIPAS39. Unexpectedly, the membrane fission protein EHD1 is also a FERARI component. Thus, FERARI appears to combine fusion activity through the SM protein VPS45 with pinching activity through EHD1 on SNX-1-positive endosomal membranes. We propose that coordination of fusion and pinching through a kiss-and-run mechanism drives cargo at endosomes into recycling pathways.

Endocytosis is essential for the communication of the cell with its environment, controlling cell growth and regulating nutritional uptake. About 70–80% of endocytosed material is recycled back from sorting endosomes to the plasma membrane through different pathways. Defects in recycling lead to a myriad of human diseases such as cancer, arthrogryposis–renal dysfunction–cholestasis syndrome, Bardet–Biedl syndrome or Alzheimer's disease^{1–8}. Yet sorting into recycling endosomes and the interaction of recycling with sorting endosomes remain poorly understood.

The identity of recycling endosomes is largely characterized by the presence of a specific Rab GTPase on the limiting membrane of the organelle. For example, Rab4 and Rab11 are present on different types of recycling endosome targeted to the plasma membrane. Rab9 is involved in recycling from the sorting endosome to the *trans*-Golgi network (TGN) and Rab10 has multiple reported roles in recycling from endosomes to the TGN or basal lateral membranes and exocytosis from the TGN^{9,10}. The different recycling pathways also highlight a robustness of the system, in that if one recycling pathway is impaired, alternative routes are still available. Yet it also underscores the difficulty in studying these pathways because of their redundancy.

The number of recycling pathways is reduced in simpler eukaryotes such as *Caenorhabditis elegans*, which lacks Rab9 and Rab4. Yet *C. elegans* maintains complex organ structures such as polarized intestinal epithelia cells, providing an excellent system to analyse recycling processes^{11,12}. In fact, the recycling protein RME-1 was discovered in *C. elegans*¹³. RME-1 and the homologous human epsin-homology domain (EHD) proteins were shown to have tubulation and vesiculation activities^{14–16}. EHD1 interacts with the Rab11 effectors Rab11FIP2 and Rab11FIP5 and is involved in Rab11-dependent recycling from tubular endosomal networks^{17,18}. The formation of these structures requires BAR domain proteins, most prominently sorting nexins (SNXs). Indeed, SNX4 associates with Rab11 recycling endosomes^{19,20}. In addition, EHD1 interacts with rabenosyn-5 to form recycling compartments²¹.

Besides the coordination of recycling pathways, sorting endosomes have to cope with incoming material from the TGN through the biosynthetic route. This cargo has to be sorted into different

domains presumably overlapping with recycling pathways. Fusion of transport containers with endosomes is regulated by tethering factors and SNAREs. CORVET and HOPS multisubunit tethering factors have been demonstrated to act on early and late endosomes, respectively^{22–25}. The yeast HOPS and CORVET complexes differ only in two subunits, which recognize Rab7 (Ypt7 in yeast) and Rab5 (Vps21 in yeast), respectively²⁵. In metazoans, two of the shared HOPS/CORVET components are duplicated. Vps16 has a homologue, VIPAS39 (SPE-39 in *C. elegans*) and the Sec1/Munc18 (SM) protein Vps33 is present as Vps33A (VPS-33.1 in *C. elegans*) and Vps33B (VPS-33.2 in *C. elegans*)²⁴. Moreover, all eukaryotes contain another SM protein, VPS45, with a proposed function in endosomal recycling²⁶.

We had speculated recently that VIPAS39 might be part of two HOPS/CORVET type of complexes, one in conjunction with Vps33B and one with VPS45, which we named class C homologues in endosome-vesicle interaction (CHEVI) and factors for endosome recycling and retromer interaction (FERARI), respectively²⁷. Since the nomenclature of retromer is ambiguous, we replaced 'retromer' by 'Rab' in FERARI. Here, we demonstrate the existence of FERARI in *C. elegans* and mammalian cells. FERARI plays a key role in Rab11-dependent recycling from sorting endosomes to the plasma membrane. We propose a model in which FERARI supports kiss-and-run of Rab11-positive structures on tubular sorting endosomes to aid the formation of recycling endosomes.

Results

FERARI is a conserved tether. We have recently postulated the existence of a tethering complex containing VIPAS39/SPE-39 and the SM protein VPS-45, which we named FERARI²⁷. To probe its existence, we coexpressed *C. elegans* GST-tagged SPE-39 and His-VPS-45 in *Escherichia coli*. His-VPS-45 co-purified with SPE-39–GST (Fig. 1a and Extended Data Fig. 3d). VPS-33.2, which together with SPE-39 is part of the CHEVI complex^{27,28}, served as a positive control, while the HOPS-specific VPS-33.1 did not bind SPE-39. These data indicate direct binding of SPE-39 to VPS-45. This interaction was confirmed by yeast-two-hybrid (Y2H) and pulldown experiments (Fig. 1b, Extended Data Fig. 2d,d' and Supplementary

¹Biozentrum, University of Basel, Basel, Switzerland. ²These authors contributed equally: Jachen A. Solinger, Harun-Or Rashid. *e-mail: anne.spang@unibas.ch

Table 3). Moreover, FERARI is conserved in mammalian cells (Fig. 1c). VPS45 has been shown to directly interact with rabenosyn-5^{29,30}. Similar to VPS45, rabenosyn-5 interacted with VIPAS39 (Fig. 1b–e and Extended Data Figs. 1b,b' and 2b,b',d,d').

On the basis of HOPS and CORVET, we speculated that FERARI might contain more subunits (Extended Data Fig. 1a). To identify additional components, we incubated the bacterially expressed SPE-39/VPS-45 complex with worm lysate and performed mass spectrometry (Supplementary Table 1), followed by Y2H assays and pulldowns from selected, streamlined candidates. We discovered two additional components of FERARI: the EHD-containing protein RME-1 and UNC-44 (Fig. 1f and Supplementary Table 3).

UNC-44 contains ankyrin motifs and a death domain. SPE-39 interacted well with RME-1 and the ankyrin motifs of UNC-44 (Fig. 1f, Supplementary Table 3 and Extended Data Figs. 1c,c',d,d' and 2a,a'). RME-1 is homologous to mammalian EHD1–4, and UNC-44 to ANK1–3. Since EHD1 has been shown to act at endosomes and EHD2 at the plasma membrane^{31,32}, we focused on EHD1. EHD1 co-precipitated and co-localized with rabenosyn-5 (Fig. 1h and Extended Data Fig. 4a,b). Much less is known about ANK1–3. However, ANK3 appears to be the ANK protein most highly expressed in HeLa cells (Extended Data Fig. 4d). ANK3 co-precipitated with endogenous VIPAS39 (Fig. 1g). Finally, endogenous VIPAS39 was pulled down with all other FERARI members (Figs. 1d,g and 3f). FERARI members also have other cellular functions, and the deletion of one component did not affect the stability of any other (Extended Data Fig. 5a,b). Our experiments revealed the existence of a conserved FERARI tether with a proposed interaction network (Fig. 1i), based on our own data (see also below) and on literature^{17,18,21,29,30}. For clarity, we will use the mammalian nomenclature in the text when referring to FERARI subunits (Fig. 1j).

Loss of FERARI affects endosomal recycling. VPS45, rabenosyn-5 and EHD1 have been implicated in recycling from sorting endosomes in mammalian cells^{30,32}. To test whether FERARI might be involved in recycling, we observed GFP-Rab11 in VIPAS39, VPS45, rabenosyn-5 and ANK3 knockout HeLa cells (Fig. 2a and Extended Data Fig. 4c). In FERARI knockout (KO) cells, Rab11-positive structures were enlarged when compared to those of control cells (Fig. 2a,b). These phenotypes were confirmed by immuno-electron microscopy (Extended Data Fig. 6).

To further test whether FERARI plays a role in Rab11-dependent recycling to the plasma membrane, we determined the recycling capacity of transferrin (Tfn). Tfn was transported less efficiently to the plasma membrane in FERARI KO cells (Fig. 2c,d). We would not expect a full block because Tfn recycling also occurs through the Rab4-dependent pathway.

The *C. elegans* intestine is an epithelium in which a pair of juxtaposed cells form a tube, the apical gut lumen (Fig. 2e). This system provides an excellent system to study membrane traffic in metazoa^{14,23–26}. We used *C. elegans* animals expressing GFP-RAB-11 and RFP-RAB-10, markers for apical and baso-lateral recycling compartments, respectively^{27,38}. In mock-treated animals, RAB-11 was mostly localized at the apical cortex, while RAB-10 was present on more internal structures (Fig. 2e). As in mammalian cells, loss of FERARI caused the enlargement of RAB-11 structures (Fig. 2e and Extended Data Fig. 5c), indicating that FERARI function is conserved. Even though CHEVI and FERARI share VIPAS39, they have distinct functions because knockdown of VPS33B did not affect RAB-11 localization (Extended Data Fig. 7a). Not only apical but also basolateral recycling was perturbed as the tubular part of the RAB-10 compartment was largely extended. Yet the size of the granular RAB-10 structures remained unchanged (Fig. 2e and Extended Data Fig. 5c). Human Tfn receptor (hTfR) has been used to study recycling in the *C. elegans* intestine³⁸. Knockdown of FERARI led to a strong reduction of the hTfR signal in the gut, suggesting that it less efficiently sorted into recycling endosomes and degraded in the lysosome (Extended Data Fig. 7b). In contrast, VPS33B(RNAi) caused hTfR to be trapped in a network-like internal structure (Extended Data Fig. 7b). We conclude that FERARI plays a role in both apical and baso-lateral recycling. Moreover, CHEVI and FERARI perform distinct functions.

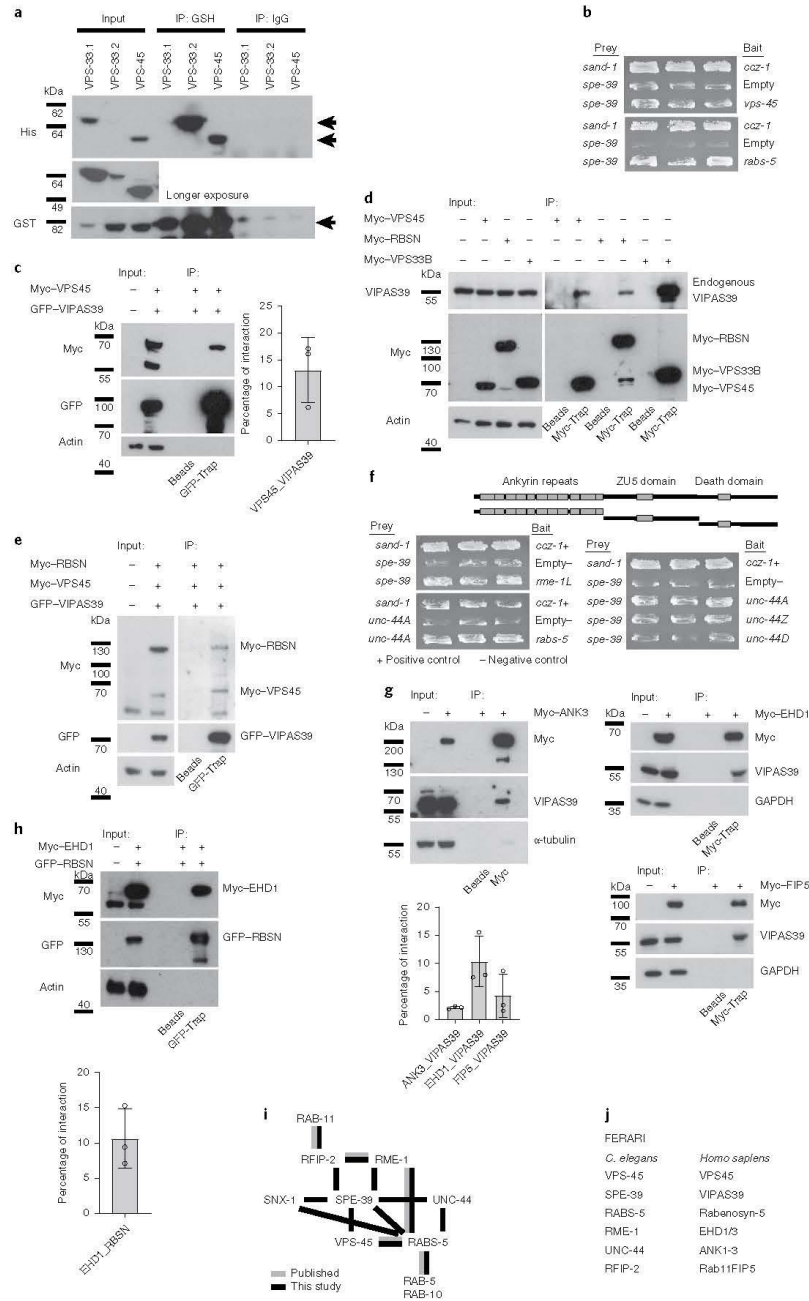
In *C. elegans* oocytes, yolk is taken up by maturing oocytes via receptor-mediated endocytosis employing the yolk receptor RME-2. FERARI(RNAi) reduced the level of yolk in oocytes (Extended Data Fig. 7c) because of impaired RME-2 recycling (Extended Data Fig. 7d). Thus, our data indicate that FERARI is involved in recycling to the plasma membrane in mammalian cells and in different *C. elegans* tissues.

Rab11FIP5 is part of FERARI and provides the link to Rab11. We observed a strong defect following loss of FERARI function on Rab11 recycling compartments. None of the FERARI components has been shown to directly bind Rab11. However, EHD1 was shown to bind the Rab11 effectors Rab11FIP2 and Rab11FIP5 in mammalian cells¹⁸. Rab11FIP5, but not Rab11FIP2, co-precipitated with GFP-rabenosyn-5 (Fig. 3a and Extended Data Fig. 3b,b',e), indicating that Rab11FIP5 is the link between Rab11 and FERARI. We also confirmed that Rab11FIP5 indeed bound to Rab11 (Fig. 3b and Extended Data Fig. 3f). To corroborate our findings, we co-expressed VIPAS39 and RAB11 with or without Rab11FIP5 (Fig. 3c). While VIPAS39 was barely detected in a RAB11–GFP pulldown, this interaction was substantially stronger in the presence of Rab11FIP5, suggesting that Rab11FIP5 could bridge the interaction between

Fig. 1 | Conserved interactions between FERARI components. **a**, Recombinant SPE-39 protein from *E. coli* interacts with VPS-45. SPE-39–GST was coexpressed with VPS-33.1, VPS-33.2 or VPS-45. Pulldowns were performed with either GSH- or IgG-beads as indicated. *n* = 3 biologically independent experiments. For quantification, see Extended Data Fig. 3d. **b**, Y2H assays show interactions between SPE-39 and VPS-45 as well as SPE-39 and RAB-5. *n* = 3 biologically independent yeast transformants were grown on plates with galactose but lacking leucine; *n* = 6 experiments were performed. The interaction between SAND-1 and CCZ-1 was used as a positive control, and an empty vector of the activation domain plasmid pJG4-5 was used as a negative control. **c**, Interaction between VIPAS39 and VPS45 in HEK293 cells. Cells were co-transfected with myc-tagged VPS45 and GFP-tagged VIPAS39. Left: co-immunoprecipitation with either control or GFP-Trap beads. Proteins were detected with antibodies against myc, GFP and actin. *n* = 3 independent experiments. Right: quantification of the interaction (mean \pm s.d.). **d**, Interaction of endogenous VIPAS39 with rabenosyn-5 and VPS45. Co-immunoprecipitation of myc-tagged rabenosyn-5, VPS45 or VPS33B, VIPAS39, myc and actin were detected. Interaction between VIPAS39 and VPS33B served as a positive control. *n* = 3 independent experiments. **e**, Interaction of VIPAS39, VPS45 and rabenosyn-5 in triple-transfected cells. myc-rabenosyn-5 and myc-VPS45 were co-immunoprecipitated with GFP-VIPAS39. *n* = 3 independent experiments. **f**, Y2H interactions between SPE-39 and RME-1, UNC-44, as well as between UNC-44 and RAB-5. UNC-44 was subcloned into three domains as indicated in the schematic drawing. *n* = 3 biologically independent yeast transformants; *n* = 6 experiments were performed. **g**, Binding of FERARI components to endogenous VIPAS39. Myc-ANK3, myc-EHD1 or myc-Rab11FIP5 was immunoprecipitated with myc beads or control beads as indicated. *n* = 3 independent experiments. The quantification (bottom left) displays the mean \pm s.d. **h**, Top: co-immunoprecipitation of myc-EHD1 and GFP-rabenosyn-5. *n* = 3 independent experiments. Bottom: the quantification of the interaction shows the mean \pm s.d. **i**, Summary of interactions between FERARI components. **j**, A table of FERARI components in *C. elegans* and humans. Unprocessed blots and statistical source data are available as source data.

VIPAS39 and RAB11. Moreover, in Rab11FIP5 KO cells, Rab11-positive structures were enlarged and TfR recycling was impaired similarly to what we had observed for other FERARI members (Fig.

3d,e; compare to Fig. 2a and Extended Data Fig. 7e). Furthermore, the interaction between EHD1 and rabenosyn-5 was weakened in Rab11FIP5 KO cells, and to a lesser extent the interaction between



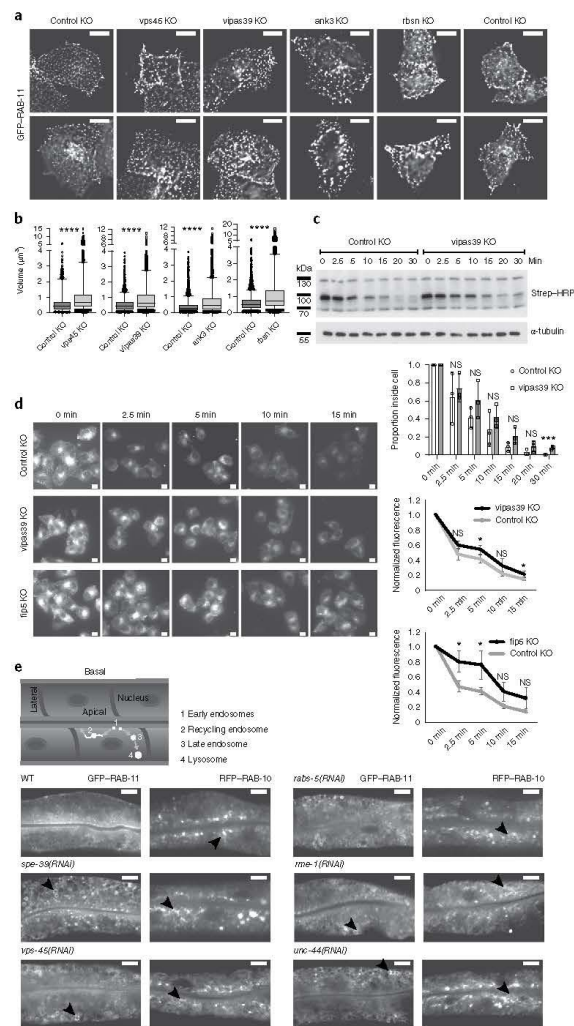


Fig. 2 | Loss of FERARI affects endosomal recycling. **a**, KO of vipas39, vps45, rbsn and ank3 causes enlargement of Rab11 compartments in HeLa cells. Representative images from live cell imaging of Rab11-GFP in control and KO cells are shown. Scale bars, 10 μ m. $n=3$ independent experiments. **b**, Quantification of the deconvolved and Fiji-processed images shown in **a**. Volumes (μ m³) were determined. For ctr KO, vipas39 KO and vps45 KO, totals of $n=6,075$, $6,104$ and $6,062$ Rab11-positive vesicles were counted; for ctr KO and ank3 KO, totals of $n=6,081$ and $n=6,056$ vesicles were counted; for ctr KO and rbsn KO, totals of $n=6,048$ and $n=6,067$ vesicles were counted. More than 2,000 vesicles from each replicate ($n=3$ independent experiments) were analysed. For the box plots, the boxes represent the 25th–75th percentile with the median and the whiskers represent the 5th–95th percentile ($P < 0.0001$). **c**, Tfn recycling is reduced in vipas39 KO cells. Pulse-chase experiment with Tfn-biotin. Internal Tfn-biotin was detected with streptavidin-HRP. Quantification is below. $n=3$ independent experiments (the data show the mean \pm s.d.). 2.5 min: $P=0.6288$; 5 min: $P=0.2351$; 10 min: $P=0.1233$; 20 min: $P=0.1445$; 30 min: $P=0.0014$. **d**, Tfn-Alexa594 recycling is reduced in FERARI KO cells. Pulse-chase experiment. Scale bars, 10 μ m. Quantification is on the right. For quantification at $t=0$: ctr, $n=153$ cells; fip5 KO, $n=166$ cells; vipas39 KO, $n=176$ cells. At $t=2.5$ min: ctr, $n=161$ cells; fip5 KO, $n=165$ cells ($P=0.0234$); vipas39 KO, $n=143$ cells ($P=0.0663$). At $t=5$ min: ctr, $n=152$ cells; fip5 KO, $n=157$ cells ($P=0.0391$); vipas39 KO, $n=162$ cells ($P=0.0420$). At $t=10$ min: ctr, $n=148$ cells; fip5 KO, $n=149$ cells ($P=0.0612$); vipas39 KO, $n=151$ cells ($P=0.1129$). At $t=15$ min: ctr, $n=146$ cells; fip5 KO, $n=152$ cells ($P=0.1031$); vipas39 KO, $n=150$ cells ($P=0.0418$) from 3 biological replicates (>40 cells per replicate). The data show the mean \pm s.d. **e**, GFP-RAB-11 and RFP-RAB-10 structures are affected by FERARI(RNAi). A schematic representation of *C. elegans* intestinal cells with endosomal compartments is shown in the top panel. GFP-RAB-11 structures are enlarged and RFP-RAB-10 networks are grossly extended in FERARI(RNAi) animals. The arrowheads point to aberrant structures. Scale bars, 10 μ m. The mean \pm s.d. is shown; $n=3$ independent experiments ($n=20$ animals); * $P < 0.05$, *** $P < 0.001$, **** $P < 0.0001$ and NS, $P > 0.05$. Two-tailed Student's *t*-tests were used for all analyses. Unprocessed blots and statistical source data are available as source data.

rabenosyn-5 and VIPAS39, suggesting that Rab11FIP5 contributes to FERARI assembly (Extended Data Fig. 3c,c' and Fig. 3f). Consistently, Rab11FIP5 co-localized with rabenosyn-5 (Extended Data Fig. 4a,b). In *C. elegans*, there is only one homologue of Rab11FIP2 and Rab11FIP5, Y39F10B.1, which we named RFIP-2. *rfip-2(RNAi)* phenocopied the effect of *FERARI(RNAi)* in the *C. elegans* intestine (Fig. 3g,h). Moreover, RFIP-2 physically interacted with FERARI components (Fig. 3i and Extended Data Fig. 3g). Therefore, we propose that Rab11FIP5 represents one branch of the RAB interaction module of FERARI (Fig. 1i,j).

FERARI may act on sorting endosomes. Our data so far suggest that FERARI functions on sorting endosomes. If this interpretation is correct, we might be able to detect an effect on the localization of the Rab proteins on sorting endosomes, RAB-5 and RAB-7. Following *FERARI(RNAi)*, the RAB-5 signal was more concentrated at the apical membrane and also part of the RAB-7 signal became enriched in the same area compared to that of mock-treated animals (Fig. 4a,b). This finding suggests that reducing recycling capacity could prematurely activate Rab conversion from RAB-5- to RAB-7-positive membranes. If this assumption was correct, disruption of Rab conversion should restore the RAB-5 localization. SAND-1 is part of a RAB-7 GEF complex and a key regulator of Rab conversion^{39,41}. Concomitant loss of SAND-1 and FERARI restored RAB-5 localization (Fig. 4c,d). Surprisingly, RAB-7-positive compartments were also partially restored under these conditions, even also moderately rescuing the hTfR transport defect (Fig. 4c–e). Likewise, the *sand-1*^{-/-} transport block in coelomocytes was also partially rescued (Extended Data Fig. 8a). Thus, loss of FERARI impacts RAB-5- and RAB-7-positive endosomes, consistent with a function of FERARI on sorting endosomes.

FERARI is required for SNX-1 active recycling compartment maintenance. SNX1 and SNX4 in mammals and the *C. elegans* homologue SNX-1 are present on the tubular part of sorting endosomes^{42,43}. Mild overexpression of mCherry-SNX-1 slightly increases the size of the tubular portions of sorting endosomes (Fig. 5a). To test whether the SNX-1-positive tubules are active recycling compartments, we blocked apical recycling by *rab-11(RNAi)*. As expected, the SNX-1 tubules were extended to long networks following *rab-11(RNAi)*. This finding suggests that RAB-11 drives recycling through these tubules and that the SNX-1 tubules are dynamic structures that respond to recycling flux. Moreover, RAB-5, RAB-7 and RAB-11 co-localized with SNX-1 tubules to a varying degree (Fig. 5b,c and Supplementary Videos 1–4), consistent with the notion that SNX-1-positive structures represent active recycling compartments on sorting endosomes. Of note, the RAB-11 signal

was more vesicular and tubular with a rather small contact site. The Golgi marker MANS-1 and the lipid droplet marker DHS-3 did not show any appreciable co-localization with SNX-1 tubules (Fig. 5b,c and Supplementary Videos 6 and 7).

Our data indicate that FERARI and SNX-1 should both be on sorting endosomes. Indeed, EHD1 decorated SNX-1 tubules with discrete puncta (Fig. 5b,c and Supplementary Video 5). When we depleted VIPAS39 or other FERARI components, the association of EHD1 with internal structures was lost, while the plasma membrane pool appeared less disturbed (Fig. 5d). This effect was not due to EHD1 degradation in the absence of FERARI (Extended Data Fig. 8b). Thus, EHD1 depends on other FERARI components for recruitment to SNX-1-positive sorting endosomes.

Next, we explored the relationship between SNX-1 and FERARI further. SNX-1 interacted specifically with *C. elegans* VIPAS39 and rabenosyn-5 in Y2H (Fig. 5g and Extended Data Figs. 1b, 2c,c' and 3a) and with endogenous VIPAS39 in mammalian cells (Extended Data Fig. 8d). Likewise, knockdown of SNX-1 or its interacting partner RME-8^{35,44} resulted in enlarged RAB-11-positive compartments, indistinguishable from those formed following loss of FERARI (compare Fig. 5e,f to Fig. 2e). These data suggest that FERARI and SNX-1/RME-8 act in the same pathway (Fig. 1i). More importantly, *FERARI(RNAi)* led to loss of the tubular SNX-1 structures (Fig. 5h), indicating that FERARI is involved in the maintenance of SNX-1 recycling compartments. This action appears to be independent of any potential role of SNX-1 in the retromer pathway, as VPS35, which is part of the cargo selective complex, did not interact with FERARI (Extended Data Fig. 8c).

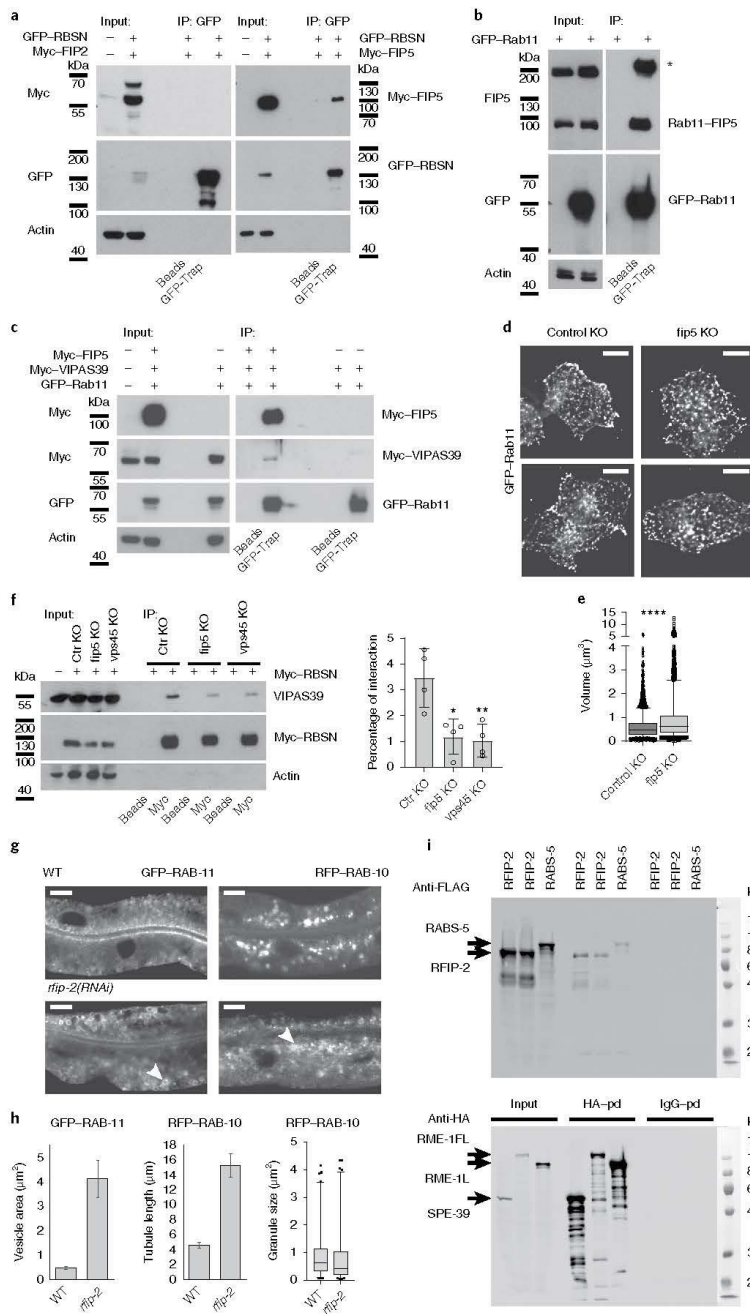
The SNAREs SYX-6 and SYX-7 act in the FERARI-dependent pathway. As a tether, FERARI should also contain a functional SNARE-binding module. The SM protein VPS-45 was shown to interact directly with the SNAREs SYX-7 and SYX-16²⁹. While *syx-7(RNAi)* caused the enlarged RAB-11 compartment phenotype characteristic of FERARI loss, *syx-16(RNAi)* had only a mild effect (Fig. 6a,b). In addition, we identified SYX-6 as another potential FERARI SNARE, while VAMP-7 and VTI-1 appeared to have no direct function in RAB-11-dependent recycling. Taken together, our results indicate that FERARI has all the hallmarks of a multi-subunit tether in that it possesses a SNARE- and a Rab-interacting module, which could bring two membrane entities together to drive membrane fusion.

Recycling endosome kiss-and-run at sorting endosomes is dependent on FERARI. FERARI is special with respect to the different functions it combines. Besides the classical tethering activities, it also contains EHD1, which acts as a pinchase¹⁴. Thus, FERARI may

Fig. 3 | Rab11FIP5 is part of FERARI and provides the link to Rab11. **a**, Rabenosyn-5 binds to Rab11FIP5 but not to Rab11FIP2. myc-tagged Rab11FIP5 but not Rab11FIP2 was co-immunoprecipitated with GFP-rabenosyn-5. Representative images are shown. *n* = 3 independent experiments. For quantification, see Extended Data Fig. 3e. **b**, A western blot of immunoprecipitation of endogenous Rab11FIP5 with GFP-Rab11. *n* = 3 independent experiments. For quantification, see Extended Data Fig. 3f. **c**, Rab11 binds to FERARI through Rab11FIP5. HEK293 cells were co-transfected with GFP-Rab11 and myc-VIPAS39 in the presence or absence of myc-Rab11FIP5. *n* = 3 independent experiments. **d**, Live cell imaging of GFP-Rab11 in *rfip5* KO HeLa cells. Scale bars, 10 μ m. *n* = 3 independent experiments. **e**, Quantification of the deconvolved and Fiji-processed images shown in **d**. GFP-Rab11-positive vesicles were counted in ctr (*n* = 6,081) and *rfip5* KO (*n* = 6,059) from *n* = 3 independent biological replicates (>2,000 vesicles per replicate). For the box plot, the box represents the 25th–75th percentile with the median and the whiskers represent the 5th–95th percentile (*P* < 0.0001). **f**, Left: interaction between RBSN and endogenous VIPAS39 is reduced in *rfip5* and *vps45* KO cells. ctr KO, *rab11fip5* KO and *vps45* KO HEK293 cells were transfected with myc-RBSN. Immunoprecipitated proteins and inputs were probed with antibodies against myc, VIPAS39 and actin. Right: quantification of interactions of *n* = 4 independent experiments. The data show the mean \pm s.d.; *P* = 0.0141 (*rfip5* KO); *P* = 0.0099 (*vps45* KO). **g**, Phenotypes of *rfip-2* knockdowns in worm intestinal cells expressing GFP-RAB-11 or RFP-RAB-10. The arrowheads point to abnormal RAB-11 and RAB-10 compartments. *n* = 3 independent RNA-mediated interference (RNAi) experiments (*n* = 20 animals). Scale bars, 10 μ m. **h**, Quantification of the *rfip-2* phenotypes shown in **g**. The mean \pm s.d. is shown. For the box plot, the box represents the 25th–75th percentile with the median and the whiskers represent the 1st–99th percentile. **i**, Interactions between proteins in the Y2H vectors were tested biochemically with pulldowns (pd). Worm RFIP-2 (Y39F10B.1) binds to RME-1 and SPE-39. Interaction between RME-1 and RAB-5 also occurs in worms. For quantification, see Extended Data Fig. 3g. **P* < 0.05, ***P* < 0.01 and *****P* < 0.0001. Two-tailed Student's *t*-tests were used for all analyses. Unprocessed blots and statistical source data are available as source data.

promote membrane fission and fusion at the recycling compartment of sorting endosomes. If this was the case, we should detect the arrival of a RAB-11-positive structure at the recycling compartment

promote membrane fission and fusion at the recycling compartment of sorting endosomes. If this was the case, we should detect the arrival of a RAB-11-positive structure at the recycling compartment



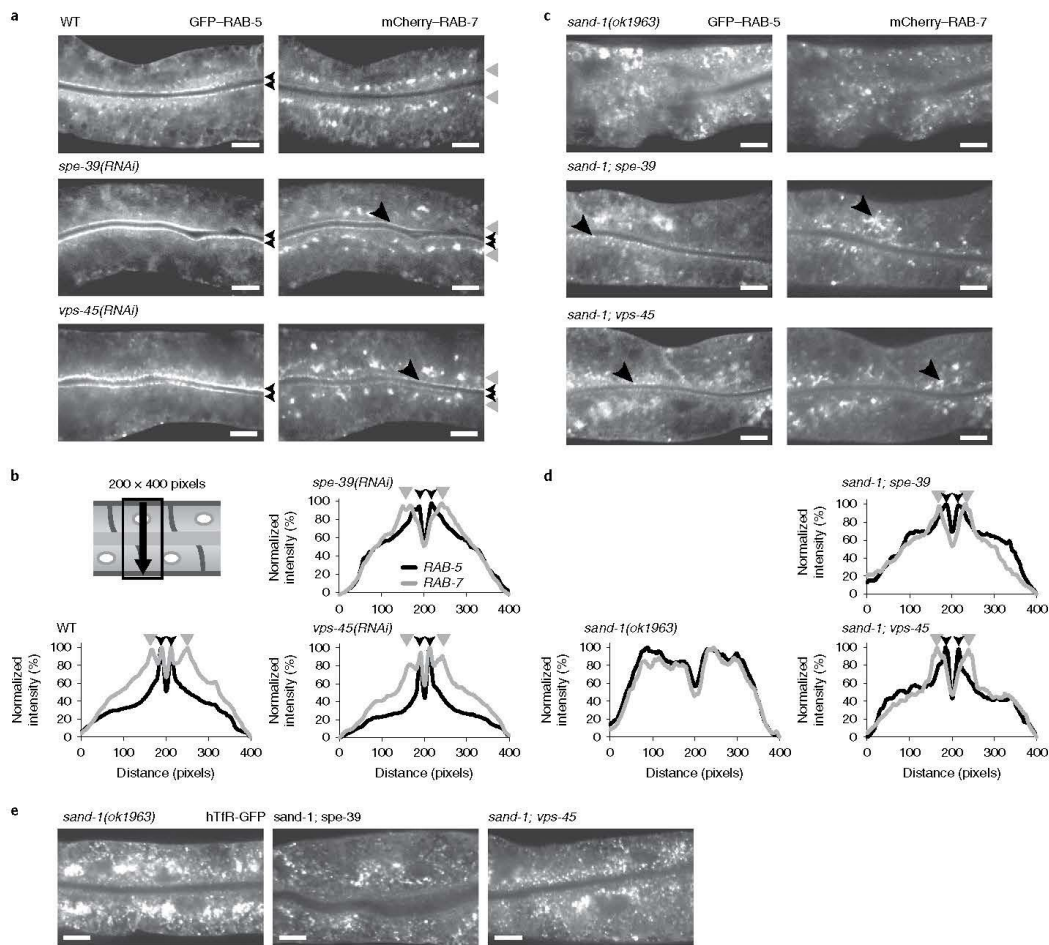


Fig. 4 | FERARI may act on sorting endosomes but is not essential for transport to lysosomes. **a**, RAB-5-positive compartments are affected by *spe-39(RNAi)* and *vps-45(RNAi)*. The GFP-RAB-5 signal remains confined to the apical membrane (small black arrowheads) and these compartments even seem to mature to RAB-7 (large black arrowheads). The general RAB-7 compartment is largely unaffected (grey arrowheads). $n=3$ independent RNAi experiments ($n=20$ animals). Scale bars, 10 μm . **b**, Quantification of RAB-5 and RAB-7 phenotypes. A schematic representation of a worm gut and the area used for quantification (line plot with 200 pixels in width) is shown in the top left panel. The small black arrowheads indicate RAB-5 peaks; the grey arrowheads indicate RAB-7 compartments. $n=5$ worms per curve. **c**, The enlarged RAB-5 compartments in *sand-1(ok1963)* worms are partially restored in *spe-39* and *vps-45* knockdowns. The dispersed and disorganized RAB-7 compartments of *sand-1(ok1963)* worms are also partially suppressed by loss of FERARI. The black arrowheads point to restored compartments. $n=3$ independent RNAi experiments ($n=20$ animals). Scale bars, 10 μm . **d**, Quantification of *sand-1* suppression phenotypes as in **b**. $n=5$ worms per curve. **e**, In *sand-1(ok1963)* worms, the degradation pathway is blocked and hTIR-GFP accumulates in very bright endosomes. The hTIR-GFP signal is reduced in *spe-39(RNAi)* and *vps-45(RNAi)*. $n=3$ independent RNAi experiments ($n=20$ animals). Scale bars, 10 μm . Statistical source data are available as source data.

low fluorescence intensities (Fig. 6e). We also observed instances in which RAB-11-positive structures were initially docked and then released (Fig. 6d and Supplementary Videos 11–13). Importantly, those RAB-11 endosomes appeared bigger and brighter (Fig. 6e). Using more sophisticated imaging enabled us to visualize RAB-11 dynamics. When we determined the residence time of RAB-11-positive structures on sorting endosomes, we noticed that the

individual residence times came in discrete intervals of about 7 s (Fig. 7a,c, Extended Data Fig. 9b and Supplementary Videos 14 and 15), indicating that the residence time increased in quanta. This quantal behaviour was abolished when FERARI function was lost (Fig. 7a,c, Extended Data Fig. 9b and Supplementary Video 16). Thus, FERARI is important for RAB-11 recycling endosome fusion and fission at sorting endosomes. A prediction from this

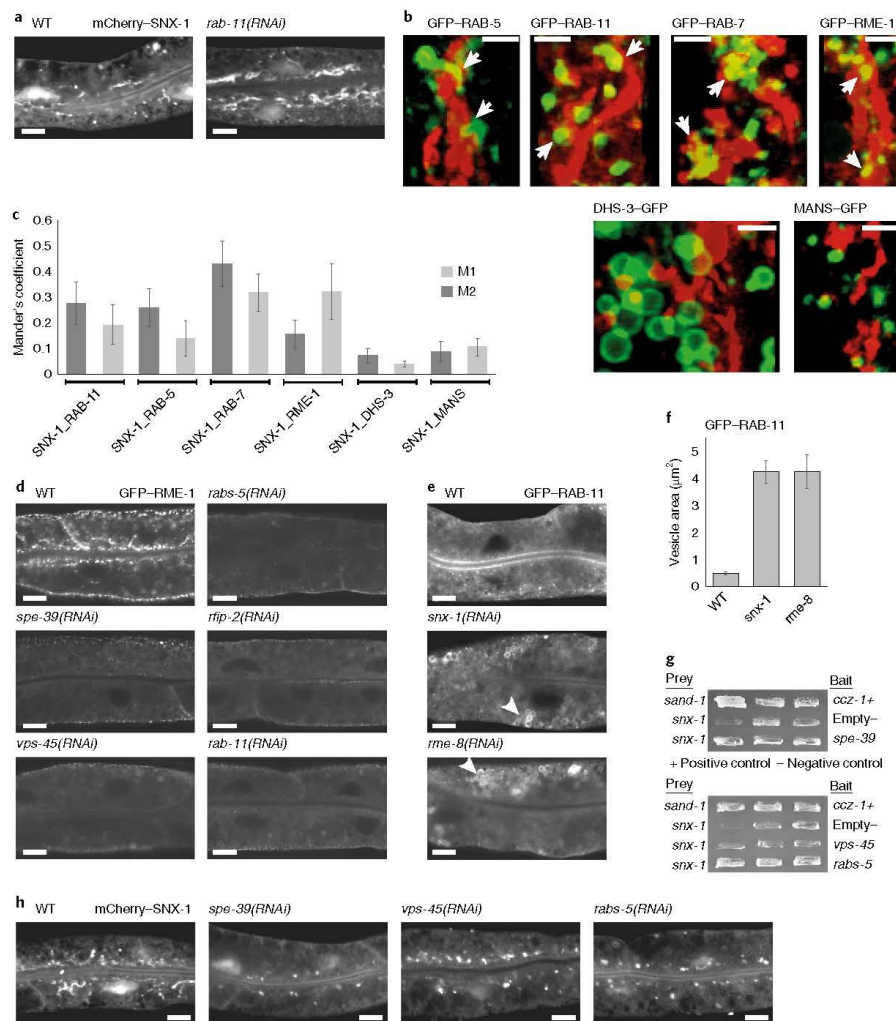


Fig. 5 | FERARI is present on and required for the maintenance of SNX-1 active recycling compartments in *C. elegans*. **a**, mCherry-SNX-1 tubules are elongated and accumulate in *rab-11(RNAi)* worms. $n=3$ independent RNAi experiments ($n=20$ animals). Scale bars, $10\ \mu\text{m}$. **b**, mCherry-SNX-1 networks sometimes coincide with the position of RAB-11, RAB-5, RAB-7 and RME-1 compartments. Worms expressing mCherry-SNX-1 and either RAB-5, RAB-11, RAB-7 or RME-1 show some overlap between the networks and the globular compartments. The white arrows point to sites of overlap. DHS-3 (lipid droplets) and MANS (Golgi) were used as controls. $n=3$ independent RNAi experiments ($n=30$ animals). Scale bars, $3\ \mu\text{m}$. **c**, Quantification of co-localization using Mander's coefficient. $n=10$ animals were measured. The mean \pm s.d. is indicated. **d**, GFP-RME-1 localization is abolished in FERARI knockdowns (*spe-39*, *vps-45*, *rabs-5*, *rfp-2* and *rab-11*). $n=3$ independent RNAi experiments ($n=20$ animals). Scale bars, $10\ \mu\text{m}$. **e**, Knockdowns of *snx-1* and its interactor *rme-8* show FERARI-like RAB-11 phenotypes. The arrowheads point to enlarged RAB-11 compartments. $n=3$ independent RNAi experiments ($n=20$ animals). Scale bars, $10\ \mu\text{m}$. **f**, Quantification of the phenotypes shown in **e**. $n=10$ vesicles each were measured in $n=6$ animals; the mean \pm s.d. is indicated. **g**, Y2H interactions of FERARI subunits with SNX-1. $n=3$ independent transformants were analysed in $n=6$ experiments. **h**, Networks formed by mCherry-SNX-1 are lost in *spe-39(RNAi)*, *vps-45(RNAi)* and *rabs-5(RNAi)* intestinal cells. $n=3$ independent RNAi experiments ($n=20$ animals). Scale bars, $10\ \mu\text{m}$. Statistical source data are available as source data.

model is that cargo molecules should behave in a similar way. hTfR and GLUT1 showed the same FERARI-dependent quantal behaviour (Fig. 7b,d,e, Extended Data Fig. 9c, Extended Data Fig. 10 and

Supplementary Videos 17–21). We surmise that RAB-11 endosomes picked up cargo and lipids at the sorting endosome, consistent with a kiss-and-run mechanism.

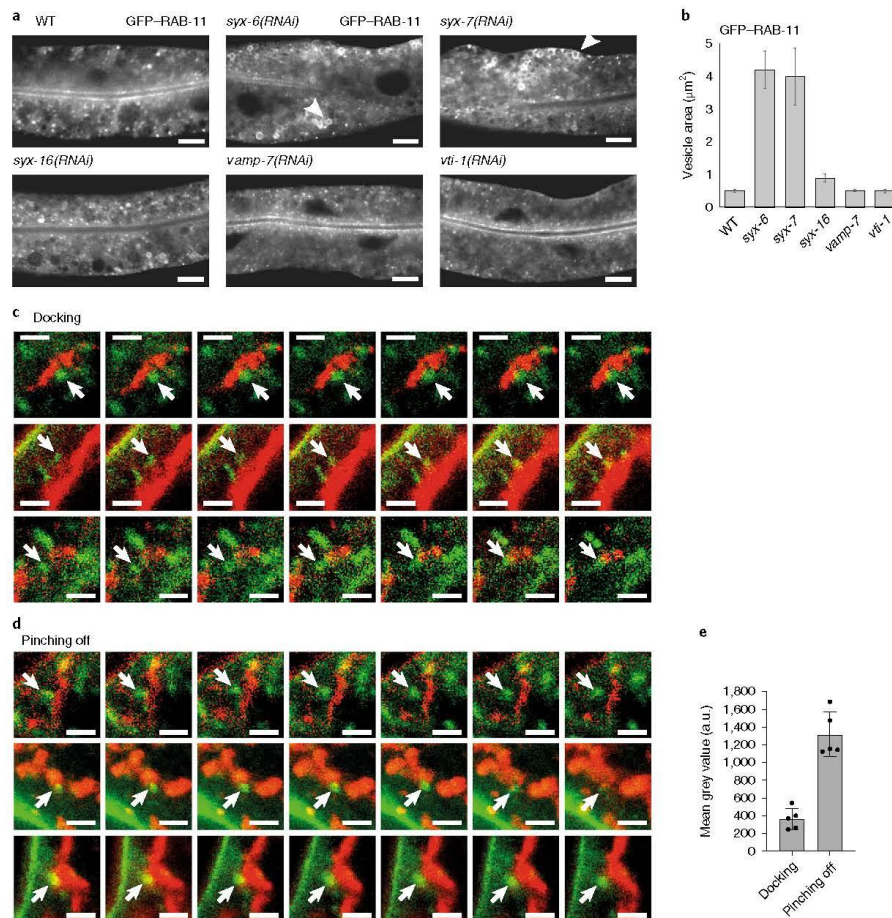


Fig. 6 | The SNAREs SYX-6 and SYX-7 act in the FERARI-dependent RAB-11 recycling pathway. a, SNARE knockdowns show distinct phenotypes on RAB-11 compartments. While *syx-6* and *syx-7(RNAi)* show enlarged RAB-11 compartments (arrowheads), *syx-16*, *vamp-7* and *vti-1(RNAi)* had no effect. $n=3$ independent RNAi experiments ($n=20$ animals). Scale bars, $10\mu\text{m}$. **b**, Quantification of the phenotypes shown in **a**. $n=10$ structures for each of $n=6$ worms was measured; mean \pm s.d. is indicated. **c**, Stills from videos with GFP-RAB-11 and mCherry-SNX-1 compartments, showing docking of globular RAB-11 to SNX-1 tubules. The arrows point to RAB-11 compartments of interest. Note the yellow overlap in the later pictures to the right. $n=3$ independent RNAi experiments ($n=30$ animals). Scale bars, $2\mu\text{m}$ (Supplementary Videos 8–10). **d**, Stills from videos showing pinching off of RAB-11 globular compartments from SNX-1 tubules. The arrows point to RAB-11 compartments starting out with some overlap (yellow) and moving away from SNX-1 tubules. The time between stills is 30 s (every third image in videos). $n=3$ independent RNAi experiments ($n=30$ animals). Scale bars, $2\mu\text{m}$ (Supplementary Videos 11–13). **e**, Docking RAB-11 compartments are less bright than pinching off RAB-11 compartments. The brightness was measured over ten frames of five videos each. $n=5$ videos were quantified; the mean \pm s.d. is indicated. Statistical source data are available as source data.

Discussion

How sorting into recycling endosomes occurs at sorting endosomes still remains enigmatic. Here, we report the existence of a multisubunit tether, FERARI, which plays a role in recycling to the apical and basal lateral domains of polarized cells in *C. elegans* and Rab11-dependent recycling in mammalian cells (Extended Data Fig. 9a). FERARI represents a tether combining a SNARE-interaction module—VPS45—with Rab interaction modules—Rab11FIP5 and rabenosyn-5²⁷. Unlike its relatives, HOPS and CORVET,

FERARI tethers membranes containing different Rab proteins. Another remarkable difference is that FERARI contains a dynamin-like protein EHD. This composition provides FERARI with two rather distinct and opposing activities: membrane fission and membrane fusion.

On the basis of our data, we propose the following model (Fig. 7f and Supplementary Video 22). We assume that FERARI members are recruited onto the sorting endosome by RAB5, where they associate with SNX1 and help to stabilize SNX1-positive

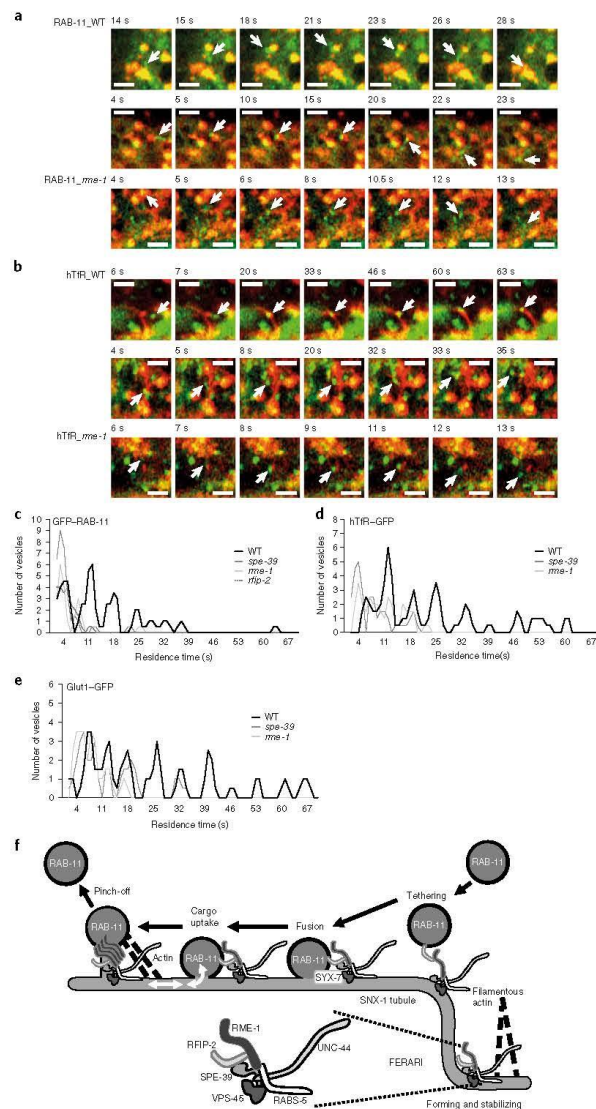


Fig. 7 | FERARI promotes kiss-and-run vesicle dynamics and quantal cargo uptake. a, Video stills of GFP-RAB-11 vesicles docking and pinching off from mCherry-SNX-1 compartments in wild-type (WT) and *mme-1(RNAi)*. The times of the frames are shown and the arrows point to RAB-11 vesicles. $n=3$ independent experiments ($n=30$ animals). Scale bars, $2\ \mu\text{m}$. (Supplementary Videos 14–16). **b**, hTIR-GFP vesicles behave in a similar way to RAB-11 vesicles. Shown are examples of hTIR vesicles in WT and *mme-1(RNAi)* worms (arrows). $n=3$ independent RNAi experiments ($n=30$ animals). Scale bars, $2\ \mu\text{m}$ (Supplementary Videos 17–20). **c–e**, Binning of vesicles according to residence times (primary data in Extended Data Fig. 9b,c). The moving average is calculated to highlight the peaks of residence times starting at approximately 4 s and continuing at around 7-s intervals. $n=65$ for WT, $n=21$ for *mme-1(RNAi)*, $n=34$ for *spe-39(RNAi)* and $n=25$ for *rftp-2(RNAi)* in **c**, $n=62$ for WT, $n=30$ for *spe-39(RNAi)* and $n=31$ for *mme-1(RNAi)* in **d**, $n=56$ for WT, $n=32$ for *spe-39(RNAi)* and $n=29$ for *mme-1(RNAi)* in **e**. **f**, A model of FERARI recycling (see also Supplementary Video 22). A putative structure of FERARI is shown below, based on interactions between the components and the approximate size of the proteins. Functions of FERARI might include forming and stabilizing SNX-1 sorting/recycling tubules. FERARI could tether RAB-11 compartments to these tubules, followed by membrane fusion through VPS-45 binding of the SNAREs SYX-6 and SYX-7. The RAB-11 compartment would be stabilized with an open pore to the SNX-1 tubule because of the presence of an RME-1 constriction ring. After sorting of cargo, the pinching activity of RME-1—potentially coupled to UNC-44 interaction with actin—will allow the RAB-11 compartment to leave the sorting station. Statistical source data are available as source data.

structures. At this point we can only speculate about the mechanism. However, ANK3 is known to link membranes to the cytoskeleton and would therefore be well suited to stabilize tubular networks. VPS-45 mediates association with the SNAREs SYX-6 and SYX-7, while RAB11-FIP5 will engage with RAB11 on a recycling structure to bring it closer to the sorting endosome. FERARI then would induce SNARE complex assembly and promote membrane fusion, similarly to what has been reported for DSL, HOPS and CORVET^{24,45,46}. Even though we anticipate full membrane fusion, our data indicate that RAB11-positive membranes do not flatten and retain their globular shape. The barrier for membrane flattening could be provided by EHD1. EHD proteins have been shown to assemble in ring structures similar to dynamin^{15,47}. In this state, cargo to be recycled to the plasma membrane and lipids could diffuse into the RAB11-positive structure. How cargo is enriched in the RAB11 domain remains unclear. We surmise that back diffusion could be limited by membrane curvature, lipid composition or other proteins. Finally, EHD would promote scission between the RAB11-positive recycling endosome and the tubular part of the sorting endosomes. Our model corresponds to a kiss-and-run model, similar to the one in neurotransmitter release, except that in our case the docked entity is not releasing but rather is taking up content. The 'flickering' in the kiss-and-run model of membrane fusion and fission is present in our system and takes about 7 s (Supplementary Video 22). In neuroendocrine cells, secretory granules maintain their shape and do not flatten out during fusion with the plasma membrane. Instead, they are released again from the plasma membrane in a process referred to as cavicapture or fuse-pinch-linger^{48,49}. The coordination of fusion and fission events could be mediated by EHD through interaction with either VPS45 or another SNARE regulator protein, SNAP29⁵⁰. Thus, FERARI provides a platform on sorting endosomes on which fission and fusion of RAB11-positive structures are coordinated. Rabenosyn-5 could potentially act as the scaffold because it can interact with all FERARI members and SNXs.

Our model is supported by our finding that the RAB-11 compartments that dock onto the sorting endosome are smaller than the ones that leave. Moreover, most components of FERARI have been implicated in recycling previously^{17,21,26,28,51}. Now our data put them into context, providing a temporally and spatially controlled concerted action. FERARI members show a varying degree of co-localization, which might be an indication for dynamic assembly on sorting endosomes. Yet FERARI was involved not only in RAB11-dependent recycling but also early on in the formation/maintenance of the tubular structures. Rabenosyn-5 and the ANK proteins might be involved in such domain formation. If this hypothesis is correct, we can expect an increase in the number of tethering modules on sorting endosomes. In fact, there is already one candidate for such an additional tether. CHEVI has been proposed to act in recycling as well as in α -granule formation, a process that requires transport from the TGN to the multivesicular body^{27,28,52}. So far only two CHEVI components, VPS33B and VIPAS39, have been identified. Given the localization of these proteins, it is likely that CHEVI acts on sorting endosomes. We propose that tethers could play a role in the formation of domains required for docking on sorting endosomes and probably also on other organelles.

Online content

Any methods, additional references, Nature Research reporting summaries, source data, extended data, supplementary information, acknowledgements, peer review information; details of author contributions and competing interests; and statements of data and code availability are available at <https://doi.org/10.1038/s41556-019-0456-5>.

Received: 5 December 2018; Accepted: 16 December 2019;
Published online: 27 January 2020

References

1. Aflatoonian, M. et al. Novel VIPAS39 mutation in a syndromic patient with arthrogryposis, renal tubular dysfunction and intrahepatic cholestasis. *Eur. J. Med. Genet.* **59**, 237–239 (2016).
2. Buggia-Prevot, V. et al. A function for EHD family proteins in unidirectional retrograde dendritic transport of BACE1 and Alzheimer's disease Abeta production. *Cell Rep.* **5**, 1552–1563 (2013).
3. Chen, C. H., Lo, R. W., Urban, D., Pluthero, F. G. & Kahr, W. H. Alpha-granule biogenesis: from disease to discovery. *Platelets* **28**, 147–154 (2017).
4. Haider, N. B. et al. Evaluation and molecular characterization of EHD1, a candidate gene for Bardet-Biedl syndrome 1 (BBS1). *Gene* **240**, 227–232 (1999).
5. Link, D. C. SNAREing a new cause of neutropenia. *Blood* **121**, 4969–4970 (2013).
6. Mellman, I. & Yarden, Y. Endocytosis and cancer. *Cold Spring Harb. Perspect. Biol.* **5**, a016949 (2013).
7. Meng, Q. et al. Increased expression of Eps15 homology domain 1 is associated with poor prognosis in resected small cell lung cancer. *J. Cancer* **6**, 990–995 (2015).
8. Tong, D. et al. Increased Eps15 homology domain 1 and RAB11FIP3 expression regulate breast cancer progression via promoting epithelial growth factor receptor recycling. *Tumour Biol.* **39**, <https://doi.org/10.1177/1010428317691010> (2017).
9. Chua, C. E. L. & Tang, B. L. Rab 10-a traffic controller in multiple cellular pathways and locations. *J. Cell Physiol.* **233**, 6483–6494 (2018).
10. Wandinger-Ness, A. & Zerial, M. Rab proteins and the compartmentalization of the endosomal system. *Cold Spring Harb. Perspect. Biol.* **6**, a022616 (2014).
11. Solinger, J. A., Poteryaev, D. & Spang, A. Application of RNAi technology and fluorescent protein markers to study membrane traffic in *C. elegans*. *Methods Mol. Biol.* **1174**, 329–347 (2014).
12. Solinger, J. A. & Spang, A. Loss of the Sec1/Munc18-family proteins VPS-33.2 and VPS-33.1 bypasses a block in endosome maturation in *Caenorhabditis elegans*. *Mol. Biol. Cell* **25**, 3909–3925 (2014).
13. Grant, B. et al. Evidence that RME-1, a conserved *C. elegans* EH-domain protein, functions in endocytic recycling. *Nat. Cell Biol.* **3**, 573–579 (2001).
14. Daumke, O. et al. Architectural and mechanistic insights into an EHD ATPase involved in membrane remodelling. *Nature* **449**, 923–927 (2007).
15. Melo, A. A. et al. Structural insights into the activation mechanism of dynamin-like EHD ATPases. *Proc. Natl. Acad. Sci. USA* **114**, 5629–5634 (2017).
16. Pant, S. et al. AMPH-1/Amphiphysin/Bin1 functions with RME-1/Ehd1 in endocytic recycling. *Nat. Cell Biol.* **11**, 1399–1410 (2009).
17. Bonifacino, J. S. & Rojas, R. Retrograde transport from endosomes to the trans-Golgi network. *Nat. Rev. Mol. Cell Biol.* **7**, 568–579 (2006).
18. Naslavsky, N., Rahajeng, J., Sharma, M., Jovic, M. & Caplan, S. Interactions between EHD proteins and Rab11-FIP2: a role for EHD3 in early endosomal transport. *Mol. Biol. Cell* **17**, 163–177 (2006).
19. Traer, C. J. et al. SNX4 coordinates endosomal sorting of TfR with dynein-mediated transport into the endocytic recycling compartment. *Nat. Cell Biol.* **9**, 1370–1380 (2007).
20. van Weering, J. R., Verkade, P. & Cullen, P. J. SNX-BAR-mediated endosome tubulation is co-ordinated with endosome maturation. *Traffic* **13**, 94–107 (2012).
21. Naslavsky, N., Boehm, M., Backlund, P. S. Jr & Caplan, S. Rabenosyn-5 and EHD1 interact and sequentially regulate protein recycling to the plasma membrane. *Mol. Biol. Cell* **15**, 2410–2422 (2004).
22. Peplowska, K., Markgraf, D. F., Ostrowicz, C. W., Bange, G. & Ungermann, C. The CORVET tethering complex interacts with the yeast Rab5 homolog Vps21 and is involved in endo-lysosomal biogenesis. *Dev. Cell* **12**, 739–750 (2007).
23. Planel, R. L. et al. Subunit organization and Rab interactions of Vps-C protein complexes that control endolysosomal membrane traffic. *Mol. Biol. Cell* **22**, 1353–1363 (2011).
24. Solinger, J. A. & Spang, A. Tethering complexes in the endocytic pathway: CORVET and HOPS. *FEBS J.* **280**, 2743–2757 (2013).
25. Ungermann, C., Price, A. & Wickner, W. A new role for a SNARE protein as a regulator of the Ypt7/Rab-dependent stage of docking. *Proc. Natl. Acad. Sci. USA* **97**, 8889–8891 (2000).
26. Rahajeng, J., Caplan, S. & Naslavsky, N. Common and distinct roles for the binding partners Rabenosyn-5 and Vps45 in the regulation of endocytic trafficking in mammalian cells. *Exp. Cell Res.* **316**, 859–874 (2010).
27. Spang, A. Membrane tethering complexes in the endosomal system. *Front. Cell Dev. Biol.* **4**, 35 (2016).
28. Rogerson, C. & Gissen, P. VPS33B and VIPAR are essential for epidermal lamellar body biogenesis and function. *Biochim. Biophys. Acta Mol. Basis Dis.* **1864**, 1609–1621 (2018).
29. Gengyo-Ando, K. et al. The SM protein VPS-45 is required for RAB-5-dependent endocytic transport in *Caenorhabditis elegans*. *EMBO Rep.* **8**, 152–157 (2007).
30. Nielsen, E. et al. Rabenosyn-5, a novel Rab5 effector, is complexed with hVPS45 and recruited to endosomes through a FYVE finger domain. *J. Cell Biol.* **151**, 601–612 (2000).

31. Guilherme, A. et al. EHD2 and the novel EH domain binding protein EHP1 couple endocytosis to the actin cytoskeleton. *J. Biol. Chem.* **279**, 10593–10605 (2004).
32. Lin, S. X., Grant, B., Hirsh, D. & Maxfield, F. R. Rme-1 regulates the distribution and function of the endocytic recycling compartment in mammalian cells. *Nat. Cell Biol.* **3**, 567–572 (2001).
33. Ackema, K. B., Sauder, U., Solinger, I. A. & Spang, A. The ArfGEF GBF-1 is required for ER structure, secretion and endocytic transport in *C. elegans*. *PLoS ONE* **8**, e67076 (2013).
34. Chen, C. C. et al. RAB-10 is required for endocytic recycling in the *Caenorhabditis elegans* intestine. *Mol. Biol. Cell* **17**, 1286–1297 (2006).
35. Sato, K., Norris, A., Sato, M. & Grant, B. D. *C. elegans* as a model for membrane traffic. *WormBook* <https://doi.org/10.1895/wormbook.1.77.2> (2014).
36. Winter, J. F. et al. *Caenorhabditis elegans* screen reveals role of PAR-5 in RAB-11-recycling endosome positioning and apicobasal cell polarity. *Nat. Cell Biol.* **14**, 666–676 (2012).
37. Sato, M., Grant, B. D., Harada, A. & Sato, K. Rab11 is required for synchronous secretion of chondroitin proteoglycans after fertilization in *Caenorhabditis elegans*. *J. Cell Sci.* **121**, 3177–3186 (2008).
38. Shi, A. et al. RAB-10-GTPase-mediated regulation of endosomal phosphatidylinositol-4,5-bisphosphate. *Proc. Natl Acad. Sci. USA* **109**, E2306–E2315 (2012).
39. Nordmann, M. et al. The Mon1–Ccz1 complex is the GEF of the late endosomal Rab7 homolog Ypt7. *Curr. Biol.* **20**, 1654–1659 (2010).
40. Poteryaev, D., Datta, S., Ackema, K., Zerial, M. & Spang, A. Identification of the switch in early-to-late endosome transition. *Cell* **141**, 497–508 (2010).
41. Poteryaev, D., Fares, H., Bowerman, B. & Spang, A. *Caenorhabditis elegans* SAND-1 is essential for RAB-7 function in endosomal traffic. *EMBO J.* **26**, 301–312 (2007).
42. Gokool, S., Tattersall, D. & Seaman, M. N. EHD1 interacts with retromer to stabilize SNX1 tubules and facilitate endosome-to-Golgi retrieval. *Traffic* **8**, 1873–1886 (2007).
43. Shi, A. et al. Regulation of endosomal clathrin and retromer-mediated endosome to Golgi retrograde transport by the J-domain protein RME-8. *EMBO J.* **28**, 3290–3302 (2009).
44. Zhang, Y., Grant, B. & Hirsh, D. RME-8, a conserved J-domain protein, is required for endocytosis in *Caenorhabditis elegans*. *Mol. Biol. Cell* **12**, 2011–2021 (2001).
45. Diefenbacher, M., Thorsteinsdottir, H. & Spang, A. The Dsl1 tethering complex actively participates in soluble NSF (N-ethylmaleimide-sensitive factor) attachment protein receptor (SNARE) complex assembly at the endoplasmic reticulum in *Saccharomyces cerevisiae*. *J. Biol. Chem.* **286**, 25027–25038 (2011).
46. Zick, M. & Wickner, W. The tethering complex HOPS catalyzes assembly of the soluble SNARE Vam7 into fusogenic *trans*-SNARE complexes. *Mol. Biol. Cell* **24**, 3746–3753 (2013).
47. Campelo, E., Fabrikant, G., McMahon, H. T. & Kozlov, M. M. Modeling membrane shaping by proteins: focus on EHD2 and N-BAR domains. *FEBS Lett.* **584**, 1830–1839 (2010).
48. Henkel, A. W. & Almers, W. Fast steps in exocytosis and endocytosis studied by capacitance measurements in endocrine cells. *Curr. Opin. Neurobiol.* **6**, 350–357 (1996).
49. Ryan, T. A. Kiss-and-run, fuse-pinch-and-linger, fuse-and-collapse: the life and times of a neurosecretory granule. *Proc. Natl Acad. Sci. USA* **100**, 2171–2173 (2003).
50. Rotem-Yehudar, R., Galperin, E. & Horowitz, M. Association of insulin-like growth factor 1 receptor with EHD1 and SNAP29. *J. Biol. Chem.* **276**, 33054–33060 (2001).
51. Lu, Q. et al. Early steps in primary cilium assembly require EHD1/EHD3-dependent ciliary vesicle formation. *Nat. Cell Biol.* **17**, 228–240 (2015).
52. Bem, D. et al. VPS33B regulates protein sorting into and maturation of alpha-granule progenitor organelles in mouse megakaryocytes. *Blood* **126**, 133–143 (2015).

Publisher's note Springer Nature remains neutral with regard to jurisdictional claims in published maps and institutional affiliations.

© The Author(s), under exclusive licence to Springer Nature Limited 2020

Methods

Worm husbandry. *C. elegans* was grown and crossed according to standard methods⁴³. RNAi was performed as previously described⁴⁴. All experiments were carried out at 20 °C, and worms were imaged at the young adult stage (with only a few eggs).

The following worm strains and transgenes were used in this study: bIs1[YP170::GFP + rol-6(su1006)]X, pwIs116 [rme-2p::rme-2::GFP::rme-2 3'UTR + unc-119(+)], pwIs429[Pvha-6::mCherry::rab-7], pwIs72[vha6p::GFP::rab-5 + unc-119(+)], pwIs90[Pvha-6::hTR::GFP; Cbr-unc-119(+)], pwIs50[Imp-1::GFP + Cb-unc-119(+)], pwIs414[Pvha-6::RFP::rab-10, Cbr-unc-119(+)], pwIs69[vha6p::GFP::rab-11 + unc-119(+)], pwIs782[Pvha-6::mCherry::SNX-1], pwIs87[Pvha-6::GFP::rme-1; Cbr-unc-119(+)], [Pdhs-3::dhs-3::GFP], pwIs481[Pvha-6::mCherry::GFP; Cbr-unc-119(+)].

Microscopy. Living worms were imaged as described previously⁴¹. Levamisole (50 mM) was used for immobilization, and 2% agarose pads were cast onto microscopy slides; worms were sealed under coverslips using Vaseline. Images were acquired using a spinning-disc confocal system Andor Revolution (Andor Technologies) mounted onto an IX-81 inverted microscope (Olympus), equipped with an IXon^{EM} + EMCCD camera (Andor Technologies). A 63×1.42 N.A. oil objective was used, where each pixel represents 0.107 µm. Solid-state 488 nm and 560 nm lasers were used for excitation and the exposure time was 100 ms. Images were averaged 4 times for oocytes and 32 times for intestine and coelomocytes. Alternatively, an Olympus Fluoview FV3000 system with a high-sensitivity spectral detector was used (photomultiplier tube voltage = 500). The objective was 60× with silicone oil, and the Galvano scan device was used. The pixel size corresponds to 0.098 µm. The sampling speed was 8.0 µs per pixel; zoom = 2.1; 488 nm (GFP) and 561 nm (RFP, mCherry) lasers were set at 4–10%. All images were processed in the same way for corresponding experiments.

Images of SNX-1 tubules with different GFP markers were obtained on a Zeiss LSM 880 microscope with Airyscan. The fast mode was used and images were processed using the Zen Black software. Worms were treated with 20 mM sodium azide to avoid any movement during image acquisition.

Videos with SNX-1 and RAB-11, hTR or Glut1 markers were taken on the LSM 880 Airyscan microscope, using the fast mode. Reducing the averaging to 2–4 times resulted in frame speeds of 0.5–1.0 s that were appropriate to the speed of the vesicles. Videos covered about two intestinal cells (about 70 µm square). Worms were treated with 50 mM levamisole and imaged as fast as possible to avoid loss of endosomal movement in the gut cells. Worms in the correct stage showed reticulated SNX-1 compartments with extruding and contracting tubules that coincided with active vesicle movement. Several videos were taken per worm and resulted in up to five vesicles showing 'kiss-and-run' behaviour per video. Small videos covering only one vesicle movement were collected from the larger videos and used to quantify the residence times. The StackReg plugin was very useful to remove the shifting worm motions and allow good tracking of single vesicles from frame to frame.

Immuno-electron microscopy. HeLa cells transfected with Rab11-GFP were prepared for immunolabelling as described in ref.²⁴. The primary antibody was rabbit anti-GFP (1:100; Abcam 6556) and the secondary was goat anti-rabbit coupled to 10-nm gold particles (BB International).

Interaction studies with worm proteins. The *C. elegans* proteins SPE-39 and VPS-45 were expressed in *E. coli* Rosetta (DE3) cells. GST-tagged SPE-39 was obtained by cloning the worm complementary DNA into the pETGEXCT vector, while His-tagged VPS-45 cDNA was cloned into the pRSF-2 Ek/LIC vector. *E. coli* cultures (500 ml) bearing both plasmids (grown in LB + amp + kan) were induced with 0.5 mM isopropyl-β-D-thiogalactoside overnight at 37 °C and collected in buffer with 50 mM HEPES pH 7.7, 300 mM NaCl, 10% glycerol and 1% Triton X-100 (with protease inhibitors) for purification. Cells were lysed with 1 mg ml⁻¹ lysozyme, 20 µg ml⁻¹ DNaseI and 2 × 30 s sonication. After a 16,000g spin, the cleared lysate was incubated overnight with Ni-NTA beads. Beads were washed four times and eluted with 250 mM imidazole. The eluate was pooled and bound overnight to glutathione beads. Worm lysate from 100-ml liquid culture (with many adults) was prepared in the same buffer (with glass beads in a FastPrep machine for 2 × 30 s). The worm extract was centrifuged at 16,000g for 30 min to yield a clear worm lysate that was added to the washed glutathione beads with bound SPE-39/VPS-45 complex. Proteins were allowed to bind overnight and finally the beads were washed four times with lysis buffer and four times with lysis buffer lacking any kind of detergents for mass spectroscopy analysis. Proteins were kept at 4 °C at all times.

Quantification of bands in both mammals and *C. elegans* was performed on non-overexposed bands for three western blots each (*n* = 3). Band-sized regions of interest (ROIs) of the same size were used to determine the mean grey values of bands in ImageJ. Inputs and pulldowns were measured and adjusted for the amounts of protein loaded. The percentage of pulldown was calculated for bait protein and prey protein. The percentage of interaction was normalized to that of the bait (assuming that full interaction could be achieved only if all of the bait was pulled down; for example, if 30% of the bait and 15% of the prey were pulled down, this would correspond to a 50% interaction between the prey and the bait).

Y2H assays were carried out using worm cDNA cloned into the vectors pEG202 (with a DNA-binding domain) and pJG4-5 (with an activation domain). The fastest results were obtained by Gibson assembly cloning (NEBuilder, NEB; E55205). pEG202 clones also obtained a 3×FLAG tag at the carboxy terminus for pulldown experiments. Growth assays were carried out with six colonies from yeast transformation (strain EGY48 + pSH18-34 plasmid for LacZ expression) for 3–7 d at 30 °C on plates lacking leucine and with addition of 2% galactose for induction of pJG4-5 expression. For pulldown experiments, 50 ml cultures of yeast were induced with 2% galactose at OD_{600nm} = 1.0 for 6 h. Cells were lysed in 50 mM HEPES pH 7.7, 300 mM NaCl, 10% glycerol and 1% Triton X-100 (with protease inhibitors) in a FastPrep device (2 × 30 s). A 25 µl volume of magnetic beads (slurry) was added for binding of tagged proteins (either anti-HA (Pierce; 88837) or anti-FLAG beads (Sigma; M8823)) and rotated overnight. After four washes, proteins were eluted with Laemmli sample buffer at 95 °C for 5 min and applied to SDS-polyacrylamide gel electrophoresis (PAGE) gels for immunoblot analysis with FLAG and HA antibodies (FLAG: Sigma; F3165, HA: Sigma HA-7 clone; H9658).

Cell culture, transfection and CRISPR-Cas9 KO in mammalian cells. HEK293 and HeLa cells were cultured and maintained in DMEM (Sigma) high-glucose medium with 10% FCS (Biococoncept), penicillin–streptomycin (1%), sodium pyruvate and L-glutamine. Cells were plated 1 d before transfection at 60–70% confluency and later transfected for 48 h using Turbofect transfection reagent (Thermo Scientific; R0532) according to the manufacturer's instructions. A 2–5 µg quantity of DNA was used per reaction based on a 10-cm dish.

For CRISPR-Cas9-mediated KO, guide RNAs were selected using the CRISPR design tool (<http://chopchop.cbu.uib.no/>). A list of oligonucleotides is provided in Supplementary Table 2. Two guide RNAs were designed from two different exons for each target gene. Annealed oligonucleotides were cloned into two different plasmids, Px458 GFP and Px459 Puro, respectively. In brief, HeLa cells were seeded at 2 × 10⁶ cells per 10-cm dish. The following day, cells were transfected with 2.5 µg of the plasmids (control vectors without insert or vectors containing a guide RNA against the target gene). Transfecting medium was exchanged with fresh medium after 4 h. Cells were treated with puromycin for 24 h after transfection followed by FACS sorting (for GFP⁺ cells) the next day. For FACS sorting after 48 h of transfection, cells were trypsinized and resuspended in cell-sorting medium (2% FCS and 2.5 mM EDTA in PBS) and sorted on a BD FACS AriaIII Cell Sorter. GFP-positive cells were collected and seeded in a new well.

Immunoprecipitation assays. HEK293 cells were co-transfected with the indicated DNA constructs. After 36–48 h of transfection, protein extracts were prepared in lysis buffer (1% NP-40, 50 mM Tris/HCl pH 7.5, 150 mM NaCl) and Halt protease inhibitor cocktail (Thermo Scientific; 186 1279) at 4 °C for 20 min followed by centrifugation at 4 °C for 20 min at 13,000 r.p.m. Immunoprecipitations were performed as previously described³⁵. In brief, protein extracts were incubated with Trap beads (nanobodies for GFP (GFP-Trap_A; gta-20-chromotek), myc (Myc-Trap_A; yta-20-chromotek), turbo-GFP (TurboGFP-Trap_A; tbt-20-chromotek) for 4 h at 4 °C with rotation, and then washed five times with lysis buffer (1 ml). Protein complexes were eluted by heating beads for 5 min at 95 °C in 2× sample buffer and resolved by SDS-PAGE on 10% and 12.5% gels followed by immunoblot analysis. Blots were developed using Amersham ECL Prime Western Blotting Detection Reagent (RPN2236) and X-ray film (Amersham Hyperfilm ECL-28906839).

Western blot analysis. Cells were collected and lysed in lysis buffer (50 mM Tris/HCl, 150 mM NaCl, 1% NP-40) containing a protease inhibitor cocktail (Roche). Protein concentrations were determined in all experiments using the Bio-RAD protein assay (Bio-RAD; 500-0006) and 20–40 µg of total protein was loaded onto either 10 or 12.5% SDS-PAGE gels before transfer onto nitrocellulose membranes (Amersham Protran; 10600003). Membranes were blocked with 5% milk, 0.1% Tween20 for 60 min at room temperature. The primary antibody incubation was overnight at 4 °C and the secondary HRP-coupled antibodies were incubated for 1 h at room temperature. The blots were developed using Amersham ECL Prime Western Blotting Detection Reagent (RPN2236) and X-ray film (Amersham Hyperfilm ECL-28906839) or the Fusion FX7 (Vilber Lourmat) image acquisition system.

Antibodies. The following antibodies were used in this study: polyclonal rabbit anti-VIPAS39 (20771-1-AP; Proteintech; 1:2,000), polyclonal rabbit anti-Rab11FIP5 (NBP1-81855; Novus Biologicals; 1:2,000), polyclonal rabbit anti-EHD1 (NBP2-56035; Novus Biologicals; 1:2,000), polyclonal rabbit anti-rabenosyn-5 (NB300-813; Novus Biologicals; 1:2,000), monoclonal mouse anti-myc (9E10) (1:3,000 for western blotting and 1:200 for immunostaining; Sigma-Aldrich; M4439), polyclonal rabbit anti-GFP (TP401; Torrey Pines; 1:3,000 for western blotting and 1:200 for immunostaining). For pulldowns, Trap beads (nanobodies) were used. GFP-Trap_A (chromotek; gta-20) was used for GFP pulldowns and myc-Trap_A (chromotek; yta-20) was used for myc pulldowns. HRP-conjugated goat anti-mouse IgG (H + L) secondary antibody (Thermo Fisher Scientific; 31430; 1:10,000) and polyclonal HRP-conjugated goat anti-rabbit IgG (Thermo Fisher Scientific; 31460; 1:10,000) were used (incubated for 1 h at room temperature) to detect bound antibodies with an ECL system (ECL prime, Amersham, RPN2232).

Alexa Fluor 488–goat anti-rabbit IgG (H + L) (Invitrogen; A-11034) and Alexa Fluor 594–goat anti-mouse IgG (H + L) cross-adsorbed secondary antibodies (Invitrogen; R37121) were used for immunofluorescence.

Immunostaining in mammalian cells. Cells were plated onto sterile 13-mm glass coverslips. Cells were fixed with 2% paraformaldehyde for 15 min, permeabilized (0.1% Triton X-100 in PBS) for 5 min and blocked with 2% BSA containing 5% goat serum in PBS for 1 h. Coverslips were incubated in primary antibodies for 2 h and washed five times in PBS followed by a 1-h incubation in fluorescently tagged secondary antibodies. After secondary antibody incubation, coverslips were washed a further five times in PBS and mounted onto glass slides using Fluoromount-G (Southernbiotech; 0100-01). Images were taken with an inverted Olympus FV1000 confocal microscope using a Plan Apochromat N 60 \times /1.40 silicon oil objective with z-stacks. Co-localization studies were performed using the ImageJ co-localization plugin JACoP.

Tfn recycling assay. The recycling assay was mainly performed according to ref.⁵⁶, with some modifications. For immunoblotting, 600,000 cells were grown in a 6-well plate. The following day, cells were starved for 1 h in serum-free medium at 37 °C and then treated with 20 μ g ml⁻¹ of Tfn-biotin for 1 h in serum-free medium. Cells were then chased with holo Tfn (100 μ g ml⁻¹) and deferoxamine mesylate (100 μ M; to prevent re-internalization) in serum-containing medium for different times. At each time point of interest, cells were washed three times with ice-cold PBS and treated with proteinase K (500 g ml⁻¹) for 30 min. To neutralize Proteinase K, cells were treated with 2 \times phenylmethylsulfonyl fluoride for 10 min. Cells were collected in a microfuge tube and washed twice with ice-cold PBS. Cells were lysed with lysis buffer and subjected to immunoblotting with streptavidin HRP.

For imaging, cells were grown in 8-well imaging chambers. The following day, cells were starved for 1 h in serum-free medium at 37 °C and then treated with 10 μ g ml⁻¹ of Tfn-Alexa-594 for 1 h in serum-free medium. Cells were then chased with holo Tfn (100 μ g ml⁻¹) and deferoxamine mesylate (100 μ M; to prevent re-internalization) in serum-containing medium for different times. At each time point of interest, cells were washed once with ice-cold PBS, treated with 0.1 M glycine (pH 3.5) for 45 s followed by two washes in ice-cold PBS, and then fixed in 4% paraformaldehyde followed by washing with PBS. Cells were then permeabilized with 0.1% Triton X-100 for 5 min, and washed three times with PBS. Cells were covered with ibidi mounting medium for imaging.

Live cell imaging. For live imaging, cells were plated in an 8-well chambered coverslips and medium was replaced with warm imaging buffer (5 mM dextrose (D(+)-glucose, H₂O, 1 mM CaCl₂, 2.7 mM KCl, 0.5 mM MgCl₂ in PBS) just before imaging. Images were taken at 37 °C on an inverted Axio Observer Zeiss microscope (Zeiss) using a Plan Apochromat N 63 \times /1.40 oil DIC M27 objective with a Photometrics Prime 95B camera. Z-stack images were processed using the OMERO client server web tool and Fiji.

DNA plasmid sources. The following commercially available plasmids were obtained: VPS33B-myc-DDK (Origene; RC203870), myc-DDK-VIPAS39 (Origene; RC202264), GFP-VIPAS39 (Sino.Bio; HG22032_ACG), myc-DDK-VPS45 (Origene; RC206027), Turbo-GFP-VPS45 (Origene; RG206027), myc-DDK-rabenosyn-5 (Origene; RC239555), GFP-rabenosyn-5 (Addgene; 37538), RFP-rabenosyn-5 (Addgene; 37537), GFP-RAB11 (Addgene; 12674), myc-DDK-ANK1 (Origene; RC220763), myc-DDK-FIP5 (Origene; RG206173), myc-DDK-EHD1 (Origene; RC211158), myc-DDK-FIP2 (Origene; RC210414). The plasmids P₄₅₈ GFP (Addgene; 48138) and P₄₅₉ Puro (Addgene; 62988) were used for cloning gRNAs.

Compartment quantifications. The length of RAB-10 tubules was measured by applying a freehand line ROI in one z plane; for the size of the RAB-11 compartments, the elliptical selection tool was used and the area in pixels was measured. Both methods might lead to an underestimate of the real sizes, because tubules and globular compartments were not measured in three-dimensional (3D) projections, but the differences between the WT and mutant phenotypes were sufficiently large so that more complicated quantification methods were not essential. In all cases, six different worms were analysed and ten structures per worm were measured (in different z planes).

The size of the RAB-10 globular compartments could be measured in a more automated way because they are very bright and sufficiently separated from each other (in contrast to those of RAB-11 where only the outlines of the enlarged compartments were visible and vesicles clustered together). Maximal z projections were carried out on the whole stack of pictures, yielding about 50–120 vesicles per worm (6 worms per condition were measured). The threshold was set and the pictures were transformed into binary images. The 'dilate' and 'watershed' functions were applied to remove single pixels and fused objects. Particles were analysed (size setting = 0-infinity and circularity = 0.5–1.0). Extremely large accumulations of objects that escaped the 'watershed' function were manually excluded from the final analyses.

Quantification of Rab11-positive endosomes. Segmentation and analysis were performed on manually chosen ROIs using a custom script for Fiji⁵⁷ as follows. First, a 3D white top-hat filter⁵⁸ was applied to the original image to homogenize

the background and used to compute 3D seeds⁵⁹ with subpixel accuracy. Next, objects were segmented on the original image using an iterative threshold⁶⁰ and converted to labels. Touching objects were then separated by a 3D watershed⁶¹ using the previously identified seeds on the label image. The resulting image was then added to the 3D ROI Manager⁶² to exclude remaining laterally touching objects and finally perform intensity and size measurements per object. A total of 1,500–2,500 Rab11-positive particles were analysed from 45–60 cells for each condition. The script is available upon request.

Quantification of the corrected total cell fluorescence for the Tfn recycling assay. Cells were selected by the freehand drawing tool in ImageJ. To obtain a background reading, a region next to a cell that had no fluorescence area was also selected. Integrated density and mean grey values of the selected areas were measured. The following formula was used to measure the corrected total cell fluorescence: CTCF = integrated density – (area of selected cell \times mean fluorescence of background readings).

The normalized value of three independent experiments was averaged.

Quantification of western blot data. Immunoblots of different proteins (antibodies) were quantified in ImageJ software. The intensity of the loading control immunoblots was used for normalization to ensure equal protein contents of the lysates. The normalized value of three independent experiments was averaged.

RNA isolation, cDNA preparation and quantitative real-time PCR. Total RNA was collected from human cells by using the RNeasy mini kit (QIAGEN_74104) according to the manufacturer's protocol. Afterwards, 1,000 ng RNA was reverse transcribed into cDNA using the cDNA synthesis kit GoScript Reverse Transcriptase and the GoScript buffer mix Oligo-dT (Promega_A2791) following the instructions given by the suppliers. A 250 nM concentration of the primers and 3 μ l of the cDNA product were then used for quantitative real-time PCR using GoTaq qPCR Master Mix (Promega_A600A) supplemented with CXR Reference Dye (Promega_C541A) that was then analysed using a StepOnePlus Real-Time PCR System (Applied Biosystem). The relative levels of the target transcripts were determined using the human β -actin transcript as a reference.

Statistics and reproducibility. All immunoblots were performed at least three times unless otherwise noted in the legend. GraphPad Prism 8.0.2 and Excel 2016 were used for the statistical analyses. Statistical analysis was performed using two-tailed *t*-tests.

Reporting Summary. Further information on research design is available in the Nature Research Reporting Summary linked to this article.

Data availability

Source Data for Figs. 1–3 (unprocessed blots), Figs. 1–7 (statistical source data), Extended Data Figs. 1–5, 7 and 8 and Extended Data Figs. 1–7 and 9 (statistical source data) are provided with the paper. All other data supporting the findings of this study are available from the corresponding author upon reasonable request.

References

- Brenner, S. The genetics of *Caenorhabditis elegans*. *Genetics* **77**, 71–94 (1974).
- Beuret, N. et al. Amyloid-like aggregation of proinsulin in diabetes insipidus and secretory granule sorting. *BMC Biol.* **15**, 5 (2017).
- Wartosch, L., Gunesdogan, U., Graham, S. C. & Luzio, J. P. Recruitment of VPS33A to HOPS by VPS16 is required for lysosome fusion with endosomes and autophagosomes. *Traffic* **16**, 727–742 (2015).
- Hsu, F., Hu, F. & Mao, Y. Spatiotemporal control of phosphatidylinositol 4-phosphate by Sac2 regulates endocytic recycling. *J. Cell Biol.* **209**, 97–110 (2015).
- Schindelin, J. et al. Fiji: an open-source platform for biological-image analysis. *Nat. Methods* **9**, 676–682 (2012).
- Legland, D., Arganda-Carreras, I. & Andrey, P. MorphoLibJ: integrated library and plugins for mathematical morphology with ImageJ. *Bioinformatics* **32**, 3532–3534 (2016).
- Tinevez, J. Y. et al. TrackMate: an open and extensible platform for single-particle tracking. *Methods* **115**, 80–90 (2017).
- Gul-Mohammed, J., Arganda-Carreras, I., Andrey, P., Galy, V. & Boudier, T. A generic classification-based method for segmentation of nuclei in 3D images of early embryos. *BMC Bioinformatics* **15**, 9 (2014).
- Ollion, J., Cochenne, J., Loll, F., Escude, C. & Boudier, T. TANGO: a generic tool for high-throughput 3D image analysis for studying nuclear organization. *Bioinformatics* **29**, 1840–1841 (2013).

Acknowledgements

We thank S. Begum and J. Fürst for excellent technical assistance with some of the experiments. The proteomics analysis was performed in the Proteomics Core Facility of the Biozentrum with the help of S. Moes and P. Jenö. The Imaging Core Facility of the Biozentrum facilitated the generation of videos and, in particular, L. Guérard

provided support for image analysis. Cells were sorted in the FACS Core Facility of the Biozentrum. We are grateful to I. G. Macara for critical comments on the manuscript. B. Grant and P. Liu are acknowledged for sharing strains. Some strains were provided by the CGC, which is funded by the NIH Office for Research Infrastructure Programs (P40 OG010440). This work was supported by the Swiss National Science Foundation (CRSII3_141956, 31003A_141207) and the University of Basel.

Author contributions

J.A.S., H.-O.R. and A.S. conceived and designed the study. J.A.S., H.-O.R. and C.P.-B. performed the experiments. J.A.S., H.-O.R., C.P.-B. and A.S. analysed and discussed the data. J.A.S. and A.S. wrote the manuscript with input from all authors.

Competing interests

The authors declare no competing interests.

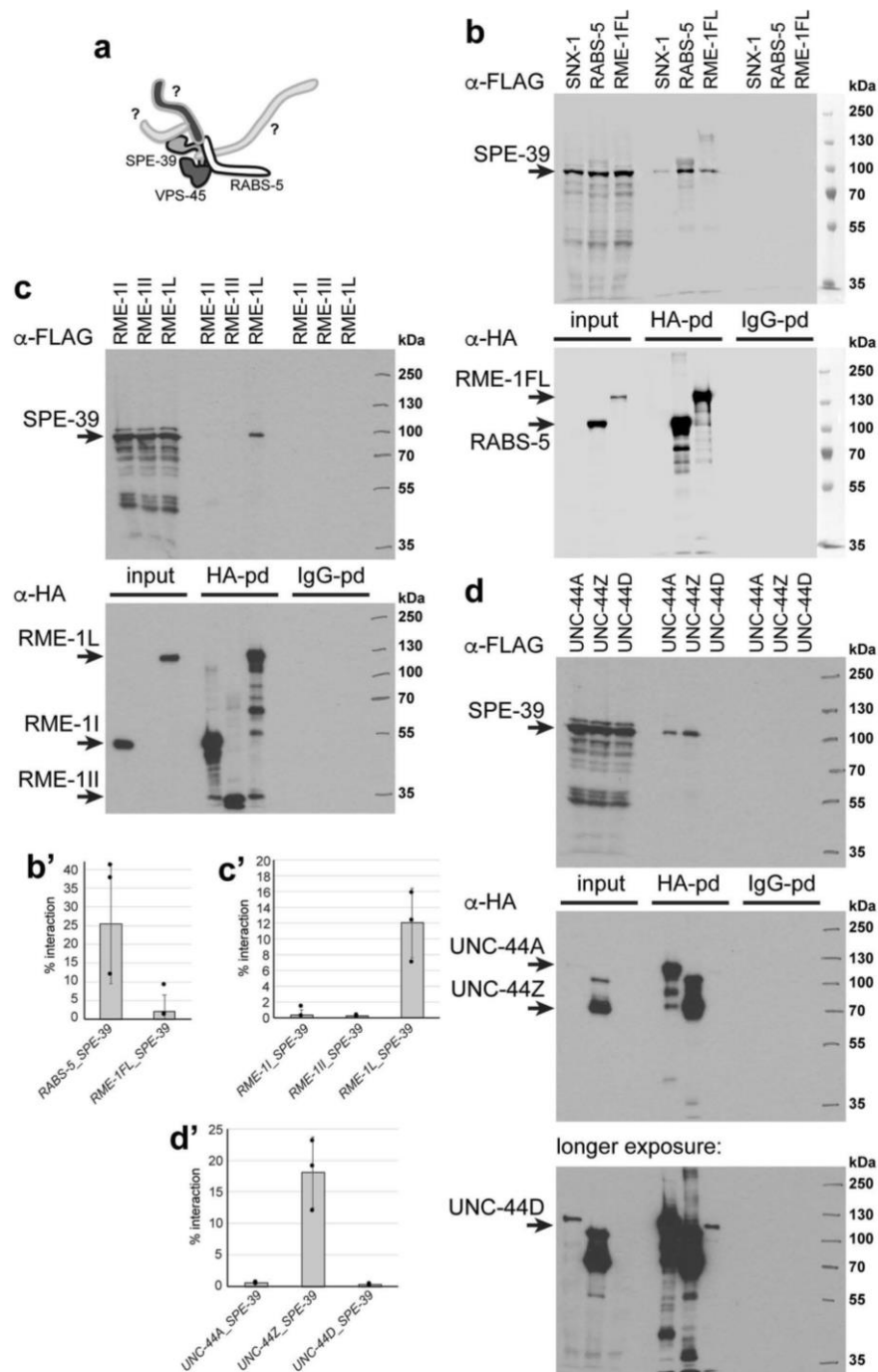
Additional information

Extended data is available for this paper at <https://doi.org/10.1038/s41556-019-0456-5>.

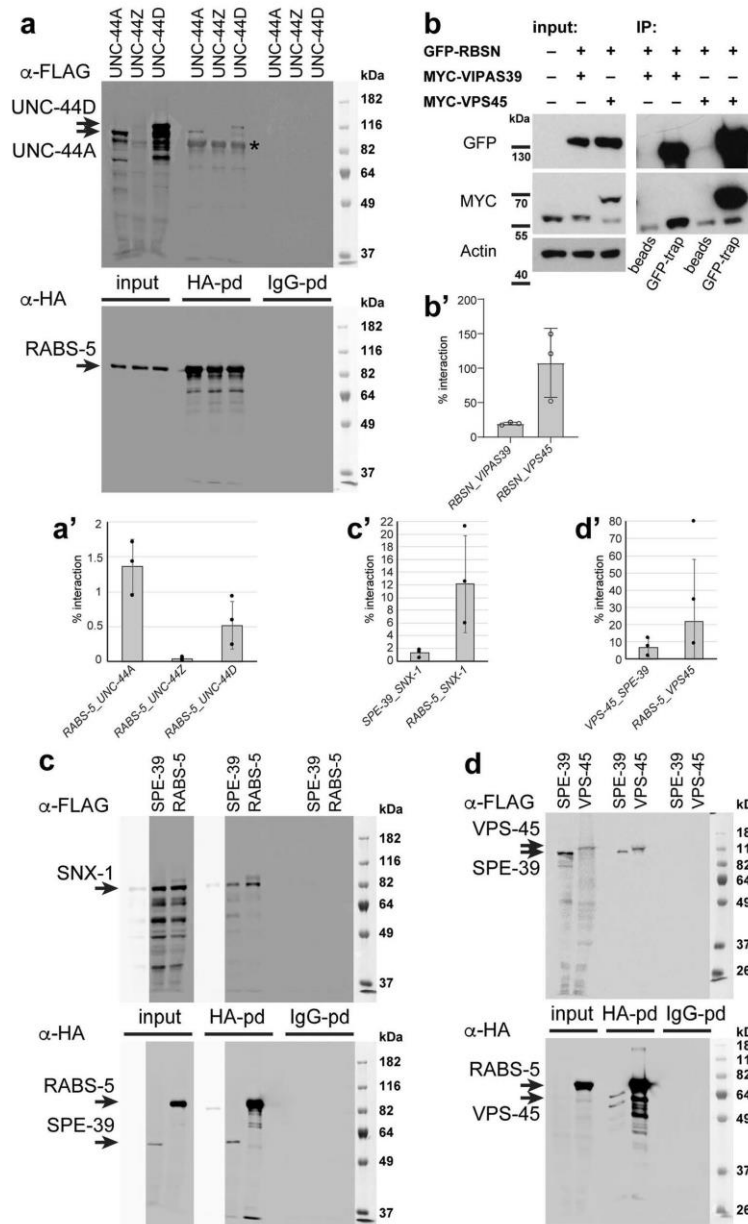
Supplementary information is available for this paper at <https://doi.org/10.1038/s41556-019-0456-5>.

Correspondence and requests for materials should be addressed to A.S.

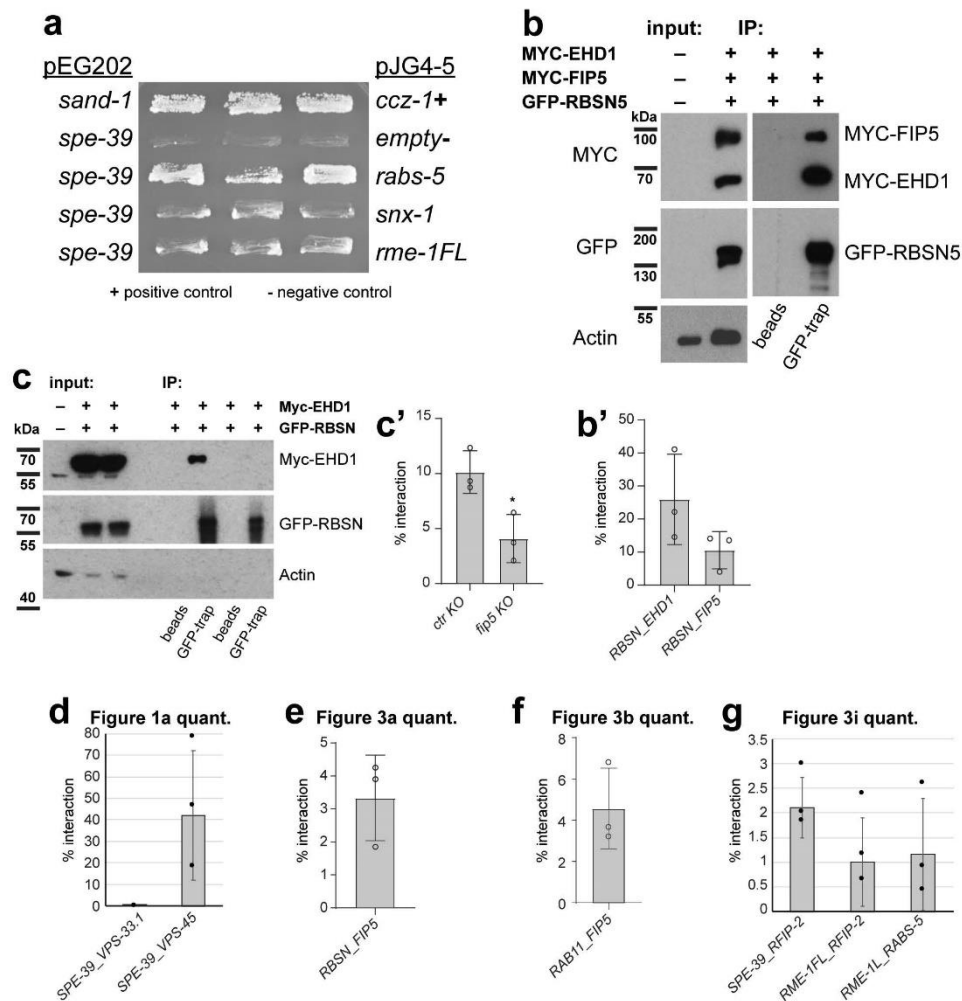
Reprints and permissions information is available at www.nature.com/reprints.



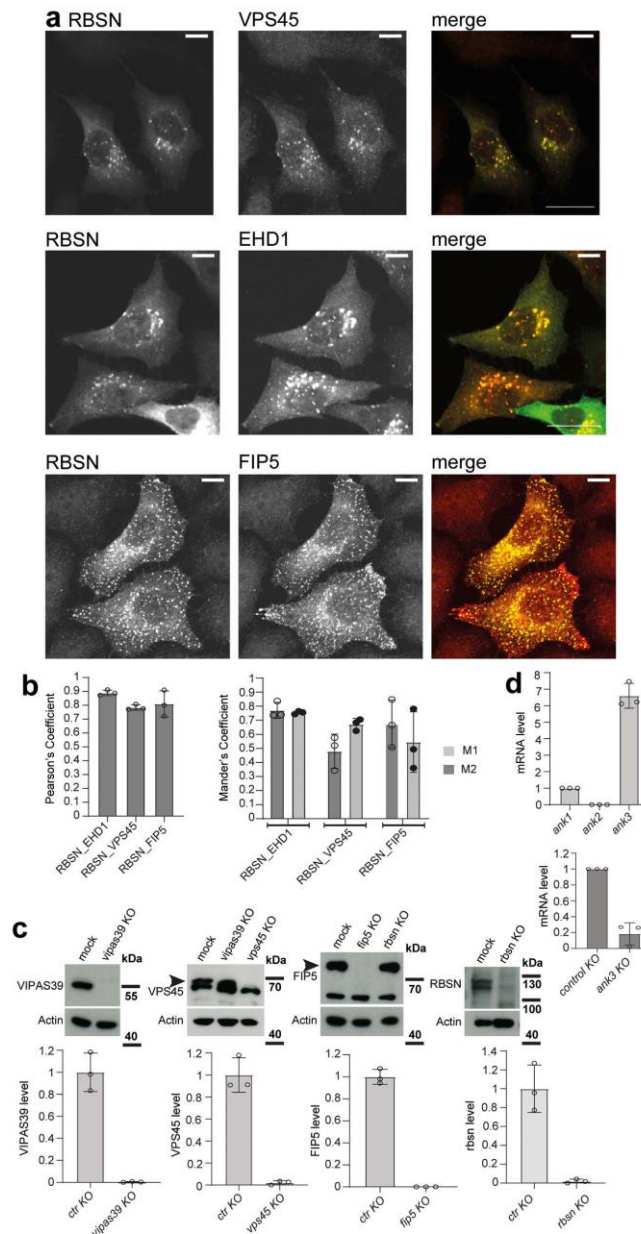
Extended Data Fig. 1 | Pull-downs of FERARI subunits show multiple interactions. **a**, Schematic drawing of the putative FERARI tether. **b**, Pull-downs were performed with extracts from yeasts expressing SPE-39-FLAG and the HA-tagged proteins indicated at the top. Control pull-downs with beads coupled to IgG were also carried out. Arrows on the left indicate the sizes of expressed proteins. $n=3$ independent experiments. Quantification is shown in (**b'**); mean \pm s. d. is given. **c**, Pull-downs showing interactions between SPE-39-FLAG and HA-RME-1 fragments. $n=3$ independent experiments. Quantification is shown in (**c'**); mean \pm s. d. is given. **d**, Pull-downs experiments using SPE-39-FLAG and fragments of UNC-44 (with HA tag). UNC-44D fragment expression is low and can be seen on longer exposure as indicated. $n=3$ independent experiments. Quantification is shown in (**d'**); mean \pm s. d. is given. See Unprocessed Blots Extended Data 1 and Statistical Source Data Extended Data 1.



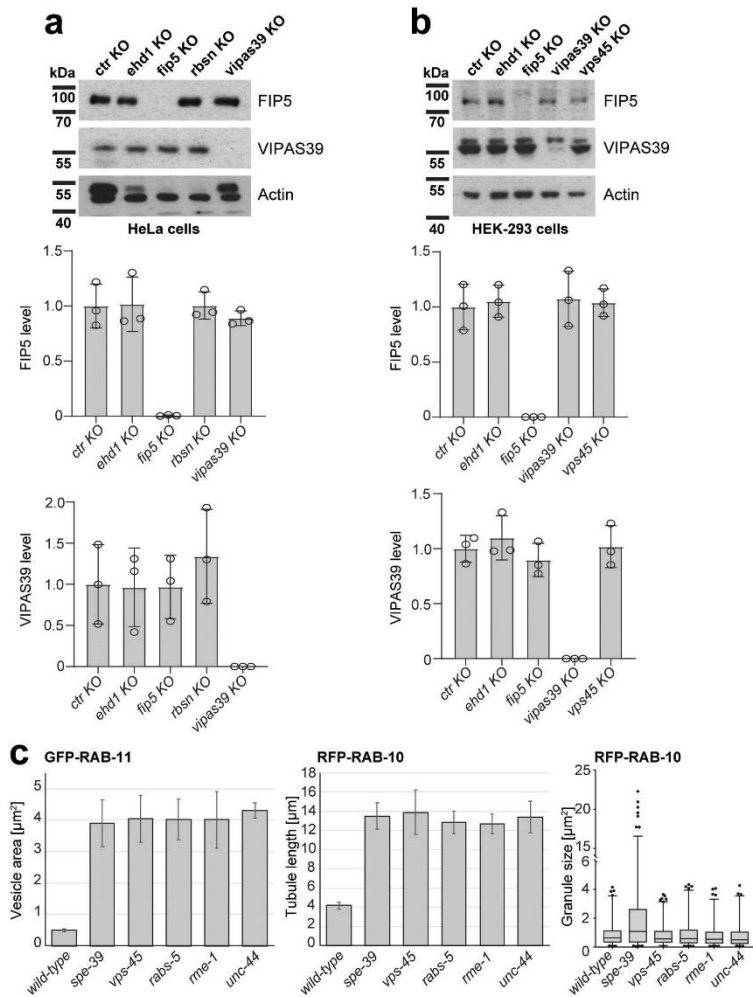
Extended Data Fig. 2 | Determination of FERARI subunits interactions. a, Pull-downs showing interaction between HA-RAB5-5 and fragments of UNC-44 (coupled to FLAG). UNC-44Z was not expressed, anti-FLAG antibody cross-reacted with RAB5-5 (indicated by asterisk). $n=3$ independent experiments. Quantification is shown in (**a'**); mean \pm s. d. is given. **b**, Western blot of the interactions between transiently over-expressed human FERARI components rabenosyn-5, VIPAS39 and VPS45. GFP-Rabenosyn-5 was precipitated with GFP-trap beads, and myc-VIPAS39 and myc-VPS45 co-precipitated. $n=3$ independent experiments. Quantification is shown in (**b'**); mean \pm s. d. is given. **c**, Pull-down experiment showing the interaction of SNX-1 with SPE-39 and RAB5-5. $n=3$ independent experiments. Quantification is shown in (**c'**); mean \pm s. d. is given. **d**, Interactions between SPE-39 and VPS-45 as well as VPS-45 and RAB5-5 in pull-down experiments. $n=3$ independent experiments. Quantification is shown in (**d'**); mean \pm s. d. is given. See Unprocessed Blots Extended Data 2 and Statistical Source Data Extended Data 2.



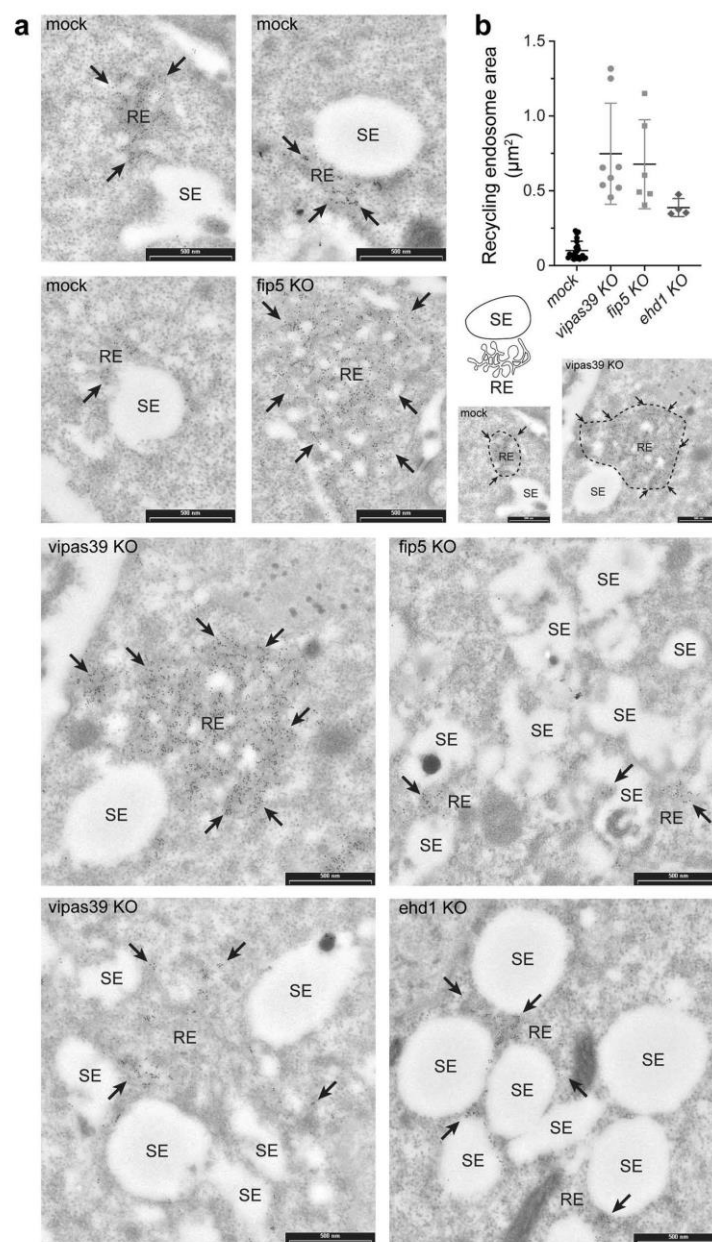
Extended Data Fig. 3 | Interactions of *C. elegans* and mammalian FERARI subunits. a, Yeast two hybrid growth assay showing interactions between SPE-39 (bait) and RABS-5, SNX-1 and RME-1 (preys). $n=3$ biologically independent experiments. **b**, Western blot depicting the interactions between human protein Rabenosyn-5 with EHD1 and Rab11FIP5, co-expressed in HEK-293 cells. GFP-Rabenosyn-5 was used as bait to co-immunoprecipitate myc-tagged EHD1 and Rab11FIP5, $n=3$ independent experiments. Quantification is shown in (**b'**); mean \pm s. d. is given. **c**, Interaction between RBSN and EHD1 is reduced in rab11fip5 KO cells. ctr KO and rab11fip5 KO HEK293 cells were co-transfected with GFP-RBSN and myc-EHD1 as indicated and myc-trap beads were used as bait. Immunoprecipitated proteins and inputs were then probed with antibodies against myc, GFP and actin. $n=3$ independent experiments. Quantification is shown in (**c'**); mean \pm s. d. is given ($P=0.0232$). **d**, Quantification of interactions shown in Fig. 1a, **e**, Fig. 3a, **f**, Fig. 3b and **g**, Fig. 3i. The mean values \pm standard deviations are shown; $n=3$ independent experiments; * $P < 0.05$, ** $P < 0.01$, *** $P < 0.001$, **** $P < 0.0001$, and n.s. $P > 0.05$. Two-tailed Student's t-tests were used for all analyses. See Unprocessed Blots Extended Data 3 and Statistical Source Data Extended Data 3.



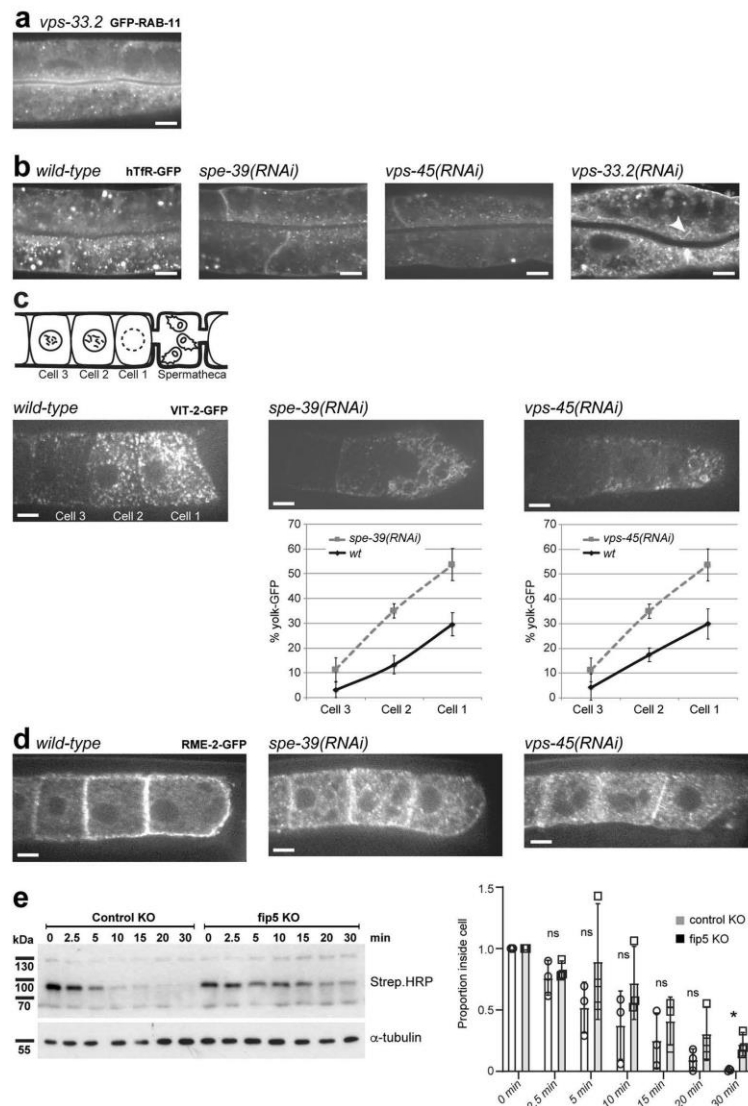
Extended Data Fig. 4 | Human FERARI components interact and co-localize in HeLa cells. a, Co-localization of rabenosyn-5 with human FERARI components VPS45, EHD1, and Rab11FIP5. HeLa cells co-transfected with GFP-Rabenosyn 5 and myc-VPS45, myc-EHD1, myc-Rab11FIP5 were subjected to immunofluorescence staining with GFP and myc antibodies. **b**, Quantification of co-localization shown in (a). $n=95$ cells were analyzed from $n=3$ independent biological replicates. Data show the mean \pm s.d. **c**, Western blot depicting the efficiencies of CRISPR-Cas9 KO of indicated proteins in HeLa cells used for analyses in Fig. 2a and 3c. Corresponding quantifications are shown below each western blot. $n=3$ independent biological replicates (Data show the mean \pm s.d.). **d**, RT-qPCR data represents levels of ank1, ank2 and ank3 mRNA in HeLa cells at endogenous level and in the ank3 KO. $n=3$ independent experiments Data show the mean \pm s.d. See Unprocessed Blots Extended Data 4 and Statistical Source Data Extended Data 4.



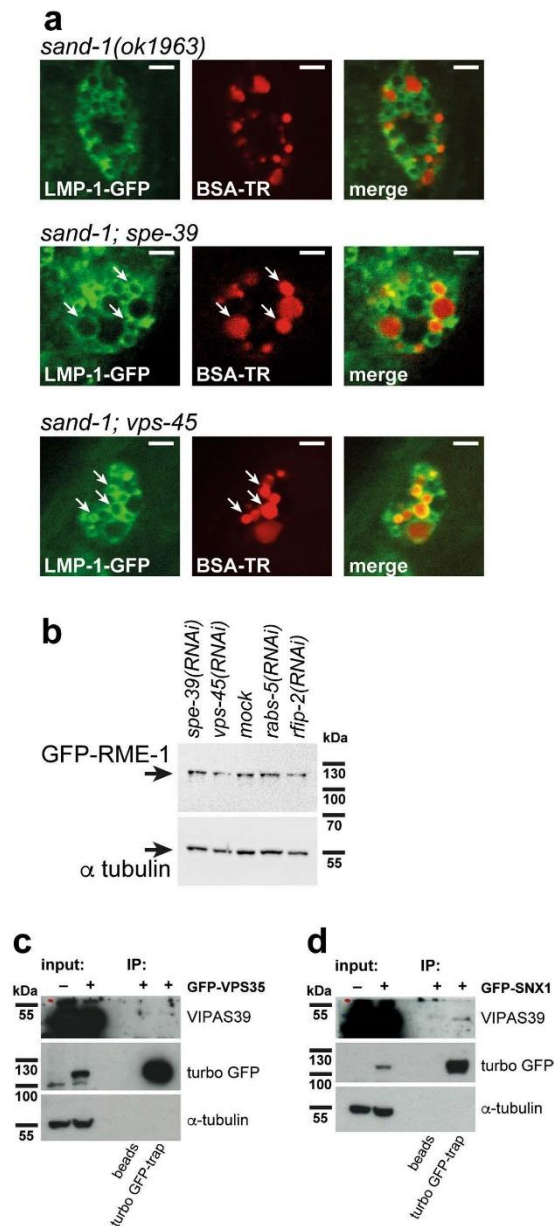
Extended Data Fig. 5 | Analysis of FERARI platform stability and phenotype. a & b. Protein stability of FERARI components in the KO cells. Endogenous levels of Rab11/FIP5 and VIPAS39 were assessed in different FERARI KO HeLa (**a**) and HEK-293 (**b**) cell lines as indicated. $n=3$ independent biological replicates. Data show the mean \pm s.d. **c.** Quantification of RAB-11 and RAB-10 phenotypes shown in Fig. 2e. RAB-11 compartments and RAB-10 tubules were measured in $n=6$ worms ($n=10$ structures each), RAB-10 globular compartments were quantified semi-automatically and comprise $n=50$ – 120 structures (per worm) in $n=6$ different worms. Mean \pm s.d. is given. For the box plot, the box represents 25–75 percentile box with median and the whiskers 1–99 percentile. See Unprocessed Blots Extended Data 5 and Statistical Source Data Extended Data 5.



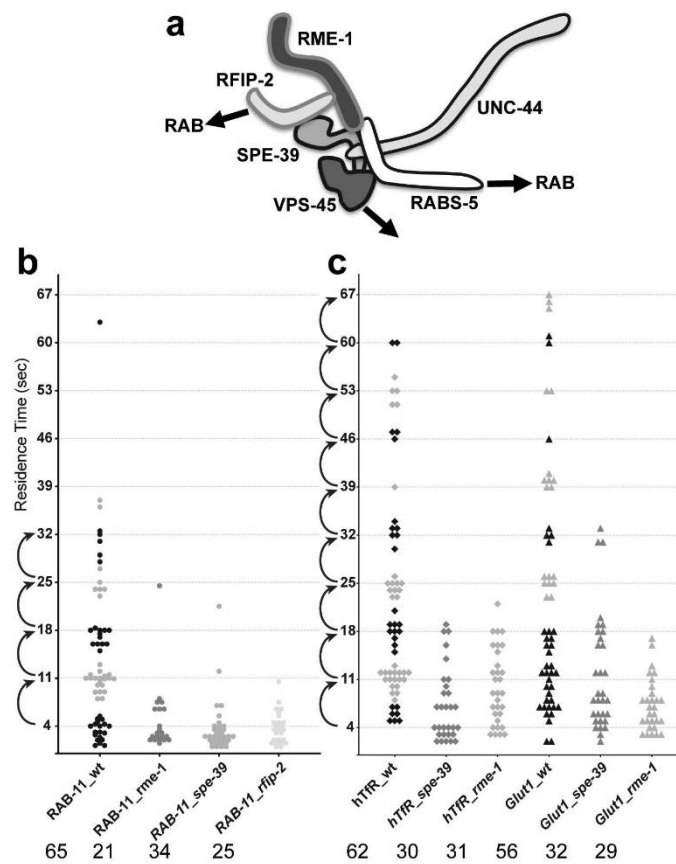
Extended Data Fig. 6 | Morphology of Rab11 compartments is affected by FERAR1 knock-downs in HeLa cells. a, Electron micrographs showing the structure of immunogold labeled Rab11 compartments. HeLa cells with the indicated CRISPR knock-outs were processed for immuno-electron microscopy. Globular sorting endosomes are marked with "SE". Tubular recycling endosomes with Rab11 signals are marked with "RE". Arrows point to densely labeled Rab11 structures containing tubular membranes. Scale bars: 500 nm. **b**, Quantification of recycling endosome sizes in different KO HeLa cells shown in (a). $n=23$ for mock, $n=8$ for *vipas39* KO, $n=6$ for *fip5* KO and $n=4$ for *ehd1* KO cells (mean \pm s.d.). n : number of cells. A schematic representation of sorting endosomes (SE) and recycling endosomes (RE) is shown. For size measurements the recycling endosomes were encircled as shown in the example pictures below the graph. Scale bars: 500 nm. See Statistical Source Data Extended Data 6.



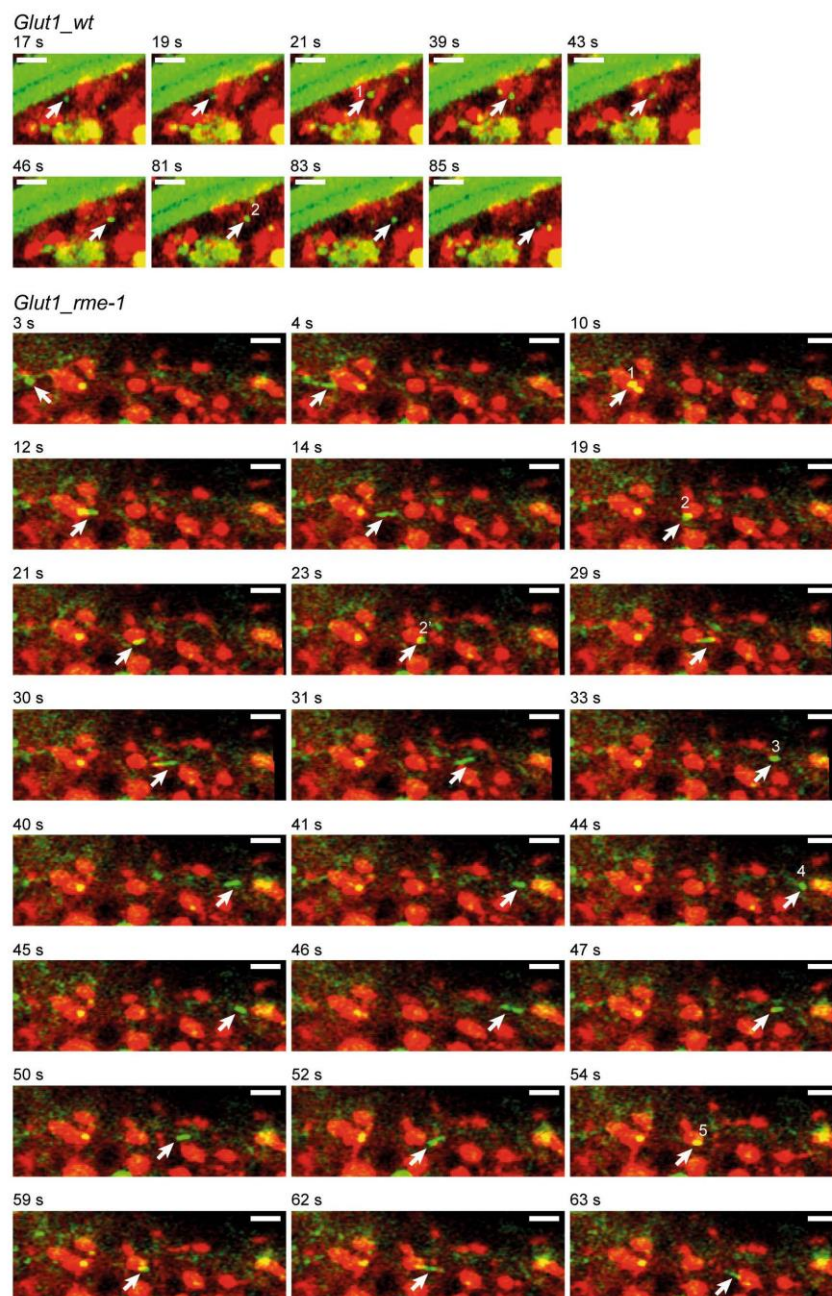
Extended Data Fig. 7 | Function of *spe-39* and *vps-45* in endosomal recycling. **a**, Knock-down of *vps-33.2* in worms has no effect on RAB-11 compartments. $n=3$ independent RNAi experiments with $n=20$ animals. Scale bar: $10\ \mu\text{m}$. **b**, Recycling of hTFR-GFP is abolished in *spe-39(RNAi)* and *vps-45(RNAi)* worms but not in *vps-33.2(RNAi)*. Most hTFR-GFP signal is lost in *spe-39(RNAi)* and *vps-45(RNAi)* worms. $n=3$ independent RNAi experiments with $n=20$ animals. Scale bars: $10\ \mu\text{m}$. **c**, Schematic representation of the last 3 oocytes prior to the spermatheca in the worm gonad. Yolk uptake defect of *spe-39(RNAi)* and *vps-45(RNAi)* worms. $n=3$ independent RNAi experiments with $n=20$ animals. Wild-type uptake of VIT-2-GFP was quantified in the first 3 oocytes before the spermatheca. The measurements were normalized to the total fluorescent signal of all 3 wild-type cells. Knock-down of *spe-39* and *vps-45* show a reduction of yolk uptake. $n=6$ gonads were quantified for each RNAi experiment. Scale bars: $10\ \mu\text{m}$. **d**, The yolk receptor RME-2-GFP is mis-localized in *spe-39(RNAi)* and *vps-45(RNAi)* worms. $n=3$ independent RNAi experiments ($n=20$ animals). Scale bars: $10\ \mu\text{m}$. **e**, Transferrin recycling is reduced in *rab11fip5KO* HeLa cells. After 1 h starvation ctrl KO and *rab11fip5KO* cells were treated with Transferrin Biotin. Cells were then chased with holo transferrin up to 30 min, and cell lysates were subjected to immunoblot with Streptavidin HRP. Quantification of the immunoblot: The mean \pm s.d. values are shown; $n=3$ independent experiments. ($P=0.5249$ at 2.5 min; $P=0.2764$ at 5 min; $P=0.2169$ at 10 min; $P=0.4093$ at 15 min; $P=0.1949$ at 20 min; $P=0.01901$ at 30 min). * $P<0.05$, ** $P<0.01$, *** $P<0.001$, **** $P<0.0001$ and n.s., $P>0.05$. Two-tailed Student's t-tests were used for all analyses. See Unprocessed Blots Extended Data 7 and Statistical Source Data Extended Data 7.



Extended Data Fig. 8 | Loss of recycling by *spe-39(RNAi)* or *vps-45(RNAi)* partially rescues a *sand-1* mutant and endogenous VIPAS39 interacts with SNX1. **a, Knock-down of *spe-39* or *vps-45* induces the degradation pathway in coelomocytes. In *sand-1(ok1963)* coelomocytes BSA-TR is not transported to the lysosomes (LMP-1 compartment). *spe-39(RNAi)* and *vps-45(RNAi)* will favor the transport of BSA-TR to coelomocytes, probably by abolishing recycling. Arrows indicate LMP-1-positive compartments containing BSA-TR. *n*=3 independent RNAi experiments (*n*=20 animals). Scale bars: 5 μm. **b**, GFP-RME-1 levels were unchanged upon *FERARI(RNAi)*. Western blot analysis of GFP-RME-1 levels in *FERARI(RNAi)* worm lysates. *n*=3 independent experiments. **c**, Endogenous VIPAS39 does not interact with Retromer subunit VPS35 in HEK-293 cells transfected with GFP-VPS35. *n*=3 independent experiments. **d**, GFP-SNX1 transfected HEK-293 cells show slight interaction between SNX1 and endogenous VIPAS39. *n*=3 independent experiments. Very weak interaction (<1%) could not be measured due to overexposed bands in the input. See Unprocessed Blots Extended Data 8.**



Extended Data Fig. 9 | Kiss-and-run at sorting endosomes is quantal. a, Schematic drawing of the *C. elegans* FERARI tether. The Rab interaction modules RFIP-2 and RABS-5 are highlighted. **b**, Quantification of GFP-RAB-11 vesicle residence times. Residence times occur in groups with an approximate 7 s interval. The longer residence times are abolished in FERARI knock-downs. **c**, Quantification of residence times of cargo vesicles containing hTfR-GFP and Glut1-GFP. The quantal distribution of residence times is similar to RAB-11 vesicles and longer residence times are abolished in FERARI RNAi conditions. Numbers of vesicles analyzed are indicated. See Statistical Source Data Extended Data 9.



Extended Data Fig. 10 | Glut1-GFP vesicle dynamics. Movie stills showing Glut1-GFP vesicles docking to and pinching off from mCherry-SNX-1 compartments in mock-treated and *rme-1(RNAi)* worms. (see also movies S20 and S21). $n=56$ for *GLUT1_wt*, $n=29$ for *GLUT1_rme-1*. n represents number of vesicles. Scale bars: 2 μm .

4. FERARI coordinates cargo flow through sorting endosomes

The following manuscript is ready to submit.

Statement of contributions: I conducted all the mammalian experiments. Jachen A. Solinger conducted all the experiments in *C. elegans*.

Professor Anne Spang and Jachen A. Solinger wrote the manuscript. Professor Anne Spang supervised the work. I wrote the figure legends and materials and methods for mammalian part.

4. FERARI coordinates cargo flow through sorting endosomes

Jachen A. Solinger, Harun-Or Rashid and Anne Spang*

Biozentrum, University of Basel, Klingelbergstrasse 70, CH-4056 Basel, Switzerland

*Corresponding Author:

Anne Spang, ORCID:0000-0002-2387-6203

Biozentrum

University of Basel

Klingelbergstrasse 70

CH-4056 Basel

Switzerland

Email: anne.spang@unibas.ch

Phone: +41 61 207 2380

Keywords: tether, recycling endosomes, endocytosis, *C. elegans*, small GTPases, SM protein, SNAREs, vesicle transport, Rab proteins, mammalian cells, CRISPR, membrane fusion, membrane fission, adaptor proteins

Abstract

Cellular organization, compartmentalization and cell-to-cell communication are crucially dependent on endosomal pathways. Sorting endosomes provide a transit point for various trafficking pathways and decide the fate of proteins: recycling, secretion or degradation. FERARI (Factors for Endosome Recycling and Rab Interactions) plays a key role in shaping these compartments and coordinates Rab GTPase function with membrane fusion and fission of vesicles through a kiss-and-run mechanism. Here we show that cargo concentration in sorting endosomes determines the length of the kiss between Rab11 and SNX1 structures, presumably by clogging the fusion stalk. Cargo flow from sorting endosomes into Rab11 structures relies on the cargo adaptor SNX6, while retention in the Rab11 endosome is dependent on AP1. Similar to Rab11, Rab5 and Rab10 positive endosomes also interact with the SNX1 tubular network through FERARI-dependent kiss-and-run. We propose that FERARI, together with cargo adaptors, coordinates the vectorial flow of cargo through sorting endosomes.

4.2 Introduction

Cells are constantly interacting and exchanging materials and signals with their surroundings. To accomplish this, they need to have efficient machineries for uptake and recycling of proteins and solutes. While the uptake of cargo through endocytosis has been extensively studied and is quite well understood, the recycling and sorting part of the cycle is less clear (Scott, Vacca, and Gruenberg 2014; Spang 2016). Many factors involved in endosomal sorting and recycling have been described (Cullen and Steinberg 2018), and microscopic analyses revealed a fascinating and complex network of dynamic tubules, where these processes take place (Klumperman and Raposo 2014). Current models concentrate on early sorting events occurring directly at Rab5-positive structures (Gallon and Cullen 2015). Sorting nexins (SNXs) with membrane tubulation activities form tubules, where adaptor proteins are recruited and attract cargo. These transport carriers acquire the appropriate Rab GTPase (e.g. Rab11) and will be pinched off to form vesicles with defined cargoes, which can be directly transported to their destination. These transport routes use retromer and retriever complexes for the transport of many different cargoes to their final destinations (K.-E. Chen, Healy, and Collins 2019). While this model addresses many features of cargo sorting and recycling it cannot explain the presence of large tubular recycling networks or how low binding affinities of cargo adaptors can ensure efficient separation and sorting of cargoes. We recently described an additional mechanism by which cargo sorting might occur at sorting endosomes. In this process, FERARI promotes a kiss-and-run between Rab11 positive recycling vesicles and the tubular sorting compartments marked by SNX1 (Solinger et al. 2020). FERARI contains proteins for tethering (Rab11FIP5, Rabenosyn 5), SNARE interactions (VPS45), binding to SNXs (VIPAS39), scaffolding and protein-protein interactions (ANK1) as well as membrane tubule stabilization and pinching (EHD1) (Solinger et al. 2020). The integration of all these factors for

recycling into one machinery allows for a tightly regulated mechanism of tethering, docking, cargo exchange and fission of vesicles. However, more studies are needed to fully understand the process of cargo sorting in endosome recycling.

In this study, we find that the length of the kiss between the recycling and the sorting endosome correlates with cargo concentration in the sorting endosome. Moreover, the cargo adaptor SNX6 on sorting endosomes regulates the flow of cargo into the recycling endosome. Unexpectedly, Rab5 and Rab10 positive endosomes also undergo FERARI mediated kiss-and-run at SNX1 endosomes with similar kinetics than Rab11 positive structures. Our data are consistent with a model in which cargo flows from Rab5 positive early endosomes through the SNX1 sorting compartment into Rab11 recycling endosomes. In this model, HRS appear to retain cargo in the Rab5 endosomes that should be going down into degradative pathway, while adaptor complex 1 (AP1) prevents cargo from diffusing back into the sorting endosomes. Therefore, interactions between cargo and their adaptors controls their vectorial flow from early to recycling endosomes.

4.3 Results

Cargo amount determines length of the kiss between RAB-11 and SNX-1 compartments.

We noticed previously that cargo vesicles containing hTfR-GFP or Glut1-GFP showed extended residence times on SNX-1 compartments compared to RAB-11 vesicles, even though these cargoes would leave the SNX-1 compartment in RAB-11 vesicles (Solinger et al. 2020). We hypothesized that cargo concentration may influence the length of the residence time (kiss). To test this hypothesis, we reduced cargo availability by downregulating hTfR-GFP and Glut1-GFP levels using RNAi against GFP (Fig. S4.7.1A-D). The length of the kiss of hTfR-GFP and Glut1-GFP vesicles was reduced and was comparable to the residence times that we had observed previously for RAB-11, but the 7 sec intervals were not perturbed by the reduced cargo levels (Fig. 4.3.1A and B, Fig. S4.7.1E-I, Solinger et al. 2020).

Next, we asked how cargo availability would influence the Rab11 residence time. We hypothesized that under high cargo concentration cargo might become stuck in the fusion pore or the stalk. As a first test, we built a model based on the stalk diameters to which EHD proteins would bind and the size of hTfR (Daumke et al. 2007), (Pant et al. 2009, 1), (Deo et al. 2018), (Lawrence et al. 1999) (Fig. 4.3.1C). Also based on the literature, cargo would prefer regions of negative membrane curvature (Roux et al. 2005), (Aimon et al. 2014). Therefore, cargo might potentially obstruct the stalk between recycling and sorting endosomes. We envisage the 7s intervals to be the time for an attempted fission event, which was abortive because cargo was still present in the stalk. In a nutshell, cargo in the stalk would directly block membrane fission.

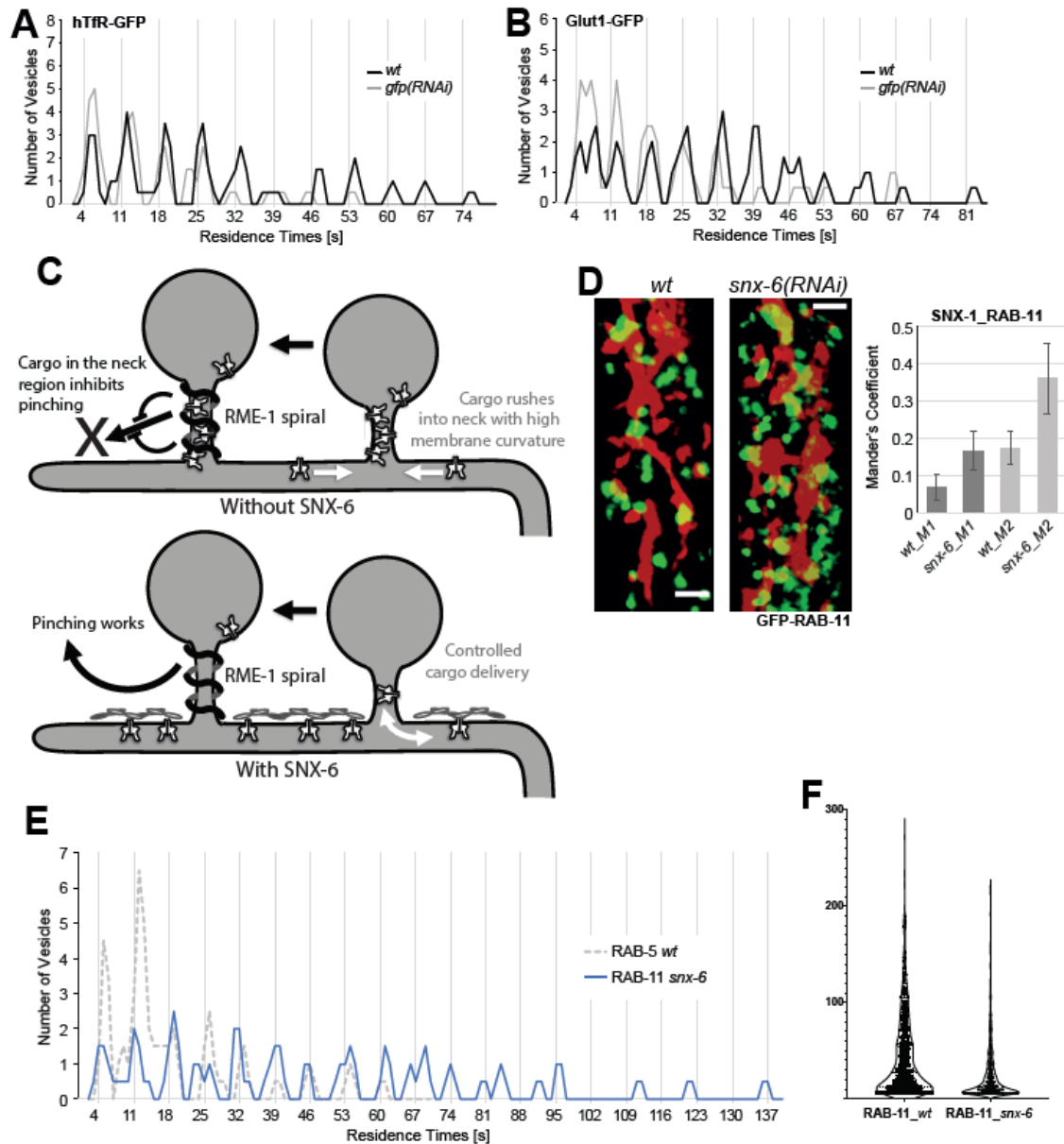


Figure 4.3.1: Cargo flow through sorting/recycling endosomes is regulated by cargo amount and cargo adaptors. (A) Residence times for hTfR-GFP vesicles decrease when cargo amount is reduced. Moving average for residence times is shown for *wild-type* (no knock-down, n=55) and *gfp(RNAi)* (n=46). Graphs with individual vesicle data are shown in Suppl. Fig. 1E. (B) Residence times for Glut1-GFP vesicles decrease when cargo amount is reduced. Residence times are plotted as in (A) for *wild-type* (no RNAi, n=56) and *gfp(RNAi)* (n=54). (C) Models for SNX-6 function and cargo flow through recycling endosomal networks. Schematic representation of possible role of SNX-6 as a cargo organizer in the SNX-1 compartment. Top shows situation without cargo adaptor SNX-6, leading to crowding in vesicle neck and blocked pinching. Bottom shows regulated cargo exchange in the presence of SNX-6. (D) Cargo adaptor *snx-6(RNAi)* leads to increased co-localization of GFP-RAB-11 vesicles with mCherry-SNX-1 networks. Quantification of Mander's coefficients on the right (n=10). (E) Knock-down of *snx-6* cargo adaptor causes very long residence times of kiss & run vesicles. The RAB-5 *wild-type* vesicles from (A) are plotted as a dashed line for comparison. Please note the elongated x-axis to accommodate vesicles with very long residence times (n=57 for RAB-11). (F) Vesicles from *snx-6* cargo adaptor knock-down worms show changes in size. RAB-11 vesicles appeared smaller (wt: n=774, *snx-6*: n=995).

SNX-6 is involved in the regulation of the length of the kiss between RAB-11 and SNX-1 compartments

To ensure proper cargo sorting into the RAB-11 recycling compartment, regulation of cargo flow is required. In fact, cargo sorting in the sorting compartment is supposed to be regulated by multiple cargo adaptors (K.-E. Chen, Healy, and Collins 2019), (Strutt et al. 2019). Mammalian cargo adaptors SNX5 and SNX6 interact with SNX1 (Simonetti et al. 2019), making them prime candidates as potential regulators of cargo sorting. To interfere with sorting into the RAB-11 vesicles, we knocked down the sole *C. elegans* homolog of SNX5/6, SNX-6. The result of the knockdown was threefold. First, we found that at least some of the Rab11 vesicles that would normally just kiss-and-run must have fused with membrane flattening yielding RAB-11 patches on the SNX-1 network (Fig. 4.3.1D). This is also highlighted by the increase in the Mander's coefficients. Second, the RAB-11 vesicles that did undergo kiss-and-run stayed there for long times (Fig. 4.3.1E and Fig. S4.7.2A). Third, in *snx-6(RNAi)* animals the RAB-11 vesicles were smaller than in control animals (Fig. 4.3.1F and Fig. S4.7.2D). All three effects are consistent with a defect in cargo sorting. In the absence of SNX-6, cargo fails to be actively sorted into the recycling vesicles, but instead cargo could diffuse into the neck and interfere with fusion pore closure thereby extending the docked stage between RAB-11 and SNX-1 compartments. Since the cargo flux into RAB-11 vesicles would be suboptimal, they would eventually leave with little cargo resulting in smaller vesicles. Finally, extended kisses could eventually lead to membrane flattening resulting in RAB-11 patches. Taken together, our results so far indicate that cargo amounts and cargo flow regulated by SNX-6 directly affect kiss-and-run and thereby most likely also FERARI function.

SNX5/6 are involved in Rab11-dependent recycling

To test whether the sorting defect caused by *snx-6(RNAi)* was conserved in mammalian cells, we knocked out SNX5 and SNX6 in HeLa cells (Fig. S4.7.3A) and assessed the co-localization of Rab11 and SNX1. Surprisingly, we observed a reduction in the co-localization between Rab11 and Snx1 in *snx5/6* KO cells (Fig. 4.3.2A-B). In part, this decrease in co-localization might be explained by the reduced stability of SNX1 upon loss of SNX5 and SNX6, presumably due to the interaction between SNX1 and SNX6 (Wassmer et al. 2007),(Simonetti et al. 2017). Likewise, we observed a reduction of SNX1-GFP in *snx5/6* KO cells (Fig. S4.7.3B). Moreover, the Rab11 compartment was increased in *snx5/6* KO cells compared to control (Fig. 4.3.2C-D). This phenotype was reminiscent of the one we had observed previously in FERARI KO cells (Solinger et al. 2020). Therefore, we asked whether SNX5 and SNX6 could interact with FERARI. FERARI members RBSN-5 and VIPAS39 specifically co-precipitated with SNX6 but not with SNX5 (Fig. 4.3.2E) indicating a link between the cargo adaptor SNX6 and the tether FERARI. Taken together our data suggest a potential role in the recruitment or stabilization of FERARI on the sorting endosomes. In addition, SNX5 and SNX6 may have additional roles. In fact,

knock-down and knockout of SNX5/6 in RPE cells was reported to yield a defect in CI-MPR retrograde transport

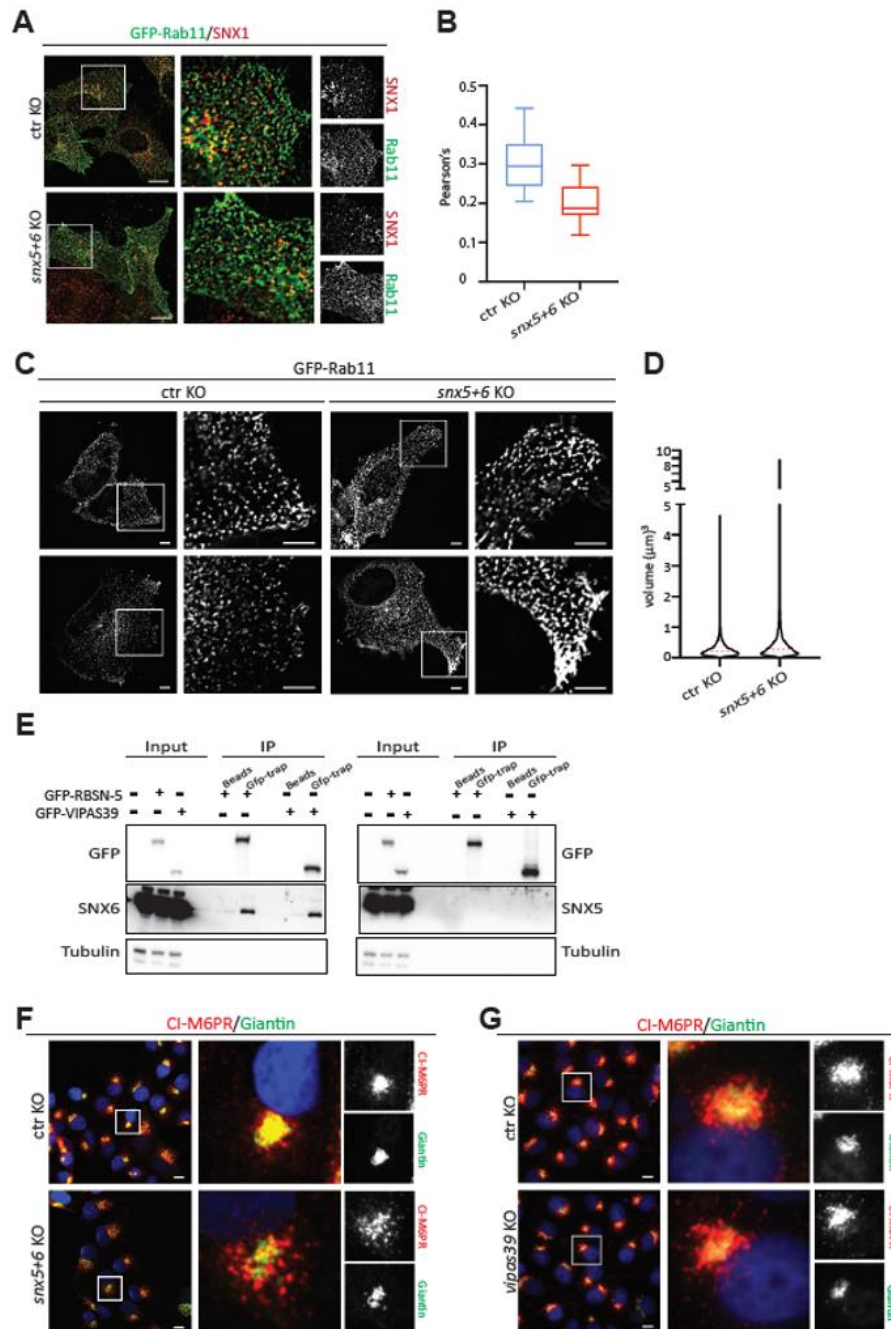


Figure 4.3.2: SNX5/6 are involved in Rab11-dependent recycling. (A) Co-localization between GFP-Rab11 and endogenous SNX1 is reduced in *snx5+6* double knock out cells. Antibodies against GFP and SNX1 were used to detect Rab11 and SNX1 by immunofluorescence, respectively. Scale bars 10 μm ; 5X magnified. (B) Quantification of the pearson's coefficient from 25 cells from each group. (C) Size of the GFP-Rab11 positive structures are enlarged in *snx5+6* double knock out cells in comparison with the CTR KO cells ($n = 3$ independent experiments) Scale bars 10 μm ; magnification 5X. (D) Volume of the GFP-Rab11 positive particles in both CTR and KO cells were determined (volume of around 10000 particles were measured from each group from two independent experiments). (E) Immunoprecipitation data showing that endogenous SNX6 (left panel), but not *snx5* (right panel), binds to FERAR1 members Rabenosyn-5 and VIPAS39 in HEK-293 cells ($n = 3$ independent experiments). (G)

(Figure 4.3.2 continued) CI-MPR trafficking is impaired in *snx5+6* KO cells. CI-MPR (red) is mostly localized in TGN (green) area in CTR KO cells and is dispersed in *snx5+6* KO cells. (H) CI-MPR localization remain unchanged in *vipas39* KO cells (n=3 independent experiments). Scale bars- 10 μ m; magnification 5X.

to the TGN (Wassmer et al. 2007), (Simonetti et al. 2017). We reproduced this phenotype in *snx5/6* KO HeLa cells (Fig. 4.3.2F). This role in retrograde transport is independent of the one that involves FERARI, as FERARI KO cells did not impede CI-MPR retrograde transport to the TGN (Fig. 4.3.2G). Our results are consistent with a role of at least SNX6 in FERARI and Rab11-dependent recycling to the plasma membrane. This role is likely conserved from *C. elegans* to mammalian cells. The difference in phenotypes is most likely related to difference in SNX1 stability, which is not affected in *C. elegans*, explained by the fact that *C. elegans* SNX-1 also represents the functional equivalent of mammalian SNX4 and might be therefore less dependent on SNX-6 binding for stability.

RAB-5-positive structures contact the SNX-1 compartment via kiss-and-run

If cargo flow and cargo adaptors are regulating the length of the RAB-11 kiss, then cargo influx into the SNX-1 compartment might likewise be regulated. Incoming cargo from the plasma membrane is transported in RAB-5 endosomes. Therefore, we explored how Rab5 endosomes would interact with the SNX-1 sorting compartment. Similar to what we had observed for RAB-11 vesicles, RAB-5 vesicles contacted the SNX-1 structures by kiss-and-run (Fig. 4.3.3A). Moreover, even the periodicity of 7 sec was the same than what we had observed for RAB-11 before (Fig. 4.3.3B and Fig. S4.7.2B). Therefore, we tested next, whether FERARI would be involved in tethering RAB-5 and SNX-1 structures. Indeed, when we knocked down FERARI members, the residence time of RAB-5 endocytic vesicles on SNX-1 structures was strongly reduced (Fig. 4.3A-B and Fig. S4.7.2B). To corroborate this finding, we measured the residence time of RAB-5 on FERARI positive structures. We observed the same 7 sec periodicity in the residence time than observed between RAB-5 and SNX-1 (Fig. 4.3.3C and Fig. S4.7.2B), indicating that FERARI is indeed responsible for RAB-5 dependent kiss-and-run of endocytic vesicles on sorting structures. These findings are consistent with cargo influx into the sorting compartment via RAB-5 endocytic vesicles. Therefore, we asked next whether the cargo adaptor SNX-6 would not only regulate cargo efflux but also cargo influx. Upon knock-down of SNX-6, we observed an increase of the co-localization of RAB-5 with SNX-1 (Fig. 4.3.3D), which might be an indication for an increase in the residence time of RAB-5 vesicles on sorting endosomes. Indeed, when we measured the residence time of RAB-5 positive vesicles on SNX-1 endosomes, we saw a large increase, similar to what we observed for RAB-11 (Fig. 4.3.3E). In contrast to the effect on RAB-11 vesicles, which were smaller in *snx-6(RNAi)* animals, RAB-5 vesicles were generally larger under the same condition (Fig. 4.3.3F and Fig. S4.7.2C). Similarly, we observed an increase in both co-localization of Rab5

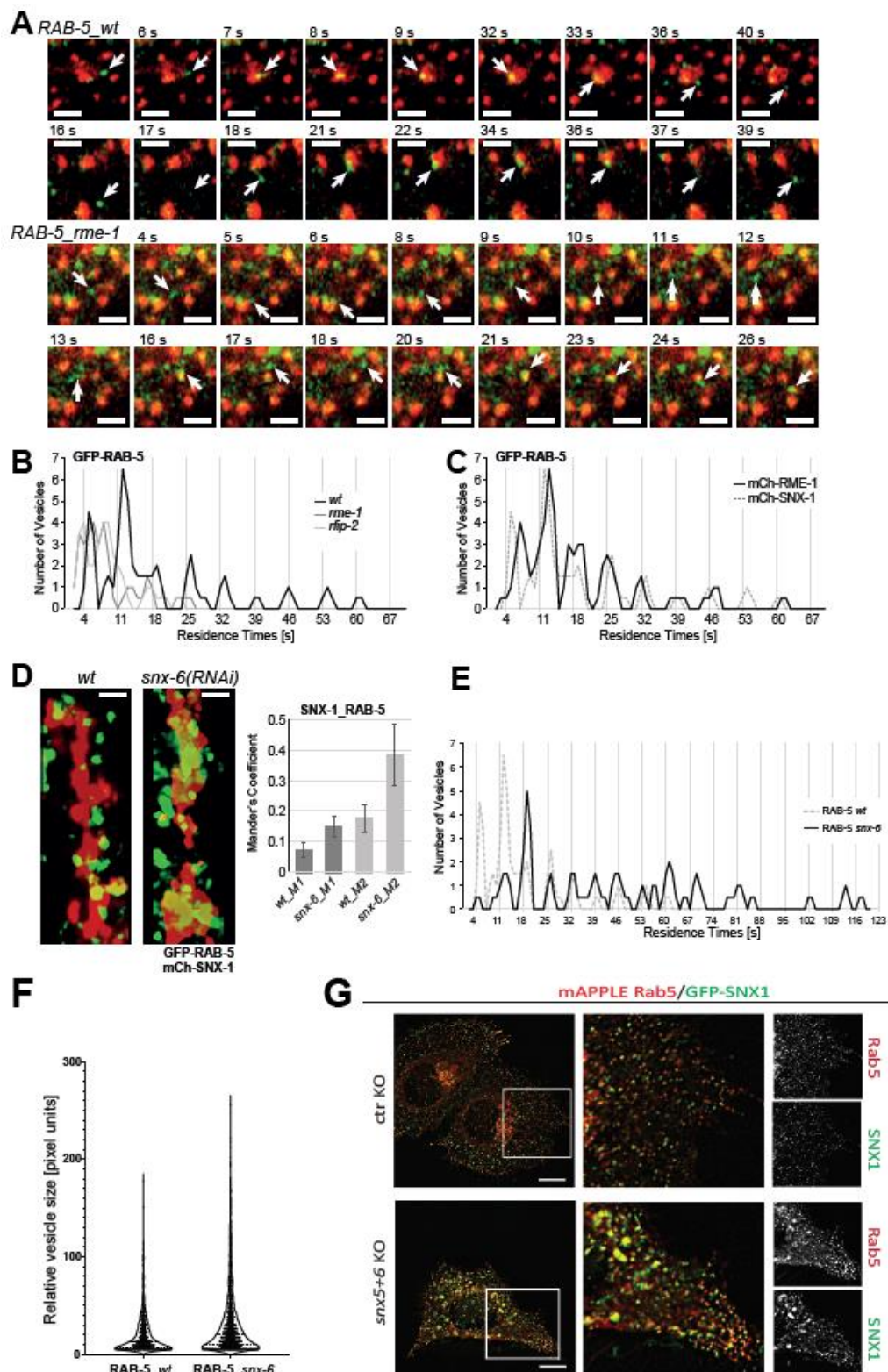


Figure 4.3.3: RAB-5 vesicles exhibit kiss & run behavior dependent on FERARI. (A) Movie stills showing kiss & run of RAB-5 vesicle (arrow) in *wild-type* and *rme-1(RNAi)* worms (see also movie). Scale bar: 2 μ m. (B) RAB-5 vesicles dock on SNX-1 networks with residence times in distinct intervals. Groups of vesicles with similar residence times appear as peaks (see also Suppl. Fig. 2B for single vesicle graph, n=53). This pattern is abolished in *rme-1* (n=33) and *rif-2* (n=35) knock-downs. (C) Residence times intervals also appear in RAB-5 vesicles docking to mCherry-RME-1 compartments (*wild-type* from (B)

(Figure 4.3.3 continued) as comparison, n=63). (D) Cargo adaptor *snx-6* knock-down increases GFP-RAB-5 vesicle co-localization with mCherry-SNX-1 compartments. Mander's coefficients on the right (n=10). : (E) Knock-down of *snx-6* cargo adaptor causes very long residence times of kiss & run vesicles. The RAB-5 *wild-type* vesicles from (A) are plotted as a dashed line for comparison. Please note the elongated x-axis to accommodate vesicles with very long residence times (n=62 for RAB-5). (F) Vesicles from *snx-6* cargo adaptor knock-down worms show changes in size. RAB-5 vesicles were larger (wt: n=828, *snx-6*: n=1459). (G) HeLa cells were co-transfected with GFP-SNX1 and mApple-Rab5. Representative images from live cell imaging of ctr and *snx5+6* KO are shown. Co-localization of Rab5 and SNX1 is increased in *snx5+6* KO cells in comparison with the ctr cells. Furthermore, the structure of both Rab5 and SNX1 looks enlarged in *snx5+6* KO cells in comparison with the ctr cells.

and SNX1 as well as the size of the co-localizing structures in *snx5/6* KO HeLa cells (Fig. 4.3.3G and Fig. S4.7.3C). Thus, it appears as if SNX-6 would trap incoming cargo from the RAB-5 compartment and thereby provide vectorial transport into the sorting compartment, while the ordered release of cargo by SNX-6 into RAB-11 vesicles would regulate efflux from the sorting compartment.

RAB-5 endocytic vesicles are expected to undergo homotypic fusion with other RAB-5-positive compartments supported by the CORVET tethering factor (Spang 2016). In our analyses of kiss-and-run, we also noticed frequent fusion events between RAB-5 vesicles (Fig. 4.3.4A, movie). This type of event was virtually never observed for RAB-11. Interestingly, the homotypic fusion and kiss-and-run could be observed on the same vesicle over time (Fig. 4.3.4A, movie), delineating possible trajectories for RAB-5 vesicles with multiple fusion and kiss-and-run actions taking place, before the vesicle would finally fuse to a larger sorting endosome.

In an effort to characterize the movements of GFP-RAB-7 vesicles, we also analyzed movies of this compartment. We never observed any kiss-and-run of RAB-7 vesicles with the SNX-1 compartment (Fig. 4.3.4B). Larger RAB-7 compartments were stably connected to SNX-1 and did not move around like the smaller vesicles (Fig. 4.3.4B and C, movies). In contrast, homotypic fusion events were frequently observed (Fig. 4.3.4C). This could be expected, based on our knowledge about HOPS tethering factor and its function in promoting fusion of RAB-7-positive compartments (Spang 2016). Taken together, these results suggest a central role of the FERARI machinery in promoting kiss-and-run of at least two types of endocytic vesicles with the sorting compartment.

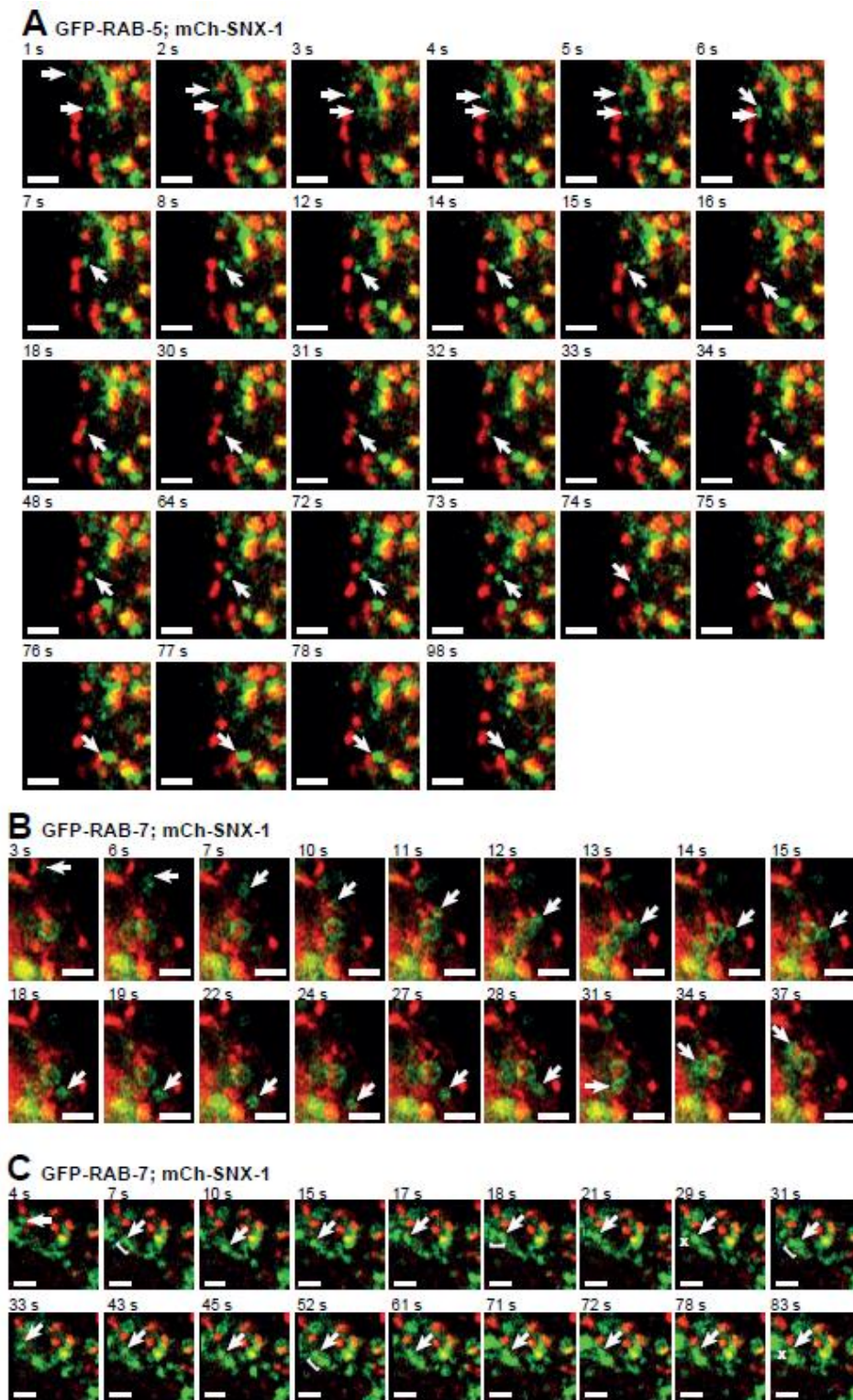


Figure 4.3.4: RAB-5 vesicles undergo homotypic fusion and kiss & run events on their way to the sorting endosome. (A) Movie stills for GFP-RAB-5 positive vesicles fusing, then docking on mCherry-SNX-1 compartment (kiss & run for 18 s) and finally fusing with a larger sorting endosome (with GFP-RAB-5 and mCherry-SNX-1 domains). Scale bar: 2 μ m. (B) RAB-7 vesicle (arrow) with no tethering or kiss & run with SNX-1 compartments (see also movie). (C) RAB-7 homotypic interactions (movie). Fusions are indicated by bracket “[” and fissions by “x”.

Kiss-and-run at SNX-1 sorting compartments might be a common feature

Given our data above, we were wondering, whether this mechanism is even more widespread and asked whether other RAB GTPases could interact with FERARI. To this end, we performed a yeast-two-hybrid assay with RAB-10, the other RAB GTPase known to act on endosomes in *C. elegans* (Fig. 4.3.5A). RAB-10 is involved in recycling to the basal-lateral membrane in polarized cells (C. C.-H. Chen et al. 2006). RAB-10 interacted with Rabenosyn 5. Notably, RAB-7 did not interact with any FERARI member in this assay, consistent with our finding that RAB-7 vesicles do not undergo FERARI mediated kiss-and-run. Encouraged by this result, we determined next the localization of RAB-10 in comparison to SNX-1. We observed RAB-10 vesicular structures docked onto the SNX-1 compartment (Fig. 4.3.5B), similar to what we had observed for RAB-11 previously (Solinger et al. 2020) and for RAB-5 (Fig. 4.3.3D). In addition, RAB-10 genetically interacts with the FERARI members VPS-45 and SPE-39 (Fig. 4.3.5C). Worms carrying the *rab-10* loss-of-function allele (*ok1494*) showed accumulations of enlarged SNX-1 compartments that were drastically enlarged by *vps-45* and *spe-39(RNAi)*.

This phenotype was not observed in *rab-10(ok1494); vps-33.2(RNAi)* worms, implying that the effect was not due to a lack of CHEVI. Since CHEVI and FERARI share the SPE-39 protein, it was important to ascertain the specificity of this phenotype.

We also knocked out Rab10 in mammalian cells (Fig. 4.3.5D). There was a trend towards enlarged SNX1 structures, but not nearly as strong as the phenotype we observed in *C. elegans* (Fig. 4.3.5E). Rab10 plays a major role in recycling to the plasma membrane in polarized epithelia (Babbey et al. 2006) and in specialized trafficking pathways such as GLUT 4 secretion and cholesterol-dependent glutamate receptor recycling (Y. Chen et al. 2012), (Glodowski et al. 2007), but might be less important in HeLa cells and therefore the phenotype would be less obvious.

Thus, at least in *C. elegans*, RAB-10 interacts physically and genetically with FERARI and RAB-10 vesicles appear to dock onto the SNX-1 sorting compartment. Moreover, these RAB-10 vesicles undergo kiss-and-run similar to RAB-5 and RAB-11, and this kiss-and-run is dependent on FERARI function (Fig. 4.3.5F-G and Fig. S4.7.2B). Finally, the co-localization between the FERARI subunit RME-1 and RAB-10 is strongly increased in *snx-6(RNAi)* animals (Fig. 4.3.5H). Therefore, different endocytic vesicles can interact with the sorting compartment presumably in order to exchange cargo.

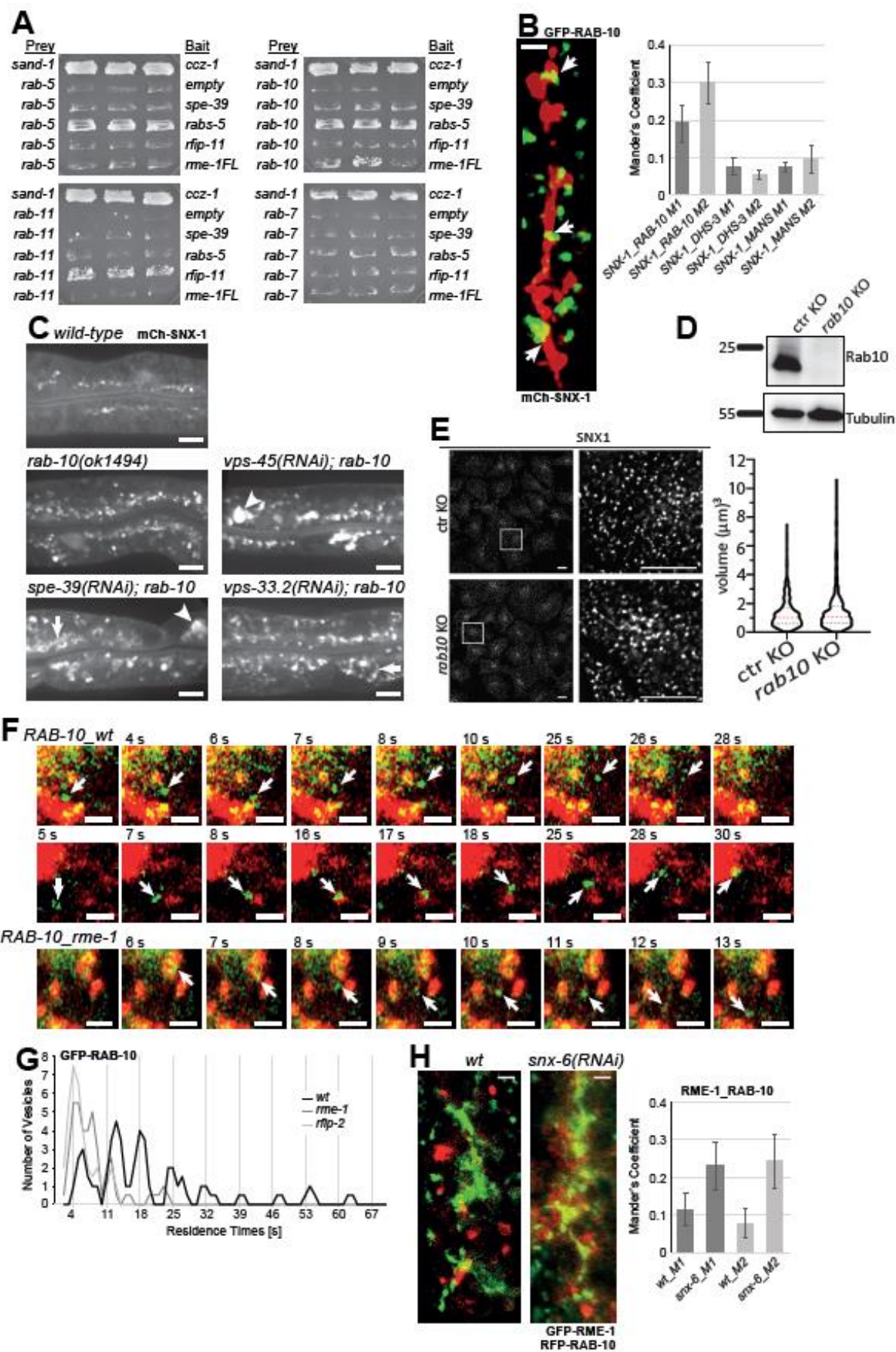


Figure 4.3.5 (previous page): Interactions of RAB-5 and RAB-10 with FERARI. (A) Yeast two-hybrid assay showing binding of RAB-5 and RAB-10 to the RAB-5 subunit of FERARI. RAB-11 interacts through RFP-2, while RAB-7 shows no interaction. n=6 independent transformants. (B) GFP-RAB-10 compartments docking onto mCherry-SNX-1 networks (see also 3D projection movie). Regions of co-localization are indicated by arrows. Quantification of co-localization by Mander's coefficients shows low but consistent overlap between RAB-10 and SNX-1, n=10. Scale bar: 2 μ m. (C) Genetic interaction between FERARI subunits and RAB-10. Knock-out worm strain *rab-10(ok1494)* causes accumulation of SNX-1 compartments, compared to *wild-type*. RNAi of *vps-45* and *spe-39* but not *vps-33.2* (CHEVI) show additional enlargement of SNX-1 (arrowheads). n=20 worms from 3 experiments. Scale bar: 10 μ m. (D) Western blot data depicting the efficiencies of CRISPR-Cas9-mediated KO of *rab10* in HeLa cells (n=3 independent experiments). (E) Size of the endogenous SNX1 structure is enlarged in *rab10* KO cells. Antibody against SNX1 was used to detect endogenous SNX1 by immunofluorescence. Violin plot showing the enlarged volume of the SNX1 structure in ctr and *rab10* KO cells (n=3 independent experiments). (F) Movie stills for RAB-10 vesicle (arrow) showing kiss & run in *rme-1(RNAi)* and *wild-type* worms. (G) RAB-10 vesicles behave in very similar manner as RAB-5 vesicles, showing residence times with quantal increases (n=51). This behavior is abolished in *rme-1* (n=40) and *rfip-2* (n=36) knock-downs. (H) Knock-down of cargo adaptor *snx-6* increases RFP-RAB-10 compartment co-localization with GFP-RME-1 FERARI member. Mander's coefficients are given on the right (n=10).

FERARI interacts with distinct sets of SNAREs for RAB-11 and RAB-10 mediated recycling

RAB-11 is chiefly responsible for recycling to the apical membrane, while RAB-10 promotes recycling to the basal-lateral membrane (Grant and Hirsh 1999),(C. C.-H. Chen et al. 2006). The fusion of the RAB-11 and RAB-10 vesicles with the sorting compartment is mediated by SNAREs. We were wondering whether the same SNAREs would be involved in the fusion event. We have shown previously that the syntaxins SYX-5 and SYX-6 are involved in the fusion of RAB-11 vesicles with the SNX-1 compartment (Solinger et al. 2020). In contrast, RAB-10 appears to use a non-overlapping set of SNAREs. The four different SNAREs *syx-16*, *vamp-7*, *vti-1* and *syx-3* indeed showed the typical elongated tubules found in FERARI knock-downs (Fig. 4.3.6A and B). The two SNAREs *syx-6* and *syx-7* shown previously to affect RAB-11 compartments did not show this effect. On the other hand, *syx-16*, *vamp-7* and *vti-1* did not show any effect on RAB-11 compartments (Solinger et al. 2020). Collectively, these data suggest that there is a specific set of SNAREs for RAB-10 interactions with FERARI. Additionally, the syntaxin SYX-3 was found to partially co-localize with SNX-1 tubular networks. Co-localization could also be observed with the FERARI subunit RME-1 and RAB-10 compartments (Fig. 4.3.6C and D). These observations point to a central role of SYX-3 in the FERARI-mediated docking of vesicles. It might be that SYX-3 is the t-SNARE on recycling tubules. Interestingly, *syx-3* also shows a RAB-11 phenotype similar to FERARI knock-downs (data not shown). Collectively our data suggest that FERARI also mediates fusion of RAB-10 vesicles with the SNX-1 compartment, using a specific set of SNAREs.

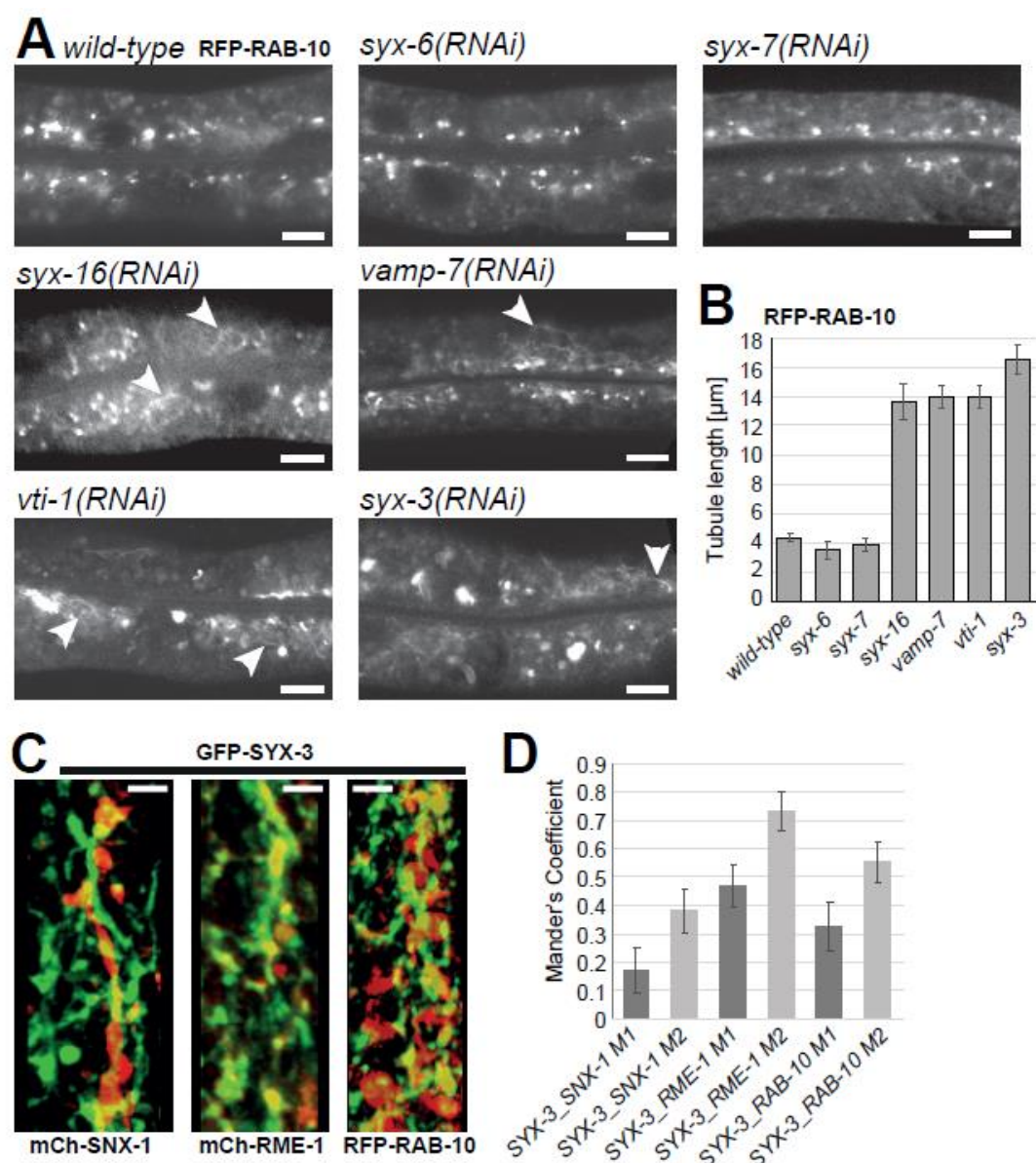


Figure 4.3.6: Specific SNAREs are used to dock RAB-10 vesicles through FERARI. (A) Knock-downs of *syx-16*, *vamp-7*, *vti-1* and *syx-3* cause FERARI-like phenotypes (long RFP-RAB-10 tubules indicated by arrowheads), while *syx-6* and *syx-7* do not. (B) Tubule length was quantified for 10 tubules in 6 worms each. (C) GFP-SYX-3 localizes to mCherry-SNX-1, mCherry-RME-1 and RFP-RAB-10 structures (movies with 3D projections). (D) Mander's coefficients are shown for n=10 worms.

Regulated cargo flux from RAB-5 endocytic vesicles into RAB-11 recycling vesicles requires additional adaptors.

Since the SNX-1 sorting compartment has at least two outlets, RAB-10 and RAB-11 vesicles, it is reasonable to assume that SNX-6 cannot be the sole factor controlling cargo flux. Indeed, different other cargo adaptors were postulated to play roles in cargo sorting during endosomal recycling. The ESCRT machinery sorts cargo for late endosomes and lysosomes away from recycling cargo (Cullen and Steinberg 2018), (Norris et al. 2017). Specific sorting nexins (SNX17

and SNX27) as well as AP1 have been described to promote recycling of cargo (Chi, Harrison, and Burd 2015), (Tan and Gleeson 2019). Therefore, we decided to analyze the effects of these cargo adaptors on cargo flow from RAB-5 endocytic vesicles into RAB-11 recycling structures via the SNX-1 sorting compartment (Fig. 4.3.7A; model). First, we turned to HGRS-1, the *C. elegans* homolog of mammalian Hrs, a subunit of ESCRT-0 involved in sequestering cargo for later inclusion into intraluminal vesicles (ILVs). HGRS should not interact with recycling cargo and therefore allow it to be transferred into the sorting compartment. GFP-HGRS-1 was frequently found on RAB-5 compartments (Fig. 4.3.7B). In addition, moving RFP-RAB-5 vesicles also often contained a domain with HGRS-1 (Fig. 4.3.7C). These results are consistent with our model that ESCRT-0 might sequester cargo away for the degradative pathway, while the remaining cargo would be free to diffuse into the SNX-1 sorting compartment. Consistent with this notion, we observed kiss-and-run between RAB-5 and SNX-1 compartments (Fig. 4.3.3A and B).

How would cargo be retained in the RAB-11 vesicles and prevented from flowing back into the SNX-1 compartment? We considered the more specialized cargo adaptors SNX-17 and SNX-27 and the adaptor complex AP1 for clathrin-dependent delivery of cargoes to the plasma membrane (refs). Blocking the retention in RAB-11 structures would result in cargo trapped in the SNX-1 sorting compartment and therefore enlargement of this compartment. When we knocked down cargo adaptors, we observed in all cases an increase in the size of the SNX-1 sorting compartment, consistent with an accumulation of cargo in these structures (Fig. 4.3.7D, black arrows, Fig. S4.7.4A). Similar to the control, a fraction of hTfR was shunt into the degradative pathway in all cases. Moreover, knockdown of SNX-17 or two subunits of AP-1 lead to accumulation of hTfR in enlarged SNX-1 positive compartments (Fig. 4.3.7D white arrows and E). In addition, we observed structures that were filled with SNX-1, which also often contained hTfR (Fig. 4.3.7D, white arrowheads and asterisks). *snx-27(RNAi)* did not share the accumulation of hTfR, indicating that it may not be involved in hTfR recycling to the plasma membrane. However, since we observed the enlargement of the SNX-1 sorting compartment, we assume that other cargo is trapped under these conditions. Taken together, our data support the hypothesis of cargo influx from RAB-5 vesicles into the SNX-1 sorting compartment, where the vectorial transport is ensured by SNX-6, while the retention of cargo into RAB-11 structures would be mediated by adaptor complexes such as AP1 or SNX-17; both processes would be coordinated by FERARI.

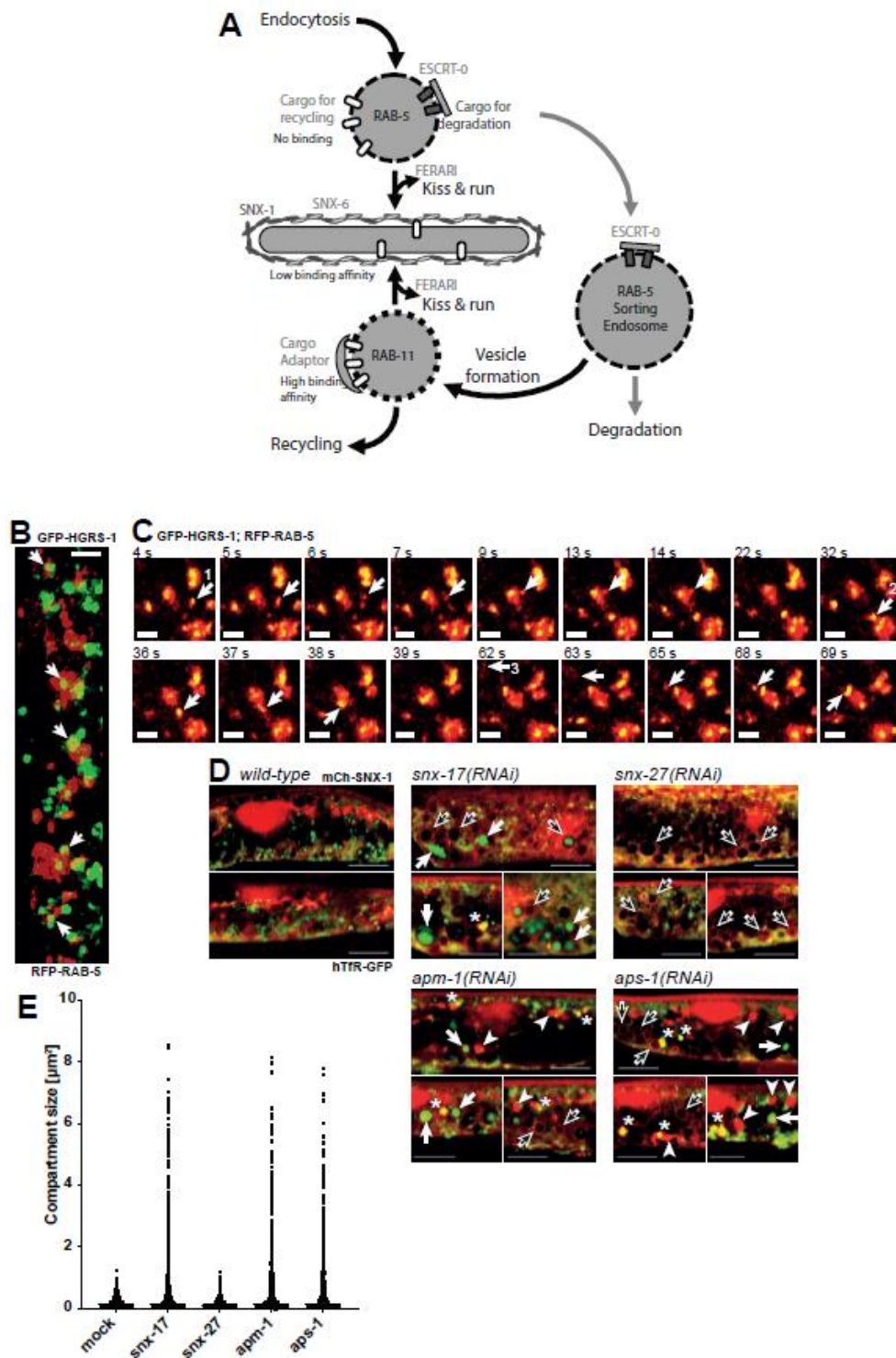


Figure 4.3.7: Effects of cargo adaptors on cargo flow (A) Cargo flow hypothesis, showing 3 subsequent steps of cargo sorting. First, RAB-5 vesicles unload non-bound recycling cargo and enrich ESCRT-bound cargo for transport into late endosomes/lysosomes. Second, low affinity binding to SNX-6 organizes cargo inside the SNX-1 tubular network. Third, higher affinity adaptors in RAB-11 vesicles are used to bind cargo for final transport to destination (e.g. plasma membrane). Subsequent steps of kiss & run ensure enrichment of wanted cargos (and loss of unwanted ones), allowing for a “proofreading” of cargo content despite low binding affinities to adaptors. (B) ESCRT-0 subunit HGRS-1 can frequently be found on RAB-5 compartments (arrows). (C) Cargo for degradation can potentially be retained on

(Figure 4.3.7 continued) moving RAB-5 vesicles by the presence of ESCRT-0 subunit HGRS-1. Movie stills showing RFP-RAB-5 vesicles fusing with a larger sorting endosome (homotypic fusion). Vesicles contain GFP-HGRS-1 domains and move with similar dynamics as small RAB-5 vesicles that perform kiss & run (see Fig. 3A+C, 4A). (D) Adaptor knock-downs affect cargo traffic through SNX-1 compartments. RNAi of *snx-17*, *snx-27*, *apm-1* or *aps-1* cause enlargement of SNX-1 compartments (black arrows: large empty round compartments, arrowheads: large filled compartments (see also Suppl. Fig.4A)). The model cargo hTfR-GFP was found in enlarged compartments as well (white arrows). These accumulations were absent in *snx-27(RNAi)* worms. Some of the hTfR accumulations co-localized with enlarged SNX-1 structures (asterisks). (E) Quantification of enlarged hTfR-GFP compartments in adaptor knock-down worms.

Kiss-and-run on sorting compartments is conserved in metazoans

Finally, we wanted to address the question of whether kiss-and-run in the endosomal system is a conserved process, as we would predict from the conservation of the function of FERARI (Solinger et al. 2020). To address this question, we first generated GFP-Rab11 knock-in cell lines using CRISPR-Cas9 (Fig. S4.7.4B). Into these cell lines, we expressed mCherry-SNX1 and performed live cell imaging using high-resolution, fast image acquisition. Indeed, we could observe kiss-and-run events between Rab11 and SNX1 compartments (Fig. 4.3.8A). Next, we used cells stably expressing mApple-Rab5 and co-expressed GFP-SNX1. Again, we were able to observe kiss-and-run between Rab5 and the SNX1 compartment (Fig. 4.3.8B). Therefore, the process, we unraveled in *C. elegans* epithelial cells is most likely conserved in mammalian cells.

4.4 Discussion

In this study, we revealed three key aspects in endocytic recycling. First, we showed that the recycling system is easily adaptable to different cargo loads it needs to process, and that the cargo concentration is a key determinant in the length of the kiss between recycling and sorting endosomes. Second, we provide strong evidence that the cargo flux and sorting in the endosomal system is dependent on cargo adaptor interactions and that the availability of these adaptors and probably binding interactions regulate sorting into different pathway. Third, our data support the notion that the FERARI tethering platform coordinates recycling by its ability to facilitate kiss-and-run of at least three types of endocytic vesicles, Rab5 early endosomes and Rab10 and Rab11 recycling endosomes with the sorting compartment.

We envisage a model in which Rab5 endocytic vesicles/early endosomes on their way form the plasma membrane inwards kiss sorting endosomes as defined by SNX1. During this kiss, cargo destined for immediate recycling could already exit the Rab5 compartment. We envisage negative selection in this process in that ubiquitinated cargo, which would interact with the ESCRT-0 component Hrs would have to remain in the Rab5 compartment, while un- or deubiquitinated cargo would be free to leave. Attraction by the negative membrane

curvature during the kiss facilitate the movement of membrane proteins and specific lipids towards the sorting endosome (Aimon et al. 2014),(Roux et al. 2005).

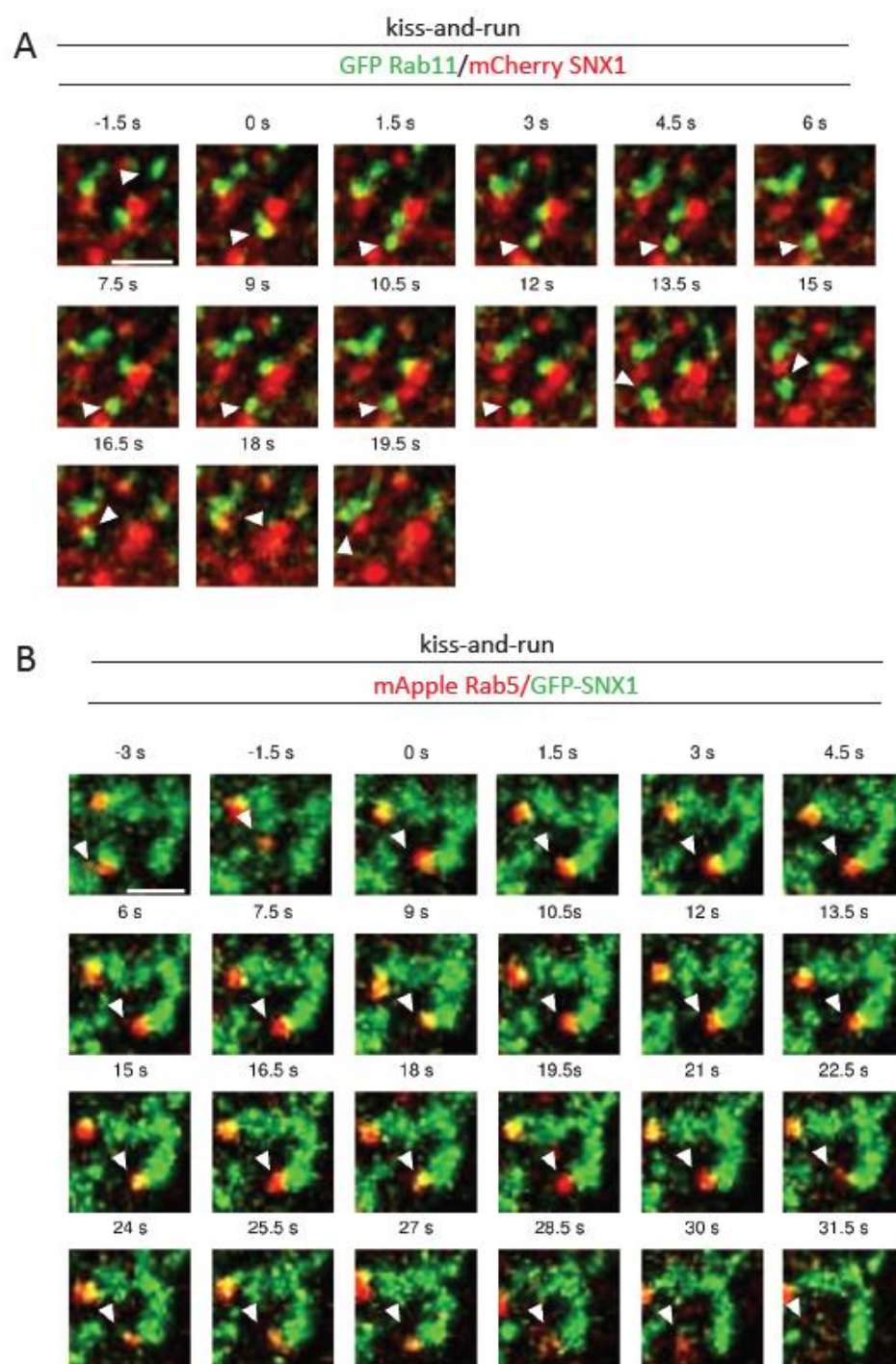


Figure 4.3.8: Kiss-and-run on sorting compartments is conserved in metazoans. (A) Movie stills for endogenously GFP-tagged RAB11 vesicle (arrow) showing kiss-and-run on mCherry-SNX1 compartment in HeLa cells. RAB11 docks on SNX1 structure at time point ‘zero’ and the kiss continues up to 9 s (n=3 independent experiments). (B) Movie stills for mApple-RAB5 vesicle showing kiss-and-run on mCherry-SNX1 compartment in HeLa cells. Snapshot from live movies showing that mApple-Rab5 is approaching GFP-SNX1 compartment. Rab5 docks on SNX1 structure at time point ‘zero’ and the kiss continues up to 30 s (n=2 independent experiments).

The length of the kiss would depend on the amount of cargo diffusing into the sorting compartment (further discussion below). Backflow of cargo would be prevented by its binding to SNX6 and potentially other cargo adaptors in the sorting compartment. In fact, we found that loss of function of SNX-17 and SNX-27 resulted in enlarged SNX-1 compartments and cargo accumulation. SNX17 and SNX27 were shown to be involved in recycling through retriever and retromer recycling pathways (Chi, Harrison, and Burd 2015), (Tan and Gleeson 2019). Combinatorial low affinity interactions of cargo with different adaptors may drive sorting in the SNX1 sorting compartment. The efflux of cargo could be into RAB-10 or RAB-11 vesicles, that would kiss in a similar way than RAB-5 endosomes. In the case of RAB-11, we surmise that AP1 is critical to retain the cargo in the RAB-11 compartment and avoid backflow into the sorting compartment. The retention could be helped by either the concentration of AP1 or to a higher affinity of the cargo for AP1 than for a SNX cargo adaptor. The presence of AP1 on tubular recycling endosomes has been shown before (Klumperman and Raposo 2014). Alternatively, there might be additional cargo adaptors and retention mechanisms. Several adaptors involved in cargo sorting from SNX-1 compartments into RAB-11 vesicles would ensure proper distribution of different types of cargo throughout the cell. It has been shown before that cargoes are not intermixing after leaving the sorting endosome (Xie et al. 2016).

We show that the length of the kiss of the RAB-11 endosomes depends on cargo availability in the sorting endosome. The ‘measure’ of the cargo concentration would be the inability to close the neck and pinching off of the vesicles caused by obstructing cargo present in the neck. We assume that steric hindrance by cargo in the neck of the kissing vesicle might block pinching, thereby ensuring enough time for complete cargo exchange. Since the cargo size is quite bulky in comparison with the pore size (Daumke et al. 2007), (Pant et al. 2009, 1), (Deo et al. 2018) and the building of a spiral or ring structure by RME-1 is essential for pinching, the presence of cargo molecules might cause an interruption of the process until cargo sorting is completed for each vesicle.

We observed that incoming RAB-5 vesicles and outgoing RAB-11 vesicles would not take a direct route, but stop several times on their way to undergo kiss-and-run. We propose that this process would ensure that vesicles will become more and more enriched in specific cargoes, after they leave the sorting endosome. During the kiss-and-run, wrongly assigned cargoes could be sorted out, resulting in a kind of “proofreading” of the cargoes and thereby increasing the fidelity of the cargo sorting process. For example, if an ILV-destined cargo is wrongly sorted during initial transport vesicle formation (out-going to recycling), it could be retrieved back to the sorting endosome by incoming RAB-5 vesicles during kiss-and-run.

Our proposed sorting model explains the observed kiss-and-run of vesicles in the endosomal system. It also provides a simple and efficient mechanism that allows for cargo sorting mistakes and step-by-step enrichment of specific cargo into different cargo carriers. The simplicity of regulating the length of cargo exchange through the presence of cargo itself would provide a way to deal with higher and lower cargo loads during cell development, changing nutrition conditions and stress.

4.5 Material and Methods

Worm husbandry

C. elegans worms were grown and crossed according to standard methods (Brenner 1974). RNAi was performed as previously described (Solinger 2014). All experiments were carried out at 20°C, and worms were imaged at the young adult stage (with only few eggs).

The following worm strains and transgenes were used in this study: *pwls206[vha6p::GFP::rab-10 + Cb unc-119(+)]*, *pwls782[Pvha-6::mCherry::SNX-1]*, *pwls414[Pvha-6::RFP::rab-10, Cb unc-119(+)]*, *dkls218[Popt-2-GFP-syx-3; Cb unc-119(+)]*, *pwls621[vha-6::mCherry-RME-1]*, *pwls72[vha6p::GFP::rab-5 + unc-119(+)]*, *pwls170[vha6p::GFP::rab-7 + Cb unc-119(+)]*, *pwls90[Pvha-6::hTfR-GFP; Cbr-unc-119(+)]*, *qxEx2247 [Pvha-6::Glut1::GFP]*, *pwls69[vha6p::GFP::rab-11 + unc-119(+)]*, *pwls87[Pvha-6::GFP::rme-1; Cbr-unc-119(+)]*, *[Pdhs-3::dhs-3::GFP]*, *pwls481[Pvha-6::mans-GFP, Cbr-unc-119(+)]*, *pwls518[vha-6::GFP-HGRS-1]*, *pwls846[Pvha-6-RFP-rab-5; Cb unc-119(+)]*, *rab-10(ok1494)*.

Microscopy

Live microscopy on worms was performed as described (Solinger 2014, 2020). In short, worms were immobilized on 2% agarose pads on microscopy slides using levamisole (50 mM); cover slips were sealed using Vaseline. Overview images (Fig. 1C, 2A, Supp. Fig. 2E) were acquired with an Olympus Fluoview FV3000 system using a high sensitivity spectral detector (HSD) at a standard voltage setting (PTM) of 500. For higher resolution, the Galvano scan device was applied. A 60x objective with silicone oil was used, resulting in a pixel size of 0.098 μm . Laser intensities were at 4-10% for both 488 (GFP) and 561 (RFP, mCherry) wavelengths. Sampling speed was 8.0 $\mu\text{s}/\text{pixel}$ with a zoom factor of 2.1. All images for corresponding experiments were processed with the same settings to insure comparable results.

High resolution 3D images and movies were obtained with a Zeiss LSM 880 microscope with Airyscan capabilities. Fast mode in the Zen Black software was used for all images. The higher than usual levamisole concentration of 50 mM was used to insure very little movement during image acquisition. For movies, resolution was traded in for speed by reducing the averaging to 2-4x, resulting in the required frame speeds of 0.5 – 1.0 seconds to follow vesicles. To catch high enough numbers of vesicles a region of approximately 70 μm^3 was covered (about 2 intestinal cells). Movement could be observed up to 30-45 min after immobilization of worms. From these overview movies, smaller regions of 70 x 70 pixels were selected, showing only 1-2 vesicles and events. These movies were then quantified. Worms in the right stage showed persistent movement in many cells and events were mainly limited by the use of only one imaging plane (due to speed limitation of the microscope). The “StackReg” plugin in Fiji was

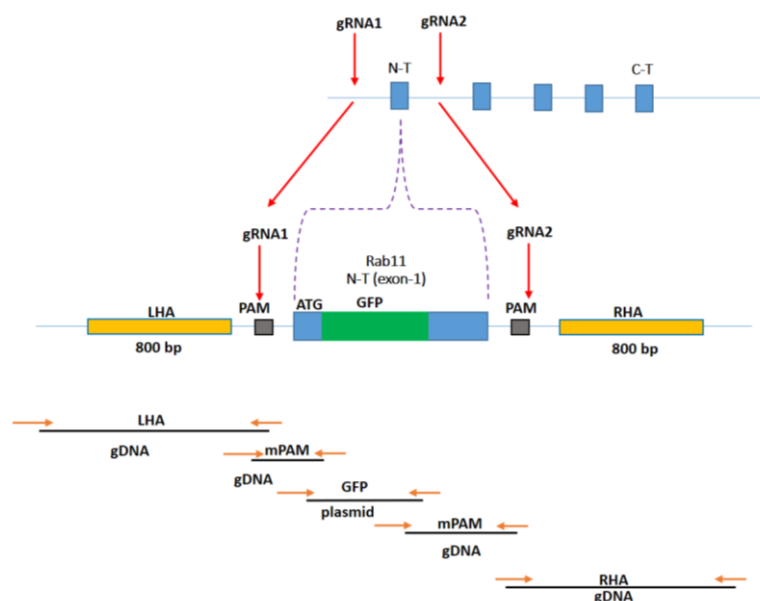
used to get rid of worm shaking and drifting motions. “Bleach correction” was used to avoid irritating blinking during repeated viewing of movies (overall, bleaching was minimal).

Compartment quantifications

RAB-10 tubule length was measured with the freehand line ROI function in Fiji. Since only one z-plane was used, this leads to an underestimation of the true length of tubules, but since FERARI phenotypes were exceptionally strong, no further measurements were deemed necessary. Mander’s Coefficients for co-localization between compartments were measured with the JACoP plugin of Fiji, using all available z-planes over whole intestinal cells for 10 worms each.

GFP-Knock-in at the Rab11 locus in HeLa cells

GFP construct was inserted into the N-terminal of Rab11 at the endogenous level by using CRISPR/Cas9 homology directed repair. The following strategy was taken to insert GFP into Rab11 genome.



HLA (Homology left arm); PAM (Protospacer adjacent motif); mPAM (mutated PAM), N-T (N terminus), RHA (Right homology arm); gRNA (guide RNA)

Two guide RNAs were designed from introns before and after first exon of Rab11. Annealed oligonucleotides were cloned into two different plasmids, Px458 mCherry (kindly provided by Mirjam Pennauer), and Px459 Puro (addgene) plasmids, respectively. Template DNA was prepared PCR method. As indicated in the scheme 5 PCR product was synthesized. GFP was synthesized by using a GFP containing plasmid as a template and for the rest, genomic DNA

from HeLa cells served as template. All these PCR products were cloned into pUC19 plasmid (Addgene; 50005) by Gibson assembly method. After transformation, sequencing was done to confirm the insertion template into the vector. 2 gRNAs containing vectors and the template containing vector were then transfected into HeLa cells by using Helix-in (OZ biosciences) transfection reagent based on the manufacturer's protocol. After 7 days of transfection, cells were FACS sorted and GFP⁺ cells were collected. For the confirmation of the GFP-knock-in, PCR and western blot were performed.

Cell culture, transfection and CRISPR–Cas9 KO in mammalian cells

HEK293 and HeLa cells were cultured and maintained in DMEM (Sigma) high-glucose medium with 10% FCS (Bioconcept), penicillin–streptomycin (1%), sodium pyruvate and L-glutamine. Cells were plated 1 d before transfection at 60–70% confluency and later transfected for 48 h using Helix-in (OZ biosciences) transfection reagent according to the manufacturer's instructions. A 1–2 µg of DNA was used per reaction based on a 10-cm dish. For CRISPR–Cas9-mediated KO, guide RNAs were selected using the CRISPR design tools (<http://chopchop.cbu.uib.no/>) and <https://www.benchling.com/>. A list of oligonucleotides is provided in Supplementary Table 1. Two guide RNAs were designed from two different exons for each target gene. Annealed oligonucleotides were cloned into two different plasmids, Px458 GFP and Px459 Puro, respectively. In brief, HeLa cells were seeded at 2×10^6 cells per 10-cm dish. The following day, cells were transfected with 2.5 µg of the plasmids (control vectors without insert or vectors containing a guide RNA against the target gene). Transfection medium was exchanged with fresh medium after 4 h. Cells were treated with puromycin for 24 h after transfection followed by FACS sorting (for GFP⁺ cells) the next day. For FACS sorting after 48 h of transfection, cells were trypsinized and resuspended in cell-sorting medium (2% FCS and 2.5 mM EDTA in PBS) and sorted on a BD FACS AriaIII Cell Sorter. GFP-positive cells were collected and seeded in a new well.

Immunoprecipitation assays

HEK293 cells were co-transfected with the indicated DNA constructs. After 36–48 h of transfection, protein extracts were prepared in lysis buffer (1% NP-40, 50 mM Tris/HCl pH 7.5, 150 mM NaCl) and Halt protease inhibitor cocktail (Thermo Scientific; 186 1279) at 4 °C for 20 min followed by centrifugation at 4 °C for 20 min at 13,000 r.p.m. Immunoprecipitations were performed as previously described⁵⁵. In brief, protein extracts were incubated with Trap beads (nanobodies for GFP (GFP-Trap_A; gta-20-chromotek), for 6 h at 4 °C with rotation, and then washed five times with lysis buffer (1 ml). Protein complexes were eluted by heating beads for 5 min at 95 °C in 2× sample buffer and resolved by SDS–PAGE on 10% and 12.5% gels followed by immunoblot analysis. Blots were developed using Amersham ECL Prime Western Blotting Detection Reagent (RPN2236) and X-ray film (Amersham Hyperfilm ECL-28906839).

Western blot analysis

Cells were collected and lysed in lysis buffer (50 mM Tris/HCl, 150 mM NaCl, 1% NP-40) containing a protease inhibitor cocktail (Roche). Protein concentrations were determined in all experiments using the Bio-RAD protein assay (Bio-RAD, 500-0006) and 20–40 µg of total protein was loaded onto either 10 to 15% SDS–PAGE gels before transfer onto nitrocellulose membranes (Amersham Protran; 10600003). Membranes were blocked with 5% milk, 0.1% Tween20 for 60 min at room temperature. The primary antibody incubation was overnight at 4 °C and the secondary HRP-coupled antibodies were incubated for 1 h at room temperature. The blots were developed using western Blotting detection kit WesternBright™ ECL (advansta; K-12045-D50) and the Fusion FX7 (Vilber Lourmat) image acquisition system.

Immunostaining in mammalian cells

Cells were plated onto sterile 13-mm glass coverslips. Cells were fixed with 2% paraformaldehyde for 15 min, permeabilized (0.1% Triton X-100 in PBS) for 5 min and blocked with 2% BSA containing 5% goat serum in PBS for 1 h. Coverslips were incubated in primary antibodies for 2 h and washed five times in PBS followed by a 1-h incubation in fluorescently tagged secondary antibodies. After secondary antibody incubation, coverslips were washed a further five times in PBS and mounted onto glass slides using Fluoromount-G (Southernbiotech; 0100-01). Images were taken with an inverted Olympus FV1000 confocal microscope using a Plan Apochromat N 60×/1.40 silicon oil objective and Axio Observer Zeiss microscope (Zeiss) with z stacks (Figure 2A, F, G). Co-localization studies were performed using the ImageJ co-localization plugin JACoP.

CI-MPR uptake and trafficking analysis

Cells were incubated with 10 µg/ml mouse anti-CI-MPR monoclonal antibody (ThermoFisher MA1-006) in serum-free DMEM for 1 hr, rinsed with PBS, fixed with 4% Paraformaldehyde, solubilized with Triton-X and immunostained with 1:500 anti-Giantin (rabbit) antibody (BioLegend cat 924302) and then fluorescent anti-rabbit and anti-mouse antibodies 1:500.

Live cell imaging

For live imaging, cells were plated in an 4-well chambered coverglass (Ibidi µ-slide; Ibidi GmbH, Germany) and medium was replaced with warm imaging buffer (5 mM dextrose (d(+)-glucose, H₂O, 1 mM CaCl₂, 2.7 mM KCl, 0.5 mM MgCl₂ in PBS) just before imaging. Images were taken at 37 °C on an inverted Axio Observer Zeiss microscope (Zeiss) using a Plan Apochromat N

63×/1.40 oil DIC M27 objective with a Photometrics Prime 95B camera (Figure 2C, 3G). Z-stack images were processed using the OMERO client server web tool and Fiji. For kiss-and-run study (Figure 8A, 8B), live movies were taken at 37 °C by using imaging buffer on a DeltaVision OMX Optical Microscope equipped with CO₂ supply. 60X/1.524 oil objective was used for image acquisition. According to Meta data frame rate is 750 mili second.

Quantification of Rab11-positive endosomes

Segmentation and analysis were performed on manually chosen ROIs using a custom script for Fiji⁵⁷ as follows. First, a 3D white top-hat filter⁵⁸ was applied to the original image to homogenize the background and used to compute 3D seeds⁵⁹ with subpixel accuracy. Next, objects were segmented on the original image using an iterative threshold⁶⁰ and converted to labels. Touching objects were then separated by a 3D watershed⁶¹ using the previously identified seeds on the label image. The resulting image was then added to the 3D ROI Manager¹⁰ to exclude remaining laterally touching objects and finally perform intensity and size measurements per object. A total of 2500-3000 Rab11-positive particles were analysed from 40-50 cells for each condition. The script is available upon request.

Antibodies

The following antibodies were used in this study: polyclonal. Polyclonal rabbit anti-GFP (TP401; Torrey Pines; 1:2,000 for western blotting and 1:200 for immunostaining), Rab10 (D36C4) Rabbit mAb (#8127, Cell signaling, 1:1000 for western blotting), Rab11 Anti-Rab11 antibody (ab3612, abcam, 1:1000 for western blotting), Recombinant Anti-SNX5 antibody (ab180520, abcam, 1:1000 for western blotting). Purified Mouse Anti-SNX1 (611482, BD biosciences, 1:100 for IF), SNX6 mouse monoclonal antibody (D-5) (sc-365965, Santa cruz, 1:1000 for western blotting), For pulldowns, Trap beads (nanobodies) were used. GFP-Trap_A (chromotek, gta-20) was used for GFP pulldowns. HRP-conjugated goat anti-mouse IgG (H + L) secondary antibody (Thermo Fisher Scientific; 31430; 1:10,000) and polyclonal HRP-conjugated goat-anti-rabbit IgG (Thermo Fisher Scientific; 31460; 1:10,000) were used (incubated for 1 h at room temperature) to detect bound antibodies with Blotting detection kit WesternBright™ ECL (advansta; K-12045-D50). Alexa Fluor 488–goat anti-rabbit IgG (H + L) (Invitrogen; A-11034) and Alexa Fluor 594–goat anti-mouse IgG (H + L) cross-adsorbed secondary antibodies (Invitrogen; R37121) were used for immunofluorescence.

DNA and Plasmid sources

The following commercially available plasmids were obtained: GFP-VIPAS39 (Sino.Bio; HG22032_ACG), GFP-Rabenosyn-5 (Addgene; 37538), turbo-GFP-SNX1 (Origene; RG201844), GFP-RAB11 (Addgene; 12674). The plasmids Px458 GFP (Addgene; 48138) and Px459 Puro (Addgene; 62988) were used for cloning gRNAs. mCherry-SNX1 was created by PCR amplifying

mCherry from mCherry-Rab11 construct (Plasmid #55124) and ligating into NotI/PmeI sites of SNX1 vector (Origene; RG201844). Turbo-GFP was deleted from the plasmid by restriction digestion (NotI/PmeI). PCR synthesized mCherry was ligated to the linearized SNX1 vector by using Roche rapid ligation kit.

4.5 References

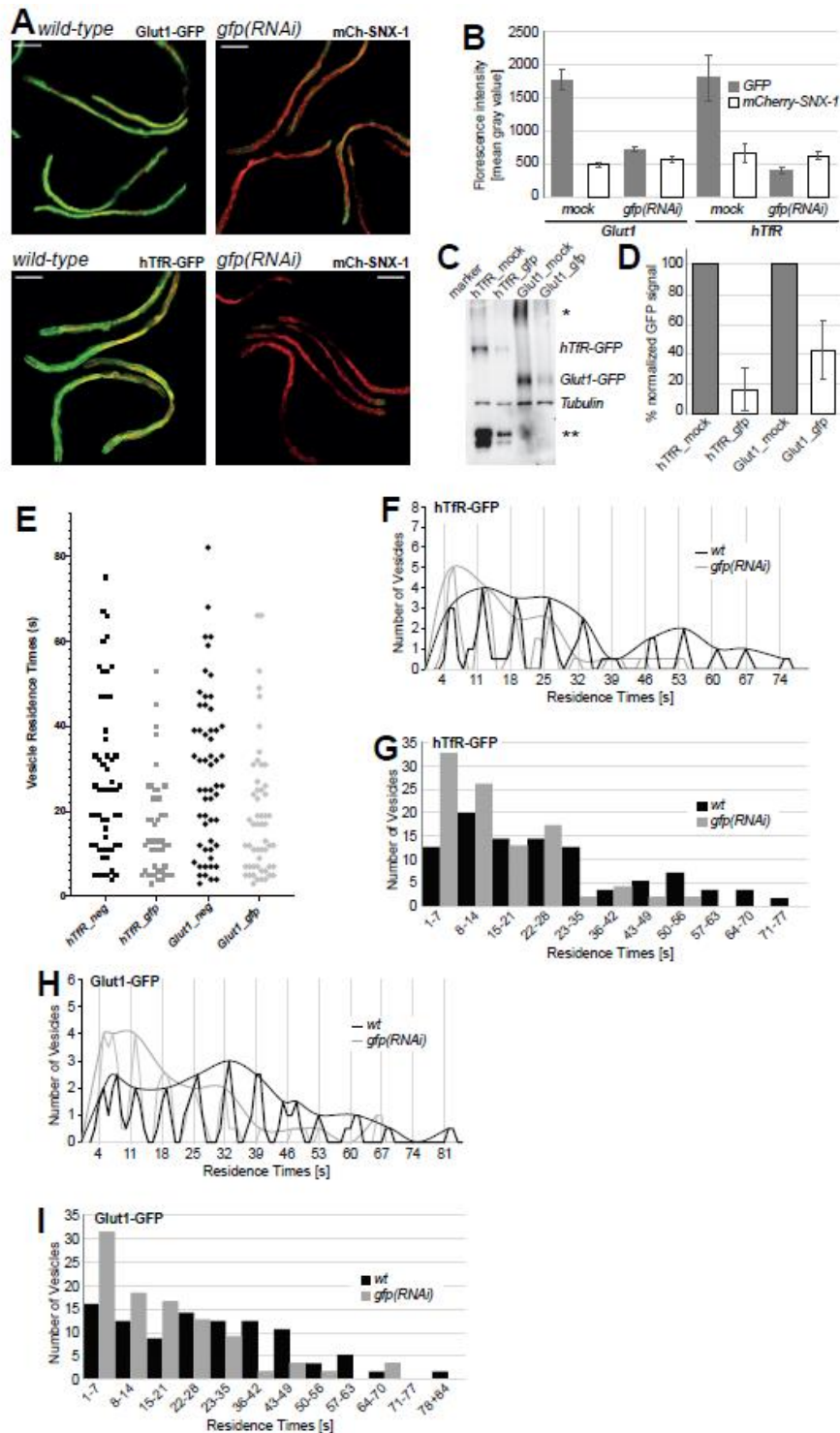
- Aimon, Sophie, Andrew Callan-Jones, Alice Berthaud, Mathieu Pinot, Gilman E. S. Toombes, and Patricia Bassereau. 2014. "Membrane Shape Modulates Transmembrane Protein Distribution." *Developmental Cell* 28 (2): 212–18. <https://doi.org/10.1016/j.devcel.2013.12.012>.
- Babbey, Clifford M., Nahid Ahktar, Exing Wang, Carlos Chih-Hsiung Chen, Barth D. Grant, and Kenneth W. Dunn. 2006. "Rab10 Regulates Membrane Transport through Early Endosomes of Polarized Madin-Darby Canine Kidney Cells." *Molecular Biology of the Cell* 17 (7): 3156–75. <https://doi.org/10.1091/mbc.e05-08-0799>.
- Chen, Carlos Chih-Hsiung, Peter J. Schweinsberg, Shilpa Vashist, Darren P. Mareiniss, Eric J. Lambie, and Barth D. Grant. 2006. "RAB-10 Is Required for Endocytic Recycling in the *Caenorhabditis Elegans* Intestine." *Molecular Biology of the Cell* 17 (3): 1286–97. <https://doi.org/10.1091/mbc.e05-08-0787>.
- Chen, Kai-En, Michael D. Healy, and Brett M. Collins. 2019. "Towards a Molecular Understanding of Endosomal Trafficking by Retromer and Retriever." *Traffic (Copenhagen, Denmark)* 20 (7): 465–78. <https://doi.org/10.1111/tra.12649>.
- Chen, Yu, Yan Wang, Jinzhong Zhang, Yongqiang Deng, Li Jiang, Eli Song, Xufeng S. Wu, John A. Hammer, Tao Xu, and Jennifer Lippincott-Schwartz. 2012. "Rab10 and Myosin-Va Mediate Insulin-Stimulated GLUT4 Storage Vesicle Translocation in Adipocytes." *The Journal of Cell Biology* 198 (4): 545–60. <https://doi.org/10.1083/jcb.201111091>.
- Chi, Richard, Megan Harrison, and Christopher Burd. 2015. "Biogenesis of Endosome-Derived Transport Carriers." *Cellular and Molecular Life Sciences : CMLS* 72 (May). <https://doi.org/10.1007/s00018-015-1935-x>.
- Cullen, Peter J., and Florian Steinberg. 2018. "To Degrade or Not to Degrade: Mechanisms and Significance of Endocytic Recycling." *Nature Reviews. Molecular Cell Biology* 19 (11): 679–96. <https://doi.org/10.1038/s41580-018-0053-7>.
- Daumke, Oliver, Richard Lundmark, Yvonne Vallis, Sascha Martens, P. Jonathan G. Butler, and Harvey T. McMahon. 2007. "Architectural and Mechanistic Insights into an EHD ATPase Involved in Membrane Remodelling." *Nature* 449 (7164): 923–27. <https://doi.org/10.1038/nature06173>.
- Deo, Raunaq, Manish S. Kushwah, Sukrut C. Kamerkar, Nagesh Y. Kadam, Srishti Dar, Kavita Babu, Anand Srivastava, and Thomas J. Pucadyil. 2018. "ATP-Dependent Membrane Remodeling Links EHD1 Functions to Endocytic Recycling." *Nature Communications* 9 (1): 5187. <https://doi.org/10.1038/s41467-018-07586-z>.
- Gallon, Matthew, and Peter J. Cullen. 2015. "Retromer and Sorting Nexins in Endosomal Sorting." *Biochemical Society Transactions* 43 (1): 33–47. <https://doi.org/10.1042/BST20140290>.
- Glodowski, Doreen R., Carlos Chih-Hsiung Chen, Henry Schaefer, Barth D. Grant, and Christopher Rongo. 2007. "RAB-10 Regulates Glutamate Receptor Recycling in a Cholesterol-Dependent Endocytosis Pathway." *Molecular Biology of the Cell* 18 (11): 4387–96. <https://doi.org/10.1091/mbc.e07-05-0486>.
- Grant, B., and D. Hirsh. 1999. "Receptor-Mediated Endocytosis in the *Caenorhabditis Elegans* Oocyte." *Molecular Biology of the Cell* 10 (12): 4311–26. <https://doi.org/10.1091/mbc.10.12.4311>.

- Klumperman, Judith, and Graça Raposo. 2014. "The Complex Ultrastructure of the Endolysosomal System." *Cold Spring Harbor Perspectives in Biology* 6 (10): a016857. <https://doi.org/10.1101/cshperspect.a016857>.
- Lawrence, C. M., S. Ray, M. Babyonyshev, R. Galluser, D. W. Borhani, and S. C. Harrison. 1999. "Crystal Structure of the Ectodomain of Human Transferrin Receptor." *Science (New York, N.Y.)* 286 (5440): 779–82. <https://doi.org/10.1126/science.286.5440.779>.
- Norris, Anne, Prasad Tammineni, Simon Wang, Julianne Gerdes, Alexandra Murr, Kelvin Y. Kwan, Qian Cai, and Barth D. Grant. 2017. "SNX-1 and RME-8 Oppose the Assembly of HGRS-1/ESCRT-0 Degradative Microdomains on Endosomes." *Proceedings of the National Academy of Sciences*, January. <https://doi.org/10.1073/pnas.1612730114>.
- Pant, Saumya, Mahak Sharma, Kruti Patel, Steve Caplan, Chavela M. Carr, and Barth D. Grant. 2009. "AMPH-1/Amphiphysin/Bin1 Functions with RME-1/Ehd1 in Endocytic Recycling." *Nature Cell Biology* 11 (12): 1399–1410. <https://doi.org/10.1038/ncb1986>.
- Roux, Aurélien, Damien Cuvelier, Pierre Nassoy, Jacques Prost, Patricia Bassereau, and Bruno Goud. 2005. "Role of Curvature and Phase Transition in Lipid Sorting and Fission of Membrane Tubules." *The EMBO Journal* 24 (8): 1537–45. <https://doi.org/10.1038/sj.emboj.7600631>.
- Scott, Cameron C., Fabrizio Vacca, and Jean Gruenberg. 2014. "Endosome Maturation, Transport and Functions." *Seminars in Cell & Developmental Biology* 31 (July): 2–10. <https://doi.org/10.1016/j.semcdb.2014.03.034>.
- Simonetti, Boris, Chris M. Danson, Kate J. Heesom, and Peter J. Cullen. 2017. "Sequence-Dependent Cargo Recognition by SNX-BARs Mediates Retromer-Independent Transport of Cl-MPR." *Journal of Cell Biology* 216 (11): 3695–3712. <https://doi.org/10.1083/jcb.201703015>.
- Simonetti, Boris, Blessy Paul, Karina Chaudhari, Saroja Weeratunga, Florian Steinberg, Madhavi Gorla, Kate J. Heesom, Greg J. Bashaw, Brett M. Collins, and Peter J. Cullen. 2019. "Molecular Identification of a BAR Domain-Containing Coat Complex for Endosomal Recycling of Transmembrane Proteins." *Nature Cell Biology* 21 (10): 1219–33. <https://doi.org/10.1038/s41556-019-0393-3>.
- Solinger, Jachen A., Harun-Or Rashid, Cristina Prescianotto-Baschong, and Anne Spang. 2020. "FERARI Is Required for Rab11-Dependent Endocytic Recycling." *Nature Cell Biology* 22 (2): 213–24. <https://doi.org/10.1038/s41556-019-0456-5>.
- Spang, Anne. 2016. "Membrane Tethering Complexes in the Endosomal System." *Frontiers in Cell and Developmental Biology* 4: 35. <https://doi.org/10.3389/fcell.2016.00035>.
- Strutt, Helen, Paul F. Langton, Neil Pearson, Kirsty J. McMillan, David Strutt, and Peter J. Cullen. 2019. "Retromer Controls Planar Polarity Protein Levels and Asymmetric Localization at Intercellular Junctions." *Current Biology: CB* 29 (3): 484–491.e6. <https://doi.org/10.1016/j.cub.2018.12.027>.
- Tan, Jing Zhi Anson, and Paul Anthony Gleeson. 2019. "Cargo Sorting at the Trans-Golgi Network for Shunting into Specific Transport Routes: Role of Arf Small G Proteins and Adaptor Complexes." *Cells* 8 (6). <https://doi.org/10.3390/cells8060531>.
- Wassmer, Thomas, Naomi Attar, Miriam V. Bujny, Jacqueline Oakley, Colin J. Traer, and Peter J. Cullen. 2007. "A Loss-of-Function Screen Reveals SNX5 and SNX6 as Potential Components of the Mammalian Retromer." *Journal of Cell Science* 120 (1): 45–54. <https://doi.org/10.1242/jcs.03302>.
- Xie, Shuwei, Kriti Bahl, James B. Reinecke, Gerald R. V. Hammond, Naava Naslavsky, and Steve Caplan. 2016. "The Endocytic Recycling Compartment Maintains Cargo Segregation Acquired upon Exit from the Sorting Endosome." *Molecular Biology of the Cell* 27 (1): 108–26. <https://doi.org/10.1091/mbc.E15-07-0514>.

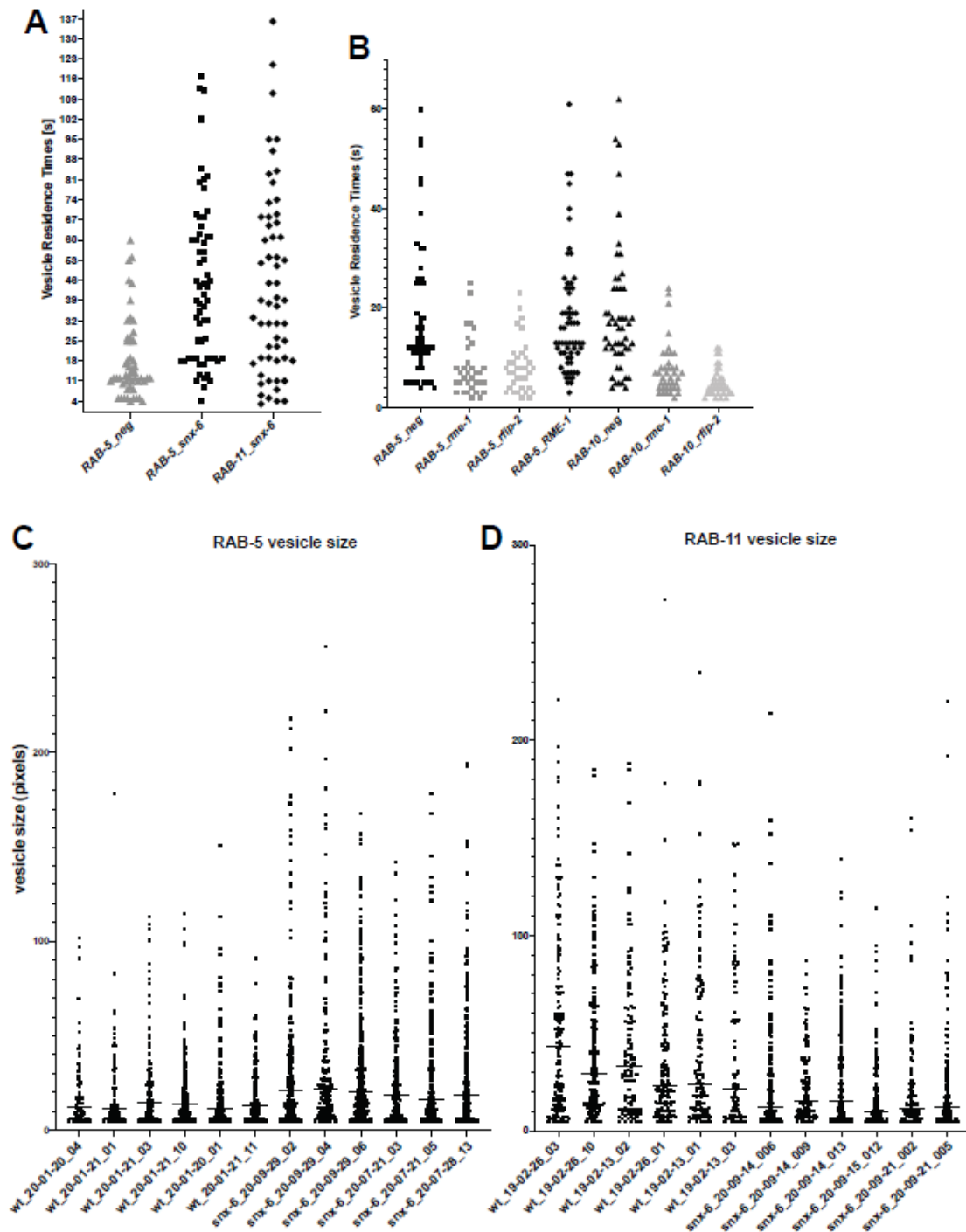
4.7 Supplementary material

List of Guide-RNAs and oligos used in this work

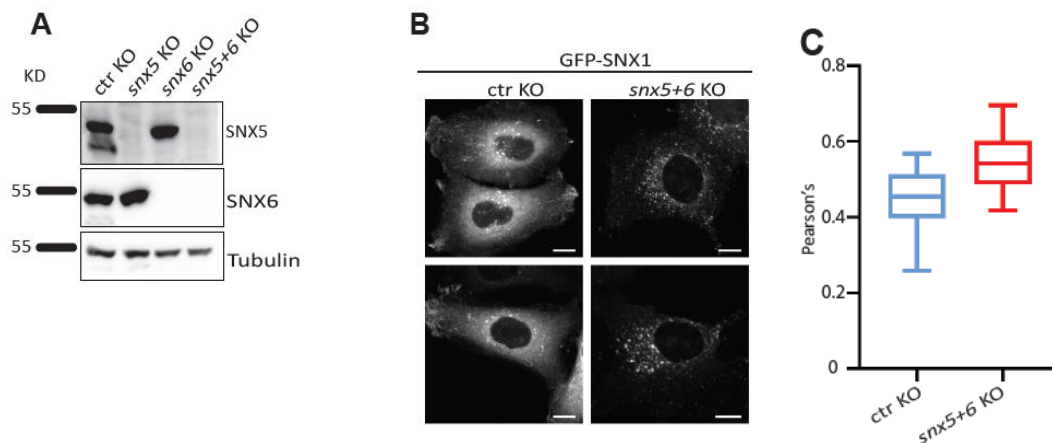
Guide-RNA	
RAB10	
guide 1 F	CACCGTGATCGGGGATTCCGGAGTG
guide 1 R	AAACCACTCCGGAATCCCCGATCAC
guide 2 F	CACCGCATTGCGCCTCTGTAGTAGG
guide 2 R	AAACCCTACTACAGAGGCGCAATGC
SNX6	
guide 1 F	CACCGATGATGGTGGGTGTTCTCCG
guide 1 R	AAACCGGAGAACACCCACCATCATC
guide 2 F	CACCGGTGCAGCGAGGAAACCGAA
guide 2 R	AAACTTCGGTTTCCTCGCTGCACC
SNX5	
guide 1 F	CACCGCGACGCGGGACTCGAGCAG
guide 1 R	AAACCTGCTCGAGTCCCGCGTCGC
guide 2 F	CACCGTTTTAAAAAGAACATTCCG
guide 2 R	AAACCGGAATGTTCTTTTAAAC
Guide-RNA for GFP knock-in into Rab11 locus	
guide 1 F	CACCGTTAAGGGGAAGTACTTCCGG
guide 1 R	AAACCCGGAAGTACTTCCCCTTAAC
guide 2 F	CACCGCTCTACACAGTCCTCGTTCG
guide 2 R	AAACCGAACGAGGACTGTGTAGAGC
Primers for GFP knock-in into Rab11 locus	
F	GCATGCCTGCAGGTCGACT TGAAATACTTATGTAAACGGACTTA
R	TTTAAGGGGAAGTACTTCCGGGATCGGCG
F	CGCCGATCCCGGAAGTACTTCCCCTTAA
R	TCCTCGCCCTTGCTCACCATTGCGCGGCCGAGGAGCGAAA
F	CTCCTCGGCCGCGCAATGGTGAGCAAGGGCGAGGAGCTGTT
R	TACTCGTCGTCGCGGGTGCCCTTGACAGCTCGTCCATGCCGAGAGTGAT
F	GAGCTGTACAAGGGCACCCGCGACGACGAGTACGACTACC
R	CGGCACGAGGGTCCACCGGGAGTGGCCCGGGTATCCGAAC
F	TGGACCCTCGTGCCGGCCACCCCTGCACTGATATAGGCCT
R	GGTACCCGGGGATCCTCTAGACAAGAAAAGAAAAGGCTAGGTGGGA



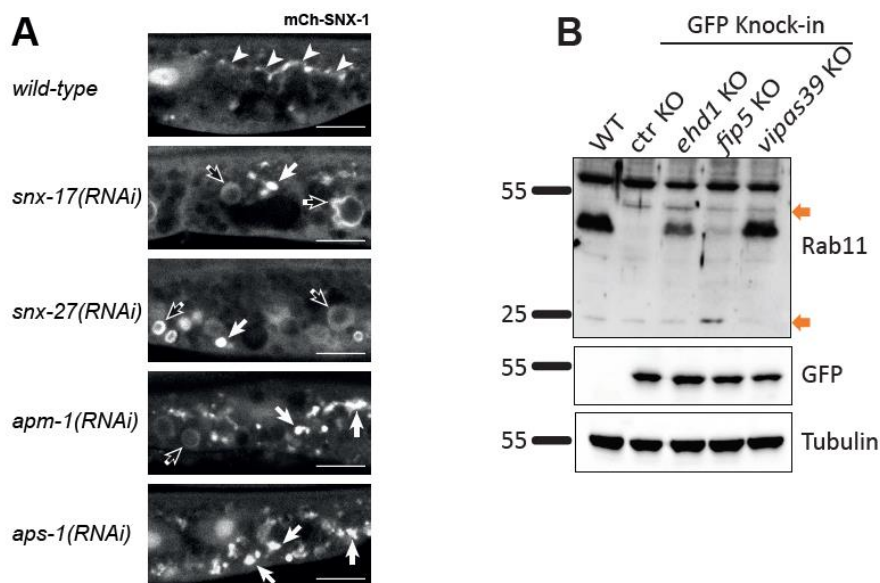
Supplementary Figure 4.7.1: (A) Example pictures of worms with mock RNAi and *gfp(RNAi)* that were used for the residence times measurements with overexpressed and reduced cargo in Fig. 4.3.1A, B. (B) Quantification of fluorescence intensity of worms shown in (A), n=30 (3 independent knock-downs). (C) Western blot data showing reduced cargo as in figure 4.3.1A, B. (D). Quantification of the western blot data in figure S1C. (E) Plots showing residence times for single vesicles doing kiss & run. These are the same vesicles used in Fig. 1A, B for the graphs with binning and moving averages, resulting in vesicle groups as peaks. (F) (H), "Bridge" graphs connecting the peaks of Fig. 1 A and B to highlight the distribution of vesicles, (F) hTfR-GFP cargo, (H) Glut1-GFP. (G), (I) Bar graphs with binning for each peak in F and H, showing the number of vesicles in each peak.



Supplementary Figure 4.7.2: (A) Residence times of vesicles in strains lacking *snx-6* cargo adaptor. Each data point represents a single vesicle that showed kiss & run behavior. For a different representation of the data refer to Fig. 4.3.1E and 3E (n=57 for RAB-11_ *snx-6*, n=62 for RAB-5_ *snx-6*). (B) Single vesicle plots for kiss & run vesicles. These graphs are a different representation of the data in Fig. 4.3.3B, C (Rab-5) and 4.3.5G (Rab-10) containing all the single vesicle residence times. (C) Size of RAB-5 vesicles in *wild-type* and *snx-6(RNAi)* worms (n=6). (D) Size of RAB-11 vesicles in *wild-type* and *snx-6(RNAi)* worms (n=6). This graph is a different representation of the data in Fig. 4.3.1F.



Supplementary Figure 4.7.3: (A) Western blot data showing the CRISPR/Cas9 mediated KO of *snx5*, *snx6* and combined KO of *snx5+6* detected by indicated antibodies. Tubulin was also detected to show equal loading. (B) Live images of ctr KO and *snx5+6* KO transiently over-expressing GFP-SNX1. Tubular structure of SNX1 is less in *snx5+6* KO cells in comparison with ctr KO cells. (C) Pearson's coefficient showing co-localization between GFP-SNX1 and mApple-Rab5. Rab5 co-localization with SNX1 is increased in *snx5+6* KO cells in comparison with ctr KO cells (around 50 cells were quantified from 2 independent experiments for each group.). Imaging data of this graph is shown in Fig. 3G.



Supplementary Figure 4.7.4: (A) mCherry-SNX-1 compartments are enlarged in cargo adaptor knock-down worms. Shown are either large hollow spheres (black arrows) or more irregularly shaped, filled structures (white arrows). The wild-type reticulated SNX-1 compartments are indicated by arrowheads. (B) GFP knock-in into the Rab11 locus in CTR and FERARI KO HeLa cells is confirmed by antibodies against GFP and Rab11. Tubulin was also detected to show the equal loading (n=3 independent experiments).

5. Purification of FERARI

Statement of contributions

Harun-Or Rashid conducted the experiments in figures 1A, 1B, and 2.

Negative stain EM, figure 3, was conducted by **Professor Camilo Perez's lab**.

Jachen A. Solinger expressed all the FERARI members in yeast other than GFP-Rabenosyn-5.

Professor Anne Spang supervised this project.

5.1 Summary

FERRARI is a multi-subunit tethering platform involved in endocytic recycling. Membrane recruitment of FERRARI is regulated by interaction with Rab5 through Rabenosyn-5. The FERRARI subunit Rab11-FIP5 captures Rab11 positive vesicles, which is followed by tethering, fusion, and fission on sorting nexin-1 positive endosomal compartments. Here, we sought to determine the overall molecular structure of the FERRARI by cryogenic electron microscopy. First, to purify FERRARI, we co-expressed differentially tagged five subunits of FERRARI, VIPAS39, VPS45, EHD1, RAB11FIP5, and ANK1 in yeast, and GFP tagged Rabenosyn-5 in HEK-293 cells. The GFP-tagged Rabenosyn-5 served as bait on GFP-trap beads. The complex was eluted by cleaving the GFP-off from Rabenosyn-5 by TEV protease. The efficiency of the purification was assessed by commassie blue and western blot. Negative stain electron microscopy data shows a homogenous sea horse-like structure of FERRARI on the EM grid. Embedding of FERRARI into vitreous ice is currently ongoing.

5.2 Introduction

Membrane-bound organelles communicate with each other via vesicular transport. Vesicles are generated at the donor membrane in a cargo-dependent manner. They are transported to and then fuse with the target membrane. Multiple fusion and fission events regulate the cargo transport along with the endolysosomal system of eukaryotic cells. Such dynamic membrane fission and fusion events are tightly controlled to maintain proper organelle identity. The molecular ingredients of both the fusion and fission processes have been identified. Diverse multiprotein complexes are central players in intracellular transport pathways. Most of them are well conserved from yeast to humans. Tethering factors regulate initial docking and tethering of vesicles to their target compartment. Multi subunit tethering complexes (MTCs) regulate membrane tethering and fusion in Rab-GTPase and SNARE dependent manner. Rab-GTPases specify the organelle identity, whereas the SNARE proteins play a central role in providing membrane specificity and catalyzing the vesicle fusion with the target membrane. Rabs and tethers provide the initial level of membrane recognition, which is then augmented by SNARE pairings.

MTCs contain 2-10 subunits, and to know their molecular architecture, it is crucial to purify the entire complex (Bröcker et al., 2010). Purified protein complex provides plenty of information about the characteristic of the complex. For example, the size of the complex, the stoichiometry of the subunits, and the overall molecular architecture can be elucidated from purified protein complexes. Furthermore, purification of the entire protein complex also provides information about the stability of the complex (Bröcker et al., 2012; Ha et al., 2016). However, purifying the protein complex as a whole is challenging because of the limitation of the available expression system. Some proteins are not highly expressed at the endogenous level, and it is challenging to express multiple proteins in human cell lines simultaneously. Furthermore, the number of protein tags is limited to specify multiple proteins. Hence, the detection of multiple proteins in a complex is difficult due to absence of good antibodies and limitations of tags. Sometimes the protein complexes are not so stable; they can only be formed in a spatiotemporal manner, and purifying such complexes is extremely tough.

Single-particle electron microscopy has been revolutionary in the determination of the ultrastructure of MTCs. Endolysosomal MTCs, CORVET and HOPS, bind with active Rab5 and Rab7, respectively. The structure of the HOPS complex is determined by single-particle EM of negatively stained HOPS particles overproduced and purified from yeast. The ultrastructure of HOPS looks like a seahorse (Fig. 5.1), which is ≈ 30 -nm in size that can adopt contracted and elongated forms. The Rab-binding subunits, Vps41 and Vps39 are, surprisingly, present on both ends of the HOPS complex. The SNARE interacting protein VPS33 localizes to the large head in addition to the two other subunits with VPS16 and VPS41. VPS18 connects the large heads with bulky tails containing VPS11 and VPS39. Recently, a 'spaghetti-dancer'-like structure has been suggested for HOPS (Chou et al., 2016). Seahorse and the spaghetti-dancer both structures show that Rab7 binds two opposite ends containing VPS41 and VPS39.

However, the difference between the two structures was caused by the difference in sample preparation. In the former study, chemical cross-linker glutaraldehyde was used to stabilize the HOPS complex resulted in a seahorse-like structure. While in the latter study chemical cross-linker glutaraldehyde was avoided.

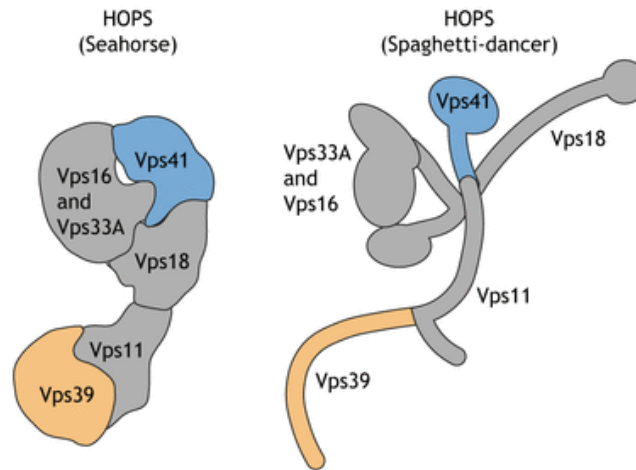


Figure 5.1: Left cartoon is depicting the structure of fusion-active yeast HOPS tethering complex elucidated by negative stain electron microscopy. This seahorse like structure of HOPS contains VPS39 and VPS41 on two opposite sides, which allows this complex to interact with two Rab7 containing compartments. Right cartoon is also depicting molecular structure of HOPS. This structure looks like a ‘spaghetti-dancer’. The difference between seahorse and spaghetti-dancer could symbolize HOPS in an ‘open’ and ‘closed’ conformation or a fixation artifact. Taken from Jan van der Beek (2019).

5.3 Results

FERARI is composed of six subunits and there is no significance sequence similarity among the subunits. The stability and the spatio-temporal regulation of FERARI tethering platform is not known. We have previously shown that FERARI members are recruited and stabilized on SNX1 positive structure (Solinger et al., 2020). To determine molecular structure of FERARI, we needed first to devise a purification scheme. To this end, we aimed to express FERARI in yeast. However, unlike HOPS tethering complex, we were unable to express all six members in yeast at the same time. More specifically, Rabenosyn-5 was not expressed in yeast while all other members were detectable. For that reason, we adapted different approach. We expressed all five members except Rabenosyn-5 in yeast. In addition, we used HEK-293 cells for expressing GFP-TEV-Rabenosyn-5. GFP served as a bait for pulling-down Rabenosyn-5 from the cell lysate.

GFP-Beads carrying rabenosyn-5 were then incubated with yeast extracts containing the other five members of FERARI. To remove Rabenosyn-5 from the GFP, we used TEV cleavage site between GFP and Rabenosyn-5. We did on bead digestion with TEV enzyme to cleave GFP from Rabenosyn-5. To optimize purification scheme, we tested three types of beads, agarose, dyna, and magnetic agarose beads and compared which type of bead was most efficient in

the pulldown and purification of FERARI proteins. To see whether we were able to purify entire FERARI complex, we performed FairBanks comassie staining and silver staining as shown in Fig. 5.2A. Interestingly, molecular weight of four FERARI members, VIPAS39, VPS45, EHD1 and Rab11-FIP5, is close to 70 KDa. Therefore, it is very difficult to distinguish them in the comassie and silver stained SDS-PAGE gels. However, in Fig 5.2A we can see several bands appearing around 70KDa in elution, suggesting that, we were able to purify FERARI.

Next, we conducted western blot experiments with specific antibody to confirm the elution of FERARI members. Our western blot data, in Fig. 5.3, shows that TEV enzyme efficiently cleaved GFP from Rabenosyn-5 and the presence of cleaved Rabenosyn-5 in elution. Furthermore, by using antibody specific to Rab11-FIP5, we can see the presence of Rab11-FIP5 mostly in the GFP-agarose bead marked lane. However, we could not detect Rab11FIP5 in case of Dyna beads and Magnetic beads. Therefore, we decided to proceed with GFP-agarose beads samples for negative stain EM. Furthermore, we have detected VIPAS39, EHD1 and ANK1 in the elution by western blot (Fig. 5.3). Altogether, we have successfully reconstituted mammalian FERARI expressed in yeast and HEK-293 cells.

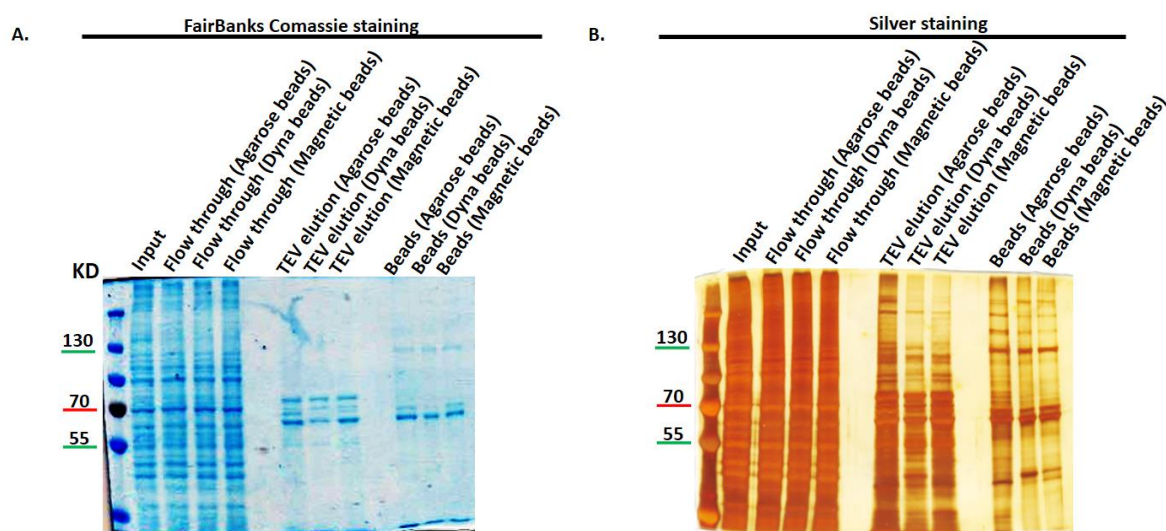


Figure 5.2. FERARI pulldown with different GFP-Beads. A,B) Samples collected in different steps of FERARI purification (a detailed description of the FERARI purification method is present in the materials and method section) were subjected to SDS-PAGE gel. (A) Fairbanks Comassie and (B) Silver staining was conducted to monitor FERARI purification.

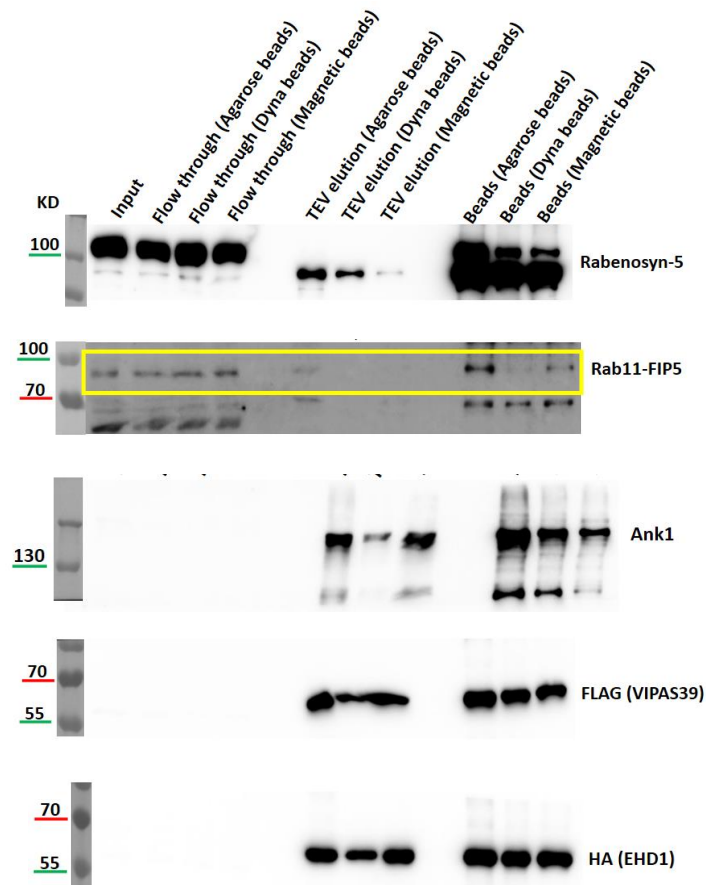


Figure 5.3. Samples collected in different steps of FERARI purification (a detailed description of the FERARI purification method is presented in the materials and method section) were subjected to immunoblot with corresponding antibodies (Rabenosyn-5, Rab11-FIP5, Ank1, VIPAS39 (FLAG), and EHD1 (HA)).

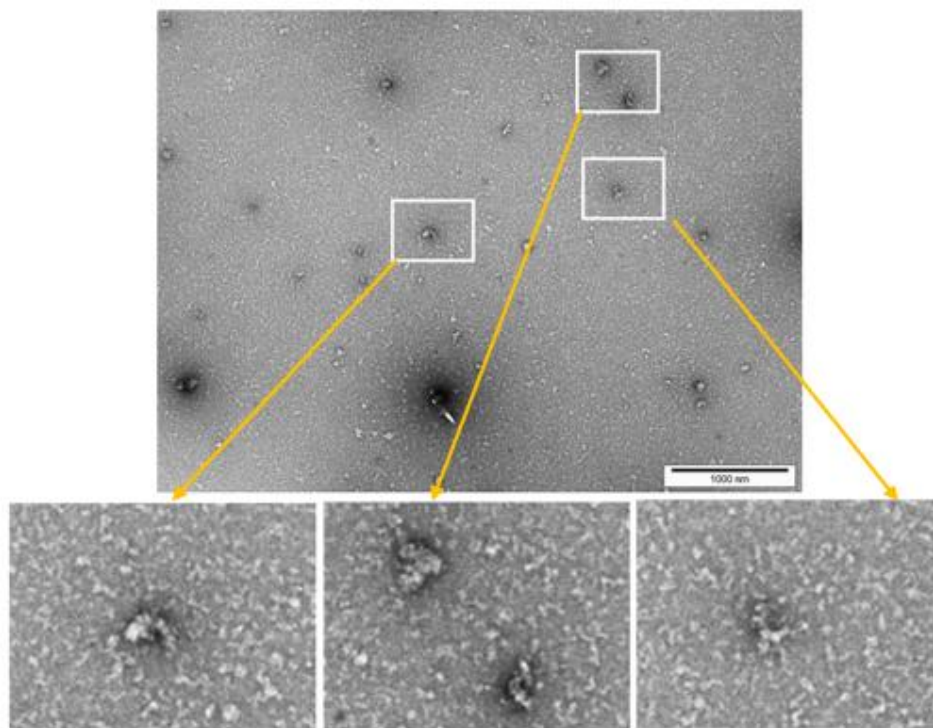
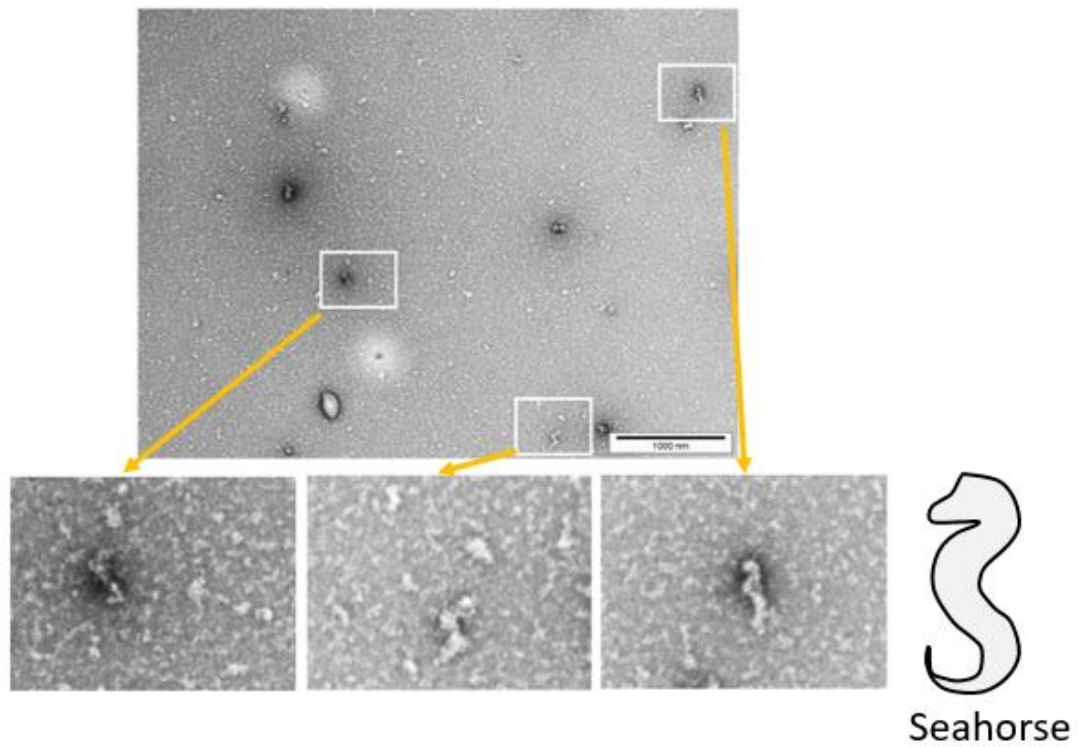


Figure 5.4: Negative stain EM data showing a seahorse like structure. Purified FERARI was loaded on EM grids and subjected to negative stain EM. Upper and lower panel showing some homogenous structures resembles a seahorse in different orientation. Magnification 4X.

Materials and methods

FERARI purification and negative stain EM

In short, GFP-TEV-RBSN was over-expressed in HEK-293 cells (4X10 cm dish, 2X10⁶ cells were seeded in each dish). Cell lysate was prepared by lysis buffer (50 mM TRIS/HCL (pH 7.5), 150 mM NaCl, 1% NP-40). Incubation of the lysate with GFP-Magnetic-Agarose Beads, Agarose beads, and Dyna beads for six hours. Beads were then washed for four times with lysis buffer. Washed beads was incubated with yeast lysate containing five other FERARI members (HA-EHD1, FLAG-VIPAS39, FLAG-Rab11FIP5, HIS-VPS45, 5. HIS-ANK1) overnight followed by four washes with lysis buffer. Beads were then Incubated with 100 µg of TEV protease diluted in 100 µl of lysis buffer for six hours followed by addition of another 50 µg of TEV protease for 6 more hours. The eluate was collected and divided into two tubes. 50 µl of laemmli buffer was added to 50 µl of elution and the mixture was heated at 95 degrees for 6 minutes. Rest of the purification was snap frozen for negative stain EM and kept at -80 degrees.

Negative stain EM protocol

Negative stain was done by Professor Camilo Perez's Lab

In short, grids were placed onto a cleaned microscope slide. For glowing discharging of grids: Slide was placed with grids on top (carbon side up) in vacuum chamber, and vacuum was pulled and glow was discharged for 30-60 s. Drops of UrAc (20-40 ul each) was pipetted onto parafilm two drops per sample. Excess stain and wash buffer from grids during staining was absorbed on Whatman paper. Stained grids were placed on another piece of labeled Whatman paper. Grid was hold with clamping forceps. 6 µl of protein solution was pipetted onto grid. After 20-45 s, buffer-protein solution was blotted off onto Whatman paper, touched to first UrAc drop, blotted off excess stain immediately, touched to second UrAc drop. Waited 10-30 s, then blotted off UrAc (take care to blot out liquid trapped in forceps). Grid was then washed by touching to a drop of buffer and blotted off the excess. Grid was placed onto labeled Whatman paper and dried dry for a few minutes, then place in grid box. Grids were visualized on the same day.

Fairbanks staining

SDS-PAGE gel was incubated in de-staining solution (7% acetic acid, 50% methanol) for 2 hours on shaker followed by incubation with solution A (25% isopropanol, 10% acetic acid, 0.05% Serva Blue G250) for another 2 hours. Afterwards SDS-PAGE gel was incubated in solution B (10% Isopropanol, 10% acetic acid, 0.005% Serva Blue G250) for 1 hour. After 1 hour, solution B was replaced with solution C (10%acetic acid, 0.002% Serva Blue G250) and the SDS-PAGE gel was incubated for another 1 hour in solution C. In the final step, we incubated the gel in solution D (10% acetic acid) for 1 hour. A picture of the gel was taken by using Canon scanner (model: Canoscan 9000F).

Silver staining

SDS-PAGE gel was incubated in fixing solution (40% ethanol, 10% acetic acid, 50% water) for 1 hour followed by washing in water for 4 times. Reducing solution (60 ml of dist. water with 10 μ l of 1 M DTT) was added to the gel and microwaved for 10-15 secs for three times. The solution was discarded after 5 minutes of shaking at RT and the gel was washed with water. 0.1% silver nitrate was used to stain the gel for 15 minutes. After a short wash with water, the gel was incubated with developing solution (3% Na_2CO_3 + 40 μ l of formaldehyde in 50 ml solution) and swirled for 30 secs. This was repeated twice more followed by washing with water briefly. Developing step was repeated once more. In second developing stage stopping solution (10% acetic acid) was added when the protein bands were sharp and the gel background starts to appear brownish. Ten minutes later, the gel was washed with water and a picture was taken.

6. FERARI regulates primary ciliogenesis

Statement of contributions

Harun-Or Rashid conducted all the experiments of this part of the thesis.

Professor Anne Spang supervised this project.

6.1 Summary

The primary cilia are microtubule-based sensory organelle that emanates from the cell surface during growth arrest. The primary cilium is found in almost all types of human cells. The primary ciliary membrane contains receptors and protein channels, and functions to organize a number of cellular signaling pathways, such as WNT and hedgehog signaling. Impaired cilia development has been implicated in ciliopathies, which is a combination of several diseases such as Polycystic Kidney Disease, Bardet-Biedl and Down syndrome, retinitis pigmentosa, Meckel-Gruber syndrome, and oral-facial-digital syndrome, and hearing loss. Impaired endocytic recycling has also been suggested to be implicated in ciliopathies.

In the cilia developmental process, a preciliary vesicle is formed on the mother centriole, followed by more extensive ciliary vesicle formation and axoneme extension that protrudes from the cell surface. Cilia development entails polarized membrane trafficking to the centrosome, which includes vesicular transport and association of different Rab-GTPases and their GAP and GEF proteins. During the ciliary development process, Rab11 is localized to the centrosome, where it plays a vital role in the activation of Rab8 through interaction with Rab8-GEF protein Rabin8. However, very little is known about how vesicular transport is coupled to cilium formation or how membrane assembly is connected to axoneme development. Furthermore, the molecular machinery involved in Rab11 recruitment at the ciliary base is not well understood. Here, we demonstrate that FERARI regulates cilia development by recruiting Rab11 at the ciliary base. Immunoprecipitation data shows the existence of the FERARI platform in retinal pigment epithelium (RPE) cells. CRISPR-mediated knock-out of FERARI members, *vipas39*, *ehd1*, and Rab11 effector protein *Rab11-fip5* causes impaired cilia development in RPE cells. While FERARI KO cells did not impair mother centriole movement and initiation of axoneme formation, the cilia were much shorter, rendering them presumably non-functional. Moreover, FERARI members were substantially localized at the ciliary base. Our study revealed an unexpected function of FERARI in cilia formation and growth.

6.2 Introduction

6.2.1 Types of cilia and their development

Cilia are conserved microtubule-based organelles protruding from the surface of virtually all types of mammalian cells. This complex and dynamic structure is divided into two sub-types: motile and non-motile cilia. The former one is also called secondary cilia. It possesses the property to beat rhythmically. By contrast, non-motile cilia or primary cilia do not have the property of rhythmic beating (Mitchison & Valente, 2017). While in all vertebrates, including humans, most cells can generate a single non-motile primary cilium, some specialized vertebrate cells are capable of generating many dozens of motile secondary cilia. These specialized multiciliated cells are found in the spinal cord, in the respiratory epithelium, and in the fallopian tube, where they generate movement of extracellular fluids. The primary cilium senses physical and biochemical extracellular signals, and differs from their multiciliated counterpart mainly in structural properties (Brooks & Wallingford, 2014).

Cilia development process or ciliogenesis is coordinated with the cell cycle. In general, primary cilia are assembled in quiescent somatic cells and during G0 and G1 phase. However, when cells enter into the S/G2 phase, cilia begin to disassemble (Dawe et al., 2007; Higgins et al., 2019). Therefore, there is an inverse relationship between cell proliferation and the development of the primary cilium. The mother centriole plays vital role in cilia formation as it serves as a physical template for basal body (BB) formation. After cell cycle exit, the mother centriole moves towards and docks to the plasma membrane (PM), and then converts into a BB. Once the BB is docked to the PM, it nucleates microtubules, which emanates along the PM and give rise to the cilium. As shown in the Fig. 6.1, extended microtubules from the BB form the main body of the cilium called axoneme. Axoneme is composed of nine sets of microtubule doublets covered by a phospholipid membrane. The ciliary membrane is continuous with the plasma membrane, but distinct in its protein and lipid properties (Avasthi & Marshall, 2012). Like mitochondria, ER and, the Golgi apparatus the cilium is a specialized cellular membrane bound organelle. However, unlike other organelles, the ciliary membrane is contiguous with the cell membrane and the base of the cilia is open to the cytoplasm (Takeda & Narita, 2012).

At the root of the cilium, inward curvature of the PM forms ciliary pocket. Axoneme elongation towards the distal tip is mostly regulated by intraflagellar transport (IFT), the two-way transport system that delivers cargo within the cilium and maintain the cilium function. IFT is crucial because protein translation is limited to the cytoplasm and the extension of axoneme requires selective import and trafficking of the ciliary protein to the distal tip. The distal region of the basal body, where the axoneme begins to extend, is known as the Transition Zone (TZ). Cargo trafficking along the cilium to tip is called anterograde transport, and the kinesin proteins catalyze this process. In contrast, retrograde IFT from ciliary tip to the cell body is dynein dependent (Pedersen & Rosenbaum, 2008; Rosenbaum & Witman, 2002; Takeda & Narita, 2012). IFT is crucial for the assembly, disassembly, and preservation of cilium. Once

the primary cilia are fully assembled, they remain highly dynamic as new tubulin molecules are recruited to the ciliary tip on a continuous basis. However, the ciliary length is not further extended because the assembly is adjusted by continuous turnover of tubulin within the cilium (Stephens, 1999).

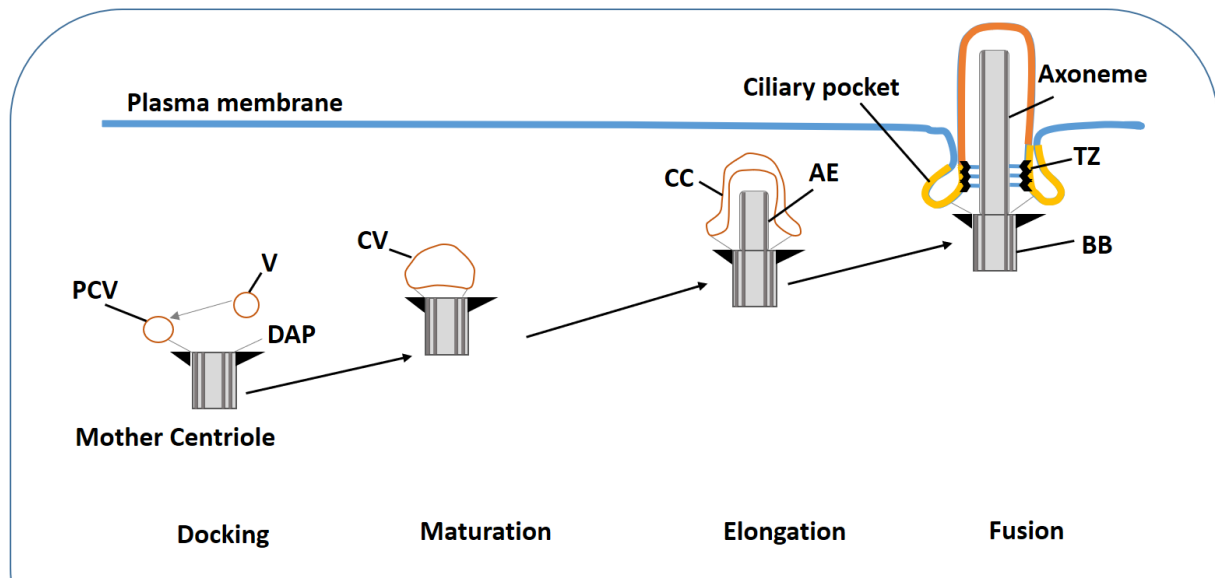


Figure 6.1: Ciliogenesis. Cilium formation starts when a mother centriole contacts a preciliary vesicle. The ciliary vesicle grows with the axoneme and gives rise to the ciliary cap, whose fusion with the plasma membrane externalizes the cilium and transforms the outer sheath into the periciliary membrane. Adapted from (Blacque et al., 2017).

PCV: Pre-ciliary vesicle; CC: Ciliary Cap; V: Vesicle; DAP: Distal Appendages; AE: Axoneme extension; BB: Basal Body; TZ: Transition Zone

6.2.2 Signaling through primary cilia

The fully grown primary cilium is enriched in receptors and ion channels that sense extracellular cues and play a vital role in signal transduction (Goetz & Anderson, 2010). The term cell antenna refers to the activity of primary cilium as it plays a central role in cell signaling during development and homeostasis. Signaling receptors present on the ciliary membrane, regulatory proteins at the basal body and the transition zone control the signaling cascade. An extensive array of signaling routes have been associated with the cilium, including Hedgehog, Notch, mTOR, Hippo, Wnt, GPCR, PDGF (and other RTKs including FGF), and TGF-beta (Clevers & Nusse, 2012; Corbit et al., 2005; Haycraft et al., 2005; Huang & Schier, 2009; Wheway et al., 2018).

The primary cilium is an ideal organelle for investigating hedgehog signaling pathways due to the abundance of the Sonic Hedgehog (shh) receptor Patched1 (PTCH1) on the ciliary membrane. Shh binding inactivates and delocalizes PTCH1 from the primary cilia, which in turn accumulates the transmembrane protein Smoothened (SMO) in cilia. This then allows Gli

activation and transport to the nucleus where it acts as transcription regulator (Corbit et al., 2005; Haycraft et al., 2005; Weiss et al., 2019; Zeng et al., 2010). The ADP-ribosylation factor (Arf)-like small GTPase (ARL13B), is a member of the ARF family of regulatory GTPases, which is highly enriched in the cilia, and is vital for ciliogenesis and Sonic Shh signaling (Larkins et al., 2011).

Hyper-activation of WNT signaling has been reported in mouse models with defected cilia (Zullo et al., 2010). Furthermore, depletion of BB components (*bbs1*, *bbs4*, and *bbs6*) interferes with Wnt signaling (Gerdes et al., 2007). Several Notch receptors are present on primary cilia and the activation of Notch is diminished in IFT depleted keratinocytes and developing embryos (Ezratty et al., 2011). Polycystin-1 (PC1) negatively regulates mTOR pathway in the kidney epithelia through interacting with tuberlin, an upstream regulator of mTOR (Shillingford et al., 2006). More recently, mTOR hyperactivation was also seen in mice kidney epithelia carrying mutant ciliary gene *Odf1* (Zullo et al., 2010). Furthermore, in zebrafish embryos rapamycin treatment was sufficient to reverse the disease causing phenotypes of depleted ciliary genes (Tobin & Beales, 2008).

6.2.3 Vesicular transport and Rab-GTPases in cilia development

Development of the primary cilium requires recruitment of pre-ciliary vesicles to a specialized form of the mother centriole called the distal appendages (Yee & Reiter, 2015). Small cytoplasmic vesicles (termed pre-ciliary vesicles, PCVs) are recruited to the distal appendages of the mother centriole before reaching the plasma membrane. PCVs are believed to generate from the Golgi and the recycling endosome¹⁸⁸. Cargo transport to and within the cilium is regulated by the coordinated function of small GTPases (Rab, Arls, and Arfs) and protein complexes, such as BBSome, exocyst, and IFT complexes. The BBSome is composed of 7 BBS subunits, BBS1, BBS2, BBS4, BBS5, BBS7, BBS8, BBS9, and BBIP10. Two IFT subcomplexes, IFT-A and IFT-B, together with the BBSome, serve as cargo adaptors for ciliogenesis (Hsiao et al., 2012; Inoue et al., 2008; Kim et al., 2010). Furthermore, IFT-A regulates retrograde protein trafficking within cilia in association with ARL13B (Nozaki et al., 2017). IFT genes principally facilitate entry/or retention of ARL13B in cilia through active transport mechanisms (Cevik et al., 2013).

Rab8 in GTP-bound form regulates the cargo protein entry into the cilium, whereas Rab11 and the BBSome, activates Rab8 at the ciliary base through recruitment of Rabin8 (Nachury et al., 2007). Rab8 is the only Rab-GTPase, identified to date, that localizes on the ciliary membrane. Although in human Retinal Pigment Epithelial (RPE) cells, GFP-Rab8a decorates both the ciliary base and the growing axoneme but it does not localize on mature ciliary membrane. As shown in Fig. 6.2, the Endocytic recycling regulator and membrane remodeling protein EHD1, in association with the Rab11-Rabin8-Rab8 cascade, work in early ciliogenesis (Knödler et al., 2010a, p. 11).

EHD-mediated membrane tubulation is crucial for ciliary vesicle formation from small preciliary vesicles or distal appendages vesicles (DAVs). EHD1 binds with a SNARE membrane fusion regulator SNAP29 by localizing at preciliary membrane, which regulates the fusion of multiple preciliary vesicles and formation of large ciliary vesicles (CV). CVs are then extended around the distal end of the mother centriole and forms ciliary cap (CC) (Bhattacharyya et al., 2016; Lu et al., 2015). EHD1 localizes to preciliary vesicular membranes and the ciliary pocket.

Recruitment of Rab8 to ciliary vesicle depends on recruitment of other proteins associated with ciliary vesicle generation, such as, the endocytic transport and recycling regulator EHD1 and IFTs. However, activation of Rab8 takes place only after ciliary vesicle assembly (Yee & Reiter, 2015). Recent studies suggest that Rab11 stimulates the activity and recruitment of Rab8 to the mother centriole and thus regulates the activation of Rab8 (Blacque et al., 2017). However, recruitment of Rab11 to the ciliary base is largely obscure.

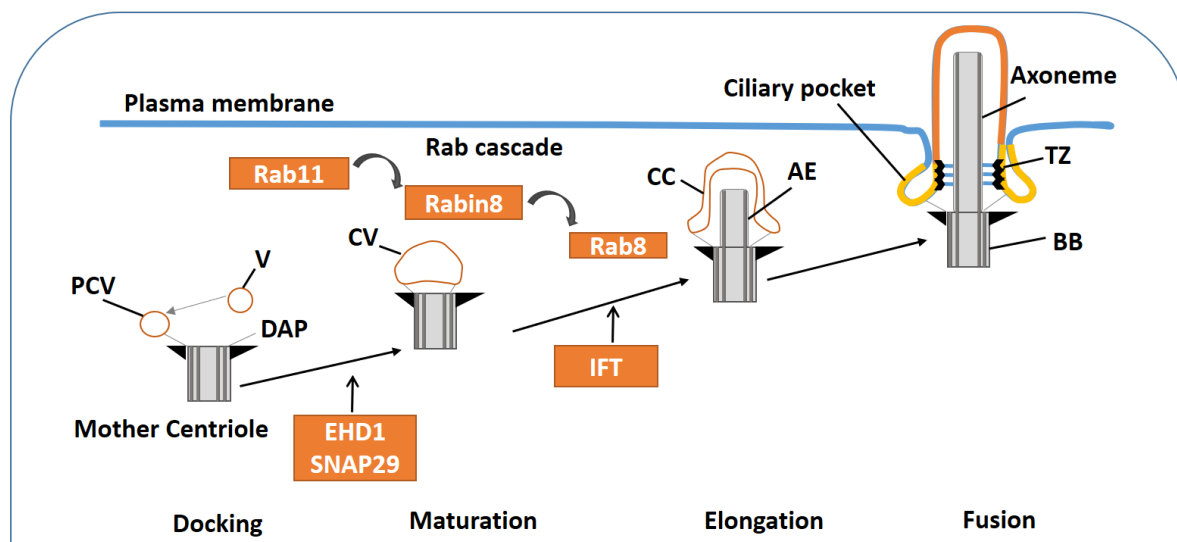


Figure 6.2: This figure is depicting the different stages of cilia development and the association of Rab-GTPases. Proposed model of RAB11-RAB8 cascade during intracellular ciliogenesis. Immediately after initiation of ciliogenesis, Rab11 recruits and activates Rab8 on the vesicles (V) that dock to the distal appendages of the mother centriole containing the preciliary vesicles, followed by the formation of small ciliary vesicles (CV). The fusion of these small vesicles is regulated by the membrane remodeling protein EHD1 and the membrane fusion protein SNAP29. A more extensive CV then caps the distal end of the mother centriole. Rab8, which is recruited and stimulated by Rab11, eventually drives membrane extension of CV. Finally, CV is fused with the plasma membrane (PM), and IFT elongates the ciliary axoneme (Ax). Adapted from (Blacque et al., 2017).

PCV: Pre-ciliary vesicle; CC: Ciliary Cap; V: Vesicle; DAP: Distal Appendages; AE: Axoneme extension; BB: Basal Body; TZ: Transition Zone

6.3 Aim of the study

Rab11 is enriched around the BB of growing primary cilia, but Rab11 does not localize on the ciliary membrane (Knödler et al., 2010a). Depletion of Rab11 results in a significant decrease in cilium length. Furthermore, Rab11 effector proteins, Rab11-FIP3 and Rab11-FIP5, have also been reported to involve cilia formation and maintenance. Moreover, vesicles required for cilia formation are mostly derived from the Golgi and Rab11 positive recycling endosome. Furthermore, Rab11 regulates the interaction between BBSome and Rabin8 crucial for ciliogenesis (Knödler et al., 2010b). Recently, Rabenosyn-5 and its binding partner VPS45, have been reported as a regulator of ciliary and pre-ciliary membrane homeostasis (Scheidel et al., 2018). We have discovered a protein platform, FERARI, regulates Rab11-mediated cargo trafficking for recycling. Rabenosyn-5, VPS45, EHD1 and Rab11-FIP5 are member of FERARI (Solinger et al., 2020). Therefore, we wanted to test the potential role of FERARI, as a platform, in ciliogenesis.

6.4 Results

FERARI is conserved in RPE cells

hTERT RPE cells are most widely used for the studies of primary cilia. To investigate the role of FERARI, a protein platform of six subunits, in ciliogenesis, we used RPE cells as a model system. First, we sought to determine whether FERARI exists in RPE cells. We found that transiently overexpressed VPS45 interacts with endogenous VIPAS39 (Fig. 6.3B). Furthermore, our immunoprecipitation data shows that endogenous Rabenosyn5 and VIPAS39 interacts with transiently overexpressed EHD1 (Fig. 6.3 C, D), confirming the existence of the FERARI platform in RPE cells similar to that we observed in HEK-293 cells (Solinger et al., 2020).

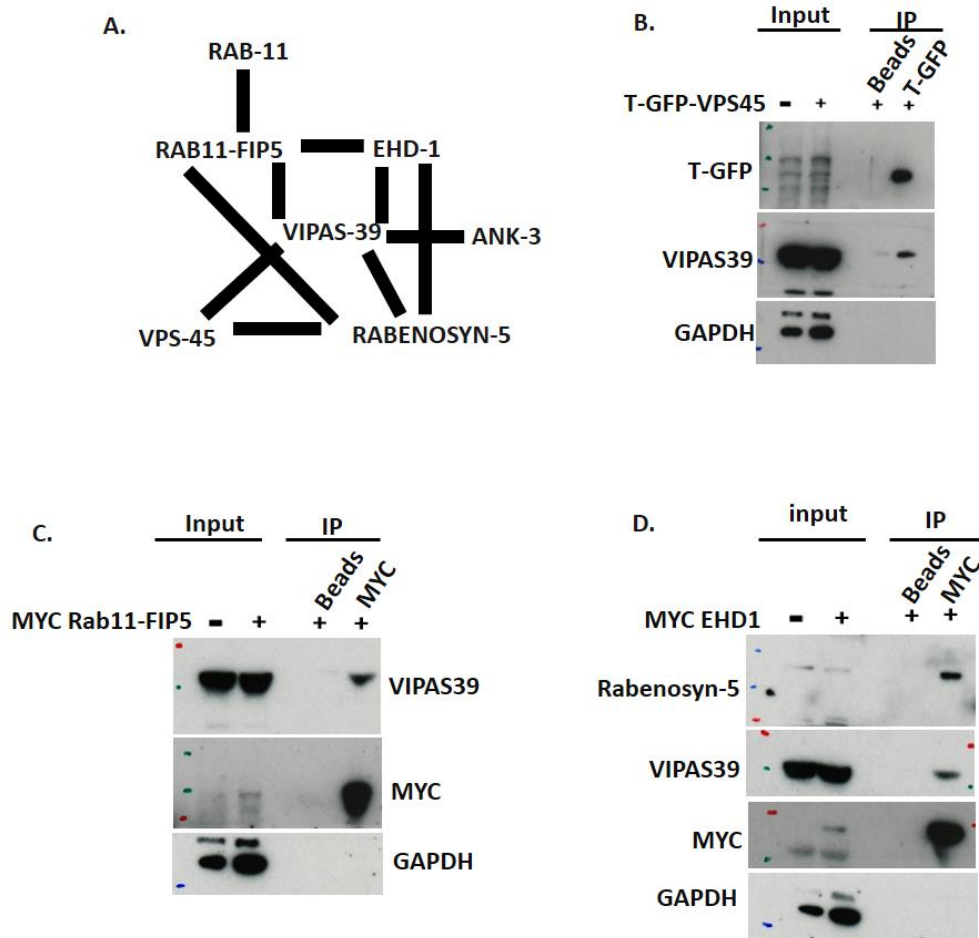


Figure 6.3: Existence of FERARI in RPE cells. A.) An interaction picture of FERARI subunits (Solinger et al., 2020). VIPAS39 is associated with all other FERARI members. B.) Interaction of endogenous VIPAS39 with VPS45. RPE cells were transfected with turbo-GFP tagged VPS45 for 48 hours, followed by immunoprecipitation with turbo-GFP nanobodies as bait. Turbo-GFP, VIPAS39, and GAPDH were detected. C.) Interaction of endogenous VIPAS39 with transiently overexpressed Rab11-FIP5. RPE cells were transfected with MYC-Rab11-FIP5 for 48 hours, followed by immunoprecipitation with MYC nano-bodies as a bait. MYC, VIPAS39, and GAPDH were detected D.) Interaction of endogenous Rabenosyn-5 and VIPAS39 with another FERARI subunit EHD1. RPE cells were transfected with MYC-EHD1 for 48 hours, followed by immunoprecipitation with MYC nano-bodies as bait. MYC, VIPAS39, and GAPDH were detected.

ARL13B interacts with FERARI subunits

Due to the abundance of ARL13B on the ciliary membrane, it has been extensively used as a ciliary marker (Dilan et al., 2019, p. 13; Kasahara et al., 2014). Multi subunit tethering complex (MTC) exocyst subunits, Sec8, Exo70, and Sec5, preferentially interacts with GTP bound form of ARL13B (Seixas et al., 2016, p. 13). Furthermore, ARL13B has also been reported to interact with FERARI subunit Rab11-FIP5 (He et al., 2018). We speculated that ARL13B might interact with other FERARI members. We investigated the interaction between endogenous ARL13B

and FERARI subunits VIPAS39 and Rabenosyn-5. Our immunoprecipitation data (Fig. 6.4) shows that endogenous ARL13B can co-immunoprecipitated with both FERARI subunits.

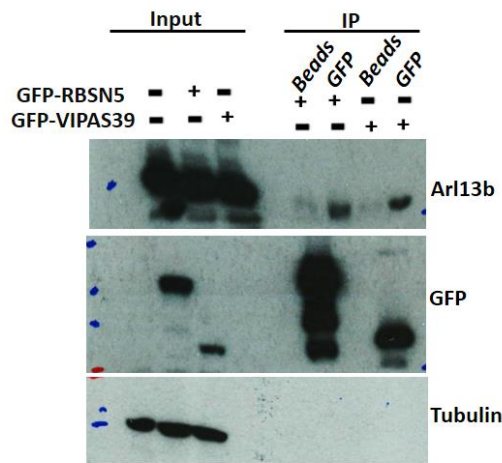


Figure 6.4: Ciliary marker ARL13B co-immunoprecipitates with FERARI subunits. Interaction of endogenous ARL13B with transiently overexpressed FERARI subunits Rabenosyn-5 and VIPAS39. RPE cells were transfected with GFP-Rabenosyn-5 and GFP-VIPAS39, individually, for 48 hours followed by immunoprecipitation with GFP nano-bodies as a bait. ARL13B, GFP and tubulin were detected by western blot.

FERARI regulates cilia size

The reverse genetics approach in *C. elegans* identified two FERARI subunits, Rabenosyn-5, and its binding partner VPS45, as a regulator of ciliary structure (Scheidel et al., 2018). Furthermore, the involvement of EHD1 has also been reported in the cilia development process (Lu et al., 2015). We hypothesize that FERARI as a platform might regulate the development of cilia. To determine whether FERARI plays a role in cilia development, I knocked-out *vipas39*, *rab11-fip5*, and *ehd1* in RPE cells, individually by CRISPR/Cas9 (Fig. 6.5 A, D, G). We have shown previously that VIPAS39 is a critical FERARI member (Solinger et al., 2020). First, to induce the cilia formation, we starved the ctr KO and *vipas39* KO RPE cells for 24 hours and analyzed the cilia length by immunofluorescence (IF), using ARL13B as cilia marker. Then we measured the length of ARL13B positive structure in ctr and KO cell lines. We found that the length of cilia was significantly reduced in *vipas39* KO cells in comparison to control (Fig. 6.5 B, C). To investigate whether the reduced cilia size in *vipas39* KO cells is the role of FERARI tethering platform or the individual role of VIPAS39, I analyzed cilia length in other FERARI KO RPE cells. Similar to that of *vipas39* KO cells, cilia length was reduced significantly in *rab11fip5* and *ehd1* KO RPE cells compared to the control (Fig. 6.5 D, E, G,H,I). FERARI appears to be involved in proper cilia formation.

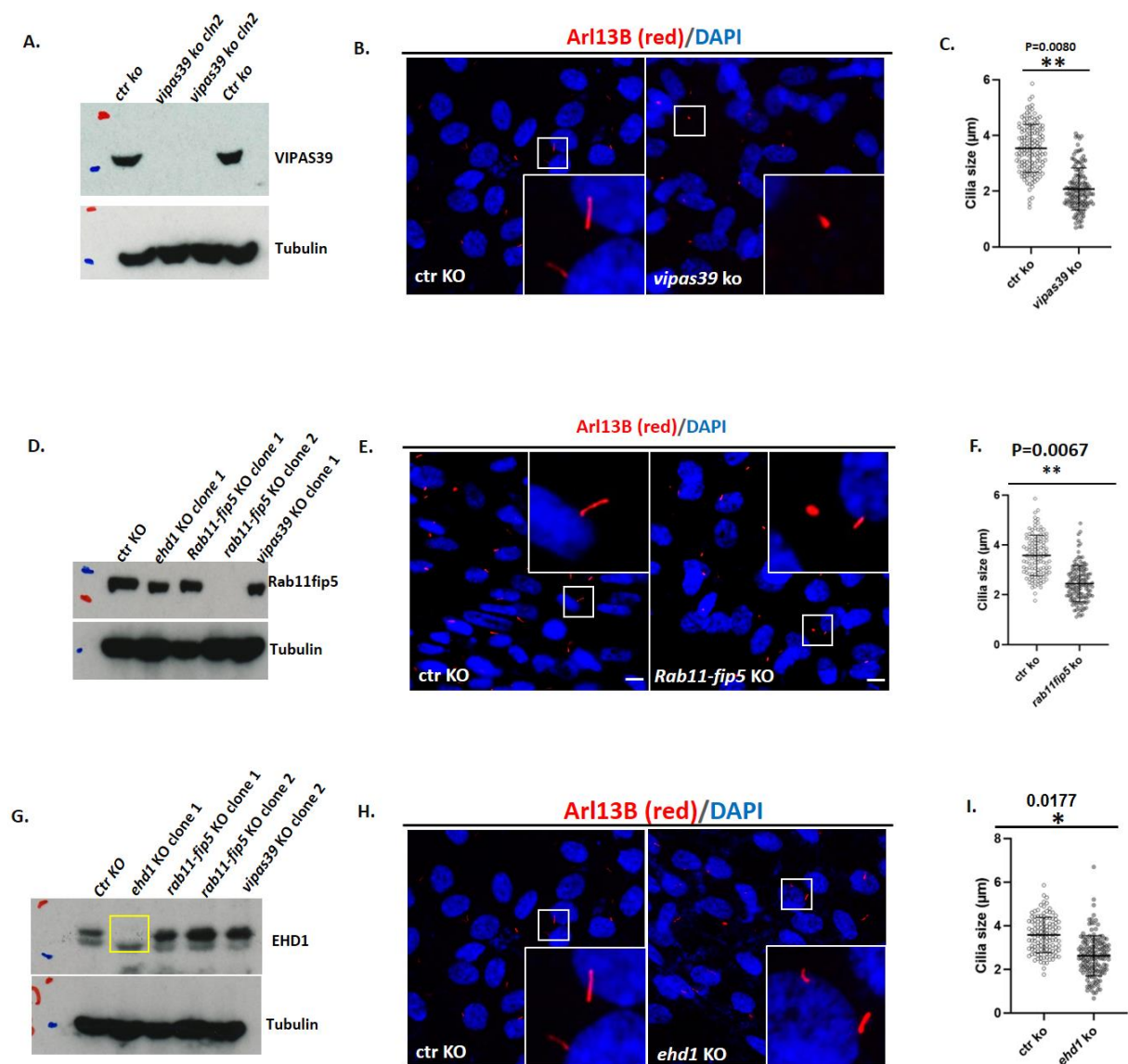


Figure 6.5: FERARI regulates cilia length. A.) CRISPR-Cas9-mediated ctr and *vipas39* KO cells were subjected to WB with antibodies against VIPAS39, and tubulin. B.) Immunofluorescence data are showing the cilia in red and the nucleus in blue. ctr KO and *vipas39* KO cells were starved for 24 hours, followed by detection of ARL13B by immunofluorescence. C.) Cilia length is significantly reduced in *vipas39* KO cells, and the length of the cilia was measured by using ImageJ software. D.) CRISPR-Cas9-mediated ctr and *rab11fip5* KO cells were subjected to WB with antibodies against Rab11-FIP5 and Tubulin. E.) ctr KO and *rab11-fip5* KO cells were starved for 24 hours, followed by detection of ARL13B by immunofluorescence. F.) Cilia length is significantly reduced in *rab11-fip5* KO cells. G.) CRISPR-Cas9-mediated ctr and *ehd1* KO cells were subjected to WB with antibodies against EHD1 and Tubulin. H.) ctr KO and *ehd1* KO cells were starved for 24 hours, followed by detection of ARL13B by immunofluorescence. I.) Cilia length is significantly reduced in *ehd1* KO cells. (Scale bars- 5 μm; Inlet magnification 4X).

FERARI is localized at the ciliary base

Our data indicates that FERARI interacts with ARL13B. Moreover, loss of FERARI impaired cilia length. Several studies suggest that FERARI members Rab11-FIP5 and EHD1 localize to cilia in RPE cells (He et al., 2018; Lu et al., 2015). Therefore, we asked next whether FERARI is localized to cilia. We conducted IF in RPE cells by using antibodies against ARL13B and FERARI subunits. In fig. 6.6, our IF data show that Rab11-FIP5 is localized at the ciliary base. This data corresponds to the previous finding of Rab11-FIP5 localization (He et al., 2018). Then we investigated the localization of EHD1. Interestingly, we observed that EHD1 is localized at both the ciliary base and the ciliary membrane decorated with ARL13B. Finally, we examined the localization of Rabenosyn-5 in RPE cells at the endogenous level. Similar to that of other FERARI subunits, Rabenosyn-5 is also highly expressed at the ciliary base (fig. 6.6 lower panel). However, Rabenosyn-5 is a bit more dispersed than Rab11-FIP5 and EHD1 surrounding the cilia. The distribution of FERARI at the ciliary base indicates its involvement in the cilia development process.

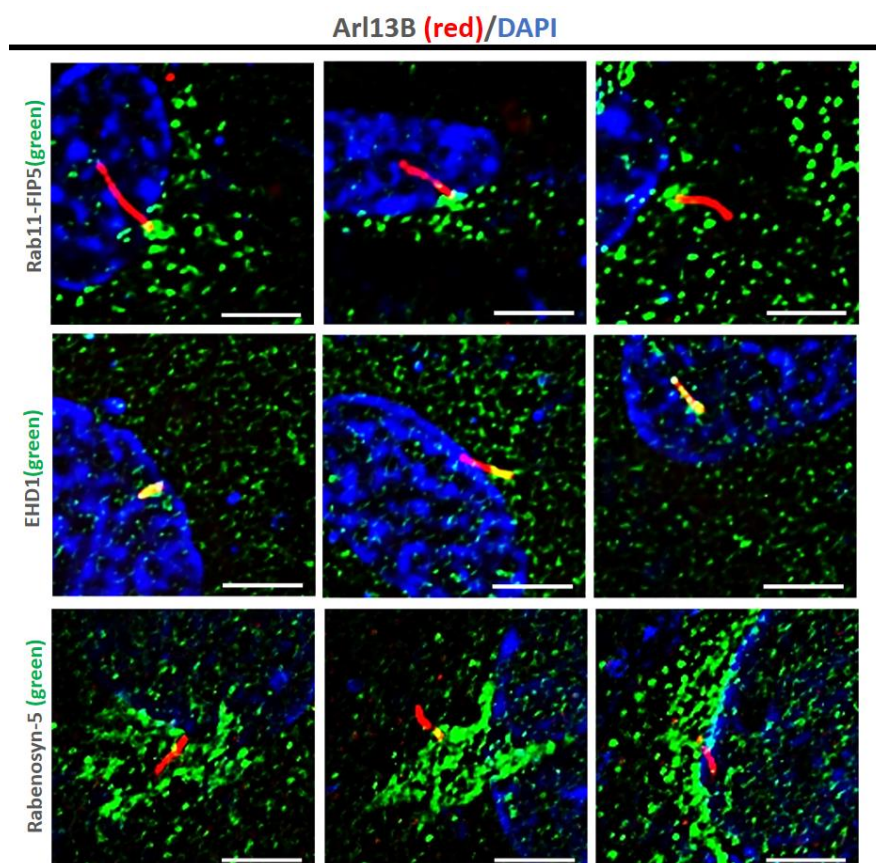


Figure 6.6. FERARI subunits localize at the ciliary base. The upper panel showing Rab11-FIP5 in green localizes at the base of the cilia in red detected by Arl13b antibody and DAPI in blue is showing the nucleus. The middle panel shows endogenous EHD1 localizes at the base of the cilia and a pool of EHD1 localizes at the ciliary membrane as well. Lower panel shows endogenous Rabenosyn-5 is highly expressed surrounding the cilia. (Scale bars- 5 μ m)

FERARI regulates the Rab11 recruitment to the developing cilia

Rab11 Stimulates the GEF activity of Rabin8 towards Rab8, and the activation of Rab8 is crucial for ciliogenesis (Westlake et al., 2011). Recent studies demonstrate that during the cilia development, transferrin receptor (TfnR) positive Rab11 vesicles are localized to the basal body under starvation condition (Jo & Kim, 2013; Kim et al., 2010; Westlake et al., 2011), suggesting that, these Rab11-positive structures are recycling endosomes. A recent study in HeLa cells demonstrated the involvement of ARL13B in Rab11 mediated endocytic recycling (Barral et al., 2012). Regulation of Rab11 mediated recycling by FERARI, its interaction with ARL13B led us to investigate the recruitment of Rab11 to the ciliary base in ctr and FERARI depleted cells. Our preliminary data indicates that transiently expressed GFP-Rab11 is highly enriched around the developing primary cilia in ctr KO cells (Fig. 6.7). In contrast, Rab11 enrichment around ARL13B is drastically reduced in *vipas39* KO cells, suggesting that, FERARI might regulate the efficient recruitment of Rab11 to the primary cilia. To corroborate this finding, I examined the GFP-Rab11 level at the ciliary base in *ehd1* KO cells. Consistent with the *viaps39* KO condition, Rab11 recruitment to the ciliary base has also impaired in the *ehd1* KO cells. Altogether, FERARI regulates the cilia length presumably by promoting efficient recruitment of Rab11 to the ciliary base.

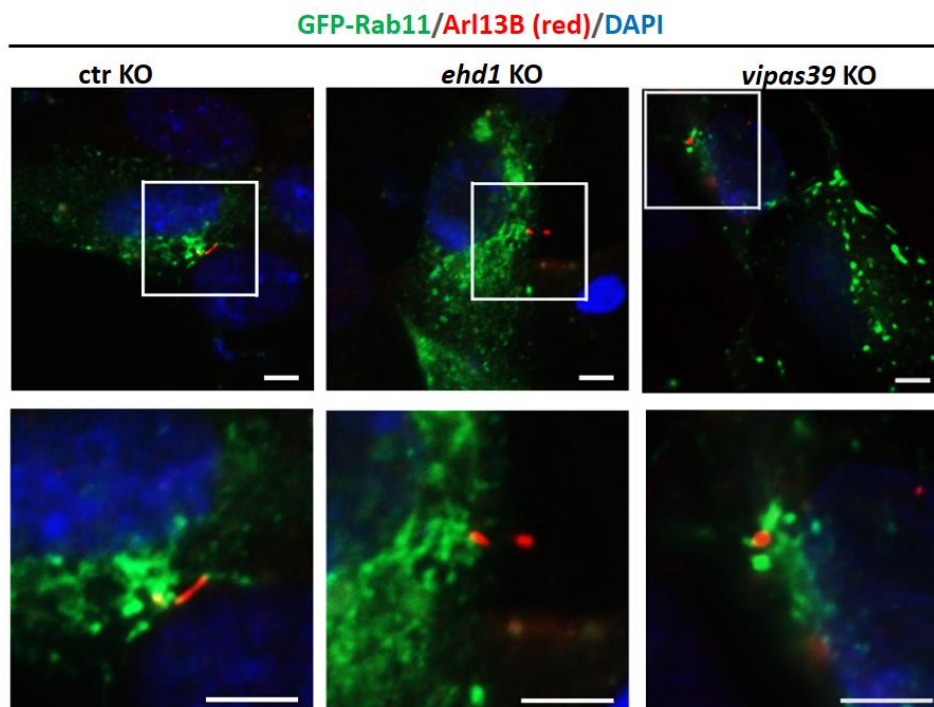


Figure 6.7: Rab11 is not efficiently recruited to the ciliary base. RPE cells were transfected with GFP-Rab11 followed by starvation for 24 hours. Immunofluorescence data show GFP-Rab11 in green, ARL13B in red, and nuclear marker DAPI in blue in three different conditions. The left, middle and, right panel is showing ctr KO, *ehd1* KO, and *vipas39* KO cells, respectively. (Scale bars- 5 μ m; magnification 3X)

6.5 Discussion and outlook

The primary cilia development includes, microtubule organization and vesicular trafficking (Hsiao et al., 2012; Leroux, 2007; Yee & Reiter, 2015). Previous studies show that the individual function of some FERARI members is crucial for ciliogenesis. However, the involvement of VIPAS39 in ciliogenesis was not known. Here in this work, I show that FERARI, as the tether, is involved in primary ciliogenesis.

In RPE cells, endogenous FERARI subunit VIPAS39 interacts with transiently expressed VPS45, Rab11-FIP5, and EHD1. Furthermore, endogenous Rabenosyn-5 also shows the interaction with transiently expressed EHD1. These interactions strongly suggest that FERARI exists in RPE cells. Most interestingly, the ciliary marker ARL13B was immunoprecipitated with two FERARI members at an endogenous level. Previously ARL13B has been shown to interact with tethering complex exocyst (Nozaki et al., 2017; Seixas et al., 2016). Therefore, it is plausible to hypothesize that the function of ARL13B might be regulated through interaction with two tethers or vice versa.

Recycling endosomal markers, Rab11 and TfnR, colocalize with the preciliary vesicles, which supply ciliary proteins crucial for the initial phase of ciliogenesis (Kim et al., 2010). These preciliary vesicles are then extended to form a ciliary vesicle with help of EHD1. Our immunofluorescence data shows that at the endogenous level, FERARI subunits are mostly localized at the ciliary base with partial overlap of EHD1 with the ARL13B decorated ciliary membrane. EHD1 is a crucial effector of ciliary vesicle development. It extends preciliary vesicle to larger ciliary vesicle, a function similar to the formation of tubulovesicular recycling endosome from sorting endosome (Deo et al., 2018; Yee & Reiter, 2015). Several studies have reported cilia length is shorter when Rab11- GDP is overexpressed or siRNA-mediated depletion of Rab11. Although the cilia length has been reduced in the Rab11 knockdown conditions, cilia development was not blocked completely (Jo & Kim, 2013). We found that cilia length was also significantly shorter in FERARI depleted cells. However, we did not see a complete block of cilia development, suggesting a possible connection between FERARI and Rab11 activity in cilia development.

Most of the signaling molecules, if not all, are transferred to cilia from the TGN and recycling endosomes through vesicles. Furthermore, cargoes can also be transported by vesicles originating from recycling compartments (Leroux, 2007). Rab11 and its effector protein, together with Arf- GTPase, regulate the cargo trafficking process to the ciliary base (Inoue et al., 2008). Furthermore, Rab11 is an upstream regulator of Rab8 that activates Rab8 and controls the downstream ciliary process. Localized activation of Rab8 at the mother centriole is crucial for ciliary membrane biogenesis. Therefore, Rab11 needs to be recruited to the ciliary base. We show that GFP-Rab11 is highly enriched at the ciliary base in ctr KO cells. Whereas, in FERARI KO cells, GFP-Rab11 localization is greatly decreased at the ciliary base. FERARI

regulates cargo trafficking via Rab11-mediated recycling pathway both in *C. elegans* and HeLa cells (Solinger et al., 2020). In RPE cells, FERARI might regulate the recruitment of Rab11 to the pericentriolar region that is crucial for ciliogenesis in RPE cells.

VPS45 and Rabenosyn-5 regulate cilia structure in neurons in *C. elegans* (Scheidel et al., 2018). In an attempt to delete VPS45 and Rabenosyn-5, I generated gRNA against both targets. However, gRNA treated single clones did not survive. Suggesting that these two proteins are crucial for the survival of RPE cells. Therefore, we would like to knock down these proteins in RPE cells by using the siRNA method and investigate cilia development. Furthermore, Rab11 regulates localized activation of Rab8 via stimulating GEF activity of Rabin8 towards Rab8. Therefore, we need to examine whether Rab8 can be activated in FERARI KO cells when Rab11 is not efficiently recruited. Recent study suggests that Rab11-FIP5 stabilizes cilia by regulating polyglutamylation of axoneme tubulin. Hypoglutamylation promotes cilia disassembly and leads to the shorter cilia size (He et al., 2018). Therefore, it would be interesting to investigate cilia import of glutamylase in FERARI KO cells. Moreover, IFT proteins play a crucial role in axoneme elongation. There are many IFT proteins, so it will be interesting to see whether FERARI regulates IFT activity. Moreover, we are now investigating PTCH1 signaling in CTR and FERARI KO RPE cells.

6.6 Materials and methods

Cell culture, transfection and CRISPR–Cas9 KO in mammalian cells

RPE cells were cultured and maintained in DMEM (Sigma) high-glucose medium with 10% FCS (Bioconcept), penicillin–streptomycin (1%), sodium pyruvate and L-glutamine. Cells were plated 1 d before transfection at 60–70% confluency and later transfected for 48 h using Helix-IN™ DNA (OZbiosciences HX11000) according to the manufacturer's instructions. A 2–5 µg quantity of DNA was used per reaction based on a 10-cm dish.

For CRISPR–Cas9-mediated KO, guide RNAs were selected using the CRISPR design tool (<http://chopchop.cbu.uib.no/>). A list of oligonucleotides is provided in the list gRNAs. Two guide RNAs were designed from two different exons for each target gene. Annealed oligonucleotides were cloned into two different plasmids, Px458 GFP (addgene; 48138) and Px459 Puro (addgene; 62988), respectively. In brief, HeLa cells were seeded at 2×10^6 cells per 10-cm dish. The following day, cells were transfected with 2.5 µg of the plasmids (control vectors without insert or vectors containing a guide RNA against the target gene). Transfecting medium was exchanged with fresh medium after 4 h. Cells were treated with puromycin for 24 h after transfection followed by FACS sorting (for GFP+ cells) the next day. For FACS sorting after 48 h of transfection, cells were trypsinized and resuspended in cell-sorting medium (2% FCS and 2.5 mM EDTA in PBS) and sorted on a BD FACS AriaIII Cell Sorter. GFP-positive cells were collected and seeded immediately in a new plate containing conditional media.

Conditional media was collected from dishes of untransfected WT RPE cells and then filter sterilized.

Immunoprecipitation assays

RPE cells were transfected with the indicated DNA constructs. After 36–48 h of transfection, protein extracts were prepared in lysis buffer (1% NP-40, 50 mM Tris/HCl pH 7.5, 150 mM NaCl) and Halt protease inhibitor cocktail (Thermo Scientific; 186 1279) at 4 °C for 20 min followed by centrifugation at 4 °C for 20 min at 13,000 rpm. Immunoprecipitations were performed as previously described (Solinger et al., 2020). In brief, protein extracts were incubated with Trap beads (nanobodies for GFP (GFP-Trap_A; gta-20-chromotek), myc (Myc-Trap_A; yta-20-chromotek), turbo-GFP (TurboGFP-Trap_A; tbta-20-chromotek)) for 4 h at 4 °C with rotation, and then washed five times with lysis buffer (1 ml). Protein complexes were eluted by heating beads for 5 min at 95 °C in 2X sample buffer and resolved by SDS–PAGE on 10% and 12.5% gels followed by immunoblot analysis. The blots were developed using WesternBright ECL solution (K12045-D50) and the Fusion FX7 (Vilber Lourmat) image acquisition system.

Western blot analysis

Cells were collected and lysed in lysis buffer (50 mM Tris/HCl pH 7.5, 150 mM NaCl, 1% NP-40) containing a protease inhibitor cocktail (Roche). Protein concentrations were determined in all experiments using the Bio-RAD protein assay (Bio-RAD, 500-0006) and 20–40 µg of total protein was loaded onto either 10 or 12.5% SDS–PAGE gels before transfer onto nitrocellulose membranes (Amersham Protran; 10600003). Membranes were blocked with 5% milk, 0.1% Tween20 for 60 min at room temperature. The primary antibody incubation was overnight at 4 °C and the secondary HRP-coupled antibodies were incubated for 1 h at room temperature. The blots were developed using WesternBright ECL solution (K12045-D50) and the Fusion FX7 (Vilber Lourmat) image acquisition system.

Antibodies

The following antibodies were used in this study: polyclonal rabbit anti-VIPAS39 (20771-1-AP; Proteintech; 1:2,000), polyclonal rabbit anti-Rab11FIP5 (NBP1-81855; Novus Biologicals; 1:2,000), polyclonal rabbit anti-EHD1 (NBP2-56035; Novus Biologicals; 1:2,000), polyclonal rabbit anti-rabenosyn-5 (NB300-813; Novus Biologicals; 1:2,000), monoclonal mouse anti-myc (9E10) (1:3,000 for western blotting and 1:200 for immunostaining; Sigma-Aldrich; M4439), polyclonal rabbit anti-GFP (TP401; Torrey Pines; 1:3,000 for western blotting and 1:200 for immunostaining). For pulldowns, Trap beads (nanobodies) were used. GFP-Trap_A

(chromotek, gta-20) was used for GFP pulldowns and myc-Trap_A (chromotek; yta-20) was used for myc pulldowns. HRP-conjugated goat anti-mouse IgG (H + L) secondary antibody (Thermo Fisher Scientific; 31430; 1:10,000) and polyclonal HRP-conjugated goat-anti-rabbit IgG (Thermo Fisher Scientific; 31460; 1:10,000) were used (incubated for 1 h at room temperature) to detect bound antibodies with an ECL system (ECL prime, Amersham, RPN2232). Alexa Fluor 488–goat anti-rabbit IgG (H + L) (Invitrogen; A-11034) and Alexa Fluor 594–goat anti-mouse IgG (H + L) cross-adsorbed secondary antibodies (Invitrogen; R37121) were used for immunofluorescence.

Immunostaining of cilia and FERARI proteins in RPE cells

Cells were plated onto sterile 13-mm glass coverslips. Cells were fixed with 4% paraformaldehyde for 15 min, permeabilized (0.1% Triton X-100 in PBS) for 5 min, and blocked with 2% BSA containing 5% goat serum in PBS for 1 h. Coverslips were incubated in primary antibodies for 2 h and washed five times in PBS, followed by a 1 h incubation with fluorescently labelled secondary antibodies. After secondary antibody incubation, coverslips were washed for five times in PBS and mounted onto glass slides using Fluoromount-G (Southernbiotech; 0100-01). Images were taken with an inverted Olympus FV1000 confocal microscope using a Plan Apochromat N 60×/1.40 silicon oil objective with z stacks. The size of the cilia was measured in the Fiji image tool.

7. Further discussion and outlook

Eukaryotic cells are populated with multiple membrane bound organelles. Inter-organelle and plasma membrane communication is mostly carried out by vesicular transport. Proteins, lipids, and different types of nutrients are incorporated into nascent vesicles originating from donor organelle/plasma membrane. These vesicles then travel along the microtubules to the destination organelle, tether and dock on the target membrane and finally fuse partially or fully to deliver the content. Such dynamic fission and fusion procedures are extremely challenging for organelle identity, and are thus tightly controlled. In endocytic branch of endomembrane trafficking system, all incoming materials from plasma membrane are targeted to the sorting endosomes (SEs). More than half of the endocytosed materials recycle back to the plasma membrane from SEs through fast and slow recycling methods. How cargoes are sorted into recycling endosomes from sorting endosomes remains largely enigmatic. Here, in this thesis I describe the existence and characterization of a multisubunit tether, FERARI, in mammalian system, which regulates Rab11-dependent recycling.

FERARI is a unique tethering platform

In the first part of my thesis, I mainly focused on the function and composition of novel tethering platform, FERARI, in human cell lines. Multi subunit tethering complexes (MTCs) have long been investigated for their role in membrane tethering and fusion. Due to the presence of multiple subunits, MTCs are multitasking, and they can combine several molecular functions. Most of the MTCs, if not all, capture moving vesicles through Rab binding subunits (Bröcker et al., 2010; Solinger & Spang, 2013). In comparison with related CORVET and HOPS, FERARI holds a unique composition of Rab binding subunits. VPS3 and VPS8, two Rab interacting subunits of CORVET, binds with Rab5 and thus regulate the fusion of Rab5 containing membranes. HOPS tethering complex interacts with Rab7 via VPS39 and VPS41, and regulates the fusion of mature endosomes with lysosomes. Interestingly, FERARI interacts with two different Rab proteins, Rab5 and Rab11, via Rabenosyn-5 and Rab11-FIP5, respectively. This unique composition of FERARI facilitates the cargo sorting to the Rab11-mediated recycling pathway from Rab5-positive sorting endosomes. Two different membranes representing different Rabs are brought together by Rab effectors Rabenosyn-5 and Rab11-FIP5, which are then followed by fusion through SNARE-interaction module—VPS45. Another remarkable difference between FERARI and its close relatives HOPS and CORVET is that FERARI comprises a dynamin-like protein EHD. This protein plays a dynamic role in membrane fission. Suggesting that FERARI combines two rather discrete and opposite activities: membrane fusion and fission (Solinger et al., 2020).

FERARI members do not share much sequence similarity and they also have other cellular functions (Solinger et al., 2020; Whyte & Munro, 2002). When we deleted one component of FERARI, it did not affect the stability of any other member. However, it seems that formation of FERARI tethering platform requires availability of all the components. Our immunoprecipitation data shows that interaction among FERARI components is

interdependent, because the binding strength between two subunits of FERARI is less when a FERARI member is knocked out. Most notably, FERARI complex is stable enough for purification and biochemical assay. We have successfully purified FERARI complex and I will discuss about this in FERARI structure part.

Role of FERARI in bridging sorting and recycling endosomes and cargo sorting into recycling vesicles

Endocytic recycling from the SE requires the formation of a transport carrier for recycling. In the Rab11-mediated recycling process, cargo transports from sorting endosomes to recycling tubules/intermediates and ERC, and finally to the plasma membrane. The current model of geometry-based sorting iterative sorting suggests that tubules generated at the sorting endosomes become ERC by recruiting Rab11 during the endosome's maturation. In contrast, the globular part of the early endosome matures into late endosome by losing Rab5 (Sönnichsen et al., 2000). The membrane fusion specificity is also changed on the globular part of sorting endosomes as it matures and CORVET is replaced by HOPS complex (Solinger & Spang, 2013). However, the cargo retrieval from degradative fate and transfer to the recycling carrier is still not well understood. We discovered that recycling vesicles are recruited on the tubular part of sorting endosomes via FERARI where they take up cargo through a kiss-and-run process.

Interestingly, we see that Rab11-positive vesicles are enlarged in FERARI depleted HeLa cells. Literature suggests that strong overexpression of constitutively active form of Rab11, Rab11Q70L, leads to the formation of enlarged Rab11 positive structures (Wilcke et al., 2000, p. 11) The possible explanation could be a partial fusion between recycling and sorting endosomes. This hypothesis was further validated by a study showing that Rab5 and Rab11 over-expression leads to a partial co-localization between these molecules. However, in our case, we can only assume that enlarged Rab11-positive structures in HeLa cells might be the consequence of the accumulation of many recycling vesicles unable to dock and fuse on the recycling tubules and transport recycling cargo to the plasma membrane due to the lack of FERARI.

Live movies in *C. elegans* and HeLa cells show that Rab11 positive vesicles are targeted to the SNX1 positive recycling compartment of sorting endosomes, where they follow a kiss-and-run process to take up cargo, suggesting that, kiss-and-run is a conserved mechanism of cargo transfer into the recycling vesicle. FERARI forms and stabilizes the SNX1 positive structures where it regulates the fusion and fission of Rab11 positive recycling vesicles. Interestingly, the time required for single fusion and fission events of individual recycling vesicles on SNX1 positive structures is significantly reduced in FERARI depleted animals. Due to the lack of tethering machinery, recycling vesicles cannot go through the fusion and fission process and thus show a chaotic movement. This brings another plausible theory that enlarged recycling

vesicles are formed through homotypic fusion between recycling endosomes that cannot dock and fuse on the SNX1 positive structures (Simonetti et al., 2019). We have also observed homotypic fusion, in several occasions, between Rab11-positive recycling vesicles in HeLa cells. However, this data requires further validation.

Membrane remodeling protein SNXs are associated with FERARI

Although much has been studied and learned about signaling cues and sorting machinery that confers cargo sorting into the lysosomal degradative pathway, recycling features of endosome export pathways are less well understood. Many studies have demonstrated receptor recycling from endosomes is an active process and have identified major sorting proteins of the sorting nexin family as hubs that can interact with various receptors and regulate them to select pathways. Microscopy analyses revealed a fascinating and complex network of dynamic tubules that regulate endosomal sorting and recycling. Multiple coat complexes, retromer, retriever, and ESCPE-1, have been described for recycling of specific cargoes where SNXs form tubules and adaptor proteins are recruited and attract (Simonetti et al., 2019). Tubing and pinching of membrane on sorting endosomes then forms recycling carriers that acquire vesicular shape and appropriate Rabs (e.g. Rab11) and travel to their target destination. In these models, it is not clear how the coats are removed from the recycling transport carriers.

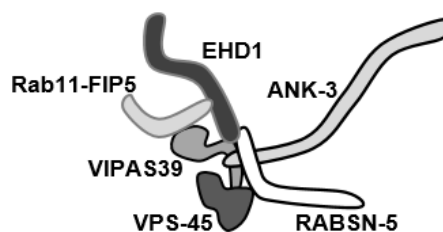
Recently, it has also been suggested that a substantial fraction of some internalized cargoes may be delivered from EEs to REs and then to the trans-Golgi network (TGN) (Lin et al., 2004; Tran et al., 2007, p. 4; Wilcke et al., 2000), suggesting that sorting can take place from RE as well. Moreover, REs are mostly composed of large endosomal tubular recycling networks and vesicles. While the tubing and pinching model explains some of the features of cargo sorting and recycling, several vital enduring questions remain unanswered: how recycling vesicles are connected to the large tubular recycling networks and how the adaptor proteins, which have very low binding affinities to the cargoes, can ensure a clean separation of cargoes.

In *C. elegans*, we discovered kiss-and-run process that explain cargo uptake by Rab11 positive recycling vesicles from SNX1 positive large tubular recycling networks. However, in HeLa cells it is challenging to look at individual events of kiss-and-run process in live movies, because of the limitation of the spatiotemporal resolution of microscopes. Nevertheless, in the second part of my thesis, to investigate whether kiss-and-run exist in mammalian system I generated GFP-Rab11 knock-in cell lines in ctr KO and FERARI KO background. In live movies, I could see the kiss-and-run of Rab11-positive vesicles on SNX1 positive structures in HeLa cells. Unlike *C.elegans*, we do not see any quantal behavior of the residence time of Rab11 positive vesicles on SNX1 positive structure. In *C. elegans* we found that duration of kiss depends on the cargo load. Duration of the kiss increases with the higher load of cargo. To know the details of the kiss-and-run process in mammalian system we are planning to overexpress a cargo and

measure the length of the kiss. Furthermore, it will be interesting to determine the residence time of different receptor containing vesicles on SNX1 positive structures.

FERARI structure: A Seahorse or a Spaghetti dancer?

All MTCs bind with numerous partners that could allow them to connect a vesicle to the proper target membrane. The molecular structure of purified MTCs, such as COG, Dsl1, and HOPS, demonstrates a complete picture of binding sites for factors on opposite membranes (Bröcker et al., 2012; Chou et al., 2016; Ha et al., 2016; Ren et al., 2009). Knowing how the Rab and SNARE binding subunits are spatially separated within the complex is crucial to understand the mechanism through which vesicle tethering and SNARE complex assembly might occur. The molecular size of a complex provides critical information about the distance it covers to capture a vesicle. It would be interesting to know whether FERARI undergoes conformational changes to fetch the vesicle in closer proximity of the SNX1 positive membrane for SNARE assembly and vesicle fusion as suggested for other MTCs. Based on the molecular structure of HOPS and our interactive map, we showed the following speculated model for FERARI (Solinger et al., 2020).



Mammalian FERARI

Figure 6.7.1 : Speculated structure of FERARI. Taken from Solinger et al. (2020)

We encountered difficulty expressing all FERARI members in yeast simultaneously. Therefore, we expressed GFP-Rabenosyn-5 in HEK-293 cells and the rest of the FERARI subunits in yeast. Extracts from both yeast and HEK-293 cells overproducing FERARI were then mixed. We were able to purify the FERARI tethering platform successfully, and western blot data of purified FERARI confirms the presence of all subunits in the elution. We see a seahorse-like structure of purified FERARI in our preliminary data collected from negative stain electron microscopy. However, this data requires further confirmation, and future studies need to be done by cryo-EM to determine the ultrastructure of FERARI.

Biological significance of FERARI

Mechanistically FERARI tethers vesicles with discrete Rab GTPases (Rab5, Rab10, and Rab11) and regulates cargo sorting into Rab11 marked vesicles. Vesicular transport is a global process

for the vast array of cellular functions. Epithelial cells rely on Rab8, Rab10, and Rab11 mediated vesicular cargo transport to develop cilia (Babbey et al., 2010, p. 10; Inoue et al., 2008, p. 11; Lara Ordóñez et al., 2019, p. 11; Lu et al., 2015). Furthermore, the contribution of MTC in ciliogenesis has also been reported repeatedly (Babbey et al., 2010; Seixas et al., 2016). Compartmentalization within cilium is maintained by selective import and export of proteins/lipids from the cytoplasm, which is controlled by the transition zone. Hence, the cilium is similar to that of other intracellular membrane-bound organelles that requires vesicular transport to communicate with other organelles and the ciliary self-development.

In the final part of my thesis, I looked into the biological significance of FERARI or the role of FERARI in cilia development, in particular. Our data suggest that FERARI exists in cilia containing RPE cells. Vesicular transport and involvement of tethering complex in cilia development further approve the possibility of FERARI involvement in cilia development. The association of half of the FERARI subunits has been described in different stages of ciliogenesis either in the mammalian system or in *C.elegans* (Bhattacharyya et al., 2016, p. 1; He et al., 2018; Scheidel et al., 2018, p. 45). However, the role of VIPAS39 seems to be novel in ciliogenesis. Our data suggest that FERARI coordinately regulates cilia development. It would be exciting to see whether kiss-and-run mediated cargo delivery plays a role in cilia development.

VIPAS39 is part of both FERARI and CHEVI

One of the core components of FERARI is VIPAS39, which is a strong binding partner of SM protein VPS33B. While HOPS and CORVET share three core proteins, EARP and GARP differ by only one subunit (Solinger & Spang, 2013). Localization of GARP complex is changed from TGN to RE when VPS53 is replaced with Syndetin, and GARP becomes EARP. Therefore, it is very likely that VIPAS39 is a part of two independent tethering complexes: FERARI and CHEVI. Although VIPAS39 is shared by FERARI and CHEVI, they play distinct roles because unlike VIPAS39, when we knockdown VPS33B it did not affect the localization of RAB-11 (Solinger et al., 2020). Recently, a direct physical interaction has been reported between CCC complex member CCDC22 and VPS33B/VIPAS39. Other members of the CCC complex did not bind to VPS33B/VIPAS39 (Hunter et al., 2018). CCC complex is associated with multiple complexes involved in cargo sorting and endocytic recycling (Bartuzi et al., 2016; Naslavsky & Caplan, 2018). Furthermore, CHEVI has been proposed to require for α -granule formation through regulating transport from TGN to the MVBs (Spang, 2016). Altogether, it is likely that CHEVI is localized on SEs. In contrast, VPS33B has been suggested to localize on LAMP1 positive compartments, and the depletion of *vps33b* causes enhanced co-localization between LAMP1 with Rab7 and accumulation of Rab7 positive structures (Galmes et al., 2015), suggesting an involvement of VPS33B in the late endosomal pathway. It will be interesting to know how *vipas39* depletion corresponds with *vps33b* depleted phenotypes. We suggest that tethers

could play vital role in the development of domains needed for docking on SEs and probably also on other organelles.

8. Abbreviation Index

Abbreviation	Term/Definition
ARF	ADP ribosylation factor
ATP	adenosine-5'-triphosphate
AX	Axoneme
BAR	Bin/Amphiphysin/Rvs domain-containing proteins
BB	basal body
bp	base pair
BSA	bovine serum albumin
CC	Ciliary Cap
CCC	COMMD/CCDC22/CCDC93
cDNA	complementary DNA, generated by reverse transcription of RNA
<i>C. elegans</i>	<i>Caenorhabditis elegans</i>
CME	Clathrin-Mediated Endocytosis
COG	Conserved Oligomeric Golgi complex
CORVET	Class C core Vacuole/Endosome Tethering
CV	Ciliary vesicle
DAP	Distal Appendages
DAPI	4',6-Diamindino-2-phenylindole dihydrochloride
DNA	deoxyribonucleic acid
dNTPs	deoxynucleotide triphosphates
DTT	dithiothreitol
EARP	Endosome-Associated Recycling Protein
ECL	enhanced chemoluminescence
<i>E. coli</i>	<i>Escherichia coli</i>
EE	Early Endosome
EEA1	Early Endosome Antigen 1
ER	endoplasmic reticulum
ERC	endocytic recycling compartment
ESCRT	Endosomal Sorting Complexes Required for Transport
FYVE domain	Fab-1, YGL023, Vps27, and EEA1 domain
GAP	GTPase-Activating Protein
GARP	Golgi-Associated Retrograde Protein Complex
GDP	guanosine-5'-diphosphate
GEF	Guanine nucleotide Exchange Factor
GFP	green fluorescent protein
GLUT4	glucose transporter type 4
GTP	guanosine-5'-triphosphate
GTPase	GTP hydrolyzing enzyme
HOPS	Homotypic fusion and Vacuole Protein Sorting

IF	Immunofluorescence
IFT	IntraFlagellar Transport
ILV	Intraluminal Vesicle
IP	immunoprecipitation
LB	lysogeny broth
LC-MS	liquid chromatography coupled to mass spectrometry
LE	Late Endosome
MVB	Multivesicular body
mRNA	messenger RNA
MW	molecular weight
Ni-NTA	Nickel-Nitrilo tetra-acetic acid agarose
PAGE	polyacrylamide gel electrophoresis
PBS	phosphate buffered saline
PCR	polymerase chain reaction
PCV	Preciliary vesicle
PH domain	Pleckstrin Homology domain
PIP	Phosphatidylinositol phospholipid
PI(4,5)P2	Phosphatidylinositol-4,5-bisPhosphate
PI(3)	Phosphatidylinositol-3-Phosphate
PM	Plasma membrane
PX domain	PhoX homology domain
qRT-PCR	quantitative reverse transcription followed by PCR
RBD	Rab binding domain
RE	Recycling Endosome
RNA	ribonucleic acid
rpm	revolutions per minute
RaBD	Rab11 binding domain
RT	room temperature
SDS	sodium dodecyl sulfate
SE	Sorting endosome
SM	Sec1/Munc18-like
SNARE	N-ethylmaleimide-sensitive factor attachment protein receptor
SNX	Sorting Nexin family Proteins
TGN	Trans-Golgi Network
t-SNARE	target membrane SNARE
TBS	tris-buffered saline solution
TBST	tris-buffered saline solution + 0.1% tween-20
TfnR	Transferrin receptor
TRAPP (I, II, III)	TRAnsport Protein Particle I (I, II, III)
TZ	Transition zone
VPS	Vacuolar Protein Sorting
v-SNARE	vesicular SNARE
WB	western blot

9. References

- Aimon, S., Callan-Jones, A., Berthaud, A., Pinot, M., Toombes, G. E. S., & Bassereau, P. (2014). Membrane shape modulates transmembrane protein distribution. *Developmental Cell*, 28(2), 212–218. <https://doi.org/10.1016/j.devcel.2013.12.012>
- Alberts, B., Johnson, A., Lewis, J., Raff, M., Roberts, K., & Walter, P. (2002a). The Molecular Mechanisms of Membrane Transport and the Maintenance of Compartmental Diversity. *Molecular Biology of the Cell. 4th Edition*. <https://www.ncbi.nlm.nih.gov/books/NBK26859/>
- Alberts, B., Johnson, A., Lewis, J., Raff, M., Roberts, K., & Walter, P. (2002b). Transport from the Trans Golgi Network to Lysosomes. *Molecular Biology of the Cell. 4th Edition*. <https://www.ncbi.nlm.nih.gov/books/NBK26844/>
- Allgood, S. C., & Neunuebel, M. R. (2018). The recycling endosome and bacterial pathogens. *Cellular Microbiology*, 20(7), e12857. <https://doi.org/10.1111/cmi.12857>
- Avasthi, P., & Marshall, W. F. (2012). Stages of Ciliogenesis and Regulation of Ciliary Length. *Differentiation; Research in Biological Diversity*, 83(2), S30–S42. <https://doi.org/10.1016/j.diff.2011.11.015>
- Babbey, C. M., Ahktar, N., Wang, E., Chen, C. C.-H., Grant, B. D., & Dunn, K. W. (2006). Rab10 regulates membrane transport through early endosomes of polarized Madin-Darby canine kidney cells. *Molecular Biology of the Cell*, 17(7), 3156–3175. <https://doi.org/10.1091/mbc.e05-08-0799>
- Babbey, C. M., Bacallao, R. L., & Dunn, K. W. (2010). Rab10 associates with primary cilia and the exocyst complex in renal epithelial cells. *American Journal of Physiology - Renal Physiology*, 299(3), F495–F506. <https://doi.org/10.1152/ajprenal.00198.2010>
- Babst, M. (2011). MVB Vesicle Formation: ESCRT-Dependent, ESCRT-Independent and Everything in Between. *Current Opinion in Cell Biology*, 23(4), 452–457. <https://doi.org/10.1016/j.ceb.2011.04.008>
- Bacaj, T., Pang, Z. P., & Südhof, T. C. (2010). Testing the SNARE/SM protein model of membrane fusion. *Proceedings of the National Academy of Sciences*, 107(52), 22365–22366. <https://doi.org/10.1073/pnas.1017268108>
- Balderhaar, H. J. kleine, & Ungermann, C. (2013). CORVET and HOPS tethering complexes – coordinators of endosome and lysosome fusion. *Journal of Cell Science*, 126(6), 1307–1316. <https://doi.org/10.1242/jcs.107805>
- Barbero, P., Bittova, L., & Pfeffer, S. R. (2002). Visualization of Rab9-mediated vesicle transport from endosomes to the trans-Golgi in living cells. *Journal of Cell Biology*, 156(3), 511–518. <https://doi.org/10.1083/jcb.200109030>
- Barral, D. C., Garg, S., Casalou, C., Watts, G. F. M., Sandoval, J. L., Ramalho, J. S., Hsu, V. W., & Brenner, M. B. (2012). Arl13b regulates endocytic recycling traffic. *Proceedings of the National Academy of Sciences of the United States of America*, 109(52), 21354–21359. <https://doi.org/10.1073/pnas.1218272110>
- Bartuzi, P., Billadeau, D. D., Favier, R., Rong, S., Dekker, D., Fedoseienko, A., Fieten, H., Wijers, M., Levels, J. H., Huijckman, N., Kloosterhuis, N., van der Molen, H., Brufau, G., Groen, A. K., Elliott, A. M., Kuivenhoven, J. A., Plecko, B., Grangl, G., McGaughan, J., ... van de Sluis, B. (2016). CCC- and WASH-mediated endosomal sorting of LDLR is required for normal clearance of circulating LDL. *Nature Communications*, 7(1), 10961. <https://doi.org/10.1038/ncomms10961>
- Beek, J. van der, Jonker, C., Welle, R. van der, Liv, N., & Klumperman, J. (2019). CORVET, CHEVI and HOPS – multisubunit tethers of the endo-lysosomal system in health and disease. *Journal of Cell Science*, 132(10). <https://doi.org/10.1242/jcs.189134>
- Behnia, R., & Munro, S. (2005). Organelle identity and the signposts for membrane traffic. *Nature*, 438(7068), 597–604. <https://doi.org/10.1038/nature04397>

- Bhattacharyya, S., Rainey, M. A., Arya, P., Mohapatra, B. C., Mushtaq, I., Dutta, S., George, M., Storck, M. D., McComb, R. D., Muirhead, D., Todd, G. L., Gould, K., Datta, K., Waes, J. G., Band, V., & Band, H. (2016). Endocytic recycling protein EHD1 regulates primary cilia morphogenesis and SHH signaling during neural tube development. *Scientific Reports*, 6(1), 20727. <https://doi.org/10.1038/srep20727>
- Blacque, O. E., Scheidel, N., & Kuhns, S. (2017). Rab GTPases in cilium formation and function. *Small GTPases*, 9(1–2), 76–94. <https://doi.org/10.1080/21541248.2017.1353847>
- Bock, J. B., Matern, H. T., Peden, A. A., & Scheller, R. H. (2001). A genomic perspective on membrane compartment organization. *Nature*, 409(6822), 839–841. <https://doi.org/10.1038/35057024>
- Bonifacino, J. S., & Glick, B. S. (2004). The Mechanisms of Vesicle Budding and Fusion. *Cell*, 116(2), 153–166. [https://doi.org/10.1016/S0092-8674\(03\)01079-1](https://doi.org/10.1016/S0092-8674(03)01079-1)
- Bouchet, J., McCaffrey, M. W., Graziani, A., & Alcover, A. (2016). The functional interplay of Rab11, FIP3 and Rho proteins on the endosomal recycling pathway controls cell shape and symmetry. *Small GTPases*, 9(4), 310–315. <https://doi.org/10.1080/21541248.2016.1224288>
- Braulke, T., & Bonifacino, J. S. (2009). Sorting of lysosomal proteins. *Biochimica et Biophysica Acta (BBA) - Molecular Cell Research*, 1793(4), 605–614. <https://doi.org/10.1016/j.bbamcr.2008.10.016>
- Brennwald, P., Kearns, B., Champion, K., Keränen, S., Bankaitis, V., & Novick, P. (1994). Sec9 is a SNAP-25-like component of a yeast SNARE complex that may be the effector of Sec4 function in exocytosis. *Cell*, 79(2), 245–258. [https://doi.org/10.1016/0092-8674\(94\)90194-5](https://doi.org/10.1016/0092-8674(94)90194-5)
- Bright, N. A., Gratian, M. J., & Luzio, J. P. (2005). Endocytic Delivery to Lysosomes Mediated by Concurrent Fusion and Kissing Events in Living Cells. *Current Biology*, 15(4), 360–365. <https://doi.org/10.1016/j.cub.2005.01.049>
- Bröcker, C., Engelbrecht-Vandré, S., & Ungermann, C. (2010). Multisubunit Tethering Complexes and Their Role in Membrane Fusion. *Current Biology*, 20(21), R943–R952. <https://doi.org/10.1016/j.cub.2010.09.015>
- Bröcker, C., Kuhlee, A., Gatsogiannis, C., Balderhaar, H. J. kleine, Hönscher, C., Engelbrecht-Vandré, S., Ungermann, C., & Raunser, S. (2012). Molecular architecture of the multisubunit homotypic fusion and vacuole protein sorting (HOPS) tethering complex. *Proceedings of the National Academy of Sciences*, 109(6), 1991–1996. <https://doi.org/10.1073/pnas.1117797109>
- Brooks, E. R., & Wallingford, J. B. (2014). Multiciliated cells: A review. *Current Biology : CB*, 24(19), R973–R982. <https://doi.org/10.1016/j.cub.2014.08.047>
- Bull, L. N., Mahmoodi, V., Baker, A. J., Jones, R., Strautnieks, S. S., Thompson, R. J., & Knisely, A. S. (2006). VPS33B mutation with ichthyosis, cholestasis, and renal dysfunction but without arthrogryposis: Incomplete ARC syndrome phenotype. *The Journal of Pediatrics*, 148(2), 269–271. <https://doi.org/10.1016/j.jpeds.2005.10.005>
- Cai, H., Reinisch, K., & Ferro-Novick, S. (2007). Coats, Tethers, Rab, and SNAREs Work Together to Mediate the Intracellular Destination of a Transport Vesicle. *Developmental Cell*, 12(5), 671–682. <https://doi.org/10.1016/j.devcel.2007.04.005>
- Campa, C. C., Margaria, J. P., Derle, A., Del Giudice, M., De Santis, M. C., Gozzelino, L., Copperi, F., Bosia, C., & Hirsch, E. (2018). Rab11 activity and PtdIns(3) P turnover removes recycling cargo from endosomes. *Nature Chemical Biology*, 14(8), 801–810. <https://doi.org/10.1038/s41589-018-0086-4>
- Caswell, P. T., Chan, M., Lindsay, A. J., McCaffrey, M. W., Boettiger, D., & Norman, J. C. (2008). Rab-coupling protein coordinates recycling of $\alpha 5 \beta 1$ integrin and EGFR1 to promote cell migration in 3D microenvironments. *The Journal of Cell Biology*, 183(1), 143–155. <https://doi.org/10.1083/jcb.200804140>
- Cavalli, V., Corti, M., & Gruenberg, J. (2001). Endocytosis and signaling cascades: A close encounter. *FEBS Letters*, 498(2), 190–196. [https://doi.org/10.1016/S0014-5793\(01\)02484-X](https://doi.org/10.1016/S0014-5793(01)02484-X)

- Cevik, S., Sanders, A. A. W. M., Wijk, E. V., Boldt, K., Clarke, L., Reeuwijk, J. van, Hori, Y., Horn, N., Hetterschijt, L., Wdowicz, A., Mullins, A., Kida, K., Kaplan, O. I., Beersum, S. E. C. van, Wu, K. M., Letteboer, S. J. F., Mans, D. A., Katada, T., Kontani, K., ... Blacque, O. E. (2013). Active Transport and Diffusion Barriers Restrict Joubert Syndrome-Associated ARL13B/ARL-13 to an Inv-like Ciliary Membrane Subdomain. *PLOS Genetics*, 9(12), e1003977. <https://doi.org/10.1371/journal.pgen.1003977>
- Chaineau, M., Ioannou, M. S., & McPherson, P. S. (2013). Rab35: GEFs, GAPs and Effectors. *Traffic*, 14(11), 1109–1117. <https://doi.org/10.1111/tra.12096>
- Chen, B., Jiang, Y., Zeng, S., Yan, J., Li, X., Zhang, Y., Zou, W., & Wang, X. (2010). Endocytic sorting and recycling require membrane phosphatidylserine asymmetry maintained by TAT-1/CHAT-1. *PLoS Genetics*, 6(12), e1001235. <https://doi.org/10.1371/journal.pgen.1001235>
- Chen, C. C.-H., Schweinsberg, P. J., Vashist, S., Mareiniss, D. P., Lambie, E. J., & Grant, B. D. (2006). RAB-10 is required for endocytic recycling in the *Caenorhabditis elegans* intestine. *Molecular Biology of the Cell*, 17(3), 1286–1297. <https://doi.org/10.1091/mbc.e05-08-0787>
- Chen, K.-E., Healy, M. D., & Collins, B. M. (2019). Towards a molecular understanding of endosomal trafficking by Retromer and Retriever. *Traffic (Copenhagen, Denmark)*, 20(7), 465–478. <https://doi.org/10.1111/tra.12649>
- Chen, Y. A., & Scheller, R. H. (2001). SNARE-mediated membrane fusion. *Nature Reviews Molecular Cell Biology*, 2(2), 98–106. <https://doi.org/10.1038/35052017>
- Chen, Y., Wang, Y., Zhang, J., Deng, Y., Jiang, L., Song, E., Wu, X. S., Hammer, J. A., Xu, T., & Lippincott-Schwartz, J. (2012). Rab10 and myosin-Va mediate insulin-stimulated GLUT4 storage vesicle translocation in adipocytes. *The Journal of Cell Biology*, 198(4), 545–560. <https://doi.org/10.1083/jcb.201111091>
- Chi, R., Harrison, M., & Burd, C. (2015). Biogenesis of endosome-derived transport carriers. *Cellular and Molecular Life Sciences : CMLS*, 72. <https://doi.org/10.1007/s00018-015-1935-x>
- Chia, P. Z. C., & Gleeson, P. A. (2014). Membrane tethering. *F1000Prime Reports*, 6. <https://doi.org/10.12703/P6-74>
- Chou, H.-T., Dukovski, D., Chambers, M. G., Reinisch, K. M., & Walz, T. (2016). CATCHR, HOPS and CORVET tethering complexes share a similar architecture. *Nature Structural & Molecular Biology*, 23(8), 761–763. <https://doi.org/10.1038/nsmb.3264>
- Choudhury, A., Sharma, D. K., Marks, D. L., & Pagano, R. E. (2004). Elevated Endosomal Cholesterol Levels in Niemann-Pick Cells Inhibit Rab4 and Perturb Membrane Recycling. *Molecular Biology of the Cell*, 15(10), 4500–4511. <https://doi.org/10.1091/mbc.E04-05-0432>
- Chua, C. E. L., & Tang, B. L. (2018). Rab 10-a traffic controller in multiple cellular pathways and locations. *Journal of Cellular Physiology*, 233(9), 6483–6494. <https://doi.org/10.1002/jcp.26503>
- Clevers, H., & Nusse, R. (2012). Wnt/ β -catenin signaling and disease. *Cell*, 149(6), 1192–1205. <https://doi.org/10.1016/j.cell.2012.05.012>
- Collins, L. L., Simon, G., Matheson, J., Wu, C., Miller, M. C., Otani, T., Yu, X., Hayashi, S., Prekeris, R., & Gould, G. W. (2012). Rab11-FIP3 is a cell cycle-regulated phosphoprotein. *BMC Cell Biology*, 13(1), 4. <https://doi.org/10.1186/1471-2121-13-4>
- Collins, R. N. (2003). “Getting It On”—GDI Displacement and Small GTPase Membrane Recruitment. *Molecular Cell*, 12(5), 1064–1066. [https://doi.org/10.1016/S1097-2765\(03\)00445-3](https://doi.org/10.1016/S1097-2765(03)00445-3)
- Corbit, K. C., Aanstad, P., Singla, V., Norman, A. R., Stainier, D. Y. R., & Reiter, J. F. (2005). Vertebrate Smoothed functions at the primary cilium. *Nature*, 437(7061), 1018–1021. <https://doi.org/10.1038/nature04117>
- Cowles, C. R., Emr, S. D., & Horazdovsky, B. F. (1994). Mutations in the VPS45 gene, a SEC1 homologue, result in vacuolar protein sorting defects and accumulation of membrane vesicles. *Journal of Cell Science*, 107 (Pt 12), 3449–3459.

- Cullen, P. J., & Steinberg, F. (2018). To degrade or not to degrade: Mechanisms and significance of endocytic recycling. *Nature Reviews. Molecular Cell Biology*, 19(11), 679–696. <https://doi.org/10.1038/s41580-018-0053-7>
- Cullinane, A. R., Straatman-Iwanowska, A., Zaucker, A., Wakabayashi, Y., Bruce, C. K., Luo, G., Rahman, F., Gürakan, F., Utine, E., Ozkan, T. B., Denecke, J., Vukovic, J., Di Rocco, M., Mandel, H., Cangul, H., Matthews, R. P., Thomas, S. G., Rappoport, J. Z., Arias, I. M., ... Gissen, P. (2010). Mutations in VIPAR cause an arthrogryposis, renal dysfunction and cholestasis syndrome phenotype with defects in epithelial polarization. *Nature Genetics*, 42(4), 303–312. <https://doi.org/10.1038/ng.538>
- Cullis, D. N., Philip, B., Baleja, J. D., & Feig, L. A. (2002). Rab11-FIP2, an Adaptor Protein Connecting Cellular Components Involved in Internalization and Recycling of Epidermal Growth Factor Receptors *. *Journal of Biological Chemistry*, 277(51), 49158–49166. <https://doi.org/10.1074/jbc.M206316200>
- Das, L., Gard, J. M. C., Prekeris, R., Nagle, R. B., Morrissey, C., Knudsen, B. S., Miranti, C. K., & Cress, A. E. (2018). Novel Regulation of Integrin Trafficking by Rab11-FIP5 in Aggressive Prostate Cancer. *Molecular Cancer Research : MCR*, 16(8), 1319–1331. <https://doi.org/10.1158/1541-7786.MCR-17-0589>
- Daumke, O., Lundmark, R., Vallis, Y., Martens, S., Butler, P. J. G., & McMahon, H. T. (2007). Architectural and mechanistic insights into an EHD ATPase involved in membrane remodelling. *Nature*, 449(7164), 923–927. <https://doi.org/10.1038/nature06173>
- Dawe, H. R., Farr, H., & Gull, K. (2007). Centriole/basal body morphogenesis and migration during ciliogenesis in animal cells. *Journal of Cell Science*, 120(1), 7–15. <https://doi.org/10.1242/jcs.03305>
- De Renzis, S., Sönnichsen, B., & Zerial, M. (2002). Divalent Rab effectors regulate the sub-compartmental organization and sorting of early endosomes. *Nature Cell Biology*, 4(2), 124–133. <https://doi.org/10.1038/ncb744>
- Deng, Z.-H., Gomez, T. S., Osborne, D. G., Phillips-Krawczak, C. A., Zhang, J.-S., & Billadeau, D. D. (2015). Nuclear FAM21 participates in NF- κ B-dependent gene regulation in pancreatic cancer cells. *Journal of Cell Science*, 128(2), 373–384. <https://doi.org/10.1242/jcs.161513>
- Deo, R., Kushwah, M. S., Kamerkar, S. C., Kadam, N. Y., Dar, S., Babu, K., Srivastava, A., & Pucadyil, T. J. (2018). ATP-dependent membrane remodeling links EHD1 functions to endocytic recycling. *Nature Communications*, 9(1), 5187. <https://doi.org/10.1038/s41467-018-07586-z>
- Derivery, E., Sousa, C., Gautier, J. J., Lombard, B., Loew, D., & Gautreau, A. (2009). The Arp2/3 activator WASH controls the fission of endosomes through a large multiprotein complex. *Developmental Cell*, 17(5), 712–723. <https://doi.org/10.1016/j.devcel.2009.09.010>
- Dickson, E. J., & Hille, B. (2019). Understanding phosphoinositides: Rare, dynamic, and essential membrane phospholipids. *The Biochemical Journal*, 476(1), 1–23. <https://doi.org/10.1042/BCJ20180022>
- Dickson, E. J., Jensen, J. B., & Hille, B. (2014). Golgi and plasma membrane pools of PI(4)P contribute to plasma membrane PI(4,5)P₂ and maintenance of KCNQ2/3 ion channel current. *Proceedings of the National Academy of Sciences*, 111(22), E2281–E2290. <https://doi.org/10.1073/pnas.1407133111>
- Diering, G. H., & Numata, M. (2014). Endosomal pH in neuronal signaling and synaptic transmission: Role of Na⁺/H⁺ exchanger NHE5. *Frontiers in Physiology*, 4. <https://doi.org/10.3389/fphys.2013.00412>
- Dilan, T. L., Moye, A. R., Salido, E. M., Saravanan, T., Koldaivelu, S., Goldberg, A. F. X., & Ramamurthy, V. (2019). ARL13B, a Joubert Syndrome-Associated Protein, Is Critical for Retinogenesis and Elaboration of Mouse Photoreceptor Outer Segments. *Journal of Neuroscience*, 39(8), 1347–1364. <https://doi.org/10.1523/JNEUROSCI.1761-18.2018>

- Dubuke, M. L., & Munson, M. (2016). The Secret Life of Tethers: The Role of Tethering Factors in SNARE Complex Regulation. *Frontiers in Cell and Developmental Biology*, 4. <https://doi.org/10.3389/fcell.2016.00042>
- Duclos, S., Corsini, R., & Desjardins, M. (2003). Remodeling of endosomes during lysosome biogenesis involves “kiss and run” fusion events regulated by rab5. *Journal of Cell Science*, 116(Pt 5), 907–918. <https://doi.org/10.1242/jcs.00259>
- Dulubova, I., Yamaguchi, T., Gao, Y., Min, S.-W., Huryeva, I., Südhof, T. C., & Rizo, J. (2002). How Tlg2p/syntaxin 16 'snares' Vps45. *The EMBO Journal*, 21(14), 3620–3631. <https://doi.org/10.1093/emboj/cdf381>
- Dunn, K. W., McGraw, T. E., & Maxfield, F. R. (1989). Iterative fractionation of recycling receptors from lysosomally destined ligands in an early sorting endosome. *Journal of Cell Biology*, 109(6), 3303–3314. <https://doi.org/10.1083/jcb.109.6.3303>
- Dutta, D., & Donaldson, J. G. (2015). Sorting of Clathrin-independent Cargo Proteins depends on Rab35 delivered by Clathrin-mediated Endocytosis. *Traffic (Copenhagen, Denmark)*, 16(9), 994–1009. <https://doi.org/10.1111/tra.12302>
- Duve, C. (1975). Exploring cells with a centrifuge. *Science (New York, N.Y.)*, 189(4198), 186–194. <https://doi.org/10.1126/science.1138375>
- Eathiraj, S., Mishra, A., Prekeris, R., & Lambright, D. G. (2006). Structural basis for Rab11-mediated recruitment of FIP3 to recycling endosomes. *Journal of Molecular Biology*, 364(2), 121–135. <https://doi.org/10.1016/j.jmb.2006.08.064>
- Evans, A. J., Daly, J. L., Anuar, A. N. K., Simonetti, B., & Cullen, P. J. (2020). Acute inactivation of retromer and ESCPE-1 leads to time-resolved defects in endosomal cargo sorting. *Journal of Cell Science*, 133(15). <https://doi.org/10.1242/jcs.246033>
- Ezratty, E. J., Stokes, N., Chai, S., Shah, A. S., Williams, S. E., & Fuchs, E. (2011). A role for the primary cilium in Notch signaling and epidermal differentiation during skin development. *Cell*, 145(7), 1129–1141. <https://doi.org/10.1016/j.cell.2011.05.030>
- Fasshauer, D., Antonin, W., Subramaniam, V., & Jahn, R. (2002). SNARE assembly and disassembly exhibit a pronounced hysteresis. *Nature Structural Biology*, 9(2), 144–151. <https://doi.org/10.1038/nsb750>
- Fasshauer, D., Sutton, R. B., Brunger, A. T., & Jahn, R. (1998). Conserved structural features of the synaptic fusion complex: SNARE proteins reclassified as Q- and R-SNAREs. *Proceedings of the National Academy of Sciences*, 95(26), 15781–15786. <https://doi.org/10.1073/pnas.95.26.15781>
- Fesce, R., Grohovaz, F., Valtorta, F., & Meldolesi, J. (1994). Neurotransmitter release: Fusion or ‘kiss-and-run’? *Trends in Cell Biology*, 4(1), 1–4. [https://doi.org/10.1016/0962-8924\(94\)90025-6](https://doi.org/10.1016/0962-8924(94)90025-6)
- Figueiredo, P. de, Doody, A., Polizotto, R. S., Drecktrah, D., Wood, S., Banta, M., Strang, M. S., & Brown, W. J. (2001). Inhibition of Transferrin Recycling and Endosome Tubulation by Phospholipase A2 Antagonists *. *Journal of Biological Chemistry*, 276(50), 47361–47370. <https://doi.org/10.1074/jbc.M108508200>
- Foley, K. P., & Klip, A. (2014). Dynamic GLUT4 sorting through a syntaxin-6 compartment in muscle cells is derailed by insulin resistance-causing ceramide. *Biology Open*, 3(5), 314–325. <https://doi.org/10.1242/bio.20147898>
- Gagescu, R., Demaurex, N., Parton, R. G., Hunziker, W., Huber, L. A., & Gruenberg, J. (2000). The Recycling Endosome of Madin-Darby Canine Kidney Cells Is a Mildly Acidic Compartment Rich in Raft Components. *Molecular Biology of the Cell*, 11(8), 2775–2791. <https://www.ncbi.nlm.nih.gov/pmc/articles/PMC14955/>
- Gallon, M., & Cullen, P. J. (2015). Retromer and sorting nexins in endosomal sorting. *Biochemical Society Transactions*, 43(1), 33–47. <https://doi.org/10.1042/BST20140290>
- Galmes, R., Brink, C. ten, Oorschot, V., Veenendaal, T., Jonker, C., Sluijs, P. van der, & Klumperman, J. (2015). Vps33B is required for delivery of endocytosed cargo to lysosomes. *Traffic*, 16(12), 1288–1305. <https://doi.org/10.1111/tra.12334>

- Gerdes, J. M., Liu, Y., Zaghloul, N. A., Leitch, C. C., Lawson, S. S., Kato, M., Beachy, P. A., Beales, P. L., DeMartino, G. N., Fisher, S., Badano, J. L., & Katsanis, N. (2007). Disruption of the basal body compromises proteasomal function and perturbs intracellular Wnt response. *Nature Genetics*, 39(11), 1350–1360. <https://doi.org/10.1038/ng.2007.12>
- Gillingham, A. K. (2017). At the ends of their tethers! How coiled-coil proteins capture vesicles at the Golgi. *Biochemical Society Transactions*, 46(1), 43–50. <https://doi.org/10.1042/BST20170188>
- Gillingham, A. K., & Munro, S. (2003). Long coiled-coil proteins and membrane traffic. *Biochimica et Biophysica Acta (BBA) - Molecular Cell Research*, 1641(2), 71–85. [https://doi.org/10.1016/S0167-4889\(03\)00088-0](https://doi.org/10.1016/S0167-4889(03)00088-0)
- Gillooly, David J., Raiborg, C., & Stenmark, H. (2003). Phosphatidylinositol 3-phosphate is found in microdomains of early endosomes. *Histochemistry and Cell Biology*, 120(6), 445–453. <https://doi.org/10.1007/s00418-003-0591-7>
- Gillooly, D.J., Morrow, I. C., Lindsay, M., Gould, R., Bryant, N. J., Gaullier, J.-M., Parton, R. G., & Stenmark, H. (2000). Localization of phosphatidylinositol 3-phosphate in yeast and mammalian cells. *EMBO Journal*, 19(17), 4577–4588. Scopus. <https://doi.org/10.1093/emboj/19.17.4577>
- Gissen, P., Johnson, C. A., Gentle, D., Hurst, L. D., Doherty, A. J., O’Kane, C. J., Kelly, D. A., & Maher, E. R. (2005). Comparative evolutionary analysis of VPS33 homologues: Genetic and functional insights. *Human Molecular Genetics*, 14(10), 1261–1270. <https://doi.org/10.1093/hmg/ddi137>
- Glodowski, D. R., Chen, C. C.-H., Schaefer, H., Grant, B. D., & Rongo, C. (2007). RAB-10 regulates glutamate receptor recycling in a cholesterol-dependent endocytosis pathway. *Molecular Biology of the Cell*, 18(11), 4387–4396. <https://doi.org/10.1091/mbc.e07-05-0486>
- Goetz, S. C., & Anderson, K. V. (2010). The primary cilium: A signalling centre during vertebrate development. *Nature Reviews. Genetics*, 11(5), 331–344. <https://doi.org/10.1038/nrg2774>
- Götte, M., & von Mollard, G. F. (1998). A new beat for the SNARE drum. *Trends in Cell Biology*, 8(6), 215–218. [https://doi.org/10.1016/s0962-8924\(98\)01272-0](https://doi.org/10.1016/s0962-8924(98)01272-0)
- Grant, B. D., & Caplan, S. (2008). Mechanisms of EHD/RME-1 Protein Function in Endocytic Transport. *Traffic (Copenhagen, Denmark)*, 9(12), 2043–2052. <https://doi.org/10.1111/j.1600-0854.2008.00834.x>
- Grant, B. D., & Donaldson, J. G. (2009). Pathways and mechanisms of endocytic recycling. *Nature Reviews Molecular Cell Biology*, 10(9), 597–608. <https://doi.org/10.1038/nrm2755>
- Grant, B., & Hirsh, D. (1999). Receptor-mediated endocytosis in the *Caenorhabditis elegans* oocyte. *Molecular Biology of the Cell*, 10(12), 4311–4326. <https://doi.org/10.1091/mbc.10.12.4311>
- Ha, J. Y., Chou, H.-T., Ungar, D., Yip, C. K., Walz, T., & Hughson, F. M. (2016). Molecular architecture of the complete COG tethering complex. *Nature Structural & Molecular Biology*, 23(8), 758–760. <https://doi.org/10.1038/nsmb.3263>
- Hanyaloglu, A. C., & von Zastrow, M. (2008). Regulation of GPCRs by endocytic membrane trafficking and its potential implications. *Annual Review of Pharmacology and Toxicology*, 48, 537–568. <https://doi.org/10.1146/annurev.pharmtox.48.113006.094830>
- Hao, M., & Maxfield, F. R. (2000). Characterization of Rapid Membrane Internalization and Recycling *. *Journal of Biological Chemistry*, 275(20), 15279–15286. <https://doi.org/10.1074/jbc.275.20.15279>
- Hattula, K., Furuholm, J., Tikkanen, J., Tanhuanpää, K., Laakkonen, P., & Peränen, J. (2006). Characterization of the Rab8-specific membrane traffic route linked to protrusion formation. *Journal of Cell Science*, 119(23), 4866–4877. <https://doi.org/10.1242/jcs.03275>
- Haycraft, C. J., Banizs, B., Aydin-Son, Y., Zhang, Q., Michaud, E. J., & Yoder, B. K. (2005). Gli2 and Gli3 Localize to Cilia and Require the Intraflagellar Transport Protein Polaris for Processing and Function. *PLoS Genetics*, 1(4). <https://doi.org/10.1371/journal.pgen.0010053>
- He, K., Ma, X., Xu, T., Li, Y., Hodge, A., Zhang, Q., Torline, J., Huang, Y., Zhao, J., Ling, K., & Hu, J. (2018). Axoneme polyglutamylation regulated by Joubert syndrome protein ARL13B controls

- ciliary targeting of signaling molecules. *Nature Communications*, 9(1), 3310. <https://doi.org/10.1038/s41467-018-05867-1>
- Helfer, E., Harbour, M. E., Henriot, V., Lakisic, G., Sousa-Blin, C., Volceanov, L., Seaman, M. N. J., & Gautreau, A. (2013). Endosomal recruitment of the WASH complex: Active sequences and mutations impairing interaction with the retromer. *Biology of the Cell*, 105(5), 191–207. <https://doi.org/10.1111/boc.201200038>
- Henkel, A. W., & Almers, W. (1996). Fast steps in exocytosis and endocytosis studied by capacitance measurements in endocrine cells. *Current Opinion in Neurobiology*, 6(3), 350–357. [https://doi.org/10.1016/S0959-4388\(96\)80119-X](https://doi.org/10.1016/S0959-4388(96)80119-X)
- Higgins, M., Obaidi, I., & McMorro, T. (2019). Primary cilia and their role in cancer (Review). *Oncology Letters*, 17(3), 3041–3047. <https://doi.org/10.3892/ol.2019.9942>
- Hong, Wanjin. (2005). SNAREs and traffic. *Biochimica et Biophysica Acta (BBA) - Molecular Cell Research*, 1744(2), 120–144. <https://doi.org/10.1016/j.bbamcr.2005.03.014>
- Hong, WanJin, & Lev, S. (2014). Tethering the assembly of SNARE complexes. *Trends in Cell Biology*, 24(1), 35–43. <https://doi.org/10.1016/j.tcb.2013.09.006>
- Hsiao, Y.-C., Tuz, K., & Ferland, R. J. (2012). Trafficking in and to the primary cilium. *Cilia*, 1, 4. <https://doi.org/10.1186/2046-2530-1-4>
- Hu, Y.-B., Dammer, E. B., Ren, R.-J., & Wang, G. (2015). The endosomal-lysosomal system: From acidification and cargo sorting to neurodegeneration. *Translational Neurodegeneration*, 4. <https://doi.org/10.1186/s40035-015-0041-1>
- Huang, P., & Schier, A. F. (2009). Dampened Hedgehog signaling but normal Wnt signaling in zebrafish without cilia. *Development*, 136(18), 3089–3098. <https://doi.org/10.1242/dev.041343>
- Hunter, M. R., Hesketh, G. G., Benedyk, T. H., Gingras, A.-C., & Graham, S. C. (2018). Proteomic and Biochemical Comparison of the Cellular Interaction Partners of Human VPS33A and VPS33B. *Journal of Molecular Biology*, 430(14), 2153–2163. <https://doi.org/10.1016/j.jmb.2018.05.019>
- Huotari, J., & Helenius, A. (2011). Endosome maturation. *The EMBO Journal*, 30(17), 3481–3500. <https://doi.org/10.1038/emboj.2011.286>
- Hutagalung, A. H., & Novick, P. J. (2011). Role of Rab GTPases in Membrane Traffic and Cell Physiology. *Physiological Reviews*, 91(1), 119–149. <https://doi.org/10.1152/physrev.00059.2009>
- Inoue, H., Ha, V. L., Prekeris, R., & Randazzo, P. A. (2008). Arf GTPase-activating protein ASAP1 interacts with Rab11 effector FIP3 and regulates pericentrosomal localization of transferrin receptor-positive recycling endosome. *Molecular Biology of the Cell*, 19(10), 4224–4237. <https://doi.org/10.1091/mbc.e08-03-0290>
- Jing, J., & Prekeris, R. (2009). Polarized endocytic transport: The roles of Rab11 and Rab11-FIPs in regulating cell polarity. *Histology and Histopathology*, 24(9), 1171–1180. <https://www.ncbi.nlm.nih.gov/pmc/articles/PMC4365979/>
- Jo, H., & Kim, J. (2013). Itinerary of vesicles to primary cilia. *Animal Cells and Systems*, 17(4), 221–227. <https://doi.org/10.1080/19768354.2013.830646>
- Jones, T., Naslavsky, N., & Caplan, S. (2020). Eps15 Homology Domain Protein 4 (EHD4) is required for Eps15 Homology Domain Protein 1 (EHD1)-mediated endosomal recruitment and fission. *PLOS ONE*, 15(9), e0239657. <https://doi.org/10.1371/journal.pone.0239657>
- Jonker, C. T. H., Galmes, R., Veenendaal, T., ten Brink, C., van der Welle, R. E. N., Liv, N., de Rooij, J., Peden, A. A., van der Sluijs, P., Margadant, C., & Klumperman, J. (2018). Vps3 and Vps8 control integrin trafficking from early to recycling endosomes and regulate integrin-dependent functions. *Nature Communications*, 9(1), 792. <https://doi.org/10.1038/s41467-018-03226-8>

- Jonker, Caspar T. H., Deo, C., Zager, P. J., Tkachuk, A. N., Weinstein, A. M., Rodriguez-Boulan, E., Lavis, L. D., & Schreiner, R. (2020). Accurate measurement of fast endocytic recycling kinetics in real time. *Journal of Cell Science*, 133(2). <https://doi.org/10.1242/jcs.231225>
- Jović, M., Kieken, F., Naslavsky, N., Sorgen, P. L., & Caplan, S. (2009). Eps15 Homology Domain 1-associated Tubules Contain Phosphatidylinositol-4-Phosphate and Phosphatidylinositol-(4,5)-Bisphosphate and Are Required for Efficient Recycling. *Molecular Biology of the Cell*, 20(11), 2731–2743. <https://doi.org/10.1091/mbc.E08-11-1102>
- Jovic, M., Sharma, M., Rahajeng, J., & Caplan, S. (2010). The early endosome: A busy sorting station for proteins at the crossroads. *Histology and Histopathology*, 25(1), 99–112. <https://www.ncbi.nlm.nih.gov/pmc/articles/PMC2810677/>
- Kasahara, K., Miyoshi, K., Murakami, S., Miyazaki, I., & Asanuma, M. (2014). Visualization of astrocytic primary cilia in the mouse brain by immunofluorescent analysis using the cilia marker Arl13b. *Acta Medica Okayama*, 68(6), 317–322. <https://doi.org/10.18926/AMO/53020>
- Katz, L., & Brennwald, P. (2000). Testing the 3Q:1R “rule”: Mutational analysis of the ionic “zero” layer in the yeast exocytic SNARE complex reveals no requirement for arginine. *Molecular Biology of the Cell*, 11(11), 3849–3858. <https://doi.org/10.1091/mbc.11.11.3849>
- Kelly, E. E., Horgan, C. P., Adams, C., Patzer, T. M., Shuilleabháin, D. M. N., Norman, J. C., & McCaffrey, M. W. (2010). Class I Rab11-family interacting proteins are binding targets for the Rab14 GTPase. *Biology of the Cell*, 102(1), 51–62. <https://doi.org/10.1042/BC20090068>
- Kim, J., Lee, J. E., Heynen-Genel, S., Suyama, E., Ono, K., Lee, K., Ideker, T., Aza-Blanc, P., & Gleeson, J. G. (2010). Functional genomic screen for modulators of ciliogenesis and cilium length. *Nature*, 464(7291), 1048–1051. <https://doi.org/10.1038/nature08895>
- Klumperman, J., & Raposo, G. (2014). The complex ultrastructure of the endolysosomal system. *Cold Spring Harbor Perspectives in Biology*, 6(10), a016857. <https://doi.org/10.1101/cshperspect.a016857>
- Knödler, A., Feng, S., Zhang, J., Zhang, X., Das, A., Peränen, J., & Guo, W. (2010a). Coordination of Rab8 and Rab11 in primary ciliogenesis. *Proceedings of the National Academy of Sciences*, 107(14), 6346–6351. <https://doi.org/10.1073/pnas.1002401107>
- Knödler, A., Feng, S., Zhang, J., Zhang, X., Das, A., Peränen, J., & Guo, W. (2010b). Coordination of Rab8 and Rab11 in primary ciliogenesis. *Proceedings of the National Academy of Sciences of the United States of America*, 107(14), 6346–6351. <https://doi.org/10.1073/pnas.1002401107>
- Lakadamyali, M., Rust, M. J., & Zhuang, X. (2006). Ligands for Clathrin-Mediated Endocytosis Are Differentially Sorted into Distinct Populations of Early Endosomes. *Cell*, 124(5), 997–1009. <https://doi.org/10.1016/j.cell.2005.12.038>
- Langemeyer, L., Fröhlich, F., & Ungermann, C. (2018). Rab GTPase Function in Endosome and Lysosome Biogenesis. *Trends in Cell Biology*, 28(11), 957–970. <https://doi.org/10.1016/j.tcb.2018.06.007>
- Lara Ordóñez, A. J., Fernández, B., Fdez, E., Romo-Lozano, M., Madero-Pérez, J., Lobbestael, E., Baekelandt, V., Aiastui, A., López de Munáin, A., Melrose, H. L., Civiero, L., & Hilfiker, S. (2019). RAB8, RAB10 and RILPL1 contribute to both LRRK2 kinase-mediated centrosomal cohesion and ciliogenesis deficits. *Human Molecular Genetics*, 28(21), 3552–3568. <https://doi.org/10.1093/hmg/ddz201>
- Larkins, C. E., Aviles, G. D. G., East, M. P., Kahn, R. A., & Caspary, T. (2011). Arl13b regulates ciliogenesis and the dynamic localization of Shh signaling proteins. *Molecular Biology of the Cell*, 22(23), 4694–4703. <https://doi.org/10.1091/mbc.E10-12-0994>
- Law, F., & Rocheleau, C. E. (2017). Vps34 and the Armus/TBC-2 Rab GAPs: Putting the brakes on the endosomal Rab5 and Rab7 GTPases. *Cellular Logistics*, 7(4), e1403530. <https://doi.org/10.1080/21592799.2017.1403530>

- Law, F., Seo, J. H., Wang, Z., DeLeon, J. L., Bolis, Y., Brown, A., Zong, W.-X., Du, G., & Rocheleau, C. E. (2017). The VPS34 PI3K negatively regulates RAB-5 during endosome maturation. *Journal of Cell Science*, 130(12), 2007–2017. <https://doi.org/10.1242/jcs.194746>
- Lawrence, C. M., Ray, S., Babyonyshev, M., Galluser, R., Borhani, D. W., & Harrison, S. C. (1999). Crystal structure of the ectodomain of human transferrin receptor. *Science (New York, N.Y.)*, 286(5440), 779–782. <https://doi.org/10.1126/science.286.5440.779>
- Lee, S., Chang, J., & Blackstone, C. (2016). FAM21 directs SNX27–retromer cargoes to the plasma membrane by preventing transport to the Golgi apparatus. *Nature Communications*, 7. <https://doi.org/10.1038/ncomms10939>
- Lees, J. A., Li, P., Kumar, N., Weisman, L. S., & Reinisch, K. M. (2020). Insights into Lysosomal PI(3,5)P2 Homeostasis from a Structural-Biochemical Analysis of the PIKfyve Lipid Kinase Complex. *Molecular Cell*, 80(4), 736–743.e4. <https://doi.org/10.1016/j.molcel.2020.10.003>
- Leloup, N., Lössl, P., Meijer, D. H., Brennich, M., Heck, A. J. R., Thies-Weesie, D. M. E., & Janssen, B. J. C. (2017). Low pH-induced conformational change and dimerization of sortilin triggers endocytosed ligand release. *Nature Communications*, 8(1), 1708. <https://doi.org/10.1038/s41467-017-01485-5>
- Leroux, M. R. (2007). Taking Vesicular Transport to the Cilium. *Cell*, 129(6), 1041–1043. <https://doi.org/10.1016/j.cell.2007.05.049>
- Lin, S. X., Mallet, W. G., Huang, A. Y., & Maxfield, F. R. (2004). Endocytosed Cation-Independent Mannose 6-Phosphate Receptor Traffics via the Endocytic Recycling Compartment en Route to the trans-Golgi Network and a Subpopulation of Late Endosomes. *Molecular Biology of the Cell*, 15(2), 721–733. <https://doi.org/10.1091/mbc.E03-07-0497>
- Lindsay, A. J., & McCaffrey, M. W. (2002). Rab11-FIP2 Functions in Transferrin Recycling and Associates with Endosomal Membranes via Its COOH-terminal Domain. *Journal of Biological Chemistry*, 277(30), 27193–27199. <https://doi.org/10.1074/jbc.M200757200>
- Lindsay, A. J., & McCaffrey, M. W. (2004). The C2 domains of the class I Rab11 family of interacting proteins target recycling vesicles to the plasma membrane. *Journal of Cell Science*, 117(19), 4365–4375. <https://doi.org/10.1242/jcs.01280>
- Liu, T.-T., Gomez, T. S., Sackey, B. K., Billadeau, D. D., & Burd, C. G. (2012). Rab GTPase regulation of retromer-mediated cargo export during endosome maturation. *Molecular Biology of the Cell*, 23(13), 2505–2515. <https://doi.org/10.1091/mbc.E11-11-0915>
- Lu, Q., Insinna, C., Ott, C., Stauffer, J., Pintado, P. A., Rahajeng, J., Baxa, U., Walia, V., Cuenca, A., Hwang, Y.-S., Daar, I. O., Lopes, S., Lippincott-Schwartz, J., Jackson, P. K., Caplan, S., & Westlake, C. J. (2015). Early steps in primary cilium assembly require EHD1/EHD3-dependent ciliary vesicle formation. *Nature Cell Biology*, 17(3), 228–240. <https://doi.org/10.1038/ncb3109>
- Luzio, J. P., Pryor, P. R., & Bright, N. A. (2007). Lysosomes: Fusion and function. *Nature Reviews Molecular Cell Biology*, 8(8), 622–632. <https://doi.org/10.1038/nrm2217>
- Machesky, L. M. (2019). Rab11FIP proteins link endocytic recycling vesicles for cytoskeletal transport and tethering. *Bioscience Reports*, 39(1). <https://doi.org/10.1042/BSR20182219>
- Mahmutefendić, H., Zagorac, G. B., & Lučin, S. M. and P. (2018). Rapid Endosomal Recycling. *Peripheral Membrane Proteins*. <https://doi.org/10.5772/intechopen.75685>
- Marat, A. L., & Haucke, V. (2016). Phosphatidylinositol 3-phosphates—At the interface between cell signalling and membrane traffic. *The EMBO Journal*, 35(6), 561–579. <https://doi.org/10.15252/embj.201593564>
- Maxfield, F. R., & McGraw, T. E. (2004). Endocytic recycling. *Nature Reviews Molecular Cell Biology*, 5(2), 121–132. <https://doi.org/10.1038/nrm1315>
- Mayinger, P. (2012). Phosphoinositides and vesicular membrane traffic. *Biochimica et Biophysica Acta*, 1821(8), 1104–1113. <https://doi.org/10.1016/j.bbalip.2012.01.002>
- McGough, I. J., de Groot, R. E. A., Jellett, A. P., Betist, M. C., Varandas, K. C., Danson, C. M., Heesom, K. J., Korswagen, H. C., & Cullen, P. J. (2018). SNX3-retromer requires an evolutionary

- conserved MON2:DOPEY2:ATP9A complex to mediate Wntless sorting and Wnt secretion. *Nature Communications*, 9(1), 3737. <https://doi.org/10.1038/s41467-018-06114-3>
- McNally, K. E., Faulkner, R., Steinberg, F., Gallon, M., Ghai, R., Pim, D., Langton, P., Pearson, N., Danson, C. M., Nägele, H., Morris, L. L., Singla, A., Overlee, B. L., Heesom, K. J., Sessions, R., Banks, L., Collins, B. M., Berger, I., Billadeau, D. D., ... Cullen, P. J. (2017a). Retriever is a multiprotein complex for retromer-independent endosomal cargo recycling. *Nature Cell Biology*, 19(10), 1214–1225. <https://doi.org/10.1038/ncb3610>
- McNally, K. E., Faulkner, R., Steinberg, F., Gallon, M., Ghai, R., Pim, D., Langton, P., Pearson, N., Danson, C. M., Nägele, H., Morris, L. M., Singla, A., Overlee, B. L., Heesom, K. J., Sessions, R., Banks, L., Collins, B. M., Berger, I., Billadeau, D. D., ... Cullen, P. J. (2017b). Retriever, a multiprotein complex for retromer-independent endosomal cargo recycling. *Nature Cell Biology*, 19(10), 1214–1225. <https://doi.org/10.1038/ncb3610>
- Melo, A. A., Hegde, B. G., Shah, C., Larsson, E., Isas, J. M., Kunz, S., Lundmark, R., Langen, R., & Daumke, O. (2017). Structural insights into the activation mechanism of dynamin-like EHD ATPases. *Proceedings of the National Academy of Sciences*, 114(22), 5629–5634. <https://doi.org/10.1073/pnas.1614075114>
- Mieczyska, M., & Munson, M. (2020). Membrane trafficking: Vesicle formation, cargo sorting and fusion. *Molecular Biology of the Cell*, 31(6), 399–400. <https://doi.org/10.1091/mbc.E19-12-0680>
- Mills, I. G., Urbé, S., & Clague, M. J. (2001). Relationships between EEA1 binding partners and their role in endosome fusion. *Journal of Cell Science*, 114(Pt 10), 1959–1965.
- Mima, J. (2017). Reconstitution of membrane tethering mediated by Rab-family small GTPases. *Biophysical Reviews*, 10(2), 543–549. <https://doi.org/10.1007/s12551-017-0358-3>
- Mindell, J. A. (2012). Lysosomal Acidification Mechanisms. *Annual Review of Physiology*, 74(1), 69–86. <https://doi.org/10.1146/annurev-physiol-012110-142317>
- Mitchison, H. M., & Valente, E. M. (2017). Motile and non-motile cilia in human pathology: From function to phenotypes. *The Journal of Pathology*, 241(2), 294–309. <https://doi.org/10.1002/path.4843>
- Morén, B., Shah, C., Howes, M. T., Schieber, N. L., McMahon, H. T., Parton, R. G., Daumke, O., & Lundmark, R. (2012). EHD2 regulates caveolar dynamics via ATP-driven targeting and oligomerization. *Molecular Biology of the Cell*, 23(7), 1316–1329. <https://doi.org/10.1091/mbc.E11-09-0787>
- Mottola, G., Classen, A.-K., González-Gaitán, M., Eaton, S., & Zerial, M. (2010). A novel function for the Rab5 effector Rabenosyn-5 in planar cell polarity. *Development*, 137(14), 2353–2364. <https://doi.org/10.1242/dev.048413>
- Mukherjee, S., Ghosh, R. N., & Maxfield, F. R. (1997). Endocytosis. *Physiological Reviews*, 77(3), 759–803. <https://doi.org/10.1152/physrev.1997.77.3.759>
- Müller, O., Bayer, M. J., Peters, C., Andersen, J. S., Mann, M., & Mayer, A. (2002). The Vtc proteins in vacuole fusion: Coupling NSF activity to V0 trans-complex formation. *The EMBO Journal*, 21(3), 259–269. <https://doi.org/10.1093/emboj/21.3.259>
- Murk, J. L. a. N., Humbel, B. M., Ziese, U., Griffith, J. M., Posthuma, G., Slot, J. W., Koster, A. J., Verkleij, A. J., Geuze, H. J., & Kleijmeer, M. J. (2003). Endosomal compartmentalization in three dimensions: Implications for membrane fusion. *Proceedings of the National Academy of Sciences*, 100(23), 13332–13337. <https://doi.org/10.1073/pnas.2232379100>
- Nachury, M. V., Loktev, A. V., Zhang, Q., Westlake, C. J., Peränen, J., Merdes, A., Slusarski, D. C., Scheller, R. H., Bazan, J. F., Sheffield, V. C., & Jackson, P. K. (2007). A core complex of BBS proteins cooperates with the GTPase Rab8 to promote ciliary membrane biogenesis. *Cell*, 129(6), 1201–1213. <https://doi.org/10.1016/j.cell.2007.03.053>
- Naslavsky, N., Boehm, M., Backlund, P. S., & Caplan, S. (2004). Rabenosyn-5 and EHD1 interact and sequentially regulate protein recycling to the plasma membrane. *Molecular Biology of the Cell*, 15(5), 2410–2422. <https://doi.org/10.1091/mbc.e03-10-0733>

- Naslavsky, N., & Caplan, S. (2018). The enigmatic endosome – sorting the ins and outs of endocytic trafficking. *Journal of Cell Science*, 131(13). <https://doi.org/10.1242/jcs.216499>
- Naslavsky, N., Rahajeng, J., Sharma, M., Jović, M., & Caplan, S. (2006). Interactions between EHD Proteins and Rab11-FIP2: A Role for EHD3 in Early Endosomal Transport. *Molecular Biology of the Cell*, 17(1), 163–177. <https://doi.org/10.1091/mbc.E05-05-0466>
- Navaroli, D. M., Bellvé, K. D., Standley, C., Lifshitz, L. M., Cardia, J., Lambright, D., Leonard, D., Fogarty, K. E., & Corvera, S. (2012). Rabenosyn-5 defines the fate of the transferrin receptor following clathrin-mediated endocytosis. *Proceedings of the National Academy of Sciences*, 109(8), E471–E480. <https://doi.org/10.1073/pnas.1115495109>
- Norris, A., Tammineni, P., Wang, S., Gerdes, J., Murr, A., Kwan, K. Y., Cai, Q., & Grant, B. D. (2017). SNX-1 and RME-8 oppose the assembly of HGRS-1/ESCRT-0 degradative microdomains on endosomes. *Proceedings of the National Academy of Sciences*. <https://doi.org/10.1073/pnas.1612730114>
- Novick, P. (2016). Regulation of membrane traffic by Rab GEF and GAP cascades. *Small GTPases*, 7(4), 252–256. <https://doi.org/10.1080/21541248.2016.1213781>
- Nozaki, S., Katoh, Y., Terada, M., Michisaka, S., Funabashi, T., Takahashi, S., Kontani, K., & Nakayama, K. (2017). Regulation of ciliary retrograde protein trafficking by the Joubert syndrome proteins ARL13B and INPP5E. *Journal of Cell Science*, 130(3), 563–576. <https://doi.org/10.1242/jcs.197004>
- Organelle assembly in yeast: Characterization of yeast mutants defective in vacuolar biogenesis and protein sorting. (1988). *The Journal of Cell Biology*, 107(4), 1369–1383. <https://www.ncbi.nlm.nih.gov/pmc/articles/PMC2115260/>
- Owen, D. J., Collins, B. M., & Evans, P. R. (2004). Adaptors for clathrin coats: Structure and function. *Annual Review of Cell and Developmental Biology*, 20, 153–191. <https://doi.org/10.1146/annurev.cellbio.20.010403.104543>
- Palade, G. (1975). Intracellular aspects of the process of protein synthesis. *Science (New York, N.Y.)*, 189(4200), 347–358. <https://doi.org/10.1126/science.1096303>
- Pant, S., Sharma, M., Patel, K., Caplan, S., Carr, C. M., & Grant, B. D. (2009). AMPH-1/Amphiphysin/Bin1 functions with RME-1/Ehd1 in endocytic recycling. *Nature Cell Biology*, 11(12), 1399–1410. <https://doi.org/10.1038/ncb1986>
- Pedersen, L. B., & Rosenbaum, J. L. (2008). Chapter Two Intraflagellar Transport (IFT): Role in Ciliary Assembly, Resorption and Signalling. In *Current Topics in Developmental Biology* (Vol. 85, pp. 23–61). Academic Press. [https://doi.org/10.1016/S0070-2153\(08\)00802-8](https://doi.org/10.1016/S0070-2153(08)00802-8)
- Pelham, H. R. B. (2002). Insights from yeast endosomes. *Current Opinion in Cell Biology*, 14(4), 454–462. [https://doi.org/10.1016/S0955-0674\(02\)00352-6](https://doi.org/10.1016/S0955-0674(02)00352-6)
- Peplowska, K., Markgraf, D. F., Ostrowicz, C. W., Bange, G., & Ungermann, C. (2007). The CORVET Tethering Complex Interacts with the Yeast Rab5 Homolog Vps21 and Is Involved in Endo-Lysosomal Biogenesis. *Developmental Cell*, 12(5), 739–750. <https://doi.org/10.1016/j.devcel.2007.03.006>
- Perini, E. D., Schaefer, R., Stöter, M., Kalaidzidis, Y., & Zerial, M. (2014). Mammalian CORVET is required for fusion and conversion of distinct early endosome subpopulations. *Traffic (Copenhagen, Denmark)*, 15(12), 1366–1389. <https://doi.org/10.1111/tra.12232>
- Perret, E., Lakkaraju, A., Deborde, S., Schreiner, R., & Rodriguez-Boulant, E. (2005). Evolving endosomes: How many varieties and why? *Current Opinion in Cell Biology*, 17(4), 423–434. <https://doi.org/10.1016/j.ceb.2005.06.008>
- Pfeffer, S. (2005). A model for Rab GTPase localization. *Biochemical Society Transactions*, 33(Pt 4), 627–630. <https://doi.org/10.1042/BST0330627>
- Pfeffer, S. R. (1999). Transport-vesicle targeting: Tethers before SNAREs. *Nature Cell Biology*, 1(1), E17–22. <https://doi.org/10.1038/8967>
- Phillips-Krawczak, C. A., Singla, A., Starokadomskyy, P., Deng, Z., Osborne, D. G., Li, H., Dick, C. J., Gomez, T. S., Koenecke, M., Zhang, J.-S., Dai, H., Sifuentes-Dominguez, L. F., Geng, L. N.,

- Kaufmann, S. H., Hein, M. Y., Wallis, M., McGaughran, J., Gecz, J., van de Sluis, B., ... Burstein, E. (2015). COMMD1 is linked to the WASH complex and regulates endosomal trafficking of the copper transporter ATP7A. *Molecular Biology of the Cell*, 26(1), 91–103. <https://doi.org/10.1091/mbc.E14-06-1073>
- Puthenveedu, M. A., Lauffer, B., Temkin, P., Vistein, R., Carlton, P., Thorn, K., Taunton, J., Weiner, O. D., Parton, R. G., & von Zastrow, M. (2010). Sequence-dependent sorting of recycling proteins by actin-stabilized endosomal microdomains. *Cell*, 143(5), 761–773. <https://doi.org/10.1016/j.cell.2010.10.003>
- Rabaptin-5a/rabaptin-4 serves as a linker between rab4 and γ 1-adaptin in membrane recycling from endosomes.* (n.d.). Retrieved February 11, 2021, from <https://www.ncbi.nlm.nih.gov/pmc/articles/PMC156754/>
- Rahajeng, J., Caplan, S., & Naslavsky, N. (2010). Common and distinct roles for the binding partners Rabenosyn-5 and Vps45 in the regulation of endocytic trafficking in mammalian cells. *Experimental Cell Research*, 316(5), 859–874. <https://doi.org/10.1016/j.yexcr.2009.11.007>
- Recycling integrins | Nature Reviews Molecular Cell Biology.* (n.d.). Retrieved February 16, 2021, from <https://www.nature.com/articles/nrm2537>
- Ren, Y., Yip, C. K., Tripathi, A., Huie, D., Jeffrey, P. D., Walz, T., & Hughson, F. M. (2009). A Structure-Based Mechanism for Vesicle Capture by the Multisubunit Tethering Complex Dsl1. *Cell*, 139(6), 1119–1129. <https://doi.org/10.1016/j.cell.2009.11.002>
- Ribeiro, L. F., Verpoort, B., Nys, J., Vennekens, K. M., Wierda, K. D., & Wit, J. de. (2019). SorCS1-mediated sorting in dendrites maintains neurexin axonal surface polarization required for synaptic function. *PLOS Biology*, 17(10), e3000466. <https://doi.org/10.1371/journal.pbio.3000466>
- Rink, J., Ghigo, E., Kalaidzidis, Y., & Zerial, M. (2005). Rab Conversion as a Mechanism of Progression from Early to Late Endosomes. *Cell*, 122(5), 735–749. <https://doi.org/10.1016/j.cell.2005.06.043>
- Robinson, D. G., & Neuhaus, J.-M. (2016). Receptor-mediated sorting of soluble vacuolar proteins: Myths, facts, and a new model. *Journal of Experimental Botany*, 67(15), 4435–4449. <https://doi.org/10.1093/jxb/erw222>
- Roccisana, J., Sadler, J. B. A., Bryant, N. J., & Gould, G. W. (2013). Sorting of GLUT4 into its insulin-sensitive store requires the Sec1/Munc18 protein mVps45. *Molecular Biology of the Cell*, 24(15), 2389–2397. <https://doi.org/10.1091/mbc.E13-01-0011>
- Rojas, R., van Vlijmen, T., Mardones, G. A., Prabhu, Y., Rojas, A. L., Mohammed, S., Heck, A. J. R., Raposo, G., van der Sluijs, P., & Bonifacino, J. S. (2008). Regulation of retromer recruitment to endosomes by sequential action of Rab5 and Rab7. *The Journal of Cell Biology*, 183(3), 513–526. <https://doi.org/10.1083/jcb.200804048>
- Rosenbaum, J. L., & Witman, G. B. (2002). Intraflagellar transport. *Nature Reviews Molecular Cell Biology*, 3(11), 813–825. <https://doi.org/10.1038/nrm952>
- Roux, A., Cuvelier, D., Nassoy, P., Prost, J., Bassereau, P., & Goud, B. (2005). Role of curvature and phase transition in lipid sorting and fission of membrane tubules. *The EMBO Journal*, 24(8), 1537–1545. <https://doi.org/10.1038/sj.emboj.7600631>
- Ryan, T. A. (2003). Kiss-and-run, fuse-pinch-and-linger, fuse-and-collapse: The life and times of a neurosecretory granule. *Proceedings of the National Academy of Sciences*, 100(5), 2171–2173. <https://doi.org/10.1073/pnas.0530260100>
- Ryder, P. V., Vistein, R., Gokhale, A., Seaman, M. N., Puthenveedu, M. A., & Faundez, V. (2013). The WASH complex, an endosomal Arp2/3 activator, interacts with the Hermansky–Pudlak syndrome complex BLOC-1 and its cargo phosphatidylinositol-4-kinase type II α . *Molecular Biology of the Cell*, 24(14), 2269–2284. <https://doi.org/10.1091/mbc.E13-02-0088>
- Scheidel, N., Kennedy, J., & Blacque, O. E. (2018). Endosome maturation factors Rabenosyn-5/VPS45 and caveolin-1 regulate ciliary membrane and polycystin-2 homeostasis. *The EMBO Journal*, 37(9). <https://doi.org/10.15252/embj.201798248>

- Schindler, C., Chen, Y., Pu, J., Guo, X., & Bonifacino, J. S. (2015). EARP is a multisubunit tethering complex involved in endocytic recycling. *Nature Cell Biology*, 17(5), 639–650. <https://doi.org/10.1038/ncb3129>
- Schmidt, O., & Teis, D. (2012). The ESCRT machinery. *Current Biology*, 22(4), R116–R120. <https://doi.org/10.1016/j.cub.2012.01.028>
- Schwartz, A. L. (1990). Cell biology of intracellular protein trafficking. *Annual Review of Immunology*, 8, 195–229. <https://doi.org/10.1146/annurev.iy.08.040190.001211>
- Scott, C. C., Vacca, F., & Gruenberg, J. (2014). Endosome maturation, transport and functions. *Seminars in Cell & Developmental Biology*, 31, 2–10. <https://doi.org/10.1016/j.semcdb.2014.03.034>
- Seaman, M. N. J. (2012). The retromer complex – endosomal protein recycling and beyond. *Journal of Cell Science*, 125(20), 4693–4702. <https://doi.org/10.1242/jcs.103440>
- Seixas, C., Choi, S. Y., Polgar, N., Umberger, N. L., East, M. P., Zuo, X., Moreiras, H., Ghossoub, R., Benmerah, A., Kahn, R. A., Fogelgren, B., Caspary, T., Lipschutz, J. H., & Barral, D. C. (2016). Arl13b and the exocyst interact synergistically in ciliogenesis. *Molecular Biology of the Cell*, 27(2), 308–320. <https://doi.org/10.1091/mbc.E15-02-0061>
- Shanks, S. G., Carpp, L. N., Struthers, M. S., McCann, R. K., & Bryant, N. J. (2012). The Sec1/Munc18 Protein Vps45 Regulates Cellular Levels of Its SNARE Binding Partners Tlg2 and Snc2 in *Saccharomyces cerevisiae*. *PLOS ONE*, 7(11), e49628. <https://doi.org/10.1371/journal.pone.0049628>
- Sharma, M., Naslavsky, N., & Caplan, S. (2008). A Role for EHD4 in the Regulation of Early Endosomal Transport. *Traffic (Copenhagen, Denmark)*, 9(6), 995–1018. <https://doi.org/10.1111/j.1600-0854.2008.00732.x>
- Shi, A., & Grant, B. D. (2013). Interactions between Rab and Arf GTPases regulate endosomal phosphatidylinositol-4,5-bisphosphate during endocytic recycling. *Small GTPases*, 4(2), 106–109. <https://doi.org/10.4161/sgtp.23477>
- Shillingford, J. M., Murcia, N. S., Larson, C. H., Low, S. H., Hedgepeth, R., Brown, N., Flask, C. A., Novick, A. C., Goldfarb, D. A., Kramer-Zucker, A., Walz, G., Piontek, K. B., Germino, G. G., & Weimbs, T. (2006). The mTOR pathway is regulated by polycystin-1, and its inhibition reverses renal cystogenesis in polycystic kidney disease. *Proceedings of the National Academy of Sciences of the United States of America*, 103(14), 5466–5471. <https://doi.org/10.1073/pnas.0509694103>
- Simonetti, B., Danson, C. M., Heesom, K. J., & Cullen, P. J. (2017). Sequence-dependent cargo recognition by SNX-BARs mediates retromer-independent transport of CI-MPR. *Journal of Cell Biology*, 216(11), 3695–3712. <https://doi.org/10.1083/jcb.201703015>
- Simonetti, B., Paul, B., Chaudhari, K., Weeratunga, S., Steinberg, F., Gorla, M., Heesom, K. J., Bashaw, G. J., Collins, B. M., & Cullen, P. J. (2019a). Molecular identification of a BAR domain-containing coat complex for endosomal recycling of transmembrane proteins. *Nature Cell Biology*, 21(10), 1219–1233. <https://doi.org/10.1038/s41556-019-0393-3>
- Simonetti, B., Paul, B., Chaudhari, K., Weeratunga, S., Steinberg, F., Gorla, M., Heesom, K. J., Bashaw, G. J., Collins, B. M., & Cullen, P. J. (2019b). Molecular identification of a BAR domain-containing coat complex for endosomal recycling of transmembrane proteins. *Nature Cell Biology*, 21(10), 1219–1233. <https://doi.org/10.1038/s41556-019-0393-3>
- Singla, A., Fedoseienko, A., Giridharan, S. S. P., Overlee, B. L., Lopez, A., Jia, D., Song, J., Huff-Hardy, K., Weisman, L., Burstein, E., & Billadeau, D. D. (2019). Endosomal PI(3)P regulation by the COMMD/CCDC22/CCDC93 (CCC) complex controls membrane protein recycling. *Nature Communications*, 10(1), 4271. <https://doi.org/10.1038/s41467-019-12221-6>
- Sneeggen, M., Pedersen, N. M., Campsteijn, C., Haugsten, E. M., Stenmark, H., & Schink, K. O. (2019). WDFY2 restrains matrix metalloproteinase secretion and cell invasion by controlling VAMP3-dependent recycling. *Nature Communications*, 10(1), 2850. <https://doi.org/10.1038/s41467-019-10794-w>

- Solinger, J. A., Rashid, H.-O., Prescianotto-Baschong, C., & Spang, A. (2020). FERARI is required for Rab11-dependent endocytic recycling. *Nature Cell Biology*, 22(2), 213–224. <https://doi.org/10.1038/s41556-019-0456-5>
- Solinger, J. A., & Spang, A. (2013). Tethering complexes in the endocytic pathway: CORVET and HOPS. *The FEBS Journal*, 280(12), 2743–2757. <https://doi.org/10.1111/febs.12151>
- Solinger, J. A., & Spang, A. (2014). Loss of the Sec1/Munc18-family proteins VPS-33.2 and VPS-33.1 bypasses a block in endosome maturation in *Caenorhabditis elegans*. *Molecular Biology of the Cell*, 25(24), 3909–3925. <https://doi.org/10.1091/mbc.E13-12-0710>
- Sönnichsen, B., De Renzis, S., Nielsen, E., Rietdorf, J., & Zerial, M. (2000). Distinct Membrane Domains on Endosomes in the Recycling Pathway Visualized by Multicolor Imaging of Rab4, Rab5, and Rab11. *The Journal of Cell Biology*, 149(4), 901–914. <https://www.ncbi.nlm.nih.gov/pmc/articles/PMC2174575/>
- Spang, A. (2016). Membrane Tethering Complexes in the Endosomal System. *Frontiers in Cell and Developmental Biology*, 4, 35. <https://doi.org/10.3389/fcell.2016.00035>
- Stefan, C. J., Trimble, W. S., Grinstein, S., Drin, G., Reinisch, K., De Camilli, P., Cohen, S., Valm, A. M., Lippincott-Schwartz, J., Levine, T. P., Iaea, D. B., Maxfield, F. R., Futter, C. E., Eden, E. R., Judith, D., van Vliet, A. R., Agostinis, P., Tooze, S. A., Sugiura, A., & McBride, H. M. (2017). Membrane dynamics and organelle biogenesis—Lipid pipelines and vesicular carriers. *BMC Biology*, 15(1), 102. <https://doi.org/10.1186/s12915-017-0432-0>
- Stephens, R. E. (1999). Turnover of Tubulin in Ciliary Outer Doublet Microtubules. *Cell Structure and Function*, 24(5), 413–418. <https://doi.org/10.1247/csf.24.413>
- Stoorvogel, W., Geuze, H. J., & Strous, G. J. (1987). Sorting of endocytosed transferrin and asialoglycoprotein occurs immediately after internalization in HepG2 cells. *Journal of Cell Biology*, 104(5), 1261–1268. <https://doi.org/10.1083/jcb.104.5.1261>
- Strutt, H., Langton, P. F., Pearson, N., McMillan, K. J., Strutt, D., & Cullen, P. J. (2019). Retromer Controls Planar Polarity Protein Levels and Asymmetric Localization at Intercellular Junctions. *Current Biology: CB*, 29(3), 484–491.e6. <https://doi.org/10.1016/j.cub.2018.12.027>
- Su, T., Bryant, D. M., Luton, F., Vergés, M., Ulrich, S. M., Hansen, K. C., Datta, A., Eastburn, D. J., Burlingame, A. L., Shokat, K. M., & Mostov, K. E. (2010). A kinase cascade leading to Rab11-FIP5 controls transcytosis of the polymeric immunoglobulin receptor. *Nature Cell Biology*, 12(12), 1143–1153. <https://doi.org/10.1038/ncb2118>
- Südhof, T. C., & Rothman, J. E. (2009). Membrane Fusion: Grappling with SNARE and SM Proteins. *Science (New York, N.Y.)*, 323(5913), 474–477. <https://doi.org/10.1126/science.1161748>
- Sun, Y., Bilan, P. J., Liu, Z., & Klip, A. (2010). Rab8A and Rab13 are activated by insulin and regulate GLUT4 translocation in muscle cells. *Proceedings of the National Academy of Sciences*, 107(46), 19909–19914. <https://doi.org/10.1073/pnas.1009523107>
- Takeda, S., & Narita, K. (2012). Structure and function of vertebrate cilia, towards a new taxonomy. *Differentiation*, 83(2), S4–S11. <https://doi.org/10.1016/j.diff.2011.11.002>
- Takemoto, K., Ebine, K., Askani, J. C., Krüger, F., Gonzalez, Z. A., Ito, E., Goh, T., Schumacher, K., Nakano, A., & Ueda, T. (2018). Distinct sets of tethering complexes, SNARE complexes, and Rab GTPases mediate membrane fusion at the vacuole in *Arabidopsis*. *Proceedings of the National Academy of Sciences of the United States of America*, 115(10), E2457–E2466. <https://doi.org/10.1073/pnas.1717839115>
- Tan, J. Z. A., & Gleeson, P. A. (2019). Cargo Sorting at the trans-Golgi Network for Shunting into Specific Transport Routes: Role of Arf Small G Proteins and Adaptor Complexes. *Cells*, 8(6). <https://doi.org/10.3390/cells8060531>
- Tan, X., Thapa, N., Choi, S., & Anderson, R. A. (2015). Emerging roles of PtdIns(4,5)P₂ – beyond the plasma membrane. *Journal of Cell Science*, 128(22), 4047–4056. <https://doi.org/10.1242/jcs.175208>

- Temkin, P., Lauffer, B., Jäger, S., Cimermancic, P., Krogan, N. J., & von Zastrow, M. (2011). SNX27 mediates retromer tubule entry and endosome-to-plasma membrane trafficking of signalling receptors. *Nature Cell Biology*, 13(6), 715–721. <https://doi.org/10.1038/ncb2252>
- Tobin, J. L., & Beales, P. L. (2008). Restoration of renal function in zebrafish models of ciliopathies. *Pediatric Nephrology (Berlin, Germany)*, 23(11), 2095–2099. <https://doi.org/10.1007/s00467-008-0898-7>
- Tran, T. H. T., Zeng, Q., & Hong, W. (2007). VAMP4 cycles from the cell surface to the trans-Golgi network via sorting and recycling endosomes. *Journal of Cell Science*, 120(6), 1028–1041. <https://doi.org/10.1242/jcs.03387>
- Urban, D., Li, L., Christensen, H., Pluthero, F. G., Chen, S. Z., Puhacz, M., Garg, P. M., Lanka, K. K., Cummings, J. J., Kramer, H., Wasmuth, J. D., Parkinson, J., & Kahr, W. H. A. (2012). The VPS33B-binding protein VPS16B is required in megakaryocyte and platelet α -granule biogenesis. *Blood*, 120(25), 5032–5040. <https://doi.org/10.1182/blood-2012-05-431205>
- Vale-Costa, S., & Amorim, M. J. (2016). Recycling Endosomes and Viral Infection. *Viruses*, 8(3), 64. <https://doi.org/10.3390/v8030064>
- van Weering, J. R. T., Sessions, R. B., Traer, C. J., Kloer, D. P., Bhatia, V. K., Stamou, D., Carlsson, S. R., Hurley, J. H., & Cullen, P. J. (2012). Molecular basis for SNX-BAR-mediated assembly of distinct endosomal sorting tubules. *The EMBO Journal*, 31(23), 4466–4480. <https://doi.org/10.1038/emboj.2012.283>
- van Weering, J. R. T., Verkade, P., & Cullen, P. J. (2010). SNX-BAR proteins in phosphoinositide-mediated, tubular-based endosomal sorting. *Seminars in Cell & Developmental Biology*, 21(4), 371–380. <https://doi.org/10.1016/j.semcdb.2009.11.009>
- van Weering, J. R. T., Verkade, P., & Cullen, P. J. (2012). SNX-BAR-mediated endosome tubulation is co-ordinated with endosome maturation. *Traffic (Copenhagen, Denmark)*, 13(1), 94–107. <https://doi.org/10.1111/j.1600-0854.2011.01297.x>
- Vazquez-Sanchez, S., Gonzalez-Lozano, M. A., Walfenzao, A., Li, K. W., & van Weering, J. R. T. (2020). The endosomal protein sorting nexin 4 is a synaptic protein. *Scientific Reports*, 10(1), 18239. <https://doi.org/10.1038/s41598-020-74694-6>
- Vellodi, A. (2005). Lysosomal storage disorders. *British Journal of Haematology*, 128(4), 413–431. <https://doi.org/10.1111/j.1365-2141.2004.05293.x>
- Wandinger-Ness, A., & Zerial, M. (2014). Rab Proteins and the Compartmentalization of the Endosomal System. *Cold Spring Harbor Perspectives in Biology*, 6(11). <https://doi.org/10.1101/cshperspect.a022616>
- Wang, F., Zhang, L., Zhang, G.-L., Wang, Z.-B., Cui, X.-S., Kim, N.-H., & Sun, S.-C. (2014). WASH complex regulates Arp2/3 complex for actin-based polar body extrusion in mouse oocytes. *Scientific Reports*, 4(1), 5596. <https://doi.org/10.1038/srep05596>
- Wang, X., Weng, M., Ke, Y., Sapp, E., DiFiglia, M., & Li, X. (2020). Kalirin Interacts with TRAPP and Regulates Rab11 and Endosomal Recycling. *Cells*, 9(5), 1132. <https://doi.org/10.3390/cells9051132>
- Wartosch, L., Günesdogan, U., Graham, S. C., & Luzio, J. P. (2015). Recruitment of VPS33A to HOPS by VPS16 Is Required for Lysosome Fusion with Endosomes and Autophagosomes. *Traffic*, 16(7), 727–742. <https://doi.org/10.1111/tra.12283>
- Wassmer, T., Attar, N., Bujny, M. V., Oakley, J., Traer, C. J., & Cullen, P. J. (2007). A loss-of-function screen reveals SNX5 and SNX6 as potential components of the mammalian retromer. *Journal of Cell Science*, 120(1), 45–54. <https://doi.org/10.1242/jcs.03302>
- Wassmer, T., Attar, N., Harterink, M., van Weering, J. R. T., Traer, C. J., Oakley, J., Goud, B., Stephens, D. J., Verkade, P., Korswagen, H. C., & Cullen, P. J. (2009). The Retromer Coat Complex Coordinates Endosomal Sorting and Dynein-Mediated Transport, with Carrier Recognition by the trans-Golgi Network. *Developmental Cell*, 17(1), 110–122. <https://doi.org/10.1016/j.devcel.2009.04.016>

- Weiss, L. E., Milenkovic, L., Yoon, J., Stearns, T., & Moerner, W. E. (2019). Motional dynamics of single Patched1 molecules in cilia are controlled by Hedgehog and cholesterol. *Proceedings of the National Academy of Sciences*, 116(12), 5550–5557. <https://doi.org/10.1073/pnas.1816747116>
- Westlake, C. J., Baye, L. M., Nachury, M. V., Wright, K. J., Ervin, K. E., Phu, L., Chalouni, C., Beck, J. S., Kirkpatrick, D. S., Slusarski, D. C., Sheffield, V. C., Scheller, R. H., & Jackson, P. K. (2011). Primary cilia membrane assembly is initiated by Rab11 and transport protein particle II (TRAPP II) complex-dependent trafficking of Rabin8 to the centrosome. *Proceedings of the National Academy of Sciences*, 108(7), 2759–2764. <https://doi.org/10.1073/pnas.1018823108>
- Whewey, G., Nazlamova, L., & Hancock, J. T. (2018). Signaling through the Primary Cilium. *Frontiers in Cell and Developmental Biology*, 6. <https://doi.org/10.3389/fcell.2018.00008>
- Whyte, J. R. C., & Munro, S. (2002). Vesicle tethering complexes in membrane traffic. *Journal of Cell Science*, 115(13), 2627–2637. <https://jcs.biologists.org/content/115/13/2627>
- Wilcke, M., Johannes, L., Galli, T., Mayau, V., Goud, B., & Salamero, J. (2000). Rab11 Regulates the Compartmentalization of Early Endosomes Required for Efficient Transport from Early Endosomes to the Trans-Golgi Network. *Journal of Cell Biology*, 151(6), 1207–1220. <https://doi.org/10.1083/jcb.151.6.1207>
- Witkos, T. M., & Lowe, M. (2015). The Golgin Family of Coiled-Coil Tethering Proteins. *Frontiers in Cell and Developmental Biology*, 3, 86. <https://doi.org/10.3389/fcell.2015.00086>
- Xie, S., Bahl, K., Reinecke, J. B., Hammond, G. R. V., Naslavsky, N., & Caplan, S. (2016). The endocytic recycling compartment maintains cargo segregation acquired upon exit from the sorting endosome. *Molecular Biology of the Cell*, 27(1), 108–126. <https://doi.org/10.1091/mbc.E15-07-0514>
- Xie, T., Nguyen, T., Hupe, M., & Wei, M. L. (2009). Multidrug resistance decreases with mutations of melanosomal regulatory genes. *Cancer Research*, 69(3), 992–999. <https://doi.org/10.1158/0008-5472.CAN-08-0506>
- Yang, H. Q., Jana, K., Rindler, M. J., & Coetzee, W. A. (2018). The trafficking protein, EHD2, positively regulates cardiac sarcolemmal KATP channel surface expression: Role in cardioprotection. *The FASEB Journal*, 32(3), 1613–1625. <https://doi.org/10.1096/fj.201700027R>
- Yee, L. E., & Reiter, J. F. (2015). Ciliary vesicle formation: A prelude to ciliogenesis. *Developmental Cell*, 32(6), 665–666. <https://doi.org/10.1016/j.devcel.2015.03.012>
- Yoon, T.-Y., & Munson, M. (2018). SNARE complex assembly and disassembly. *Current Biology: CB*, 28(8), R397–R401. <https://doi.org/10.1016/j.cub.2018.01.005>
- Yu, H., Shen, C., Liu, Y., Menasche, B. L., Ouyang, Y., Stowell, M. H. B., & Shen, J. (2018). SNARE zippering requires activation by SNARE-like peptides in Sec1/Munc18 proteins. *Proceedings of the National Academy of Sciences*, 115(36), E8421–E8429. <https://doi.org/10.1073/pnas.1802645115>
- Yudowski, G. A., Puthenveedu, M. A., Henry, A. G., & von Zastrow, M. (2009). Cargo-mediated regulation of a rapid Rab4-dependent recycling pathway. *Molecular Biology of the Cell*, 20(11), 2774–2784. <https://doi.org/10.1091/mbc.e08-08-0892>
- Zeng, H., Jia, J., & Liu, A. (2010). Coordinated Translocation of Mammalian Gli Proteins and Suppressor of Fused to the Primary Cilium. *PLOS ONE*, 5(12), e15900. <https://doi.org/10.1371/journal.pone.0015900>
- Zerial, M., & McBride, H. (2001). Rab proteins as membrane organizers. *Nature Reviews Molecular Cell Biology*, 2(2), 107–117. <https://doi.org/10.1038/35052055>
- Zullo, A., Iaconis, D., Barra, A., Cantone, A., Messaddeq, N., Capasso, G., Dollé, P., Igarashi, P., & Franco, B. (2010). Kidney-specific inactivation of Odf1 leads to renal cystic disease associated with upregulation of the mTOR pathway. *Human Molecular Genetics*, 19(14), 2792–2803. <https://doi.org/10.1093/hmg/ddq180>

10. Acknowledgements

This work was performed in the group of Prof. Dr. Anne Spang at the Biozentrum of the University of Basel (Switzerland). First and foremost, I would like to thank my supervisor **Prof. Anne Spang** for giving me the opportunity to conduct my PhD in her lab. I am very grateful for her guidance and support that I received throughout the years. I am also grateful to my Ph.D. committee members, Professor Martin Spiess and Professor Jean Gruenberg for their support and good input.

I am thankful to the technical and administrative staff of the 5th floor and the Spang lab, Brigitte Olufsen, Maja Güntensperger, Dora Stetak, Cedrin Kueng, Jonas Fürst, Elisabete, and Fatima Reis. The IMCF-Biozentrum for their support and advice with image acquisition and analysis. Especially Alexia, Laurent and Kai for their technical and image analysis support.

I am grateful to **Dr. Jachen Solinger** for his amazing work in *C. elegans* and for the critical and careful reading of my thesis. Thanks to **Dr. Maria Podinovskaya**, for her advice on tissue culture and CRISPR/Cas9 method and imaging.

All members of the Spang Lab whom I work with, **Julia Stevens, Dr. Kiril Tishinov, Dr. Emmanouil Kyriakakis, Artan Ademi, Pascal Ankli, Dr. Timo Stahl, Dr. Thomas Gross, Dr. Congwei Wang, Dr. Ludovic Enkler, Dr. Debdatto Mookherjee, Dr. Carla Elizabeth Cadena del Castillo, Shirley Dixit, Viktória Szentgyörgyi, and Danie Ott**. I feel very privileged working with these talented scientists.

All the 5th-floor members, especially Dr. Dominik Buser for the advice and experimental help.

Special thanks to my wife, my best friend and colleague **Sheuli Begum** for all the help and mental support. Overall, thanks for always been there, every day, every minute, every moment. Without you, nothing would be possible.

Last but not least, a very big thank goes to my family and friends for being patient, for always understanding, and for supporting me through these years. Without them, I would not have been able to accomplish any of this.

11. Curriculum Vitae

Harun-Or Rashid

Date of birth: 01.01.1990

Nationality: Bangladeshi

Address: St. Johannis Ring 90, 4056 Basel, Switzerland

Email: h.rashid@unibas.ch

EDUCATION

2016 – 2021 Ph.D. in Cell Biology | Focal area Growth and Development

Biozentrum, University of Basel, Basel, Switzerland

2013 – 2016 Masters in medical science | Chonbuk National University, Jeonju, South Korea

2007 – 2011 Bachelor of pharmacy | Northern University Bangladesh, Dhaka, Bangladesh

FELLOWSHIPS AND HONORS

2013 - 2016 Brain Korea (BK) Research scholarship

2016 Notable Korean scientist (IBRIC, South Korea)

2007-2011 Best student award (every semester)

Selected Publications

Solinger JA*, **Harun-Or Rashid** *, et al. FERARI is required for Rab11-dependent endocytic recycling. *Nat Cell Biol.* PMID: 31988382. (*equal contribution)

Bahar E, Akter KM, Lee GH, Lee HY, **Harun-Or Rashid** et al. β -Cell protection and antidiabetic activities of *Crassocephalum crepidioides* (Asteraceae) Benth. S. Moore extract against alloxan-induced oxidative stress via regulation of apoptosis and reactive oxygen species (ROS). *BMC Complement Altern Med.* PMID: 28356096

Bahar E, Lee GH, Bhattarai KR, Lee HY, Choi MK, **Harun-Or Rashid** et al. Polyphenolic Extract of *Euphorbia supina* Attenuates Manganese-Induced Neurotoxicity by Enhancing Antioxidant Activity through Regulation of ER Stress and ER Stress-Mediated Apoptosis. *Int J Mol Sci.* PMID: 28146110

Harun-Or Rashid, et al. (2015) ER stress: Autophagy induction, inhibition and selection, *Autophagy*. PMID: 26389781

Raj Kumar Yadav, Geum-Hwa Lee, Hwa-Young Lee, Bo Li, Han-Eul Jung, **Harun-Or Rashid** et al. TMBIM6 (transmembrane BAX inhibitor motif containing 6) enhances autophagy and reduces renal dysfunction in a cyclosporine A-induced nephrotoxicity model. *Autophagy*. PMID: 26305401

Harun-Or Rashid et al. Endoplasmic reticulum stress in the regulation of liver diseases: Involvement of Regulated IRE1 α and β -dependent decay and miRNA. *J Gastroenterol Hepatol.* PMID: 27774654.